



2016-10-01

Rotational Strength and Stiffness of Shallowly Embedded Base Connections in Steel Moment Frames

Kevin N. Hanks
Brigham Young University

Follow this and additional works at: <https://scholarsarchive.byu.edu/etd>

 Part of the [Civil and Environmental Engineering Commons](#)

BYU ScholarsArchive Citation

Hanks, Kevin N., "Rotational Strength and Stiffness of Shallowly Embedded Base Connections in Steel Moment Frames" (2016). *All Theses and Dissertations*. 6261.
<https://scholarsarchive.byu.edu/etd/6261>

This Thesis is brought to you for free and open access by BYU ScholarsArchive. It has been accepted for inclusion in All Theses and Dissertations by an authorized administrator of BYU ScholarsArchive. For more information, please contact scholarsarchive@byu.edu.

Rotational Strength and Stiffness of Shallowly Embedded
Base Connections in Steel Moment Frames

Kevin N. Hanks

A thesis submitted to the faculty of
Brigham Young University
in partial fulfillment of the requirements for the degree of
Master of Science

Paul W. Richards, Chair
Richard J. Balling
Kyle M. Rollins

Department of Civil and Environmental Engineering
Brigham Young University

Copyright © 2016 Kevin N. Hanks

All Rights Reserved

ABSTRACT

Rotational Strength and Stiffness of Shallowly Embedded Base Connections in Steel Moment Frames

Kevin N. Hanks

Department of Civil and Environmental Engineering, BYU
Master of Science

Shallowly embedded column base connections with unreinforced block out concrete are a common method of connecting steel columns to their foundation. There has been little research done to accurately quantify the effects of this block out concrete on the connection strength and rigidity, and therefore there is nothing to aid the practicing engineer in accounting for this in structural analysis. Due to this lack of understanding, engineers have typically ignored the effects of shallow block out concrete in their analysis, presumably leading to a conservative design.

Recent research has attempted to fill this gap in understanding. Several methods have been proposed that seek to quantify the effects of shallow block out concrete on a column base connection. Barnwell proposed a model that predicts the strength of a connection. Both Jones and Tryon used numerical modeling to predict the rotational stiffness of the connection.

An experimental study was carried out to investigate the validity of these proposed models. A total of 8 test specimens were created at 2/3 scale with varying column sizes, connection details, and embedment depths. The columns were loaded laterally and cyclically at increasing displacements until the connection failed.

The results show that the strength model proposed by Barnwell is reasonable and appropriate, and when applied to this series of physical tests produce predictions that have an observed/predicted ratio of between 0.95 to 1.39. The results also show that methods for estimating the rotational stiffness of the connection at the top of the block out concrete, as proposed by Jones and Tryon also produce reasonable values that had observed/predicted ratios of between 0.93 to 1.47.

An alternative model for determining a design value for the rotational stiffness of a shallowly embedded column base plate is also proposed. When the embedment depth to column depth ratio is greater than 1.22, the connection is sufficiently rigid and at small deflections (less than 1% story drift) may be accurately modelled with infinite rotational stiffness (a “fixed” connection) at the base of the column.

Keywords: steel columns, spread footings, shallowly embedded connection, block out, base plates, anchor bolts, lateral stiffness, rotational stiffness

ACKNOWLEDGEMENTS

This research would not have been possible without the support of a number of people, to whom I am indebted. First I would like to acknowledge the effort and support of my committee chair: Dr. Paul Richards, whose constant support, feedback, encouragement and advice was invaluable to me throughout the entire process. My wife, Naomi and my children, Brooklyn and Lily have likewise been supportive. Their cheerleading efforts provide the motivation for my work. David Anderson and his army of lab assistants provided endless support in the structures lab as the test specimens were built and tested. Ashley Sadler was my right hand during construction, and put her blood and sweat (quite literally) into the project. Both Trevor Jones and Joshua Tryon collaborated with me on the concepts and predictive models used herein. Several members of the professional community provided input and feedback on the design and testing concepts, of which I am grateful, namely: Barry Arnold (ARW Engineers), Graham Oxborrow (Reaveley Engineers + Associates), and Timothy Sobieraj (Burns & McDonnell). Finally, I would like to acknowledge Tom Schlafly, the director of research at the American Institute of Steel Construction (AISC), whose funding made this entire project possible.

TABLE OF CONTENTS

ABSTRACT	ii
TABLE OF CONTENTS.....	iv
LIST OF TABLES	xiii
LIST OF FIGURES	xv
1 Introduction.....	1
2 Literature review	5
2.1 Exposed Base Plate Connections	5
2.1.1 DeWolf and Sarisley (1980)	5
2.1.2 Thambiratnam and Paramasivam (1986)	9
2.1.3 Fisher and Kloiber (2006).....	11
2.1.4 Kanvinde and Deierlein (2011).....	18
2.1.5 Kanvinde, Grilli et al. (2011).....	21
2.1.6 Kanvinde, Jordan et al. (2013).....	25
2.2 Embedded Base Plate Connections.....	30
2.2.1 Pertold, Xiao et al. (2000a).....	30
2.2.2 Pertold, Xiao et al. (2000b).....	33
2.2.3 Grilli and Kinvinde (2015).....	37
2.3 Composite Moment Connections.....	40

2.3.1	Marcakis and Mitchell (1980).....	40
2.3.2	Sheikh, Deierlein et al. (1989)	47
2.3.3	Deierlein, Sheikh et al. (1989)	52
2.3.4	Shahrooz, Remmetter et al. (1993)	55
2.3.5	Motter (2014)	58
2.4	Steel Pile-to-Pile-Cap Connections.....	61
2.4.1	Xiao, Wu et al. (2006).....	61
2.4.2	Eastman (2011)	65
2.4.3	Richards, Rollins et al. (2011)	69
2.5	Shallowly Embedded Column Base Plates	73
2.5.1	Cui and Nakashima (2011)	73
2.5.2	Barnwell (2015)	78
2.5.3	Jones (2016).....	81
2.5.4	Tryon (2016)	83
3	Methods.....	89
3.1	Overview	89
3.2	Test Matrix.....	92
3.3	Specimen Design	92
3.3.1	Member Size Selection	93
3.3.2	Design Methodology.....	94

3.3.2.1	Base Plate Design	94
3.3.2.2	Column-to-Base Plate Weld Design.....	97
3.3.2.3	Anchor Bolt Design	97
3.3.2.4	Shear Lug Design	98
3.3.2.5	Concrete Base Design.....	99
3.3.2.6	Concrete Floor Slab Design.....	100
3.3.2.7	Concrete Block Out Design	102
3.4	Construction Process.....	102
3.4.1	Base Mat Construction.....	102
3.4.2	Top Mat Construction & Column Installation	112
3.4.3	Block out Construction	119
3.4.4	Specimen Placement & Test Setup	127
3.5	Testing Equipment and Instrumentation.....	136
3.5.1	Actuator.....	136
3.5.2	String Potentiometers.....	136
3.5.3	Strain Gages	139
3.6	Loading Protocol.....	142
4	Results	145
4.1	Material Tests.....	145
4.1.1	Concrete Tests.....	145

4.1.2	Steel Tests	149
4.2	Test Observations.....	152
4.2.1	Test Observations - Specimen D1.....	152
4.2.2	Test Observations - Specimen D2.....	155
4.2.3	Test Observations - Specimen D3.....	158
4.2.4	Test Observations - Specimen D4.....	162
4.2.5	Test Observations - Specimen F1	166
4.2.6	Test Observations - Specimen F2	168
4.2.7	Test Observations - Specimen F3	172
4.2.8	Test Observations - Specimen F4	175
4.3	Backbone Curve.....	179
4.3.1	Backbone Curve – All.....	181
4.3.2	Backbone Curve - D1.....	183
4.3.3	Backbone Curve - D2.....	184
4.3.4	Backbone Curve - D3.....	185
4.3.5	Backbone Curve - D4.....	186
4.3.6	Backbone Curve - F1	187
4.3.7	Backbone Curve - F2	188
4.3.8	Backbone Curve - F3	189
4.3.9	Backbone Curve - F4	190

4.3.10	Backbone Curve – Discussion	191
4.4	Hysteresis Curve	192
4.4.1	Hysteresis Curve - D1	193
4.4.2	Hysteresis Curve – D2	194
4.4.3	Hysteresis Curve – D3	195
4.4.4	Hysteresis Curve – D4	196
4.4.5	Hysteresis Curve – F1	197
4.4.6	Hysteresis Curve – F2	198
4.4.7	Hysteresis Curve – F3	199
4.4.8	Hysteresis Curve – F4	200
4.4.9	Hysteresis Curve – Discussion.....	201
4.5	Rotational Stiffness	202
4.5.1	Rotational Stiffness – D1	208
4.5.2	Rotational Stiffness – D2	208
4.5.3	Rotational Stiffness – D3	209
4.5.4	Rotational Stiffness – D4	209
4.5.5	Rotational Stiffness – F1	210
4.5.6	Rotational Stiffness – F2	210
4.5.7	Rotational Stiffness – F3	211
4.5.8	Rotational Stiffness – F4	211

4.5.9	Rotational Stiffness – Discussion	212
4.6	Anchor Bolt Strain	213
4.6.1	Anchor Bolt Strain, Anchor Bolt A1	216
4.6.2	Anchor Bolt Strain, Anchor Bolt A2	218
4.6.3	Anchor Bolt Strain – Discussion.....	220
4.7	Column Strain	221
4.7.1	Column Strain – D1	222
4.7.2	Column Strain – D2	223
4.7.3	Column Strain – D3	224
4.7.4	Column Strain – D4	225
4.7.5	Column Strain – F1	226
4.7.6	Column Strain – F2	227
4.7.7	Column Strain – F3	228
4.7.8	Column Strain – F4	229
4.7.9	Column Strain – Discussion.....	230
5	Discussion.....	231
5.1	Performance of Test Setup.....	231
5.1.1	Reaction Frame	231
5.1.2	Base Lateral Support.....	235
5.1.3	Out-of-Plane Reaction Frame	236

5.2	Performance of Specimen Design.....	239
5.2.1	Performance of Base Mat.....	240
5.2.2	Performance of Top Mat and Block Out.....	242
5.2.3	Performance of Shear Lug	244
5.2.4	Performance of Anchor Bolts	245
5.3	Connection Strength.....	248
5.4	Connection Stiffness	256
5.5	Design Example	264
5.5.1	Design Example #1: Moment Frame with a “Fixed” Base.....	265
5.5.2	Design Example #2: Moment Frame with a “Pinned” Base.....	268
6	Conclusions.....	271
	References	274
	Appendix A: Test Specimen Design Drawings.....	277
A.1	Design Drawings for Specimen D1	278
A.2	Design Drawings for Specimen D2.....	282
A.3	Design Drawings for Specimen D3	286
A.4	Design Drawings for Specimen D4.....	290
A.5	Design Drawings for Specimen F1	294
A.6	Design Drawings for Specimen F2	298
A.7	Design Drawings for Specimen F3	302

A.8 Design Drawings for Specimen F4	306
Appendix B: Design calculations	310
B.1 Base Plate Design for Specimens D1, D2, D3, & D4	311
B.2 Anchor Bolt Design for Specimens D1, D2, & D3	315
B.3 Anchor Bolt Design for Specimen D4.....	320
B.4 Maximum Expected Reaction Forces for Specimens D1, D2, D3, & D4	325
B.5 Base Plate Design for Specimens F1, F2, F3, & F4	332
B.6 Anchor Bolt Design for Specimens F1, F2, & F3	336
B.7 Anchor Bolt Design for Specimen F4	341
B.8 Maximum Expected Reaction Forces for Specimens F1, F2, F3, & F4.....	346
B.9 Shear lug weld design for all Specimens.....	353
B.10 Base Slab Bending Capacity and Reinforcement Design.....	357
B.11 Design Example #1: Portal Frame Design with a “fixed” base.....	364
B.12 Design Example #2: Portal Frame Design with a “Pinned” Base	378
Appendix C: Miscellaneous Drawings	387
C.1 Design Drawing for the Anchor Bolts and Embedded Plates	388
C.2 Design Drawing for the Anchor Bolt and Shear Key Pocket Template	390
C.3 Design Drawing for the Corbel	392
C.4 Design Drawing for the Actuator Extension Piece.....	394
C.5 Design Drawing for the Base Lateral Support Steel.....	396

C.6 Design Drawing for the Overall Test Specimen Setup.....	398
C.7 Actuator Schematic.....	400

LIST OF TABLES

Table 2-1: Summary of Test Results and Comparisons to Predictive Methods (DeWolf and Sarisley 1980)	9
Table 2-2: Test Matrix and Results (Grilli and Kanvinde 2015)	39
Table 2-3: Summary of Test Results (Sheikh, Deierlein et al. 1989)	51
Table 2-4: Summary of Test Results (Deierlein, Sheikh et al. 1989)	55
Table 2-5: Test Matrix (Motter 2014)	61
Table 2-6: Test Matrix (Xiao, Wu et al. 2006).....	62
Table 2-7: Test Specimen Design (Richards, Rollins et al. 2011)	72
Table 2-8: Specimen Parameters - First Test Round (Barnwell 2015)	80
Table 2-9: Specimen Parameters - Second Test Round (Barnwell 2015).....	80
Table 2-10: Experimental vs. Theoretical Rotational Stiffness of Barnwell's Physical Test Specimens (Tryon 2016)	85
Table 3-1: Test Matrix.....	92
Table 3-2: Summary of Member Size Selection	94
Table 3-3: Required Flexural Strength of Column Bases	95
Table 3-4: Concrete Mix Design for Block Out Concrete	119
Table 3-5: Procedure Used to Mix Block Out Concrete	120
Table 3-6: Report of Functioning and Non-Functioning Strain Gages	142
Table 3-7: Loading Protocol	143
Table 4-1: Summary of Concrete Cylinder Tests for the Base Mat.....	146
Table 4-2: Summary of Concrete Cylinder Tests for the Top Mat	147

Table 4-3: Summary of Concrete Cylinder Tests for the Block Out	148
Table 4-4: Key Information from Tensile Tests.....	150
Table 4-5: Rotational Stiffness at First Peak of 0.75% Story Drift Cycle	206
Table 4-6: Rotational Stiffness Before and After Concrete Cold Joint Break	207
Table 5-1: Observed Strength of Each Test Specimen.....	250
Table 5-2: Observed Specimen Yield Strength vs. Predicted Strengths	253
Table 5-3: Predicted vs. Observed Rotational Stiffness, β	259
Table 5-4: Design Example #1: Summary of Design Methods.....	266
Table 5-5: Design Example #1: Summary of Detailed Design Results	267
Table 5-6: Design Example #2: Summary of Design Methods.....	269
Table 5-7: Design Example #1: Summary of Detailed Design Results	270

LIST OF FIGURES

Figure 1-1: Typical Details for (a) Exposed Column Base Plate, (b) Embedded Column Base Plate, and (c) Shallowly Embedded Column Base Plate	2
Figure 1-2: Examples of Composite Connections: (a) Concrete Column and Steel Beam Connection, and (b) Steel Pile to Concrete Pile Cap	4
Figure 2-1: Stress and Strain Distribution Model for the Working Stress Method (DeWolf and Sarisley 1980).....	6
Figure 2-2: Stress Distribution for the Ultimate Strength Method (DeWolf and Sarisley 1980).....	7
Figure 2-3: Specimen (a) Elevation and (b) Plan View (Thambiratnam and Paramasivam 1986)	10
Figure 2-4: Model of Exposed Base Connection with Large Moment (Fisher and Kloiber 2006)	12
Figure 2-5: Model of Friction Mechanism (Fisher and Kloiber 2006)	16
Figure 2-6: Model of Bearing Mechanism Using (a) Shear Lug, and (b) Embedded Column (Fisher and Kloiber 2006)	17
Figure 2-7: Model of a Basic Moment Frame Under Lateral Load With (a) Pinned Base and (b) Fixed Base Connections (Kanvinde, Grilli et al. 2011)	22
Figure 2-8: Model of the Various Deformations Contributing to the Rotational Stiffness of an Exposed Base Connection (Kanvinde, Grilli et al. 2011)	23
Figure 2-9: Overview of Finite Element Model of Base Plate (Kanvinde, Jordan et al. 2013).....	26

Figure 2-10: Comparison of Contours of Vertical Displacement on the Base Plate (a) as Measured Directly Through Laser Scanning, and (b) From Finite Element Simulations (Kanvinde, Jordan et al. 2013)	27
Figure 2-11: Comparison of Anchor Rod Forces Estimated From Tests as well as Finite Element Simulations (Kanvinde, Jordan et al. 2013)	28
Figure 2-12: Comparison of Actual Stress Configuration Underneath a Base Plate for a Flexible Base Plate (Simulation #5) and a Stiff Base Plate (Simulation #6) (Kanvinde, Jordan et al. 2013).....	29
Figure 2-13: Example of an Embedded Column Base Connection (Pertold, Xiao et al. 2000a).....	30
Figure 2-14: Test Setup to Isolate and Test (a) Steel-Concrete Bond/Skin Friction, and (b) Concrete Bearing/Punching Shear (Pertold, Xiao et al. 2000a)	32
Figure 2-15: Model of Stress Distribution for an Embedded Column (Pertold, Xiao et al. 2000b)	34
Figure 2-16: Comparison of Experimental Values vs. Predicted from the Proposed Model Under Bending Loads (Pertold, Xiao et al. 2000b)	36
Figure 2-17: Illustration of Embedded Column Base Connection, Subjected to Axial and Lateral Loads (Grilli and Kanvinde 2015)	38
Figure 2-18: Typical Wall Panel and Beam-to-Column Composite Connections (Marcakis and Mitchell 1980).....	41
Figure 2-19: Test Setup for Test Series #1 (Marcakis and Mitchell 1980).....	42
Figure 2-20: Setup for Test Series #2 (Marcakis and Mitchell 1980).....	44

Figure 2-21: Specimens Isolating the Stress Directly Above and Below the Embedded Steel Member (Marcakis and Mitchell 1980)	45
Figure 2-22: Typical Composite Test Specimen (Sheikh, Deierlein et al. 1989)	48
Figure 2-23: Reinforcing Steel Details (Sheikh, Deierlein et al. 1989)	49
Figure 2-24: (a) Bearing (Stiffener) Plate Details; (b) Extended FHP, Steel Column, and Shear Stud Details (Sheikh, Deierlein et al. 1989).....	50
Figure 2-25: Contributions to the Panel Shear (a) Steel Web Panel; (b) Concrete Compression Strut; (c) Concrete Compression Field (Deierlein, Sheikh et al. 1989)	52
Figure 2-26: Example of a Coupling Beam Seated in the Plane of a Concrete (Shahrooz, Remmetter et al. 1993)	56
Figure 2-27: Typical Test Design (Shahrooz, Remmetter et al. 1993)	57
Figure 2-28: Model for Simulating Beam Effective Fixed Point (Shahrooz, Remmetter et al. 1993).....	58
Figure 2-29: View of Complete Test Assembly (Motter 2014)	60
Figure 2-30: Test Variables (Motter 2014)	60
Figure 2-31: Typical Steel Pile-to-Concrete-Pile Cap Connection (Xiao, Wu et al. 2006)	62
Figure 2-32: Typical Test Setup (Xiao, Wu et al. 2006).....	63
Figure 2-33: Typical Test Specimen Design (Eastman 2011)	65
Figure 2-34: Elastic Connection Stiffness vs. Normalized Pile Embedment Depth (Eastman 2011)	67

Figure 2-35: Model of the Elastic Stresses Developed by the Embedded Pile (Eastman 2011)	68
Figure 2-36: Comparison of Model for Elastic Strength With the Tested Elastic Strength of Specimens (Eastman 2011)	68
Figure 2-37: Example of Detail for (a) Fixed Pile Connection, and (b) Pinned Pile Connection (Richards, Rollins et al. 2011)	69
Figure 2-38: Moment Resisting Mechanisms: (a) Concrete Bearing/Embedment Mechanism, (b) Flexural Reinforcement Mechanism (Richards, Rollins et al. 2011)	70
Figure 2-39: Friction Mechanism (Richards, Rollins et al. 2011)	71
Figure 2-40: Model of Location of Compression Resultant (Barnwell 2015)	81
Figure 2-41: Example of the Effects of Base Plate Thickness on the Stiffness of a Column Base Connection, W8x48 Column Size (Jones 2016)	82
Figure 2-42: Model for an Embedded Column Base Connection (Tryon 2016)	83
Figure 2-43: Tryon's Model for Rotational Stiffness vs. Embedment Length, Compared with Barnwell Physical Tests (Tryon 2016)	85
Figure 2-44: Tryon's Normalized Rotational Stiffness vs. Embedment Curve for W10 Family (Tryon 2016)	86
Figure 2-45: Tryon's Normalized Rotational Stiffness vs. Embedment Curve for W14 Family (Tryon 2016)	86
Figure 3-1: Model of Lateral Force-Resisting Moment Frame with a Fixed Base	89
Figure 3-2: Test Setup General Layout - Elevation View Perpendicular to Loading	90
Figure 3-3: Test Setup General Layout - Elevation View Parallel to Loading	91

Figure 3-4: Test Setup General Layout - Plan View	91
Figure 3-5: Example Base Plate Design (for D-Specimens).....	96
Figure 3-6: Typical Concrete Base Mat Reinforcement	101
Figure 3-7: Typical Base Mat Prepared for Concrete Pour.....	104
Figure 3-8: Rebar Mats for the (a) Base Mat, and (b) Top Mat, Tied atop Templates	105
Figure 3-9: Anchor Bolt/Shear Lug Pocket Template (a) Top View, (b) Bottom View	106
Figure 3-10: Fully Assembled Base Mat Rebar Cage.....	107
Figure 3-11: Concrete Symon Form Setup	107
Figure 3-12: PVC in Place to Create Tie-Down Holes	108
Figure 3-13: Steel Pencil Rods in Place to Hold the Sides of the Concrete Form	110
Figure 3-14: Base Mat Concrete Pour	111
Figure 3-15: Completed Base Mat Pour.....	111
Figure 3-16: Exposed Anchor Bolts and Shear Key Pocket	112
Figure 3-17: Finished Top Mat	112
Figure 3-18: Top Floor Mat Preparations (a) 8 inch Floor Slab, (b) 16 inch Floor Slab	114
Figure 3-19: (a) First Lift Complete for the Concrete Pouring of an 16 inch Top Floor Mat, (b) Completed Concrete Pouring for a 16 inch Top Mat.....	114
Figure 3-20: (a) 8 inch Top Floor Mat Specimen with Concrete Forms Removed (b) Close up of Block out for a 16 inch Top Floor Mat with Forms Removed	115
Figure 3-21: (a) Column Placement and Adjusting, (b) Anchor Bolts	116

Figure 3-22: Column Base Prepped for Grout Pour.....	118
Figure 3-23: Finished Grout for Specimen D2.....	118
Figure 3-24: (a) Electric Mixer Used to Mix Concrete in 0.2 yd ³ Batches, (b) Material Measured out in Buckets	121
Figure 3-25: Block Out Concrete Placement	122
Figure 3-26: Placed Block Out Concrete	123
Figure 3-27: Finished Specimen D1, No Block Out	124
Figure 3-28: Finished Specimen F2, 8 inch Block Out.....	125
Figure 3-29: Finished Specimen F3, 16 inch Block Out.....	126
Figure 3-30: Bird's-Eye View of all Completed Specimens	127
Figure 3-31: Specimen in Place and Ready for Testing.....	128
Figure 3-32: Moving Specimens Using the Lab Overhead Crane Using (a) Original Bent-Rebar Pick Points, and (b) Post-Installed Pick Points	129
Figure 3-33: Post-Installed Crane Pick Points on Specimens D2, D3, D4, F2, F3, & F4	130
Figure 3-34: Base Preparations, (a) 2x4 Frame Built to Contain Hydrocal Mixture, (b) Floor Prepared with Form Release and Clay Donuts.....	132
Figure 3-35: Corbel-to-Column Connection, Seen from Above with Actuator Arm Ready to Move into Place	133
Figure 3-36: Out-of-Plane Reaction Frame.....	135
Figure 3-37: String Potentiometer Attachment Methods into (a) Steel Locations, and (b) Concrete Locations	137
Figure 3-38: String Potentiometers Attached Onto Wooden Plank	137

Figure 3-39: String Potentiometer Locations and Names	138
Figure 3-40: Threaded Rod Anchor Bolt Prepared for Strain Gage	140
Figure 3-41: Strain Gage Locations and Names, Typical for Each Specimen.....	141
Figure 3-42: Loading Protocol - Graphical Representation	144
Figure 4-1: Tensile Test on Threaded Anchor Rod.....	150
Figure 4-2: Tensile Test, 1 inch DIA Threaded Rod, ASTM F1554 Gr. 36 Steel	151
Figure 4-3: Tensile Test, 1 1/8 inch DIA Threaded Rod, ASTM F1554 Gr. 36 Steel	151
Figure 4-4: Specimen D1 (a) Start of Testing, and (b) End of Testing.....	152
Figure 4-5: Specimen D1, Crack in the Base Mat.....	154
Figure 4-6: Specimen D1, Anchor Bolts Under Tensile and Compressive Stresses.....	154
Figure 4-7: Specimen D2 (a) Start of Testing, and (b) End of Testing.....	155
Figure 4-8: Specimen D2, Vertical Crack in Top Mat.....	156
Figure 4-9: Specimen D2, Cracks in Base Mat.....	157
Figure 4-10: Specimen D2, Top of Concrete at Conclusion of Testing (7% Drift).....	158
Figure 4-11: Specimen D3 (a) Start of Testing, and (b) End of Testing.....	159
Figure 4-12: Specimen D3, Vertical Crack in Top Mat.....	160
Figure 4-13: Specimen D3, Cracks in Base Mat.....	160
Figure 4-14: Specimen D3, Top of Concrete at Conclusion of Testing (10% Drift).....	162
Figure 4-15: Specimen D4 (a) Start of Testing, and (b) End of Testing.....	163
Figure 4-16: Specimen D4, Vertical Cracks in Top Mat	164
Figure 4-17: Specimen D4, Base Mat at the Conclusion of Testing.....	164
Figure 4-18: Specimen D4, Top of Concrete at Conclusion of Testing.....	165
Figure 4-19: Specimen F1 (a) Start of Testing, and (b) End of Testing	166

Figure 4-20: Specimen F1, Grout and Top Surface of Concrete Failing	167
Figure 4-21: Specimen F1, Anchor Bolts Under Tensile and Compressive Stresses	168
Figure 4-22: Specimen F2 (a) Start of Testing, and (b) End of Testing	169
Figure 4-23: Specimen F2, Vertical Crack in Top Mat.....	170
Figure 4-24: Specimen F2, Block Out Distress at Conclusion of Testing	171
Figure 4-25: Specimen F3 (a) Start of Testing, and (b) End of Testing	172
Figure 4-26: Specimen F3, Vertical Cracks in Top Mat	173
Figure 4-27: Specimen F3, Vertical Crack in Top Mat at Conclusion of Testing, Back Side	174
Figure 4-28: Specimen F3, Block Out Concrete at Conclusion of Testing (9% Drift)....	174
Figure 4-29: Specimen F4 (a) Start of Testing, and (b) End of Testing	175
Figure 4-30: Specimen F4, Vertical Crack in Top Mat.....	177
Figure 4-31: Specimen F4, Vertical Crack in Top Mat at Conclusion of Testing	177
Figure 4-32: Specimen F4, Surface of Block out at Conclusion of Testing (10% Drift)	178
Figure 4-33: Model for Deflection of a Cantilevered Beam	179
Figure 4-34: Backbone Curve - All D-Series Tests	181
Figure 4-35: Backbone Curve – All D-Series Tests, up to 1%	181
Figure 4-36: Backbone Curves - All F-series Tests	182
Figure 4-37: Backbone Curve - All F-Series Tests, up to 1% Drift.....	182
Figure 4-38: Specimen D1 - Backbone Curve; Entire Testing Protocol.....	183
Figure 4-39: Specimen D1 - Backbone Curve; up to 1% Story Drift	183
Figure 4-40: Specimen D2 - Backbone Curve; Entire Testing Protocol.....	184

Figure 4-41: Specimen D2 - Backbone Curve; up to 1% Story Drift	184
Figure 4-42: Specimen D3 - Backbone Curve; Entire Testing Protocol	185
Figure 4-43: Specimen D3 - Backbone Curve; up to 1% Story Drift	185
Figure 4-44: Specimen D4 - Backbone Curve; Entire Testing Protocol	186
Figure 4-45: Specimen D4 - Backbone Curve; up to 1% Story Drift	186
Figure 4-46: Specimen F1 - Backbone Curve; Entire Testing Protocol	187
Figure 4-47: Specimen F1 - Backbone Curve; up to 1% Story Drift	187
Figure 4-48: Specimen F2 - Backbone Curve; Entire Testing Protocol	188
Figure 4-49: Specimen F2 - Backbone Curve; up to 1% Story Drift	188
Figure 4-50: Specimen F3 - Backbone Curve; Entire Testing Protocol	189
Figure 4-51: Specimen F3 - Backbone Curve; up to 1% Story Drift	189
Figure 4-52: Specimen F4 - Backbone Curve, Entire Testing Protocol	190
Figure 4-53: Specimen F4 - Backbone Curve; up to 1% Story Drift	190
Figure 4-54: Specimen D1 - Hysteresis; Entire Testing Protocol	193
Figure 4-55: Specimen D1 – Hysteresis; up to 1% Story Drift	193
Figure 4-56: Specimen D2 - Hysteresis; Entire Testing Protocol	194
Figure 4-57: Specimen D2 - Hysteresis; up to 1% Story Drift	194
Figure 4-58: Specimen D3 - Hysteresis; Entire Testing Protocol	195
Figure 4-59: Specimen D3 - Hysteresis; up to 1% Story Drift	195
Figure 4-60: Specimen D4 - Hysteresis; Entire Testing Protocol	196
Figure 4-61: Specimen D4 - Hysteresis; up to 1% Story Drift	196
Figure 4-62: Specimen F1 - Hysteresis; Entire Testing Protocol	197
Figure 4-63: Specimen F1 - Hysteresis; up to 1% Story Drift	197

Figure 4-64: Specimen F2 - Hysteresis; Entire Testing Protocol.....	198
Figure 4-65: Specimen F2 - Hysteresis; up to 1% Story Drift	198
Figure 4-66: Specimen F3 - Hysteresis; Entire Testing Protocol.....	199
Figure 4-67: Specimen F3 - Hysteresis; up to 1% Story Drift	199
Figure 4-68: Specimen F4 - Hysteresis; Entire Testing Protocol.....	200
Figure 4-69: Specimen F4 - Hysteresis; up to 1% Story Drift	200
Figure 4-70: Rotational Spring Model and Location at Each Specimen.....	202
Figure 4-71: Angle of Rotation at Point of Interest	204
Figure 4-72: Model for Contributions to Total Deflection	205
Figure 4-73: Rotational Stiffness for Test Specimen D1	208
Figure 4-74: Rotational Stiffness for Test Specimen D2	208
Figure 4-75: Rotational Stiffness for Test Specimen D3	209
Figure 4-76: Rotational Stiffness for Test Specimen D4	209
Figure 4-77: Rotational Stiffness for Test Specimen F1	210
Figure 4-78: Rotational Stiffness for Test Specimen F2	210
Figure 4-79: Rotational Stiffness for Test Specimen F3	211
Figure 4-80: Rotational Stiffness for Test Specimen F4	211
Figure 4-81: Predictive Models as Proposed by: (a) (DeWolf and Sarisley 1980), and (b) (Barnwell 2015).....	213
Figure 4-82: Strain in Anchor Bolt A1, D-Series Tests	216
Figure 4-83: Strain in Anchor Bolt A1, F-Series Tests.....	217
Figure 4-84: Strain in Anchor Bolt A2, D-Series Tests	218
Figure 4-85: Strain in Anchor Bolt A2, F-Series Tests.....	219

Figure 4-86: Strain in Column Flanges, Specimen D1	222
Figure 4-87: Strain in Column Flanges, Specimen D2	223
Figure 4-88: Strain in Column Flanges, Specimen D3	224
Figure 4-89: Strain in Column Flanges, Specimen D4	225
Figure 4-90: Strain in Column Flanges, Specimen F1	226
Figure 4-91: Strain in Column Flanges, Specimen F2	227
Figure 4-92: Strain in Column Flanges, Specimen F3	228
Figure 4-93: Strain in Column Flanges, Specimen F4	229
Figure 5-1: Typical Hysteresis Plot of Reaction Frame During Testing; Specimen F3	232
Figure 5-2: Reaction Frame (a) Test Setup, and (b) Resultant Forces	233
Figure 5-3: Reaction Frame Base	234
Figure 5-4: Lateral Movement of Base Mat for (a) D-Series Specimens and (b) F- Series Specimens	236
Figure 5-5: (a) Plan View of the Out-of-Plane String Pot Setup [Not To Scale], and (b) Model of Relative Distances	237
Figure 5-6: Adjusted Out-of-Plane Movement (a) D-Series Tests and (b) F-Series Tests	239
Figure 5-7: Anchor Bolts with Differering Strains; Specimen F2 After Testing and With Block out Concrete Removed	247
Figure 5-8: Anchor Bolts Post Test, Specimen D2	247
Figure 5-9: Anchor Bolt Strain Data for Specimen D3	249
Figure 5-10: Backbone Curve for Specimen F2 (Copy of Figure 4-48)	250

Figure 5-11: Observed Strength of D-Series Specimens	251
Figure 5-12: Observed Strength of F-Series Specimens	251
Figure 5-13: Observed Specimen Strength vs. Predicted Strengths, D-Specimens	254
Figure 5-14: Observed Specimen Strength vs. Predicted Strengths, F-Specimens.....	254
Figure 5-15: Rotational Stiffness of Column Base Connection at Top of Embedment Concrete, Modelled as a Rotational Spring	257
Figure 5-16: Predicted vs. Observed Rotational Stiffness, D-Series Specimens	260
Figure 5-17: Predicted vs. Observed Rotational Stiffness, F-Series Specimens.....	260
Figure 5-18: Rotational Stiffness of Column Base Connection, Modelled at the Base of the Column as a "Fixed" Connection.....	263
Figure 5-19: Design Example #1: Results of Design Using Conventional Design Methods.....	267
Figure 5-20: Design Example #1: Results of Design Using New Design Methods	267
Figure 5-21: Design Example #2: Results of Design Using Conventional Design Methods.....	270
Figure 5-22: Design Example #2: Results of Design Using New Design Methods	270

1 INTRODUCTION

Steel structures come in a wide variety of shapes and sizes, but share a common trait: they must be secured to the ground. Typically, a steel structure is anchored to a reinforced concrete foundation. The connection then, between the steel structure and its foundation is of the utmost importance. These base connections, “arguably...are the most important type of structural connections, transferring forces from the entire structure into the foundation” (Kanvinde and Deierlein 2011). These connections must be able to transfer the large vertical (gravity) loads from the structure, and in many cases the lateral and rotational loads imposed by lateral loads on the structure. There are many methods of connecting the steel column to its foundation, but the three most common types of base plate details are as follows:

1. Exposed. See Figure 1-1 (a). An exposed base plate is the simplest of the three connection types mentioned, but is unable to transfer large lateral and moment forces into the foundation without special detailing. It is often used in industrial applications, where aesthetics is not a concern.
2. Embedded. See Figure 1-1(b). An embedded base plate is the most complicated of the three, and is able to transfer large lateral and moment forces into the foundation. It can also be more expensive as it requires supplemental reinforcement and careful coordination between steel and concrete contractors. This type is often used in Seismic Lateral Resisting Systems (SLRS) to create a “fixed” base.

3. Shallowly embedded. See Figure 1-1(c). Engineers seeking the simplicity of the exposed connection with the aesthetic finish of an embedded one use the shallowly embedded connection. The column base is encased in unreinforced block out concrete. This has become the most common type of base plate connection detail in non-industrial applications.

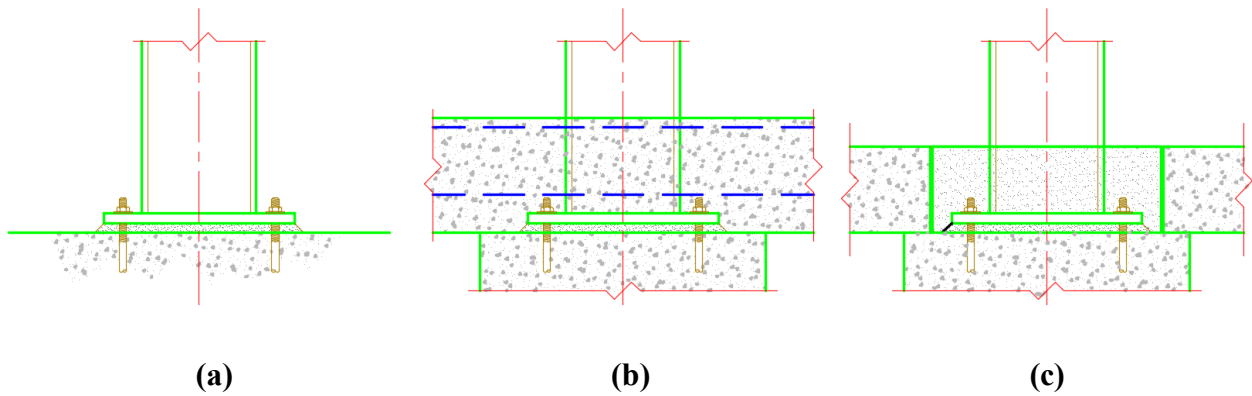


Figure 1-1: Typical Details for (a) Exposed Column Base Plate, (b) Embedded Column Base Plate, and (c) Shallowly Embedded Column Base Plate

While the shallowly embedded column base plate is the most common, it is also the least understood. Significant research has been performed on exposed base plates [(Thambiratnam and Paramasivam 1986); (Fisher and Kloiber 2006); (Kanvinde and Deierlein 2011); (Kanvinde, Grilli et al. 2011); (Kanvinde, Jordan et al. 2013)], as well as embedded base plates [(Pertold, Xiao et al. 2000a); (Grilli and Kanvinde 2015)]. This research has led to a broad understanding of the behavior of these types of connections, producing codes and design guides for use by

practicing engineers [(Fisher and Kloiber 2006); (Grilli and Kanvinde 2013), (Pertold, Xiao et al. 2000a)]. In contrast, attention on shallowly embedded base plates has been sparse.

Due to the scarcity of understanding and research surrounding shallowly embedded base plate connections, there is little to guide the practicing engineer in modeling these connections. Thus, during the design phase engineers typically treat a shallowly embedded base plate the same way they would an exposed base plate connection, and any contribution to the connection from the embedment concrete is ignored. This presumably conservative approach ignores any of the possible benefits of the embedment on the strength and rigidity of the connection, simply because those effects have not been studied and quantified.

Recent research into similar connections, those with various steel members embedded into concrete, suggest that the embedment concrete does indeed provide a quantifiable effect and that ignoring it is very conservative. Tests involving composite beam-column moment connections (Figure 1-2(a)) [(Shahrooz, Remmetter et al. 1993); (Motter 2014)], and steel pile to pile-cap connections (Figure 1-2(b)) [(Hutchinson, Chai et al. 2005); (Xiao, Wu et al. 2006); (Eastman 2011); (Richards, Rollins et al. 2011)] have shown that the contributions of the surrounding concrete on even a shallowly embedded steel shape are significant enough to warrant consideration. Recent exploratory research into shallowly embedded column base plates [(Cui and Nakashima 2011); (Barnwell 2015); (Tryon 2016); (Jones 2016)] confirm this. Barnwell, Tryon, and Jones, in particular showed through physical testing and numerical modeling that ignoring the contribution of the embedment concrete is conservative, and that this concrete adds significantly to both the strength and rigidity of the connection.

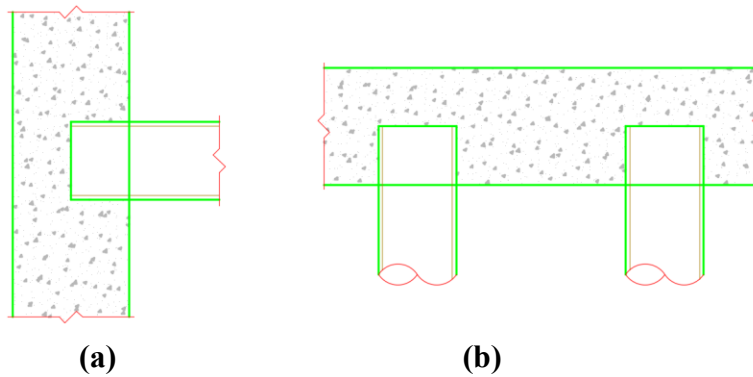


Figure 1-2: Examples of Composite Connections: (a) Concrete Column and Steel Beam Connection, and (b) Steel Pile to Concrete Pile Cap

This research continues the work performed by Barnwell, Tryon, and Jones to quantify the effects of the block out concrete on the behavior of this important connection. All three of these researchers have attempted to produce a model that will predict the behavior of a shallowly embedded steel column base connection. A main goal of this research, then, is to validate their theories and provide physical test data with which to compare their models.

A better understanding of the behavior of shallowly embedded column base plates will aid the practicing engineer in more accurately modeling a structure. This will result in more efficient, less expensive steel structures. Research into these connection types focuses on a detail that is already widely used and accepted in practice. There is a potential for substantial cost savings using this existing detail simply by understanding and more accurately modeling this connection during the design phase of a project.

2 LITERATURE REVIEW

2.1 Exposed Base Plate Connections

2.1.1 DeWolf and Sarisley (1980)

In 1980, a study was performed that investigated a gap in the then-current understanding of exposed base plates under moment loads. The authors, (DeWolf and Sarisley 1980) recognized that while the concept of a base plate experiencing axial load has been studied, little attention had been given to base plates experiencing a large moment load in addition to an axial load. They identified two possible methods for the design and evaluation of exposed base plates under a moment load. Their intent was to test specimens and compare the results of those tests to the predicted failure loads from these methods.

Method 1 is called the working stress method. This method is based on the assumed behavior of the system at the design or service load. It assumes that the moment induced by an eccentric axial load is resisted by 2 main mechanisms: tension in the anchor bolts on the trailing edge of the base plate, and compression in the concrete on the leading edge, whose stress distribution is triangular in shape. See Figure 2-1.

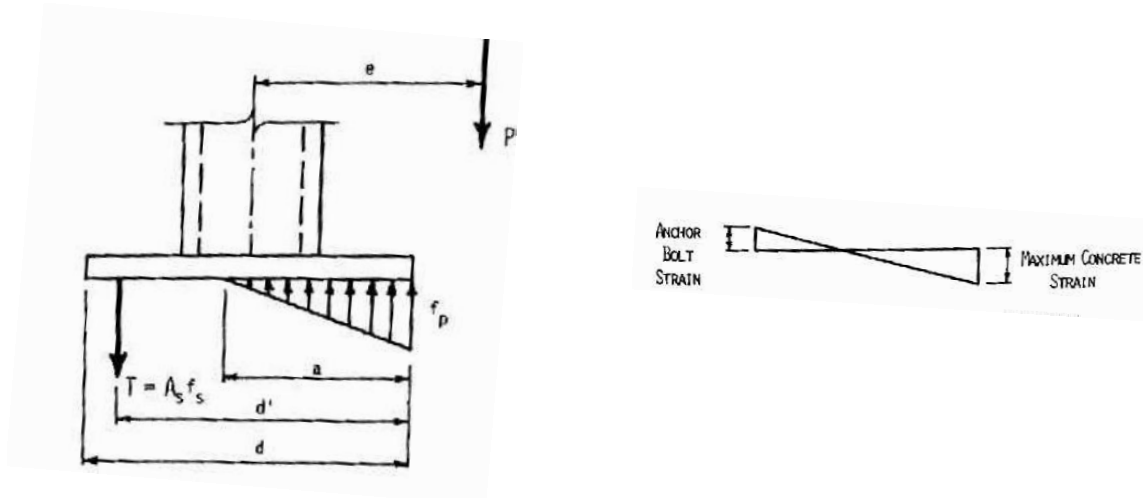


Figure 2-1: Stress and Strain Distribution Model for the Working Stress Method (DeWolf and Sarisley 1980)

Given the geometry of the plate (d, d') and the eccentricity of the load (e), there are four unknowns: tension in the anchor bolt group (T), the length of the compression stress block (a), the maximum compressive load on the concrete (f_p), and the predicted load at failure (P). The goal is to determine the predicted load at failure, or the capacity of the connection. To solve for these unknowns, one of two approaches is used.

The first approach is to assume that the maximum stress in the concrete is the same as its allowable stress at service loads (f_c), so $f_p = f_c$. Using that assumption, elementary statics principles lend a solution for a and T . Finally, the allowable load (P) for a given eccentricity is determined. This approach assumes that the stresses in the anchor bolt and the concrete are independent.

The second approach is to make the “strain compatibility assumption”, illustrated in Figure 2-1. This assumes that the stresses in the anchor bolts and the concrete are dependent on each

other. Assuming this allows for f_p , T , a , and P to be found analytically. In order for the strain in the anchor bolts and concrete to be compatible, the base plate would need to exhibit perfectly rigid behavior. DeWolf and Sarisley felt this unreasonable, and thus favor use of the first approach to determine the predicted failure loads of their specimen.

Method 2 is called the ultimate stress method. This method is based on the assumption that the anchor bolt is yielding (thus $f_s = f_y$) and that the stress distribution in the concrete is a rectangular stress block of magnitude f_p . The magnitude f_p is assumed to be equal to $0.85 \cdot f'_c$, similar to the value used in concrete beam and column design. See Figure 2-2.

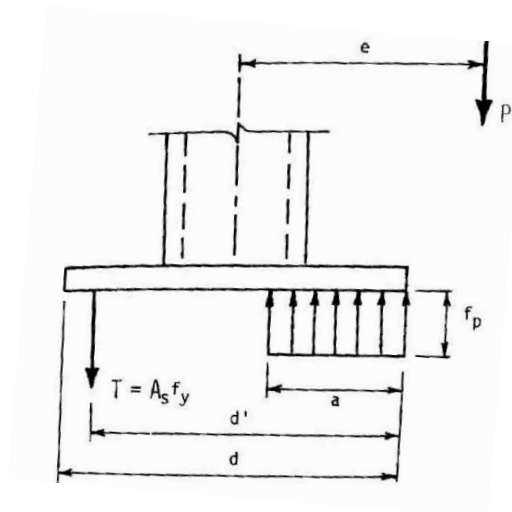


Figure 2-2: Stress Distribution for the Ultimate Strength Method (DeWolf and Sarisley 1980)

Given the axial load (P), the eccentricity (e), the geometry of the plate (d, d'), and the material properties of the anchor bolts and concrete (f_y and f'_c), the unknown width of the compression stress block (a) is determined. From there, one can solve for the predicted load at failure (P) by summing the vertical forces acting on the model.

The authors tested 16 total specimens to failure. Loads were applied as axial loads, at various eccentricities, to induce moment. The specimens investigated three variables:

1. Anchor bolt size. Diameters used were: 0.465 in, 0.748 in, and 0.990 in.
2. Base plate thickness. Thicknesses used were: 0.754 in, 0.884 in, and 0.990 in.
3. Ratio of Axial Load to Moment. Eccentricities used were: 0 in, 3 in, 6 in, 9 in.

The authors compared the failure loads (P_e) of the specimens to the predicted failure loads from the working stress method (P_{ws} , using the first approach discussed) and the ultimate strength method (P_u). A safety factor for each specimen was also determined from the ratio of the test failure load to the predicted failure load. See Table 2-1 for a summary of the results of these tests.

From these results, the authors concluded that both methods of calculating the strength of an exposed base plate connection are reasonable. The mean safety factor for the working stress method was 2.16, and for the ultimate stress method was 1.11. While reasonable, both methods are conservative and do not account for all the mechanisms associated with resisting the applied loads. The authors of this paper stated that they preferred the ultimate stress method as it more accurately predicts the actual behavior of the base plate, and that it reflects on the industry trend toward limit design.

Table 2-1: Summary of Test Results and Comparisons to Predictive Methods (DeWolf and Sarisley 1980)

Specimen	Base plate thickness (in)	Eccentricity of load (in)	Anchor bolt diameter (in)	Test Failure Load P_e (kips)	Working stress method		Ultimate strength method	
					Predicted load	Comparison	Predicted load	Comparison
					P_{ws} (kips)	P_e / P_{ws}	P_u (kips)	P_e / P_u
1	0.884	0.0	-	155.0	-	-	-	-
2	0.884	3.0	0.465	80.0	34.0	2.35	74.6	1.07
3	0.884	6.0	0.465	25.2	11.6	2.17	21.3	1.18
4	0.884	9.0	0.465	12.5	5.7	2.19	9.9	1.26
5	0.884	0.0	-	150.0	-	-	-	-
6	0.884	3.0	0.748	89.5	-	-	80.7	1.11
7	0.884	6.0	0.748	46.0	20.6	2.23	41.0	1.12
8	0.884	9.0	0.748	29.5	13.0	2.27	24.7	1.19
9	0.884	0.0	-	144.0	-	-	-	-
10	0.884	3.0	0.995	90.0	-	-	82.3	1.09
11	0.884	6.0	0.995	47.0	22.3	2.11	45.1	1.04
12	0.884	9.0	0.995	30.5	14.9	2.05	28.5	1.07
13	0.990	6.0	0.748	48.0	20.6	2.33	41.0	1.17
14	0.990	9.0	0.748	27.4	13.0	2.11	24.7	1.11
15	0.754	6.0	0.748	39.8	20.6	1.93	41.0	0.97
16	0.754	9.0	0.750	25.6	13.0	1.97	24.7	1.04

2.1.2 Thambiratnam and Paramasivam (1986)

The authors of this paper, (Thambiratnam and Paramasivam 1986), designed a test that would isolate the base plate itself and analyze its behavior under axial and moment loads. They wanted to determine what effect the base plate alone plays on the overall capacity of the connection.

They built twelve total specimens and loaded them to failure. See Figure 2-3. Loads were applied as vertical axial loads, at various eccentricities that would induce bending in the connection. There were only two variables:

1. Base plate thickness. Thicknesses used were: 0.625 in, 0.75 in, and 0.875 in.
2. Ratio of Axial Load to Moment. Eccentricities used were: 1 in, 3 in, 5 in, and 7 in.

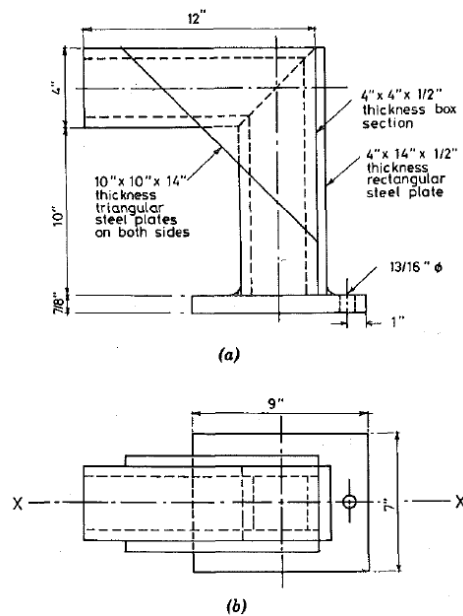


Figure 2-3: Specimen (a) Elevation and (b) Plan View (Thambiratnam and Paramasivam 1986)

The authors wanted to compare the test results with the current design methods, so like DeWolf and Sarisley, they made predictions on the failure load using the working stress method. They found that the mean safety factor (ratio of test failure to predicted failure), was 1.35. In

order to isolate bending in the base plate as a failure mechanism, they oversized the anchor bolt and used concrete with a high compressive strength. The authors state that in their tests, neither the concrete nor the anchor bolts came close to failure, and the loss of strength in the connection was attributed in every case to yielding of the base plate. This difference, they state, accounts for the much lower safety factor than was calculated in the tests done by DeWolf and Sarisley.

These tests highlight two important points regarding exposed base plate connections. First, they point out that the then current methods of predicting allowable loads are inaccurate for thin (flexible) base plates experiencing large moment loads. This is because the design methods of the time (the working stress model) do not account for flexibility in the base plate. Secondly, they point out that counterintuitively, a thicker base plate does not always yield the strongest connection. A very flexible base plate tends to yield, while a very stiff base plate tended to lift up off its leading edge, causing excessive strain in the anchor bolts. They stated that there is an optimal thickness of the base plate that the connection strength, though they admitted that additional testing would be required to determine what that would be.

2.1.3 Fisher and Kloiber (2006)

Research of the type thus discussed resulted in a design guide (Fisher and Kloiber 2006) published by the American Institute of Steel Construction. Its purpose was to consolidate the available research into a guide that would aide practicing engineers in designing an exposed base plate. Fisher and Kloiber begin the section on designing column base plates with large moments with this explanation: “When the magnitude of the bending moment is large relative to the column axial load, anchor rods are required to connect the base plate to the concrete foundation so that the base does not tip nor fail the concrete in bearing at the compressed edge.”

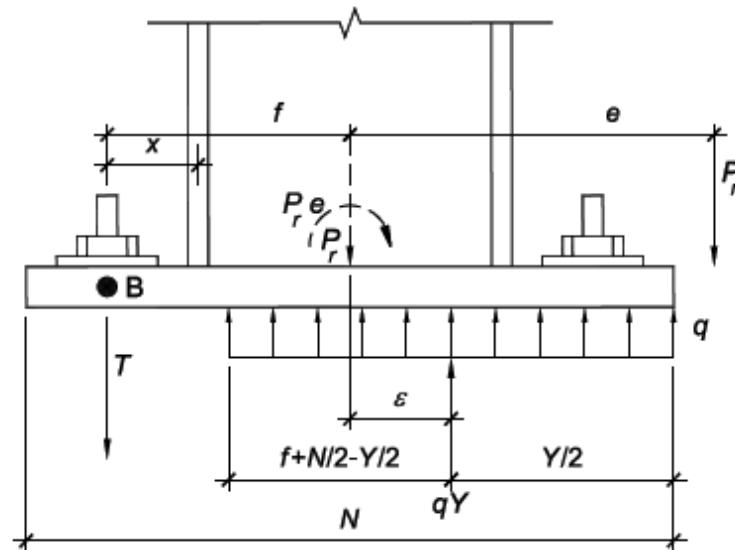


Figure 2-4: Model of Exposed Base Connection with Large Moment (Fisher and Kloiber 2006)

A base plate is defined as having a bending moment magnitude “large relative to the column axial load” when equation (2.1.1) is satisfied.

$$e > e_{crit} \quad (2.1.1)$$

Where:

$$e_{crit} = \frac{N}{2} - \frac{P_r}{2 \cdot q_{max}}$$

e = eccentricity of the column axial load. When only the column axial load (P_r) and the moment (M_r) at the base are given, e is calculated by the equation $e = M_r / P_r$.

e_{crit} = critical eccentricity – any eccentricity lower than this critical eccentricity is treated as a column base plate with “small moments”, a topic covered in this review.

N = base plate dimension parallel to the eccentricity dimension.

P_r = column axial load

$$q_{\max} = f_{p(\max)} \cdot B$$

$$f_{p(\max)} = \phi \left(0.85 \cdot f_c' \right) \left(\sqrt{\frac{A_2}{A_1}} \right) \leq \phi \cdot 1.7 \cdot f_c'$$

ϕ = ACI specified strength reduction factor = 0.65

A_1 = area of base plate

A_2 = maximum area of the portion of the supporting surface that is geometrically similar to and concentric with the loaded area.

f_c' = compressive strength of the concrete supporting the column

The general design procedure then lists the following steps for the design of a base plate connection (while this method is presented for both LRFD and ASD methods, only the LRFD is summarized here):

1. Determine the axial load (P_r) and moment (M_r).
2. Pick a trial base plate size $N \times B$.

3. Determine the equivalent eccentricity (e), and the critical eccentricity (e_{crit}). If $e > e_{crit}$, then continue on to step four. Otherwise, the connection is considered as having “small moments”, a condition not covered in this summary. Refer to the Design Guide section 3.3 for this case.
4. Determine the equivalent bearing length (Y) using equation (2.1.2), and the tensile force in the anchor rods, (T) using equation (2.1.3).

$$Y = \left(f + \frac{N}{2} \right) \pm \sqrt{\left(f + \frac{N}{2} \right)^2 - \frac{2 \cdot P_r \cdot (e + f)}{q_{\max}}} \quad (2.1.2)$$

(note that if the portion under the square root is negative, then the base plate configuration chosen does not yield a solution. Return to step 2, choose a larger base plate size and continue)

$$T = q_{\max} \cdot Y - P_r \quad (2.1.3)$$

5. Determine the required minimum base plate thickness ($t_{p(req)}$) at the bearing interface: equations (2.1.4) & (2.1.5), and tension interfaces: equation (2.1.6). Choose the larger value.

$$t_{p(req)} = 1.5 \cdot m \cdot \sqrt{\frac{f_{p(\max)}}{F_y}} \quad \text{for } Y \geq m \quad (2.1.4)$$

$$t_{p(req)} = 2.11 \cdot \sqrt{\frac{f_{p(\max)} \cdot Y \cdot \left(m - \frac{Y}{2} \right)}{F_y}} \quad \text{for } Y < m \quad (2.1.5)$$

$$t_{p(req)} = 2.11 \cdot \sqrt{\frac{T \cdot \left(f - \frac{d}{2} + \frac{t_f}{2} \right)}{B \cdot F_y}} \quad (2.1.6)$$

where:

$$m = \frac{N - 0.95d}{2}$$

$$n = \frac{B - 0.8b_f}{2}$$

(note: when $n > m$, substitute n for m in equation (2.1.4) or (2.1.5))

d = depth of wide flange column section

t_f = column flange thickness

6. Determine the anchor rod size appropriate for the tensile loading.

The design guide also provides a procedure for determining the shear strength of a connection. It provides guidance for the shear strength given three different mechanisms

1. Friction between the base plate and grout or concrete surface. Figure 2-5. This mechanism will always be present provided there is a net downward axial load (P_u) on the column. The engineer must use the loading combination with the most unfavorable arrangement of factored compressive loads. If the net axial load ends up being negative (an uplift load), then the shear resistance from friction is non-existent. The method of determining the available shear resistance from friction can be determined using equation (2.1.7).

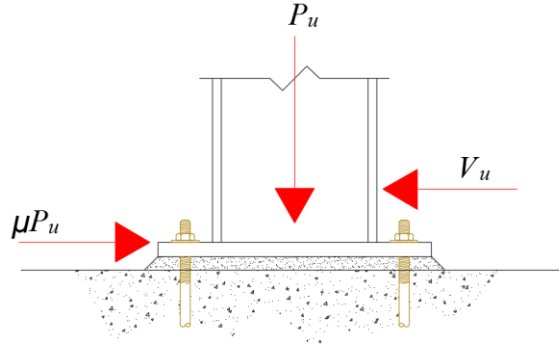


**Figure 2-5: Model of Friction Mechanism
(Fisher and Kloiber 2006)**

$$\phi V_{nf} = \phi \mu P_u \leq 0.2 f'_c A_c \quad (2.1.7)$$

where:

V_u = shear demand on the column base

ϕV_{nf} = available shear resistance from friction

ϕ = strength reduction factor = 0.6

μ = coefficient of friction = 0.55 (steel on grout); 0.70 (steel on concrete)

P_u = lowest factored axial load on the column from load combinations

A_c = area of the base plate

If the shear demand (V_u) is greater than the available shear resistance (ϕV_{nf}), then the difference must be resisted by one of the two remaining mechanisms.

2. Bearing against concrete. This mechanism is caused by a shear lug bearing against a shear pocket or by the column and base plate bearing against concrete or grout, as in the case of an embedded column. See Figure 2-6.

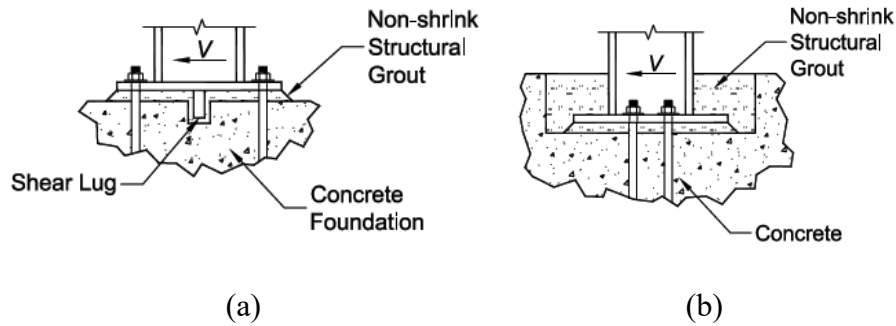


Figure 2-6: Model of Bearing Mechanism Using (a) Shear Lug, and (b) Embedded Column (Fisher and Kloiber 2006)

For bearing against a shear lug, use equation (2.1.8). For bearing of a column & base plate against grout or concrete, as in the case of an embedded column, use equation (2.1.9).

$$\phi V_{nbrg} = \phi 1.3 f_c' A_l \quad (2.1.8)$$

$$\phi V_{nbrg} = 0.55 f_c' A_{brg} \quad (2.1.9)$$

where:

ϕV_{nbrg} = available shear resistance from bearing

ϕ = strength reduction factor = 0.60

A_l = embedded area of shear lug (not including the portion of the lug in contact with the grout above the surface of the concrete foundation)

A_{brg} = contact area between the base plate and column against the grout/concrete

3. Shear in the anchor rods. This mechanism will not be summarized herein, as it is not the subject of this paper. Suffice to say that the design of shear resistance of the anchor bolts must take into account two mechanisms: first, bending of the bolts in reverse curvature with the effective length taken as half the thickness of the washer plus the thickness of the base plate. Second, concrete breakout capacity, per the concrete capacity design (CCD) method. This mechanism is explained in Section 3.5.3 of the guide, which in turn references the procedure outlined in ACI 318 Appendix D.

2.1.4 Kanvinde and Deierlein (2011)

Fairly recently a series of tests were performed (Kanvinde and Deierlein 2011) on exposed base plates with the purpose of evaluating their behavior under a variety of loading conditions, and comparing those results with recommendations from the AISC Design Guide discussed above. They came up with an innovative testing mechanism that could impart large lateral shear loads at the base in addition to axial loads. This allowed them to test the accuracy of the models and recommendations from the AISC Design Guide.

They constructed a total of 20 specimens, and loaded each to failure. The loading conditions varied based on the failure mechanisms they were interested in. These were:

1. Axial and Moment Loads. The first seven specimens were loaded to failure with an axial load at varying eccentricities, similar to the two previous tests mentioned.
2. Axial and Shear Loads. The next seven specimens were loaded with a constant axial load (both a compressive and a tensile load), then a lateral shear force at the base of the column until failure.
3. Weld Capacity. The final six specimens were created to isolate the weld that attaches the base plate to the bottom of the column. These were loaded with an axial and moment load until the weld failed. Very similar test to that done by (Myers, Kanvinde et al. 2009).

While the authors didn't publish their raw data regarding these tests, they state the following conclusions:

1. Moment Capacity
 - a. All of the specimens tested showed "excellent deformation capacity". The connections did not lose any of their rotational strength until they experienced a rotation corresponding to 7%-10% of a total story drift. For reference, AISC seismic provisions for a beam-to-column moment connected require a connection to withstand a rotation corresponding to minimum 4% story drift. This indicates that an exposed base plate connection has higher potential for energy dissipation than previously thought.
 - b. Relating their results to the strength predictions from the AISC design guide, they found that the actual strength of a connection was 80% stronger

than what was predicted, indicating a fair amount of conservatism in the design guide. They discovered that the design guide was more accurate when yielding of the anchor bolt governed the strength, and less so when yielding of the base plate governed.

2. Shear Capacity

- a. The authors recommended a coefficient of friction between the bottom of the base plate and the grout of 0.45. The AISC design guide suggests a value of 0.55.
- b. When the shear load is resisted by the anchor bolts, they concluded that the current recommendations from the design guide were accurate. The effective length of the bolt is taken as the thickness of the base plate plus $\frac{1}{2}$ the thickness of the washer. The bolts bend in double curvature, and should be checked for the interaction between axial forces due to flexure and axial loads with the shear loads.
- c. When a shear key pocket and a shear lug are used, the authors recommend using the “concrete capacity design” rather than the “45 degree cone method”. They stated that due to the size effect in concrete (Bažant 1984), failure from shear loads was controlled by fracture initiation.

3. Weld Capacity

- a. The authors concluded that both the complete joint penetration (CJP) weld, and the partial joint penetration (PJP) weld (with a reinforcing fillet weld)

performed more than adequately and are appropriate for use in seismic design.

- b. They also discovered that the PJP weld actually performed slightly better than the CJP weld. They attribute this result to the presence of an access weld hole required in a CJP weld, where stresses are magnified.
- c. Both of these conclusions echo results reported in the similar tests done on weld details in column base plates (Myers, Kanvinde et al. 2009).

2.1.5 Kanvinde, Grilli et al. (2011)

The studies summarized thus far have focused on the strength of an exposed base plate connection. There has been little mention of another important characteristic of these connection types: their rotational stiffness. During design, engineers typically classify this stiffness in one of two idealized ways: either as “pinned” or “fixed”. A pinned connection is one that displays no rotational stiffness, while a fixed connection is one with infinite rotational stiffness. See Figure 2-7.

The authors of this paper (Kanvinde, Grilli et al. 2011) state that while no connection is truly pinned or fixed, the true rotational stiffness of a base connection lies somewhere in between these ideals on a spectrum. The true rotational stiffness of a base connections lies somewhere in between. Any connection behaves more like a rotational spring, and some are stiffer than others. By classifying a base as truly fixed, the engineer neglects the true behavior of a connection and may under-design a system. When classifying a base as pinned, the engineer neglects the inherent stiffness of the connection and may be conservative in the design of a system.

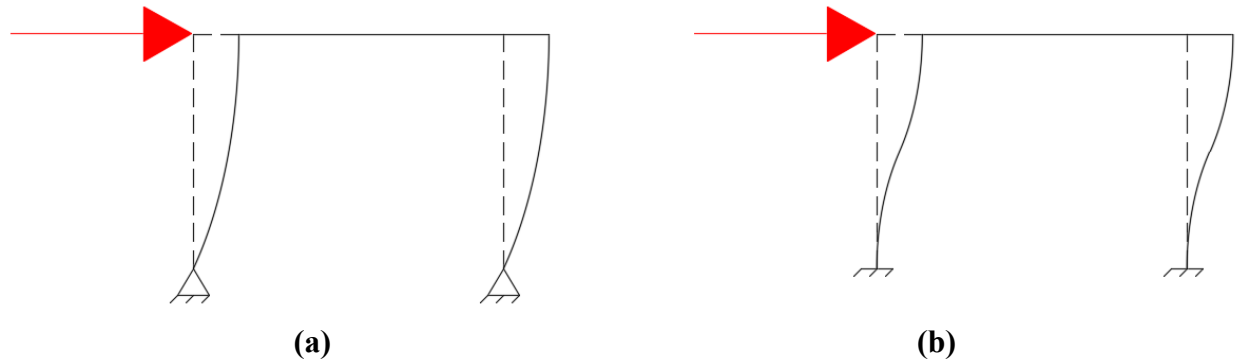


Figure 2-7: Model of a Basic Moment Frame Under Lateral Load With (a) Pinned Base and (b) Fixed Base Connections (Kanvinde, Grilli et al. 2011)

The true rotational stiffness of a base connection affects several aspects of a structural system response. This includes the overall structural reliability, the internal force distribution, system deformations, and the column effective length. Thus, accurately determining the rotational stiffness of a connection leads to a more accurate overall design, and contribute to both safety and economy.

Kanvinde proposes a step-by-step method for classifying the rotational stiffness of a connection. While the exact procedure is not summarized in detail here, the rotational stiffness is determined from four components, as shown in Figure 2-8.

The components whose deformations define the rotation flexibility include:

1. Elongation of the anchor rods in tension.
2. Bending of the base plate on the tension side.
3. Bending of the base plate on the compression side.
4. Deformation of the concrete under the compression side of the plate.

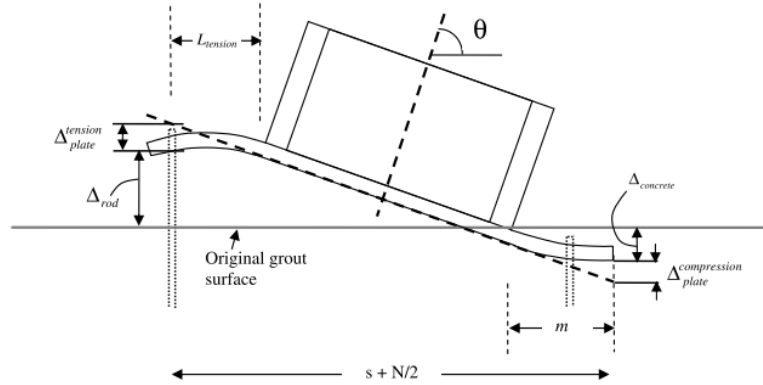


Figure 2-8: Model of the Various Deformations Contributing to the Rotational Stiffness of an Exposed Base Connection (Kanvinde, Grilli et al. 2011)

The authors chose various tests previously performed to validate the rotational stiffness acquired from this method. The results of this comparison was that the method described briefly above can reasonably predict the actual behavior of the connection. They discovered that for cases with high eccentricity, the ratio of the tested stiffness versus the calculated stiffness

$(\frac{\beta_y^{test}}{\beta_y^{method}})$ was an average of 1.08, with a coefficient of variation of 0.12.

The authors note that this method predicted values very poorly for the condition of low eccentricity, and thus cannot recommend this method for those cases. Also, there are built-in inaccuracies which should be understood. There are assumptions made in the AISC Design Guide which are inherently present in this model. The shape of the stress block underneath the compression flange of the column is assumed to be rectangular and does not reflect actual conditions, a finding that will be confirmed by the next paper discussed. The method also

assumes that the base plate on the tension side of the connection bends as a cantilever beam, when in reality it will exhibit biaxial bending around the anchor bolts.

The authors conclude that because of these limitations, this method be employed only for base plates with a large eccentricity and a geometry similar to those tested here. Connections with significantly more stiff or flexible base plates, different bolt patterns, etc. should not use this method.

Since the test specimens used in this thesis are similar in nature to those this method is intended to predict, the model and its accompanying equations are used to predict the behavior of one of the test specimens. Since the model proposed here does not take into account any contributions to the rotational stiffness from concrete embedment, the following equations produce a prediction for three of the test specimens, namely D1, D2, & D3. The contributions of each of the components are shown below in equations (2.1.10) through (2.1.13). The amount of rotation expected at the column base is calculated using equation (2.1.14), and finally the stiffness of the connection is shown below in equation (2.1.15). This value will be compared to the actual observed stiffness of the specimens in section 5.4.

$$\Delta_{rod} = \frac{T_{rod} \cdot L_{rod}}{A_{rod} \cdot E_{rod}} = \frac{(31.3kip) \cdot (20in)}{(0.606in^2) \cdot (18,000ksi)} = 0.057in \quad (2.1.10)$$

$$\begin{aligned} \Delta_{plate}^{tension} &= \left(\frac{T \cdot L_{tension}^3}{3 \cdot E_{plate} \cdot I_{plate}} \right) + \frac{T \cdot L_{tension}}{A_{s_plate} \cdot G_{plate}} \\ &= \left(\frac{(125.2 \text{ kip}) \cdot (2.0625 \text{ in})^3}{3 \cdot (29,000 \text{ ksi}) \cdot (15.2 \text{ in}^4)} \right) + \frac{(125.2 \text{ kip}) \cdot (2.0625 \text{ in})}{(30 \text{ in}^2) \cdot (11,154 \text{ ksi})} \\ &= 0.0016 \text{ in} \end{aligned} \quad (2.1.11)$$

$$\begin{aligned}
\Delta_{plate}^{compression} &= \frac{f_{\max} \cdot B}{8 \cdot E_{plate} \cdot I_{plate}} \cdot \left(m^4 - \frac{1}{3} \cdot (m - Y)^3 \cdot (3 \cdot m + Y) \right) \\
&\quad + \frac{f_{\max} \cdot B \cdot Y}{A_{s_plate} \cdot G_{plate}} \cdot \left(m - Y + \frac{Y^2}{2} \right) \\
&= \frac{(9.4 \text{ ksi}) \cdot (16 \text{ in})}{8 \cdot (36 \text{ ksi}) \cdot (15.2 \text{ in}^4)} \cdot \\
&\quad \left((4.06 \text{ in})^4 - \frac{1}{3} \cdot (4.06 \text{ in} - 0.837 \text{ in})^3 \cdot (3 \cdot 4.06 \text{ in} + 0.837 \text{ in}) \right) \\
&\quad + \frac{(9.4 \text{ ksi}) \cdot (16 \text{ in}) \cdot (0.837 \text{ in})}{(30 \text{ in}^2) \cdot (11,154 \text{ ksi})} \cdot \left(4.06 \text{ in} - 0.837 \text{ in} + \frac{(0.837 \text{ in})^2}{2} \right) \\
&= 0.0067 \text{ in}
\end{aligned} \tag{2.1.12}$$

$$\Delta_{concrete} = \frac{f_{\max}}{E_{conc}} \cdot d_{footing} = \frac{(9.35 \text{ ksi})}{(11022 \text{ ksi})} \cdot (24 \text{ in}) = 0.0204 \text{ in} \tag{2.1.13}$$

$$\begin{aligned}
\theta_y &= \frac{\Delta_{rod} + \Delta_{plate}^{tension} + \Delta_{plate}^{compression} + \Delta_{concrete}}{s + N/2} \\
&= \frac{(0.057 \text{ in}) + (0.0016 \text{ in}) + (0.0067 \text{ in}) + (0.0204 \text{ in})}{(9 \text{ in}) + (11 \text{ in})} \\
&= 0.0043 \text{ radians}
\end{aligned} \tag{2.1.14}$$

$$\begin{aligned}
\beta_y &= \frac{M_y}{\theta_y} = \frac{(204.3 \text{ kip} \cdot \text{ft})}{(0.0043 \text{ radians})} \\
&= 47,463 \frac{\text{kip} \cdot \text{ft}}{\text{radians}} = 569,559 \frac{\text{kip} \cdot \text{in}}{\text{radians}}
\end{aligned} \tag{2.1.15}$$

2.1.6 Kanvinde, Jordan et al. (2013)

Recognizing that all previous methods of predicting the behavior of the connection rely on simplified methods and assumptions, the authors of this paper (Kanvinde, Jordan et al. 2013) leveraged computer software to analyze the exposed base plate in a finite element model. The interactions of all the separate components in a base plate under load is complex, so in all the

previous methods simplifying assumptions are made. Although the total interaction of all these components has been tested and analyzed, there has not been an opportunity to isolate and examine each individual component. This limitation inhibits an accurate prediction when these individual components are different than those tested.

Kanvinde et al. created a finite element model with the capabilities of isolating and analyzing all the components in an exposed base plate connection. This allows for a better understanding of a connection, and more accurate predictions of their behavior. Refer to Figure 2-9 for an image of the finite element model created for this purpose.

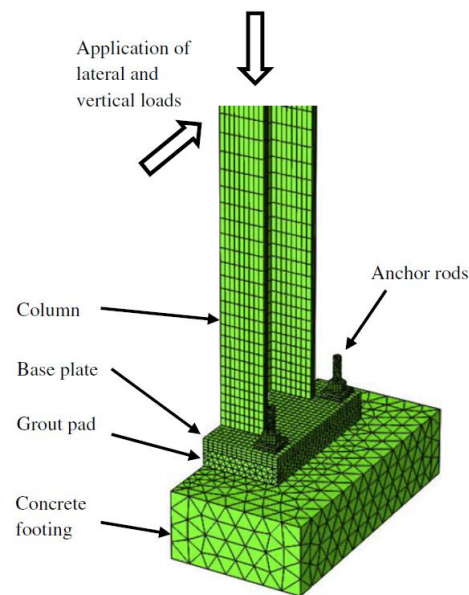


Figure 2-9: Overview of Finite Element Model of Base Plate (Kanvinde, Jordan et al. 2013)

The results gathered from the computer model were validated against actual test data. The computer models were created to replicate actual test specimens created and tested by (Gomez, Kanvinde et al. 2010). Comparison of the computer model to test data provide the validation. Refer to Figure 2-10 and Figure 2-11 for several examples of this comparison.

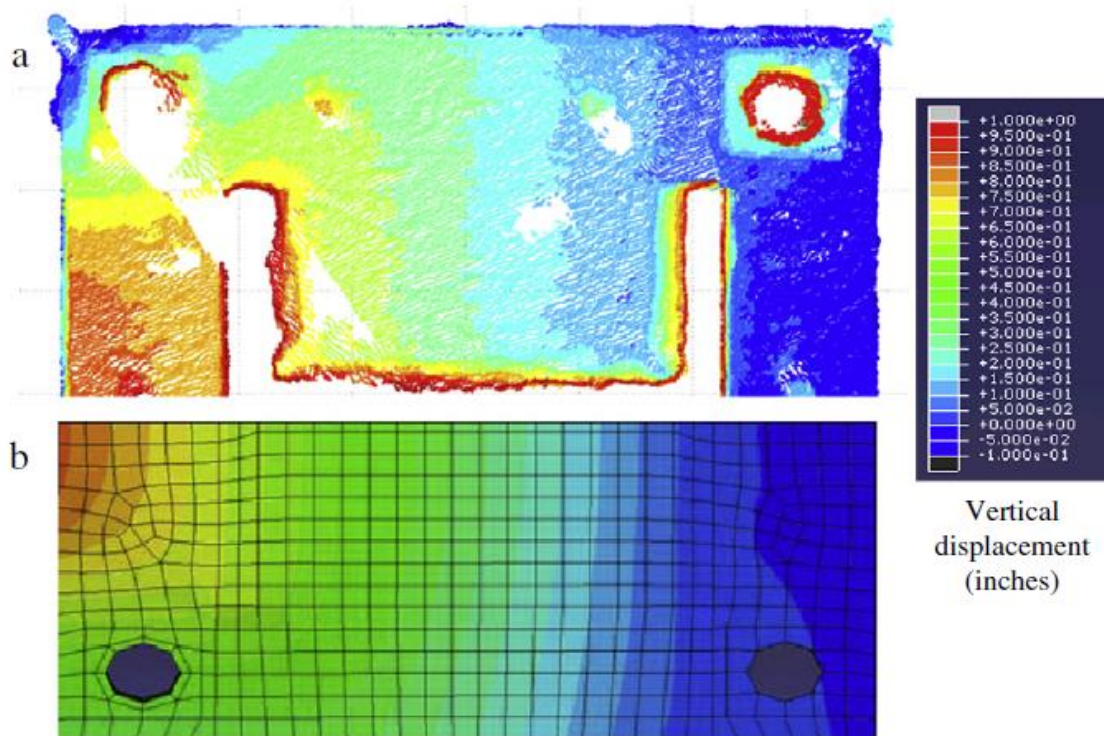


Figure 2-10: Comparison of Contours of Vertical Displacement on the Base Plate (a) as Measured Directly Through Laser Scanning, and (b) From Finite Element Simulations (Kanvinde, Jordan et al. 2013)

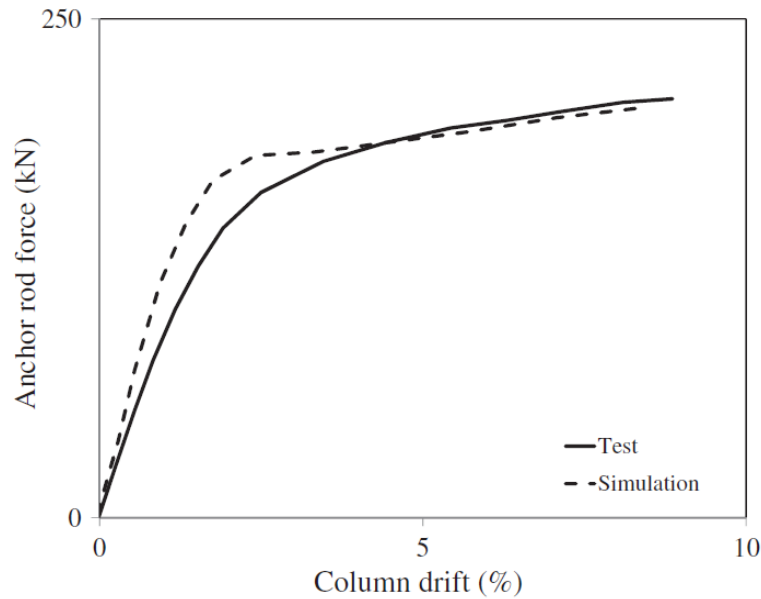


Figure 2-11: Comparison of Anchor Rod Forces Estimated From Tests as well as Finite Element Simulations (Kanvinde, Jordan et al. 2013)

Based on these observations, the authors conclude that the current methods of computing rotational strength are adequate. The complexities involved in perfectly predicting the behavior of a connection are too great to be accounted for in design. They advocate for a balance between simplicity and accuracy.

Kanvinde et al. noted that a thicker base plate increased the capacity of the connection, while the base plate thickness is not even a variable in the current design methods. They recommend that for base plates thicker than 75 Mm (3 inches - the thickest base plate tested in literature), the available moment capacity be amplified by a factor based on the increased thickness. See equation (2.1.16).

$$M_{comp}^{modified} = M_{comp}^{method} \cdot (1.02 \cdot (t_{plate} - 75 \text{ mm})) \text{ for } t_{plate} > 75 \text{ mm} \quad (2.1.16)$$

where:

M_{comp}^{mod} = the modified rotational strength of an exposed base plate connection

M_{comp}^{method} = the rotational strength of a connection, calculated per current methods.

t_{plate} = thickness of base plate (mm)

The key conceptual finding from this study was that the stress distribution under the compression end of the base plate rarely resembles the rectangular stress block used in the AISC design guide 1. Stiffer base plates tend to concentrate the stresses near the toe of the plate, while thinner plates bend, and concentrate the stresses near the compression flange of the column, as per Figure 2-12.

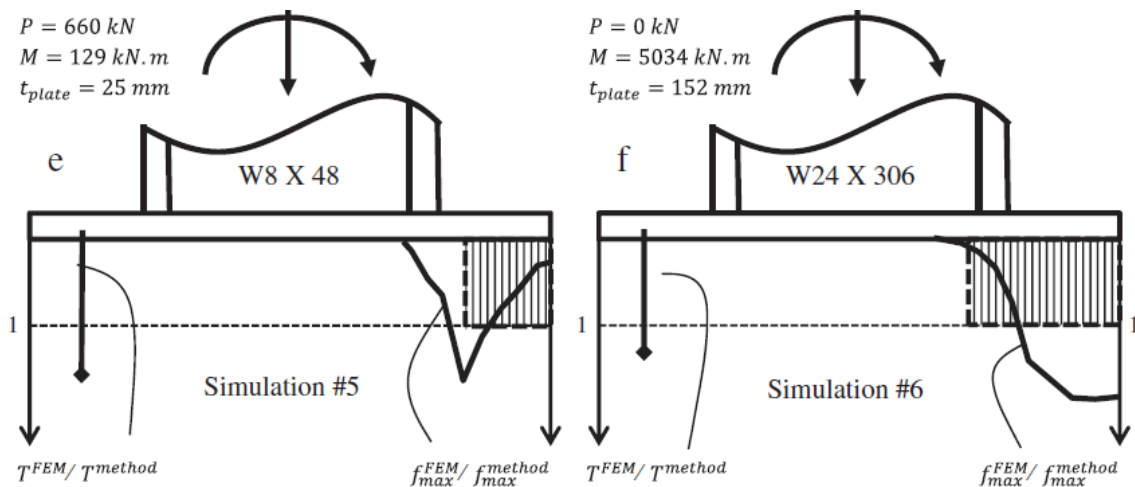


Figure 2-12: Comparison of Actual Stress Configuration Underneath a Base Plate for a Flexible Base Plate (Simulation #5) and a Stiff Base Plate (Simulation #6) (Kanvinde, Jordan et al. 2013)

Despite this difference between the model and actual behavior, the authors confirm that the AISC design guide still closely predicted forces in the anchor bolts, and was appropriate for use.

2.2 Embedded Base Plate Connections

2.2.1 Pertold, Xiao et al. (2000a)

The concept of an embedded column has long been used in an attempt to both strengthen the column base connection and hide and/or eliminate the base plate and anchor bolt assembly, providing a smooth aesthetically pleasing finish as per Figure 2-13. This type of base plate detail utilizes no anchor bolts, and uses wood wedges to temporarily hold the column in place until the concrete filling cures. Research into the behavior of these types of columns had until this point, focused on the rotational strength of such connections. The authors of this paper (Pertold, Xiao et al. 2000a) wanted to investigate the axial resistance of these types of connections.

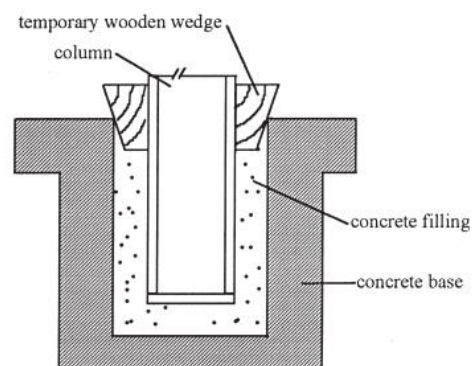


Figure 2-13: Example of an Embedded Column Base Connection (Pertold, Xia et al. 2000a)

They identified two main mechanisms providing axial resistance in an embedded column: first, the skin friction at the interface between the steel column and the surrounding concrete, and second, the bearing of the bottom of the column onto the concrete itself. The authors believed that due to the lack of understanding regarding these mechanisms, the embedment depths for embedded columns are often unnecessarily lengthened, leading to a conservative design. For example, at that time, engineers typically ignored the contribution of skin friction due to the lack of experimental data. There is an argument for cost savings, they argue, simply by understanding and quantifying the benefits of this connection.

Six total physical specimens were created to isolate and test the mechanisms listed above.

1. Three specimens were created to isolate the skin friction from the steel-concrete interface of the column. A steel column was embedded in an unreinforced concrete block, and a void was placed below the column itself, so the only axial resistance came from friction. The columns were then loaded axially to failure. See Figure 2-14(a) for this test setup.
2. Three specimens were created to isolate the concrete bearing mechanism. The sides of the steel column were greased in an attempt to negate any skin friction, so the only mechanism opposing axial load was bearing. The concrete below the column varied from 120 mm (2 specimens) to 220 mm (1 specimen). Again, these specimens were loaded axially to failure. See Figure 2-14(b) for this test setup.

The authors conclude that both mechanisms contribute significantly to the axial strength of the embedded connection. The tests indicated a high stiffness, and a failure load that was nearly as high as the nominal design strength of the column. The authors conclude that the bond

strength between the steel and concrete is very high. This bond strength, they admit, is conditional upon the load being medium to long term static loading, with very little lateral load or bending on the column. Also, the bond displayed essentially no residual strength after failure making it unsuitable for use in seismic applications.

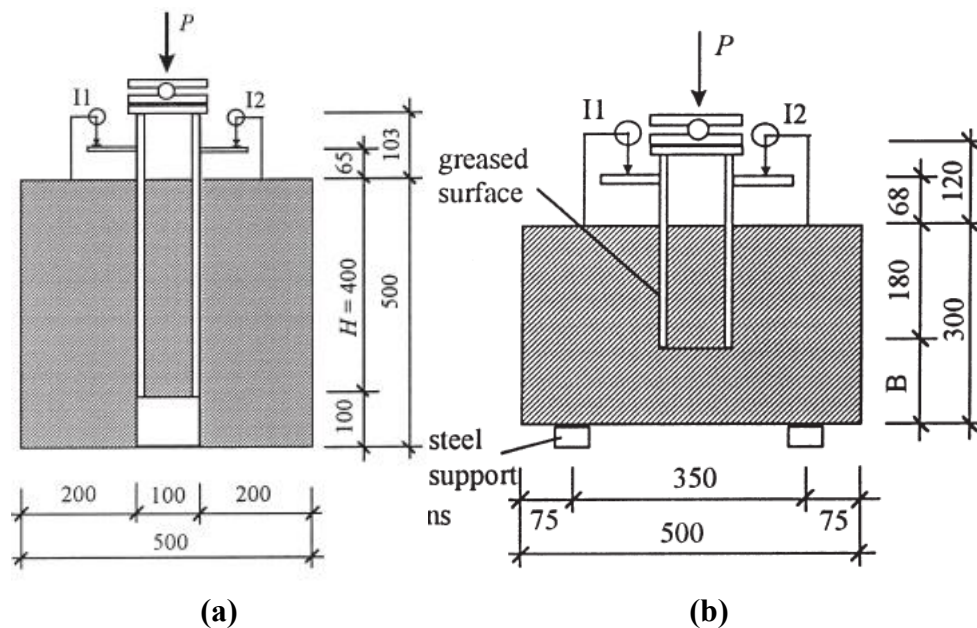


Figure 2-14: Test Setup to Isolate and Test (a) Steel-Concrete Bond/Skin Friction, and (b) Concrete Bearing/Punching Shear (Pertold, Xiao et al. 2000a)

The second set of tests indicated that in all cases, the failure mechanism was punching shear. The column punched out a truncated cone in the bottom of the concrete block. For the two depths tested, there was no concrete crushing observed at the column base. As expected, there was little warning of imminent failure, and the punching failure was brittle, happening suddenly.

Overall, these experiments show that a significant amount of vertical load can be transferred from the column to the concrete base using both the bearing and the bond strength. They even note that for common base geometries, the contribution of the steel/concrete bond can outweigh that of the bearing mechanism. A numerical model for predicting the capacity will be outlined in the next section.

2.2.2 Pertold, Xiao et al. (2000b)

While the previous paper described and summarized the physical tests that were performed, the authors (Pertold, Xiao et al. 2000b) continued their work in this paper, consolidating the knowledge gained in those experiments into a design model that can be used in the design of embedded columns. The design is based on the model shown in Figure 2-15.

Two critical dimensions in design of these types of connection are the effective flange width, b_{eff} , and the embedment depth of the column, H (Note that the top 50 mm of the embedment is ignored when determining H). The effective width can be calculated from equation (2.2.1). The following guide is limited by the relationship between the embedment depth of the column and the effective flange width, as shown in equation (2.2.2).

$$b_{eff} = \min \left\{ \begin{array}{l} b_c + 0.5h_c \\ 2b_c - t_{wc} \end{array} \right\} \quad (2.2.1)$$

$$b_{eff} \leq H \leq 2b_{eff} \quad (2.2.2)$$

where:

t_{fc} = thickness of the column flange

t_{wc} = thickness of the column web

h_c = depth of the column section

b_c = width of the column section

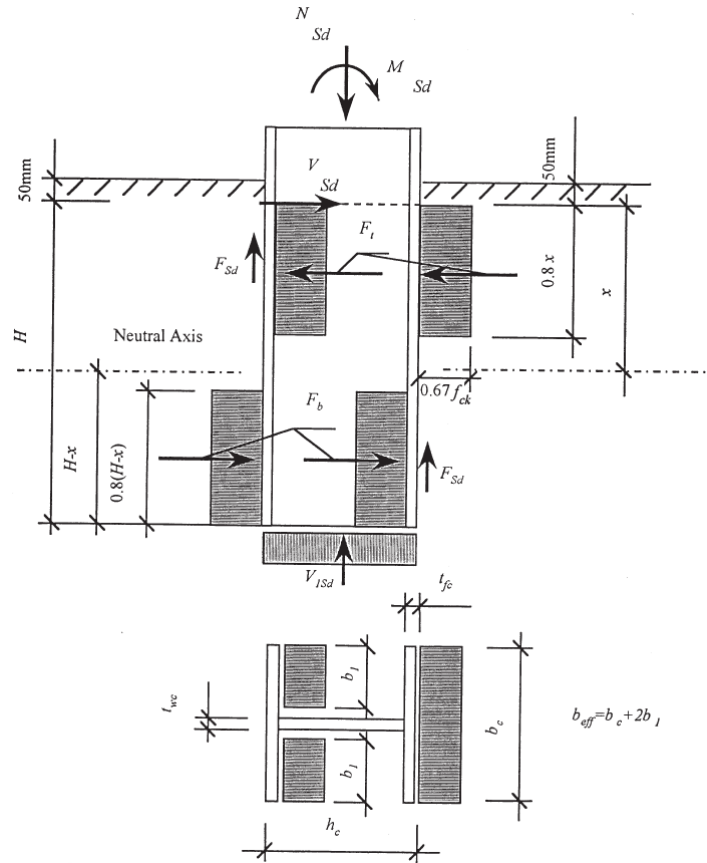


Figure 2-15: Model of Stress Distribution for an Embedded Column (Pertold, Xiao et al. 2000b)

The required column embedment depth for a set of given loading conditions is summarized in equation (2.2.3).

$$H = \frac{1.56V_{sd} + \sqrt{4.74 \cdot V_{sd}^2 + 6.22 \cdot M_{sd} f_{ck} b_{eff}}}{b_{eff} f_{cd}} \quad (2.2.3)$$

where:

H = required embedment depth to develop the bending capacity of the column

V_{sd} = applied shear load

M_{sd} = applied moment load

f_{ck} = 28-day concrete compressive strength (similar to f_c') of embedment concrete

f_{cd} = 28-day concrete compressive strength (similar to f_c') of base concrete

b_{eff} = effective flange width, see equation (2.2.1).

The authors also give design models for the shear and axial resistance of embedded columns based on their embedment length, but those models will not be summarized here.

The proposed model for determining the required embedment depth was compared with the results from the authors' empirical results, (Pertold, Xiao et al. 2000a). The authors state that the actual embedment length required versus the calculated length required is in "good agreement". This comparison can be seen in Figure 2-16.

Based on these results, the authors conclude that the proposed model is appropriate for use for columns similar to those tested. The model is considered comprehensive and can be applied to embedded column bases subject to bending moments, shear, and axial forces.

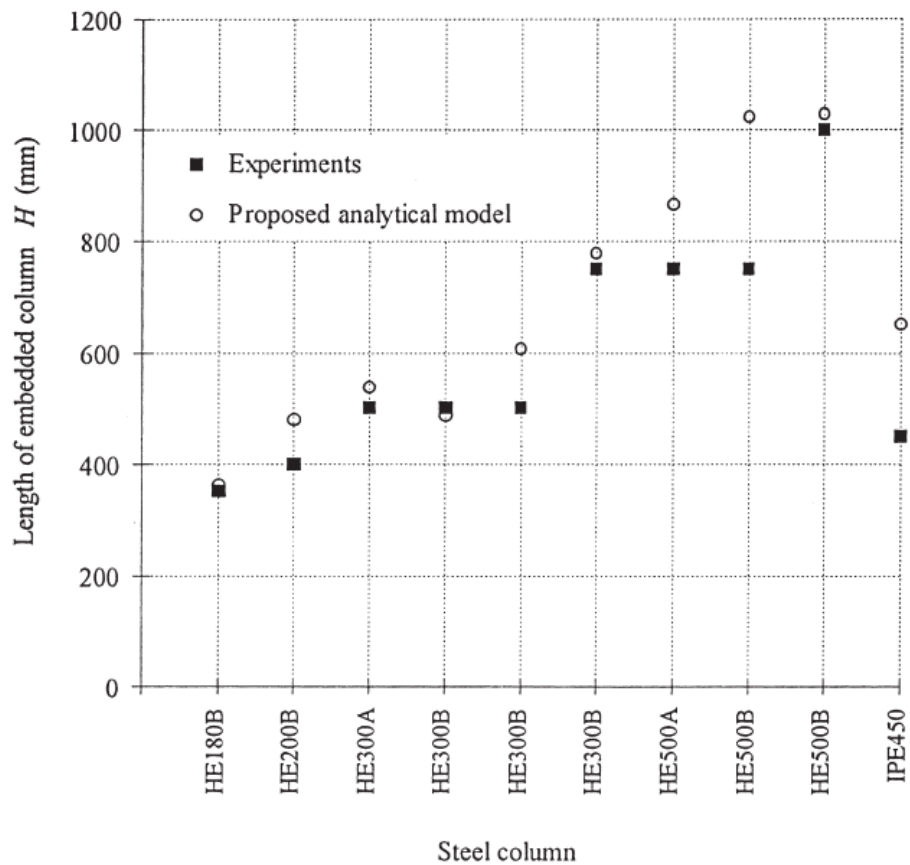


Figure 2-16: Comparison of Experimental Values vs. Predicted from the Proposed Model Under Bending Loads (Pertold, Xiao et al. 2000b)

2.2.3 Grilli and Kanvinde (2015)

The previous papers discussed offered understanding and a design guide for embedded columns under static loads. More recently, these authors (Grilli and Kanvinde 2015) wanted to study the performance of embedded column base connections under seismic loads. See Figure 2-17 for an illustration of the connection used in this study. They sought to add knowledge of embedded column base connections and further understand their 1) load resistance and failure mechanisms, 2) strength, 3) rotational stiffness, and 4) deformation capacity and energy dissipation characteristics.

Five total physical specimens were created and tested under a variety of loading conditions. They also tested a connection detail that was more representative of current practice and design. Mainly, they included a base plate at the bottom of the column (included for uplift resistance), and stiffener plates at the top of the embedment (included for compression resistance). Three main variables were tested:

1. Embedment depth of the columns (defined as the distance between the top of the base plate to the top of the embedment concrete): 20 inches & 30 inches.
2. Column flange width (note that the columns chosen are especially stiff and heavy, in an effort to minimize bending in the column and force a failure in the base connection): W14x370 (16.5 inch flange width), and W18x311 (12.0 inch flange width).
3. Axial Load on the column: 100 k (compression), 0 kip, -150 kip (tension).

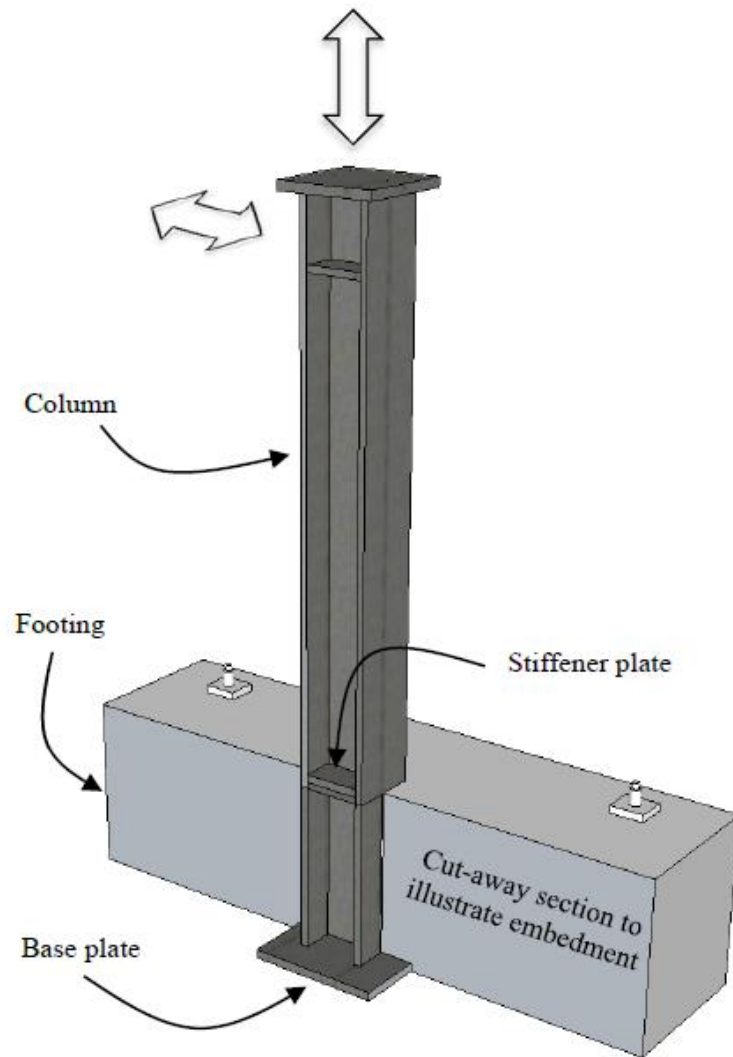


Figure 2-17: Illustration of Embedded Column Base Connection, Subjected to Axial and Lateral Loads (Grilli and Kanvinde 2015)

The test matrix and test results are summarized below in Table 2-2.

Table 2-2: Test Matrix and Results (Grilli and Kanvinde 2015)

Test #	Column Size, (b_f [mm])	P [kN]	d_{embed} [mm]	Base Plate, $t_p \times N \times B$ [mm]	Z [m]	M_{base}^{max} [kN-m]	β_{base}^{test*} [10^5 kN-m/rad]	$\frac{\Delta_{test}}{\Delta_{fixed}}$ ***	$\frac{M_{base}^y}{M_{base}^{max}}$	Λ_{max} (%)
1	W14x370 (419)	445 (C)	508	$51 \times 762 \times 762$	2.84	2579(+)	3.23	1.21	0.87	3.85
				2613(-)		0.69			3.82	
2	W18x311 (305)			$51 \times 864 \times 711$	2.84	2324(+)	3.84	1.16	0.709	3.01
				2168(-)		0.66			2.89	
3	W14x370 (419)	0	762	$51 \times 762 \times 762$	3.10	3741(+)	3.07	1.30	0.72	6.97
		3444(-)				0.67			7.77	
4		445 (C)				4124 (+)	3.38	1.30	0.66	6.48
						3612(-)			0.81	5.09
5		667 (T)				3800 (+)	3.25	1.29	0.73	2.72**
						3464(-)			0.72	2.65**
							Mean	1.25	0.72	4.98
							CoV	0.05	0.07	0.38

* Average stiffness of both directions

** Test terminated due to slip prior to failure (Mean, COV does not include these data points)

*** Notional columns used for Tests #1-5 are W14X145, W14X132, W14X193, W14X211, and W14X193 respectively.

The authors arrived at the following conclusions based on the results of their tests:

1. An embedded column base connection does have greater strength and stiffness when compared to a comparable exposed base connection.
2. Increasing the embedment depth increases the strength of the connection.

3. Increasing the column flange width increases the strength of the connection.
4. Application of compressive axial load on the column increased the strength significantly when compared to the specimen with no axial load.
5. Application of tensile axial load had little effect on the strength when compared with no axial load.
6. As the specimens were tested laterally, cracks were formed in the concrete which grew with each successive load. This caused both the strength and the stiffness to decrease incrementally until failure.

A design model is proposed by the authors that could be used as a design guide for future connections, but that design model is not summarized here.

2.3 Composite Moment Connections

2.3.1 Marcakis and Mitchell (1980)

As far back as 1980 (Marcakis and Mitchell 1980), the concept of a composite connection (a member connection involving two different materials) was investigated. The authors of this paper sought to investigate the connection of steel beam connected into a precast concrete member. This type of connection is very similar to an embedded steel column base, whereas the embedded steel section is subject to a lateral load that causes a moment in the connection. Refer to Figure 2-18 for typical composite connections.

As an exploratory study into this type of connection, the authors devised experiments that would test a wide range of possible variables affecting their behavior. Their objectives involved understanding the performance given the following variables:

1. Axial load on the column/wall. (The axial stress in the concrete surrounding the embedded steel member)
2. Amount of concrete cover.
3. Addition of supplemental reinforcement welded to the embedded steel member.
4. Geometry/shape of the embedded steel member.
5. Amount and type of loading on the embedded steel member.

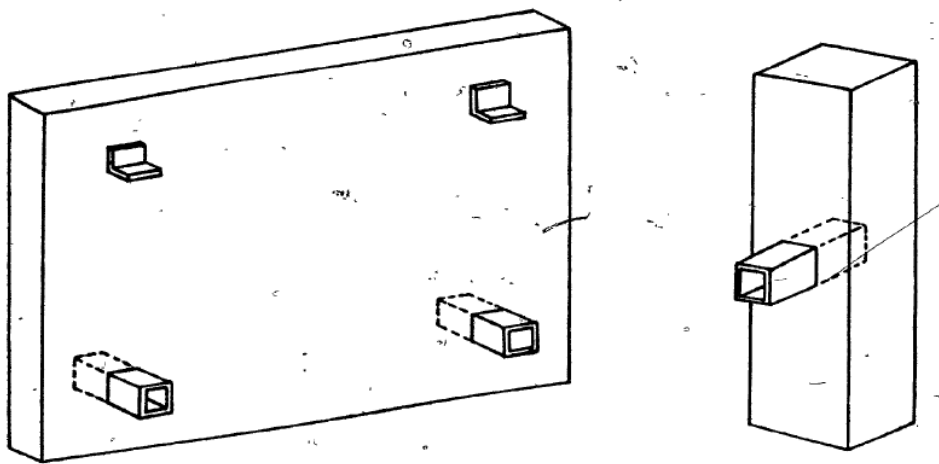


Figure 2-18: Typical Wall Panel and Beam-to-Column Composite Connections (Marcakis and Mitchell 1980)

The authors tested a total of 21 specimens, divided up into 3 main test series.

1. Series 1

- a. Four total specimens. All four specimens included an HSS 4x4x1/4 beam embedded into a concrete column. Embedment depth kept constant at 6 inches. Axial load on the concrete column varied from 1 kip to 90 kip. Steel beam was loaded vertically to failure. Refer to Figure 2-19.

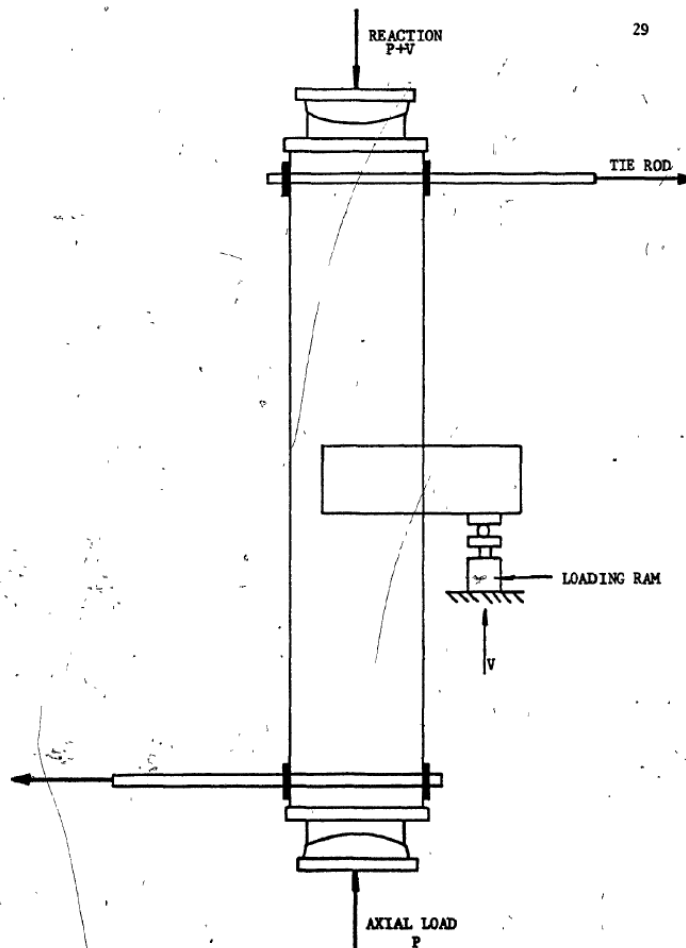


Figure 2-19: Test Setup for Test Series #1 (Marcakis and Mitchell 1980)

2. Series 2

- a. Thirteen total specimens.
- b. Five specimens – HSS 6x4x3/8 beams with constant embedment depth of 7 inches. Axial load on the concrete column varied from 0 kip to 240 kips.
- c. One specimen – similar to first five of the series, with the exception that a W6x25 shape was used. The flanges of the wide flange member were trimmed to match the width of the HSS 6x4 member.
- d. Two specimens – similar to first five of the series, with the addition of supplemental reinforcement welded to the HSS member.
- e. Three specimens – similar to first five of the series, but with varying amounts of concrete cover surrounding the HSS member.
- f. Three specimens – similar to the first five of the series, with the exception that rather than a 7 inch embedment depth, the HSS member passes completely through the concrete column. Refer to Figure 2-20.

3. Series 3

- a. Four total specimens
- b. One specimen – includes a solid 4 inch x 4 inch steel member embedded into a concrete column. This column was built especially wide to isolate the steel member from the normal reinforcement in the column. The idea was to create a favorable condition for the spreading of the load into the concrete column.

- c. One specimen. Similar to the first test in the series, with the exception that styrofoam blocks were placed adjacent to the steel member while pouring the concrete so as to create a void and isolate the forces directly above and below the steel member.

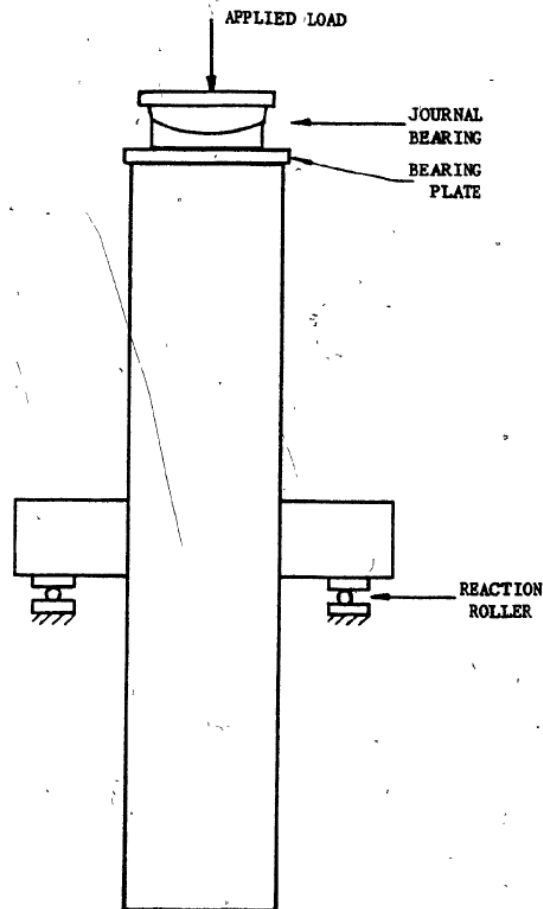


**Figure 2-20: Setup for Test Series #2
(Marcakis and Mitchell 1980)**

- d. One specimen. Similar to the second test in the series, with the exception that the steel member passes completely through the column, and is tested in pure moment. Refer to Figure 2-21.
- e. One specimen. Similar to the third test in the series with the exception that that steel member used was an HSS 6x4x3/8.

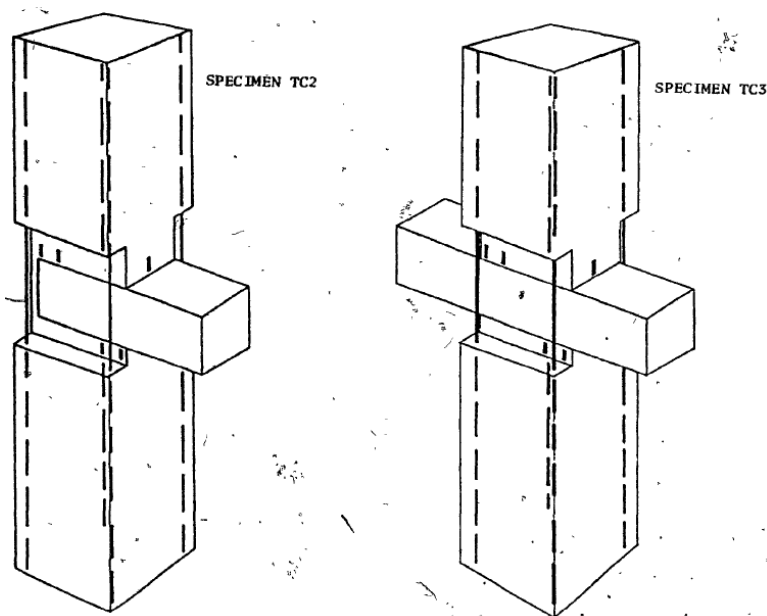


Figure 2-21: Specimens Isolating the Stress Directly Above and Below the Embedded Steel Member (Marcakis and Mitchell 1980)

The conclusions that the authors made from the test results are as follows:

1. Effective width of the connection: The effective width of the connection can be taken as the smaller of 1) the width of the confining concrete core measured to the outside of the column ties, or 2) twice the width of the embedded structural steel member.
2. Effect of the shape of the embedded steel member: The wide flange shape was able to develop greater capacity when compared with a similarly-sized HSS member. This is due, presumably, to the larger compression surface area.
3. The addition of supplemental reinforcement welded to the top & bottom of the steel shape dramatically increased the strength of the connection. The reinforcement helped mitigate the negative effects of the concrete around the connection cracking under stress.
4. The axial load on the column (and thus the stress in the concrete at the connection) played a large role in the performance of the connection. The authors noticed that as the axial load increased, there was a decrease in the ductility of the connection. The strength of the member also increased as the load on the column increased, up to 50% of the column capacity. As axial loads increased above 50% of the column capacity, the strength actually decreased. As long as the axial stress in the column was less than 70% of the column capacity, then the connection strength was greater than when there was zero stress in the column concrete.

The authors developed a reliable design model that can be used for the design of similar connections. Because the configuration of the connections tested here are different from the

shallowly embedded column bases treated in this paper, the equations for the strength model will not be summarized here.

2.3.2 Sheikh, Deierlein et al. (1989)

These authors (Sheikh, Deierlein et al. 1989) took the research of Marcakis and Mitchell a step further in 1989 and researched specific composite connections. They recognized that in taller buildings, from 40-70 stories, the cost of the building's columns became more expensive compared to the other structural elements. Thus it became advantageous to optimize the column design. Steel is more economical (due to construction costs) for the girders, beams, and flooring systems. For the columns, concrete becomes a much more economical option. Thus, a structural system that utilizes concrete columns and steel beams is desirable.

The connection and interaction of these two systems is the focus of this research. Previously, designers relied on very simple shear connections mostly because of the lack of research on how these two systems interacted. The authors postulate that a composite connection of this type can utilize much more of the available strength from the connection.

Fifteen total test specimens were created at 2/3 scale. Refer to Figure 2-22 for a typical test specimen. Seven of these were tested under a steadily increasing (static) load, while eight were tested with reverse cyclic loading. The column consisted of reinforced concrete, 20 inch x 20 inch square. The beams were a built-up W18 section (ASTM A36 steel), and were continuous through the column. The beam size was chosen so that the flexural strength of the beam was stronger than the anticipated capacity of the connection. This was done to isolate the connection and attempt to make it fail before a plastic hinge was formed in the beam. The column

reinforcement ties were present in the depth of the beam. Holes were drilled in the webs of the beams to facilitate this reinforcement. See Figure 2-23 for the reinforcing steel details.

A variety of different details were tested as shown in Figure 2-24. All of these details attempted to develop composite action between the two materials.

The results from these tests show that composite connections of this nature are reliable and provide adequate stiffness under service loads and ductile failure at ultimate loads. Under cyclic loading these connections exhibit toughness comparable to reinforced concrete connections designed for seismic loading. The summary of these test results can be found in Table 2-3.

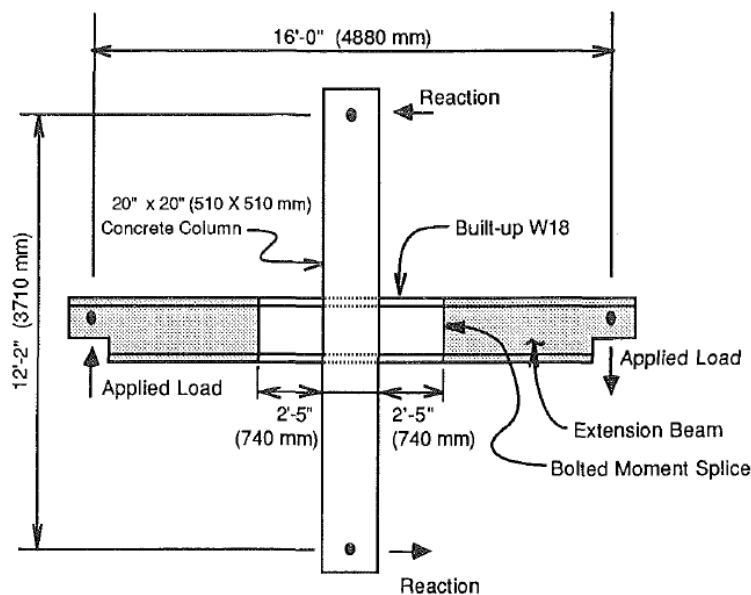


Figure 2-22: Typical Composite Test Specimen
(Sheikh, Deierlein et al. 1989)

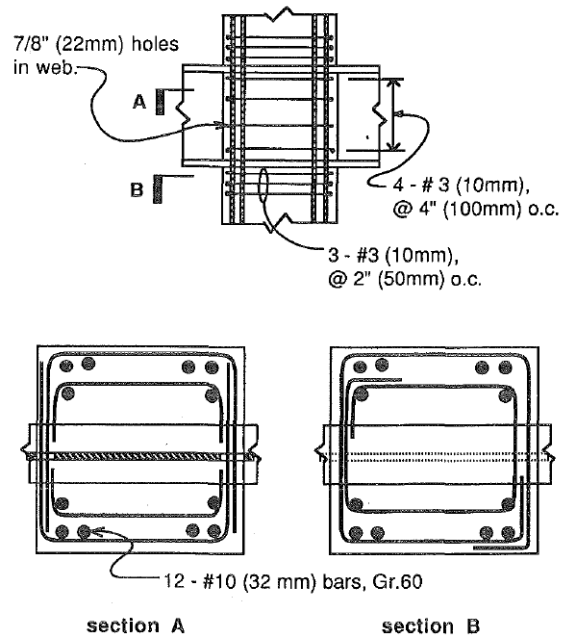


Figure 2-23: Reinforcing Steel Details
(Sheikh, Deierlein et al. 1989)

One of the more important findings from these tests were the effects that different details had on the strength of the connection. Any detail that mobilized the concrete in compression added significantly to the connection strength. Specimen #3 was a plain beam, and served as a benchmark for all the other tests. It relied on nothing more than friction and bond between the concrete and steel to develop composite action. Specimens #4, 5, 7, 9, & 10 show the effect of including a face bearing plate that creates a concrete “compression strut” inside the flanges of the beam. Adding this simple detail increased the strength by 61-76%, when compared with the plain beam from specimen #3. These tests also showed that the thickness of the plate used did not have a significant effect on the strength, and that the additional strength is derived from the concrete compression strut. A larger stiffness plate (engaging a larger concrete compression strut) did add strength to the connection.

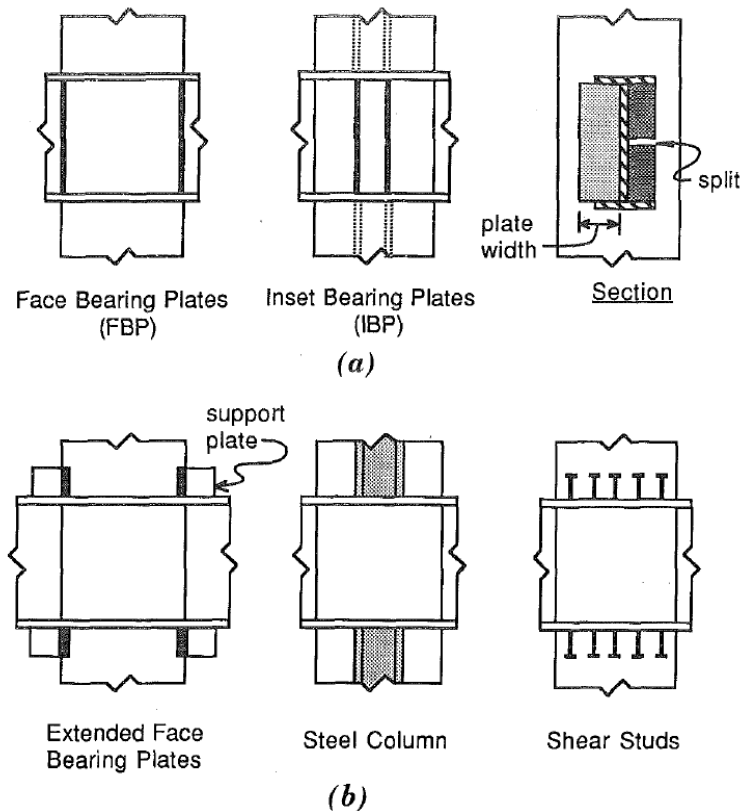


Figure 2-24: (a) Bearing (Stiffener) Plate Details; (b) Extended FHP, Steel Column, and Shear Stud Details (Sheikh, Deierlein et al. 1989)

Specimens 8 and 12-17 showed the effect of engaging the concrete in compression outside the column flanges. Specimen 8 included face bearing plates that caused a compression field both within the beam depth and outside it. Adding this simple detail allowed the connection to carry a load 180% greater than that of the plain beam from specimen 3. Specimens 12 & 13 created composite action via welded studs on the flanges of the beam, and alone carried 174% of the load of the plain beam. Specimens 14-17 all had steel columns attached to the beam, and the authors suggest that the addition of the steel column allowed the connection to carry 153% of the load of the plain beam.

Table 2-3: Summary of Test Results (Sheikh, Deierlein et al. 1989)

Specimen number (1)	Joint detail (2)	f'_c (ksi) (3)	Strength (kips) (4)	Comparison ratio (5)	Mode of failure (6)
3	Plain beam	4.5	16.5	1.00	Panel shear
4	FBP (0.375 × 8 × 16 in., A 36)	4.3	26.6	1.61	Panel shear
5	Thick FBP (0.875 × 8 × 16 in., Gr. 50)	4.3	28.2	1.71	Panel shear
6	FBP (0.375 × 8 × 16 in., A36) with styrofoam backing; Two web doubler plates (0.5 in. thick, Gr. 50)	4.0	35.8	2.17	Vertical bearing
7	Wide FBP (0.875 × 12 × 16 in., Gr. 50)	4.0	33.8	2.05	Panel shear
8	Extended FBP [0.875 × 8 × 25.5 in. (4 in. extension), Gr. 50]	3.6	46.2	2.80	Panel shear
9	FBP (0.875 × 8 × 16 in., Gr. 50); Cut-out steel-web inside joint	3.7	26.2	1.59	Panel shear
10	Split FBP (2.375 × 8 × 7.5 in., A36)	4.7	29.0	1.76	Panel shear
11	FBP (0.375 × 8 × 16 in., A36); Two web doubler plates (0.125-in. thick, A36); Dywidag bars (8-#8-3 ft., Gr. 60)	4.7	47.0	2.85	Panel shear
12	Shear studs (15-0.5 in. ϕ × 4 in., each flange)	5.0	28.7	1.74	Panel shear
13	Shear studs (15-0.5 in. ϕ × 4 in., each flange); FBP (0.375 × 8 × 16 in., A36)	5.0	42.8	2.59	Panel shear
14	Steel column (W5 × 18.5, Gr. 50); IBP (0.375 × 8 × 16 in., A36)	4.0	33.8	2.05	Panel shear
15	Steel column (W5 × 18.5, Gr. 50); FBP (0.375 × 8 × 16 in., A36)	4.0	37.0	2.24	Panel shear
16	Steel column (W5 × 18.5, Gr. 50); FBP (0.375 × 8 × 16 in., A36); clip angles (L4 × 4 × 0.375 in., A36)	3.8	37.3	2.26	Panel shear and angle yielding
17	Steel column (W5 × 18.5, Gr. 50); FBP (0.375 × 8 × 16 in., A36); Dywidag bars (8-#8-3 ft., Gr. 60)	3.9	36.8	2.23	Panel shear

Note: 1 in. = 25.4 mm; 1 ksi = 6.89 MPa; 1 kip = 4.45 kN.

Specimen 11 was designed to evaluate the effect of vertical reinforcement (“Dywidag” reinforcing bars). These vertical bars were welded to the column flanges, and reinforced the concrete both in compression and in tension. Coupled with web doubler plates, this detail carried a load 285% great than the plain beam.

A composite connection of this type is therefore a reliable method of connecting steel and concrete members. The strength of the connection is significantly improved by engaging the concrete in compression. This is accomplished with the addition of details that form either a compression strut inside the steel beam depth or a compression field outside the beam depth.

2.3.3 Deierlein, Sheikh et al. (1989)

As a companion to the previous paper, these authors (Deierlein, Sheikh et al. 1989) attempted to create a reliable model to design composite connections. They proposed a model that predicts the nominal strength of the connection. The strength is governed by the “shear panel strength”, and is highly dependent on the joint detail provided (as shown in the previous paper). The panel shear is carried by three mechanisms, as shown in Figure 2-25.

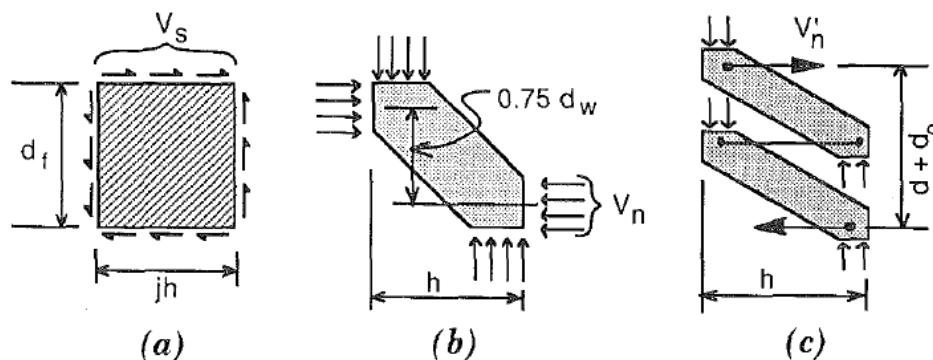


Figure 2-25: Contributions to the Panel Shear (a) Steel Web Panel; (b) Concrete Compression Strut; (c) Concrete Compression Field (Deierlein, Sheikh et al. 1989)

The steel web panel is similar to that found in a normal structural steel connection and is mobilized regardless of the exact detailing options used. The shear panel strength is calculated using equation (2.3.1).

$$V_s = 0.6F_{yw}t_wjh \quad (2.3.1)$$

Where:

V_s = Panel Shear strength

$0.6F_{yw}$ = shear yield stress of the web steel

t_w = web thickness

jh = length of the panel. This depends on the location of the vertical force couple, not the width of the concrete column. Finding this distance is not discussed here.

The concrete compression strut is engaged by the inclusion of face bearing plates inside the depth of the beam to bear against the concrete as the joint and the steel panels deform. This strut is similar to that used in the design of reinforced concrete joints. Its strength can be calculated from equation (2.3.2).

$$V_n = 0.63\sqrt{f'_c} \cdot b_p h \quad (2.3.2)$$

Where:

V_n = Horizontal force resisted by the concrete compression strut

f'_c = concrete 28-day compressive strength

b_p = bearing plate width (limited to 1.5 times the beam flange width, b_f).

h = column width

The concrete compression field is mobilized by details outside the beam depth that engage the concrete outside the beam in compression (shear studs, face bearing plates, vertical reinforcement attached to the flange, or steel columns). The strength can be determined from equation (2.3.3).

$$V_n^* = 0.63\sqrt{f_c^*} \cdot b_o h \leq V_c^* + V_s^* \quad (2.3.3)$$

Where:

V_n^* = Horizontal force resisted by the concrete compression field

b_o = effective compression field width

V_c^* & V_s^* = concrete and reinforcement components required to carry the shear V_n^*

After creating this model, the authors compared results they got with the empirical results summarized in the previous paper. These results are summarized Table 2-4. In all cases, the model under predicted the actual strength of the connection. The ratio of the model-predicted strength versus the tested strength ranged from 0.65 – 0.96, showing that the proposed model is a conservative method of predicting strength.

Table 2-4: Summary of Test Results (Deierlein, Sheikh et al. 1989)

Specimen number (1)	Description (2)	Nominal Strength (kips)			Notes (6)
		Measured (3)	Calculated (4)	Ratio (5)	
1	Plain beam	17.0	14.0	0.83	No FBP
2	FBP	22.5	15.6	0.69	Bearing failure
3	Plain beam	16.5	10.8	0.65	No FBP
4	FBP	26.6	24.2	0.91	—
5	FBP (extra thick)	28.2	24.2	0.86	—
6	FBP, web doubler plates	35.8	30.4	0.85	Bearing failure
7	Wide FBP	33.8	31.2	0.92	—
8	Extended FBP	46.2	44.3	0.96	—
10	FBP (split)	29.0	25.2	0.87	—
11	FBP, web doubler plates, Dywidag bars	47.0	44.8	0.95	—
15	FBP, steel column	37.0	34.1	0.92	—
16	FBP, steel column, clip angles	37.3	34.7	0.93	—
17	FBP, steel column, Dywidag bars	36.9	35.6	0.96	—

2.3.4 Shahrooz, Remmetter et al. (1993)

Further research went into composite connections (Shahrooz, Remmetter et al. 1993), and the authors of this paper focused their studies on composite coupled walls under seismic loads. This occurs when concrete shear walls are connected in plane by a steel beam, which could be a lintel over a window or doorway. As the shear walls are deformed under lateral seismic loads, the steel beam is loaded cyclically and transfers large shear and moment loads into the shear wall. This situation is very similar to the tests performed by Sheikh and Deierlein, except that rather than having the steel beam connecting into a concrete column, the beam is connected into the plane of a concrete shear wall. Refer to Figure 2-26 for simple illustration of this.

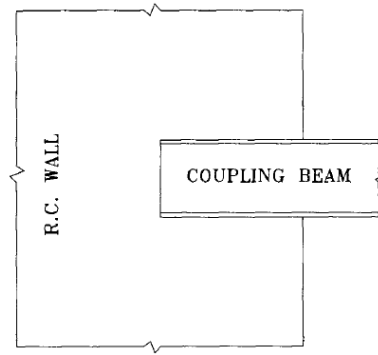


Figure 2-26: Example of a Coupling Seated in the Plane of a Concrete (Shahrooz, Remmetter et al. 1993)

The motivation for this research is two-fold: under various loading conditions and reinforcing details, what is the 1) strength, and the 2) stiffness of the connection. Both of these values are important in the design of seismic connections.

They designed three total specimens at 1/2 scale and tested them to failure. All specimens consisted of a reinforced concrete wall and a short embedded coupling beam. See Figure 2-27 for a sketch of the test design. The wall was loaded with a vertical static axial load, and the coupling beam was loaded with a cyclic vertical load. The cyclic load was the same for all three specimens, and the static load acting on the wall was placed at different locations on the wall to simulate different levels of stresses around the embedment length. The designs of the three specimens were identical, except the 3rd, which included supplemental reinforcing bars welded to the top and bottom flange of the coupling beam just inside the face of the wall.

connection became. Under cyclic loading, cracks tended to develop in the concrete, reducing the stiffness as time progressed. The addition of supplemental reinforcement (in specimen #3) around the coupling beam increased the stiffness and reduced the influence of cracks.

The authors proposed a stiffness model to use in design. They suggested that the connection could be effectively “fixed”, but at a point inside the wall rather than at the face, as shown in Figure 2-28. This distance (e) was determined to be approximately $1/3$ of the embedment length from the face of the wall.

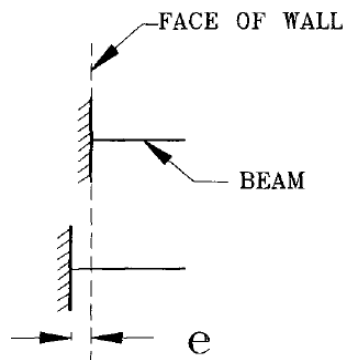


Figure 2-28: Model for Simulating Beam Effective Fixed Point (Shahrooz, Remmetter et al. 1993)

2.3.5 Motter (2014)

This author (Motter 2014) continued research into this type of composite connection, but built full-scale models for testing. Motter summarized the importance of this connection in

seismic design by stating that “the coupling beams act as fuses to limit the lateral force demands on a building and dissipate earthquake energy. Favorable performance of coupling beams is characterized by large inelastic deformation capacity... in addition to predictable strength and stiffness.” His purpose was to validate previous research with large-scale models.

A total of four physical specimens were created. Figure 2-29 shows the specimen assembly for the first two tests. As shown, two simultaneous tests were built into either side of the reinforced concrete wall. The second two tests were similarly designed. Figure 2-30 shows the various variables that were accounted for in the tests, and Table 2-5 gives the test matrix used.

The results of the tests echoed those previously done: that the composite connection is adequate at transferring large loads between the different elements.

Regarding the required embedment length required to develop the strength of the coupling beam encased in the concrete wall, the authors recommend using equation H4-2 found in the 2010 AISC Seismic Provisions (not given here).

The authors came to the following conclusions based on the results of these tests:

1. The nominal plastic flexural strength of the coupling beam is based both on the expected yield stress of the steel beam and the concrete modeled in compression using the uniform magnitude (Whitney) stress block. Due to the lack of fixity at the face of the wall, the nominal flexural strength is computed based on a point inside the wall, $1/3$ the distance of the embedment.

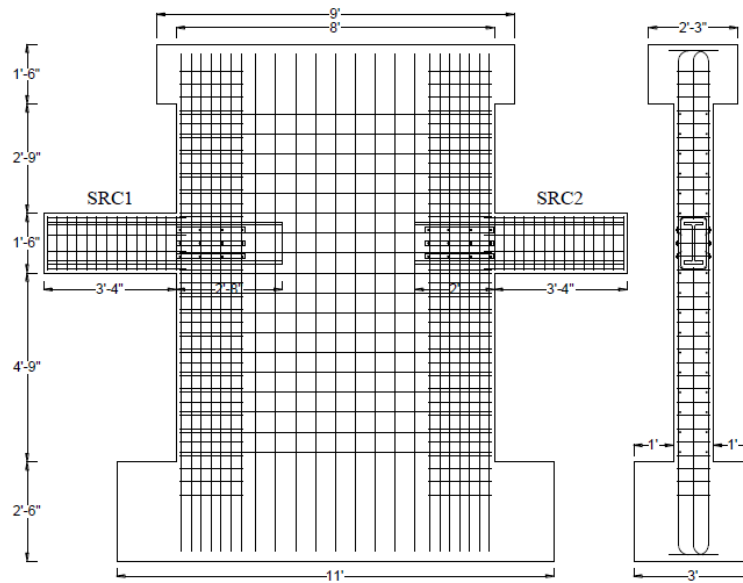


Figure 2-29: View of Complete Test Assembly (Motter 2014)

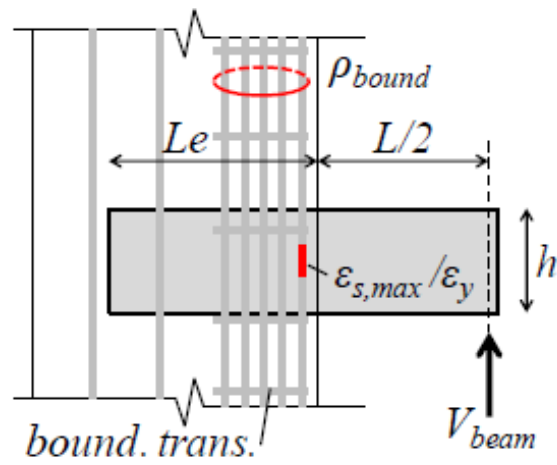


Figure 2-30: Test Variables (Motter 2014)

Table 2-5: Test Matrix (Motter 2014)

	$\alpha = L/h$	L_e (in.)	ρ_{bound}	bound trans.	f'_c (ksi)	$\varepsilon_{s,max}/\varepsilon_y$
SRC1	3.33	32	0.024	OBE	7.4	0.53
SRC2	3.33	24	0.033	OBE	7.4	0.83
SRC3	2.40	26	0.017	OBE	5.0	1.09
SRC4	3.33	24	0.006	Other	4.6	0.57

2. For design of the embedment length, they recommend the use of the embedment equation found in the 2010 AISC Seismic Provisions.
3. They recommend designing the coupling beam span as a rigid body with rotational springs at the beam-wall interfaces. A spring stiffness of $M_{pe} / \theta_y = 1.33\%$ (where θ_y is the chord rotation at yield), or $75 \cdot M_{pe} / \text{radian}$ is appropriate for use.
4. The 2010 AISC Seismic Provisions require the use of auxiliary reinforcement welded to the beam flanges and the use of bearing plates at the face of the wall. The authors conclude that given sufficient embedment length these requirements are unnecessary.

2.4 Steel Pile-to-Pile-Cap Connections

2.4.1 Xiao, Wu et al. (2006)

Another situation that has received attention from researchers recently is that of a steel pile-to-concrete-pile cap connection (Xiao, Wu et al. 2006). The configuration is very similar to that of a shallow-embedded steel column: A steel member (usually an HP section, or a round pipe) is embedded a short distance into reinforced concrete and subjected to axial loads and some

lateral moment-inducing loads. In some cases, reinforcing bars are attached to the steel section and embedded into the concrete in an attempt to tie the two members together and encourage composite action. Refer to Figure 2-31 for the pile-to-pile cap connection studied.

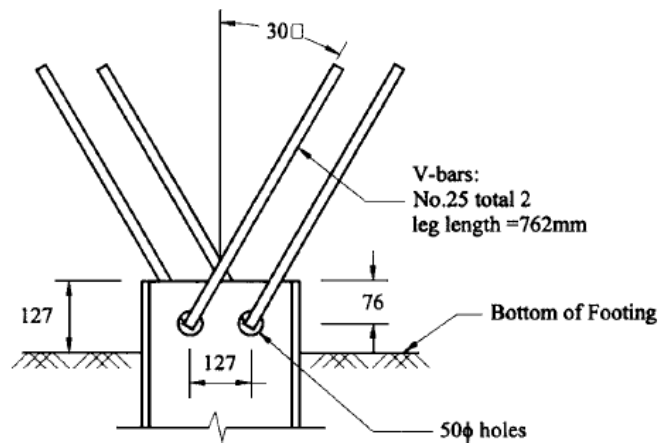


Figure 2-31: Typical Steel Pile-to-Concrete-Pile Cap Connection (Xiao, Wu et al. 2006)

Table 2-6: Test Matrix (Xiao, Wu et al. 2006)

Model specimens	Orientation of HP pile	Loading condition	Concrete strength f'_c (MPa)	Axial load (kN)
HP-S-V	Strong direction	Cyclic vertical loading only	41.1	Varies
HP-W-V	Weak direction	Cyclic vertical loading only	37.9	Varies
HP-S-L	Strong direction	Cyclic lateral loading with constant vertical load	41.1	1,779
HP-W-L	Weak direction	Cyclic lateral loading with constant vertical load	41.1	1,779
HP-S-VL	Strong direction	Proportionally varied cyclic lateral and vertical loading	37.9	Varies ^a

^aInitial axial load was 890 kN.

Typically, this connection, like the shallowly embedded concrete column, is conservatively designed as a “pinned” connection. Any benefits to the rotational strength of the connection offered by the surrounding concrete or the embedded reinforcing bars is ignored. In an attempt to quantify the contributions of these mechanisms, Xiao built and tested a total of five specimens that represented a typical California bridge pile cap and subjected them to various loading conditions.

The test specimens were built and tested upside down, so the footing rested against the floor and the steel pile extended up out of the footing. The steel pile used was an HP 14x89, and this was embedded 5 inches into a 4 foot cubic block of reinforced concrete. The main variables tested were the configuration of the pile (bending in strong-axis or weak-axis) and the loading condition of the pile. Refer to Table 2-6 for the test matrix used. Figure 2-32 shows the typical test setup.

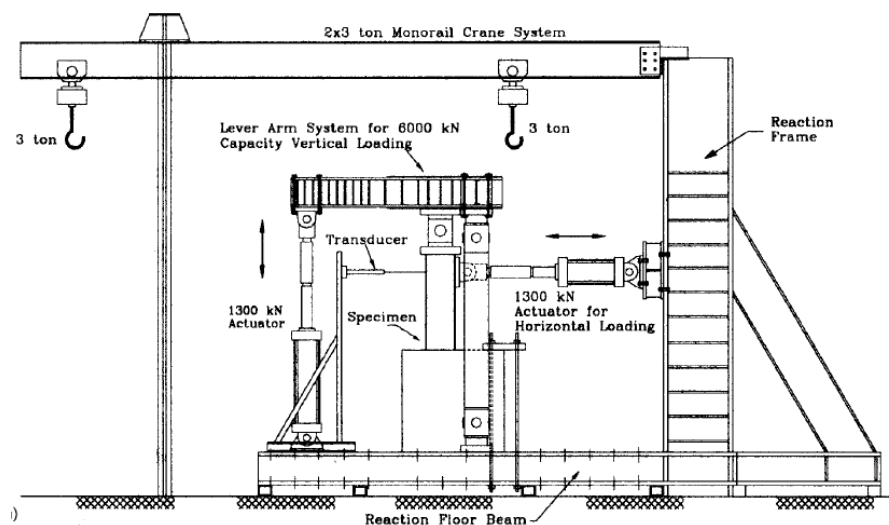


Figure 2-32: Typical Test Setup (Xiao, Wu et al. 2006)

The results from these tests lead the authors to make conclusions similar to those from the composite connection tests: namely that a connection of this type, embedded even a very short distance, develops significant moment capacity. Specifically, the authors listed the following conclusions:

1. The current connection detail shown cannot develop the full tensile capacity of the steel HP pile. The author attributes this partly to the assumption that only one of the steel reinforcing bars is engaged at a time. In determining the tensile capacity of a connection like this, the author recommends using the yield capacity of only one of the v-shaped reinforcing bars. The author recommends considering welding the anchorage bars to the pile web to ensure contribution from both bars, though he admits this was not specifically tested for this project.
2. Although typically designed as a “pinned” connection, this configuration can transfer a substantial moment. Equation for estimating the flexural strength are given in the paper. (Note that these design equations are modifications of the equations first proposed by (Marcakis and Mitchell 1980))
3. The moment is transferred from the HP pile to the pile cap via two mechanisms: flexural resisting mechanism (tension in the reinforcing bar, compression of the concrete at the other end), and an embedment mechanism (compression of the concrete on the sides of the steel HP pile).
4. Often, concrete blocks rupture near the edge of the concrete footing controls the load-carrying capacity of the connection. Upon rupture of this type, the embedment mechanism described above disappears, while the flexural resisting mechanism remains the only thing transferring forces.

2.4.2 Eastman (2011)

This author (Eastman 2011) continued research into steel piles embedded into reinforced concrete pile caps in 2011. He expanded on the knowledge provided by Xiao by expanding the test parameters to include other variables. Eastman wanted to experiment with circular pipe (a common shape used for steel piles), in lieu of the HP shapes used by Xiao. The tests he designed used a standard 12.75 inch diameter pipe embedded at various depths into the concrete pile cap. He also included a cover plate, another common detail for piles. See Figure 2-33 for the typical test design. Specimens were loaded laterally to failure. Eastman's key interests were to investigate the strength of the connection at various depths, as well as the rotational stiffness of the connection.

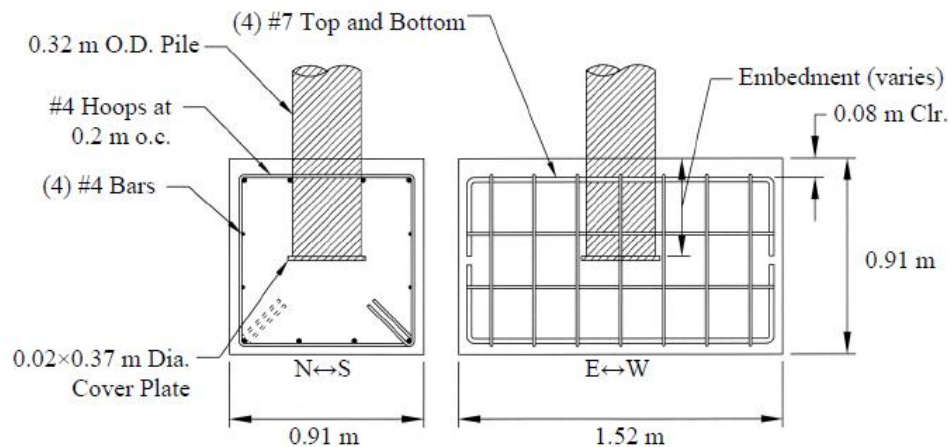


Figure 2-33: Typical Test Specimen Design (Eastman 2011)

There was only 1 variable tested in these experiments: the embedment depth of the pile. The embedment depths were measured in relation to the diameter of the pile. They were:

1. $1.5 \times \text{Diameter}$ (17.9 inches)
2. $0.5 \times \text{Diameter}$ (6.25 inches)
3. $0.4 \times \text{Diameter}$ (4.56 inches)

Like Xiao, Eastman showed with these tests that a steel shape, even a round one, embedded into concrete could transfer a large amount of rotational force. In addition, he showed what effect the embedment depth had on the behavior of the connection. Eastman concluded that:

1. The pile embedded 1.5 times its diameter was able to develop the entire bending strength of the pile.
2. Even a pile with minimal embedment can develop a significant moment-resisting capacity. The pile embedded 0.5 times its diameter still resisted over 1/3 of the moment resisted by the 1.5D pile.
3. The connection produces significant rotational stiffness. See Figure 2-34 for the stiffness values reported. Even the shallowly embedded piles developed a large fraction of the resistance produced by the deep pile. The stiffness is not, however, infinite, as is the assumption in models that use a “fixed” connection. To accurately model the connection in design, the rotational stiffness is better modeled as a rotational spring.

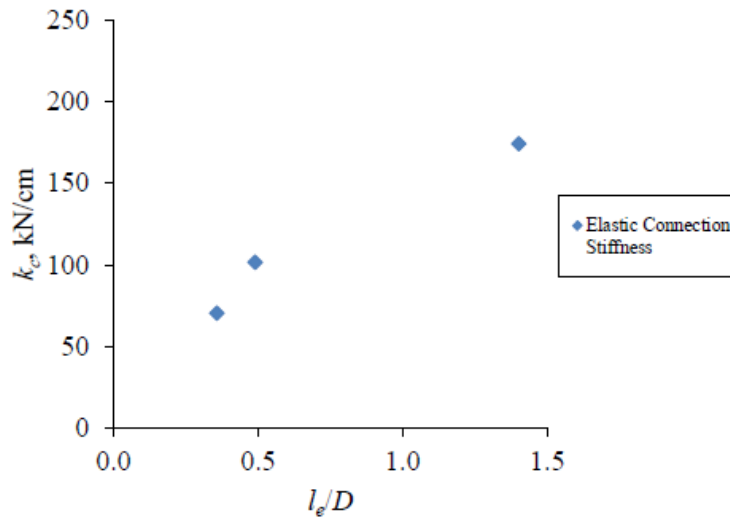


Figure 2-34: Elastic Connection Stiffness vs. Normalized Pile Embedment Depth (Eastman 2011)

Eastman took the results from this test and developed a model to estimate the elastic strength of the connection. The model proposed is a version of the model proposed by (Marcakis and Mitchell 1980). The difference lies in the inclusion of the end-bearing plate; Eastman included an end-bearing force to his model. See Figure 2-35 for the stresses included in this model.

The tested strengths of each of the specimens were compared with the predicted values. three different methods of determining the maximum stress under the embedment plate were used. The method that showed the best prediction was the method that assumed that the bearing stress (σ_e) is limited by the friction force developed between the pile and the concrete at the back of the connection. A friction coefficient of 0.35 was used ($C_e = (0.35) \cdot C_b$). Refer to Figure 2-36 for the graph of this comparison.

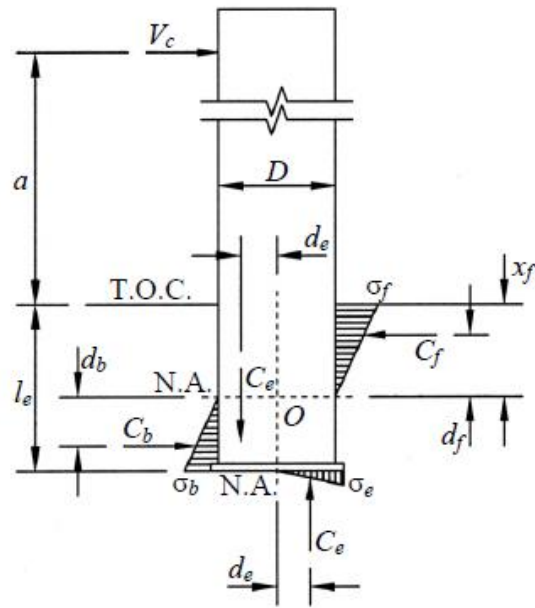


Figure 2-35: Model of the Elastic Stresses Developed by the Embedded Pile (Eastman 2011)

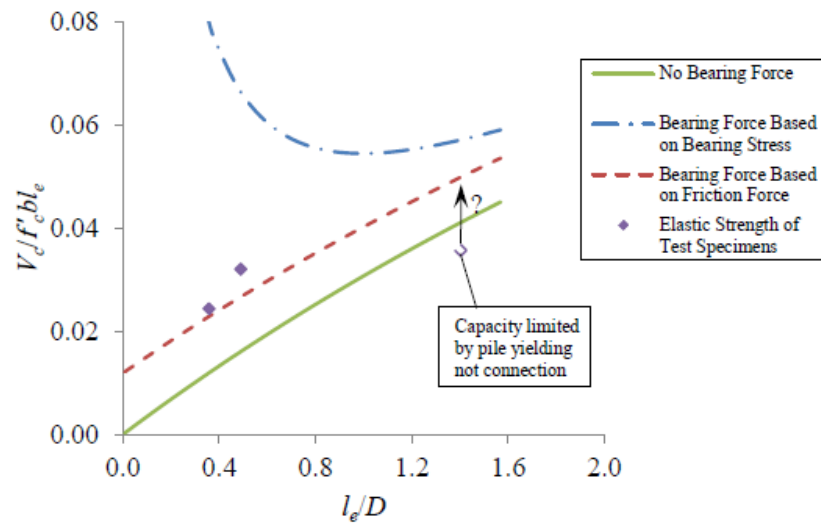


Figure 2-36: Comparison of Model for Elastic Strength With the Tested Elastic Strength of Specimens (Eastman 2011)

2.4.3 Richards, Rollins et al. (2011)

Bridges and DOT structures often rely on deep foundations to support heavy structural loads. These deep piles are connected to a concrete pile cap. Often (as has been discussed previously), these connections are designed as “pinned” connections. This connection can often be critical to the performance of a foundation system during lateral seismic loads, so it is a major concern to the designers when they are trying to control deflection of the system. In an attempt to introduce rotational stiffness and create a more “fixed” connection, designers often resort to filling the pile with concrete, and including large amounts of reinforcement to tie the pile to the pile cap. This is done at great cost to a project, especially when hundreds or even thousands of piles are needed. See Figure 2-37 for an example of a “fixed” pile connection detail.

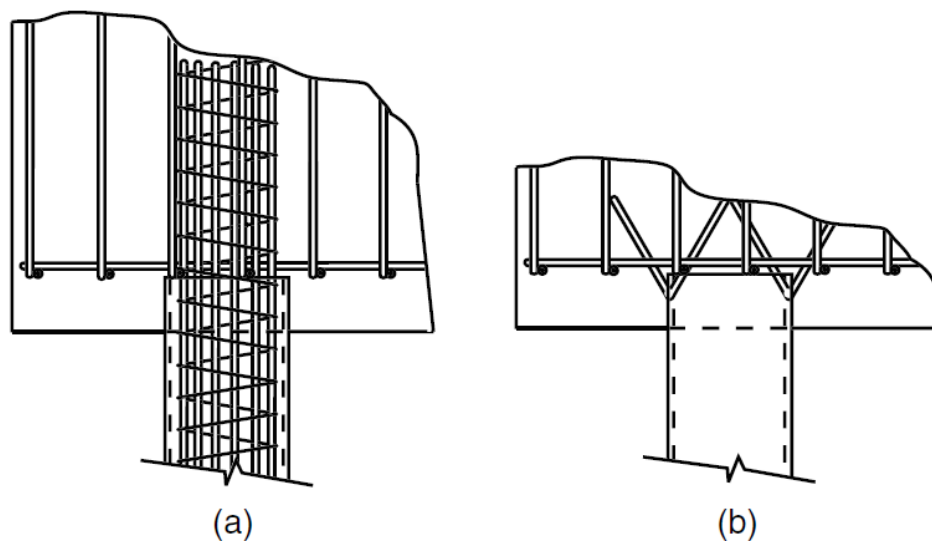


Figure 2-37: Example of Detail for (a) Fixed Pile Connection, and (b) Pinned Pile Connection (Richards, Rollins et al. 2011)

Creation of the “fixed” pile connection relies on two main mechanisms: 1) bearing of the concrete to the sides of the pile, as described by (Marcakis and Mitchell 1980), and 2) the couple created by the supplemental reinforcement. These mechanisms are shown in Figure 2-38.

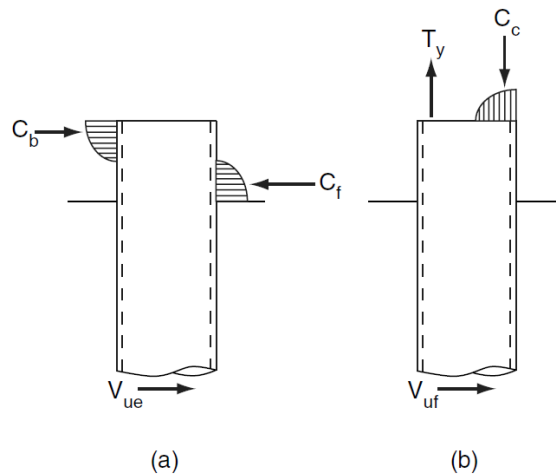


Figure 2-38: Moment Resisting Mechanisms:
(a) Concrete Bearing/Embedment
Mechanism, (b) Flexural Reinforcement
Mechanism (Richards, Rollins et al. 2011)

The motivation for this research was that the authors wanted to investigate the strength and stiffness of several different connection details. They recognized that there was a mechanism that contributed to both the strength and stiffness: friction between the concrete and the pile. This friction is caused by the bond between the steel pile and the surrounding concrete, and actually assisted in resisting the moment in the pile, as shown in Figure 2-39.

The authors realized that without supplemental reinforcement, the only mechanisms contributing to the moment capacity of the connection would be the embedment and the friction mechanism. They wanted to determine if a fixed connection could be created relying solely upon those two mechanisms. If so, then a designer could confidently rely on the benefits of a fixed connection while avoiding the increased cost of supplemental reinforcement.

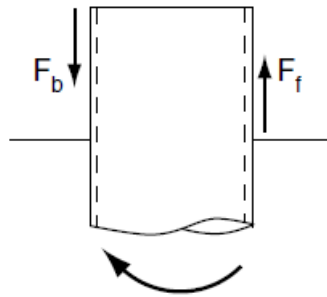


Figure 2-39: Friction Mechanism (Richards, Rollins et al. 2011)

Four full-scale test specimens were created for testing. Each specimen consisted of a reinforced concrete pile cap measuring 0.91m X 0.91m X 1.8 m. Connected to this pile cap were two steel piles, each driven into the ground to a depth of 12.2 m. The piles were 0.3m diameter with 9.5mm wall thickness. An actuator was attached to the side of the pile cap and anchored to a much larger and stiffer set of piles. The actuator induced lateral loads into the pile cap, which was resisted by shear and bending at the pile connection point. The test variables were the embedment depth of the pile, and the reinforcement details used. See Table 2-7.

Based on the results of these tests, the following relevant conclusions were made:

1. Pipe piles with even a minimal amount of embedment depth and reinforcement can develop significant moments. The general practice of treating these connections in design as “pinned” is conservative.
2. The current methods for computing moment capacity of embedded piles under-predict the actual capacity of the embedded pile.,

Table 2-7: Test Specimen Design (Richards, Rollins et al. 2011)

Specimen	Pile cap embedment (m)	Pile-to-cap reinforcement	Concrete fill in pile
1	0.15	Yes ^a	Yes ^b
2	0.30	Yes	Yes
3	0.30	No	No
4	0.61	No	Yes

^aPile-to-cap reinforcement consisted of four #6 longitudinal bars and #4 spiral with 0.15 m pitch, extending from 1.2 m below grade up to the top reinforcement grid in the pile cap.

^b28 MPa concrete used to fill piles.

3. The friction mechanism described above may significantly increase the moment capacity of the connection, though they admit that further testing would need to be performed that isolates this mechanism to accurately predict its involvement.

4. While a shallow embedment may be adequate for developing the flexural capacity of the pile, a longer embedment may be required to avoid supplemental shear reinforcing in the cap.

2.5 Shallowly Embedded Column Base Plates

2.5.1 Cui and Nakashima (2011)

Japanese researchers (Cui and Nakashima 2011) have done limited work on shallowly embedded column bases. The detail investigated is used for column base plates: the shallowly embedded column base. This detail is used when a column is anchored to a reinforced grade beam or pedestal, then the floor slab is poured directly over the base, creating a smooth, aesthetic finish.

Typically, the contribution of the floor slab to the strength and stiffness of the connection has been neglected. The connection is either designed as a “pinned” connection, or heavily detailed to create a “fixed” base. Any contribution of the small amount of embedment concrete is ignored during the design phase. The authors of this paper wanted to investigate and quantify the contributions of the slab. They also wanted to test several reinforcement details and see if by adding supplemental reinforcement, the stiffness of the connection could be such that it would produce a fixed column base, similar to a deeply embedded column base.

They created eight physical specimens, at 2/3 scale. All eight of the columns were square HSS 200 mm tubes with thickness of 9 mm (7 specimens) and 12 mm (1 specimen). Base plates were all 25 mm thick and 300 mm square. A total of twelve D13 anchor bolts were spaced evenly around the base plate. The foundation “beam” was designed to be large and stiff enough

that failure of the anchor bolts in the base plate would govern the strength of the connection. One specimen was designed as the control of the test, and was a simple exposed base plate connection without the shallow embedment concrete. The remaining seven specimens included various supplemental reinforcement configurations and slab shapes.

The columns were all loaded axially with a 115 kip load (corresponding to approximately 0.2 times the axial yield capacity of the 0.9 mm thick tube). A separate lateral actuator then loaded the columns laterally.

The columns were loaded with a static axial load that was approximately 0.2 times the yield axial capacity of the column. The columns were then loaded laterally to failure or a displacement of 0.1 radians, whichever occurred first. The results of these tests showed that the shallow embedment contributed greatly to the overall performance of the connection.

The strength of the connection, when compared with the baseline exposed based plate specimen, increased significantly with the presence of concrete cover and supplemental reinforcement. The tests showed that for the thickest embedment (200 mm, or 1.0 times the depth of the HSS column), along with supplemental reinforcement, the strength increased by 2.0 over a similar but exposed base plate.

The stiffness of the connection also increased with the addition of embedment. The stiffness increased over the baseline test by 1.1 for the column with 100 mm embedment (1/2 times column depth), and by 1.5 for the 200 mm embedded column. Interestingly, the authors conclude that neither the addition of supplemental reinforcement nor the shape of the slab had a significant improvement on the stiffness of the connection.

The deformation capacity of the connection also increased with the addition of embedment concrete and reinforcement. The supplemental reinforcement provided the greatest increase in the deformation capacity. The strength of the connection began to decrease at a column rotation of 0.03 radians, but with the supplemental reinforcement, the connection maintained 90% of its strength up through a rotation of 0.06 radians.

The main failure mode for the connection was punching shear failure in the embedment concrete above the trailing end of the column. The failure mode could be shifted to column local buckling (formation of a plastic hinge), when the embedment and reinforcement were increased sufficiently to make the connection stronger than the column.

The authors proposed a prediction model for future design of similar connections using HSS columns. The column is evaluated at the bottom of the base plate, and is modeled as having three modes of flexural resistance. The total strength of the connection is taken as the sum of these three resistance modes.

1. Contribution of exposed base plate. The flexural strength of this mode follows the procedure as described in AISC Design Guide No.1, and the Architectural Institute of Japan. This is estimated for three different loading cases:

- a. When the anchor bolts on the tension side take smaller forces than the yield strength (high compression load, low moment)

$$M_e = (N_u - N) d_t \quad (2.5.1)$$

- b. When the anchor bolts on the compression side take tensile forces (high tensile force on column, low moment)

$$M_e = (N + 2T_u)d_t \quad (2.5.2)$$

c. Otherwise (high moment load)

$$M_e = T_u d_t + \frac{(N + T_u)D}{2} \left(1 - \frac{N + T_u}{N_u} \right) \quad (2.5.3)$$

Where

M_e = Maximum bending strength of the column base in bending

N = Axial force in the column transferred to the column base

N_u = maximum compressive strength of the concrete under the base plate, estimated as

$$0.85BDf_c.$$

$B \& D$ = dimension of base plate parallel and perpendicular to moment axis, respectively

T_u = maximum tensile strength of the anchor bolts acting in the tension region.

d_t = dimension from centerline of column to the anchor bolt group in tension

2. Contribution of the concrete slab. This moment resistance is assumed to be given by two mechanisms: direct bearing of the slab adjacent to the compression side of the column, and the punching resistance of the slab in uplift on the tension side of the base plate (note that this punching resistance governed the strength of nearly all of the test specimens from this group).

- a. The strength of the concrete in direct bearing of the slab adjacent the compression side of the concrete is given as:

$$M_{cc} = v_c \cdot f'_c \cdot 0.8d \cdot (0.6d + t_{bp}) \quad (2.5.4)$$

- b. The strength of the reinforced concrete punching resistance on the uplift side of the baseplate is given as:

$$M_{ct} = Q \cdot D_t$$

$$Q = \frac{1 - \sin 45^\circ}{2} A \cdot v_t f'_c \cdot \cos 45^\circ \quad (2.5.5)$$

Where:

A = area of the punching-shear surface, given as:

$$A = B \cdot \frac{d}{\cos 45^\circ} + \frac{\pi}{2} \cdot \left(\frac{d}{\cos 45^\circ} \right)^2 + (B - C) \cdot \left(\frac{d}{\cos 45^\circ} \right) \quad (2.5.6)$$

D_t = Distance from centerline of the column to the centerline of the base plate region resisting uplift.

$$D_t = \frac{B + C}{4} \quad (2.5.7)$$

C = depth of the HSS column.

d = embedment depth of column, from top of concrete to the top of the base plate.

v_c & v_t = effectiveness factors for bearing and punching shear, respectively

$$v_c = 0.85$$

$$v_t = 0.7 - \frac{f'_c}{200} \quad (2.5.8)$$

3. Contribution of supplemental reinforcement in the concrete slab. This is given as:

$$M_{st} = A_r \sigma_y \cdot \cos 45^\circ \cdot 8l \quad (2.5.9)$$

Where:

A_r = cross section of reinforcing bars resisting moment

σ_y = yield strength of reinforcing bars

l = horizontal distance from the centroid of the column section to the reinforcing bars.

The authors were able to use the empirical tests to verify the model and equations summarized. The calculated strengths provided reasonable estimates of actual moment capacity, with the predicted values ranging between 82-92% of the experimental strengths. This model provides a reasonable and conservative method for predicting the design strength of a connection.

2.5.2 Barnwell (2015)

Recently, Barnwell researched a specific type of shallow-embedded column base plate: One created using a block out. When a floor slab is poured, a portion of the floor is blocked out and the steel column is later anchored to the footing below in that block out. After the steel column has been set and anchored, the block out is then filled in with unreinforced concrete, leaving a smooth, aesthetic finish.

Like other shallowly embedded column types investigated here, Barnwell reports that in design, the block out concrete is ignored, and the column is considered to be “pinned” at the

base. Any benefits from the block out concrete are ignored by designers, simply because those benefits have not been researched and quantified.

Barnwell created a total of twelve specimens (at 2/3 scale) to investigate the effect of the block out on the stiffness and strength of the connection. The test matrix can be seen in Table 2-8 and Table 2-9. The specimens were not loaded axially. An actuator was used to exert cyclic lateral loads at the tops of the column to induce lateral and moment loads at the base. Specimens were loaded until failure.

Based on the tests performed, Barnwell reached the following conclusions:

1. All embedded connections showed higher strength than that predicted by the AISC Steel Design Guide 1. The columns embedded only 8 inches (1x the column depth) on average show bending strength 86% greater than the Design Guide predicted strength. The column embedded 16 inches (2x the column depth) showed an average increase in bending strength of 144%. Thus, like the other test performed on embedded steel members, even a small amount of concrete embedment has a significant effect on the strength of the connection. Methods that ignore the contributions of the block out concrete are conservative.
2. The stiffness of the connection also increased with the addition of the block out. In the strong direction, the 8-in embedded columns showed a stiffness of 12.57-16.65 kip/in, while the deeper 16-in embedded columns had a stiffness of 14.66-21.31 kip/in. Barnwell concludes that adding additional embedment will not continue to increase the rotational stiffness of the connection, and that even the shallow specimens approached the highest stiffness possible.

**Table 2-8: Specimen Parameters - First Test Round
(Barnwell 2015)**

Specimen	Embedment [in]	Orientation	Shape
A1	8	Strong	W8×35
A2	8	Strong	W8×48
A3	8	Weak	W8×35
A4	8	Weak	W8×48
B1	16	Strong	W8×35
B2	16	Strong	W8×48
B3	16	Weak	W8×35
B4	16	Weak	W8×48

**Table 2-9: Specimen Parameters - Second
Test Round (Barnwell 2015)**

Specimen	Embedment [in]	Orientation	Shape	Braced Slab
CA2	8	Strong	W8×48	Y
DA2	8	Strong	W8×48	N
CB2	16	Strong	W8×48	Y
DB2	16	Strong	W8×48	N

3. The resultant compression block was not located underneath the baseplate, as is the case with an exposed column base connection. Rather, the resultant compression block is located underneath the slab-on-grade concrete a distance farther than the edge of the base plate.
4. Barnwell proposed a model that predicts the rotational strength of the connection. In his model, a 45° line is drawn from the compression face of the column to the top of the slab/footing interface. This location marks the approximate location for

the compression resultant. See Figure 2-40. Using this model, Barnwell was able to predict the capacity of the twelve specimens to within 20% of tested strengths.

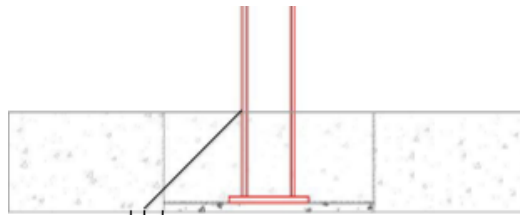


Figure 2-40: Model of Location of Compression Resultant (Barnwell 2015)

2.5.3 Jones (2016)

Jones continued the work done by Barnwell, and sought to study the effects of embedment depth on the stiffness of a shallowly embedded column connection by creating a computer model using finite element methods. He used the physical tests performed by Barnwell as a benchmark to calibrate his finite element models.

Jones discovered that the behavior of the connection is highly dependent on the connection between the steel column and the surrounding concrete. Determining methods of capturing the properties of this interface became a focus of his efforts. Several methods of approximating the properties of this interface were experimented with and evaluated based on the physical tests performed by Barnwell.

A key finding of this work showed the significance of the base plate to the rotational stiffness of the connection. For connections with little or no embedment, the stiffness (thickness) of the base plate plays a crucial role in the rotational stiffness of the connection. As the embedment depth increases, the contribution of the column bearing against the embedment concrete increases, and the contribution of the base plate to the stiffness decreases, as shown in Figure 2-41. Thus for deeper embedment lengths, the stiffness of the base plate becomes negligible.

Jones was able to use his modeling techniques to provide prediction of the performance of the physical tests associated with this thesis. He obtained details of the designs for the eight test specimens (see Section 3.3) built for this thesis and modelled them. The comparison between his predictions and the actual performance will be discussed in section 5.4 of this thesis.

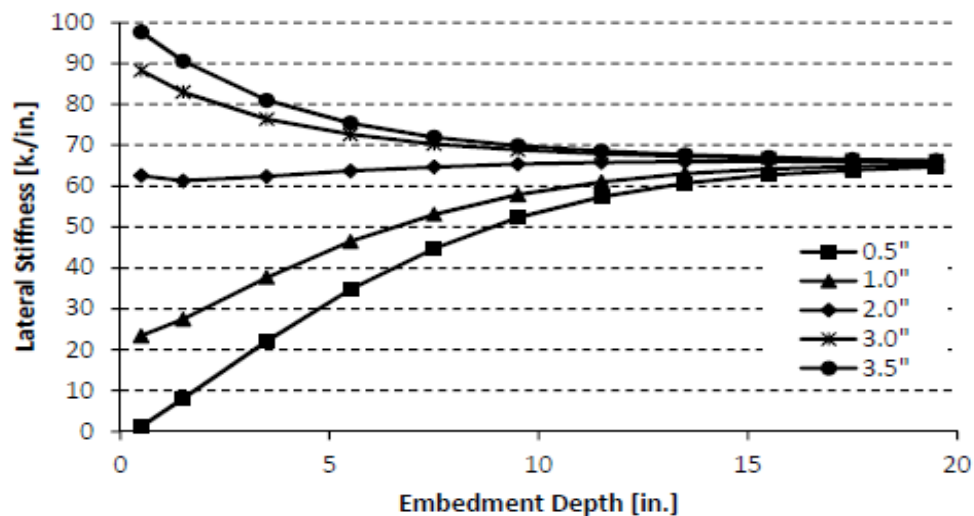


Figure 2-41: Example of the Effects of Base Plate Thickness on the Stiffness of a Column Base Connection, W8x48 Column Size (Jones 2016)

2.5.4 Tryon (2016)

Like Jones, Tryon's work involved using numerical models to predict the behavior of shallowly embedded column base connections. Tryon cleverly adapted the work performed by (Hetényi 1971) on the closed-form solution to a beam of infinite length supported on an elastic foundation. Tryon was able to adapt this work to the situation of an embedded column, equating the column steel to the “beam of infinite length” and the surrounding block out concrete to the “elastic foundation”.

Tryon created a model (Figure 2-42) that broke down an embedded column into three parts: the exposed column portion, the embedded column portion, and the base plate. By analyzing these three portions separately, a model was created for the predicted behavior of the connection.

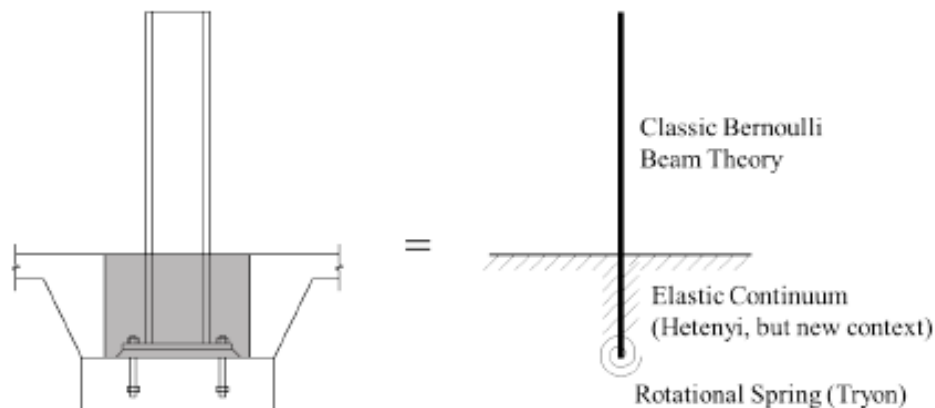


Figure 2-42: Model for an Embedded Column Base Connection (Tryon 2016)

Tryon was able to directly compare the results of his model to the physical experiments performed by Barnwell. Use of this model requires a parameter known as the modulus of subgrade reaction (k), which in the Hetényi model represents the spring constant of the material that the infinite beam bears on. For this adjusted model, the modulus of subgrade reaction is a characteristic of the concrete that the steel column bears against and is directly related to its modulus of elasticity. The characteristic could not be directly measured for Barnwell's physical tests, so a range of approximate values between 300 and 600 kip/in³ was determined for the comparison. The results are tabulated in Table 2-10.

A relationship between the rotational stiffness of the connection and the embedment depth of the column was also produced, see Figure 2-43. These curves show that for expected values of the modulus of subgrade reaction, the rotational stiffness of the connection increases as the embedment depth increases. The stiffness does reach an equilibrium point after which it remains constant even if the embedment depth increases. A key observation of Tryon is that at an embedment depth of roughly 2 times the depth of the column, the rotational stiffness is maxed, and additional embedment depth has no benefit on the rotational stiffness of the connection. This value is confirmed by (Castilla, Martin et al. 1984).

Tryon was able to produce normalized rotational-stiffness vs. embedment curves for a variety of wide-flange column shapes. These curves assume a modulus of subgrade reaction (k_o) of 500 kip/in³, and a concrete 28-day compressive strength of 4000 psi. Two of these curves are shown, the W10 family (Figure 2-44) and the W14 family (Figure 2-45). These curves can be used as a comparison to the tests performed for this thesis. Note that the shapes used in this thesis are a W10x77, and a W14x53. Tryon also created simplified equations that approximate the values found in the curves, and can be used in lieu of the curves, see EQ (2.5.10). This

Equation is meant to be used for all common shapes bent about the strong axis orientation. The comparison between this prediction and the actual results are shown in Section 5.

Table 2-10: Experimental vs. Theoretical Rotational Stiffness of Barnwell's Physical Test Specimens (Tryon 2016)

Specimen	Rotational Stiffness [1000 kip-in/rad]		
	Experimental	$k_0 = 300 \text{ kip/in}^3$	$k_0 = 600 \text{ kip/in}^3$
A1	196	168	285
A2	232	193	335
CA2	206	193	335
B1	433	405	526
B2	636	496	670
B3	184	161	202
CB2	640	496	670
Error [%]		19.6	16.4

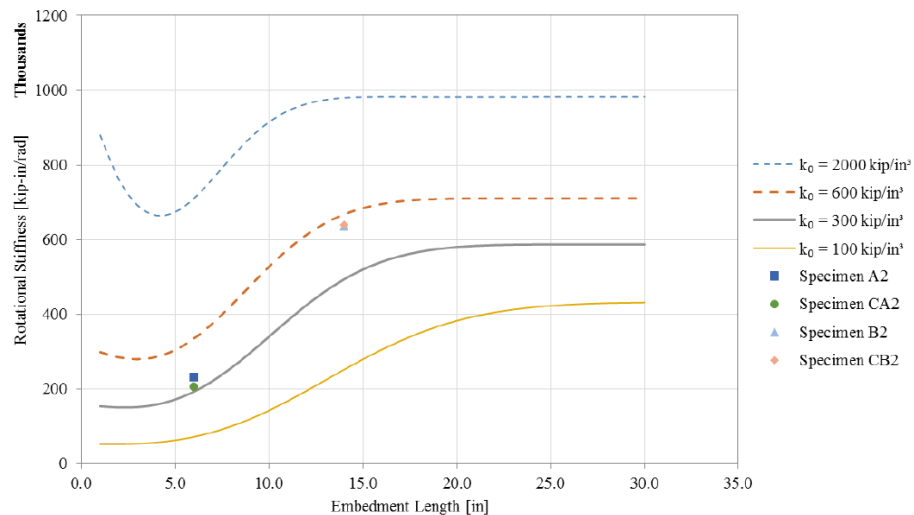


Figure 2-43: Tryon's Model for Rotational Stiffness vs. Embedment Length, Compared with Barnwell Physical Tests (Tryon 2016)

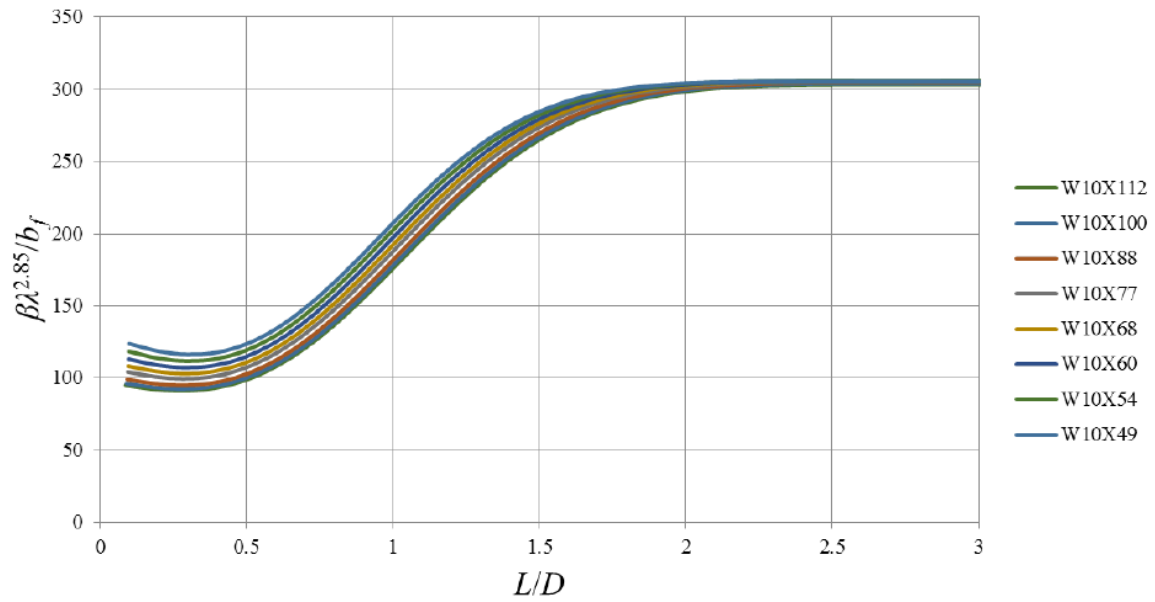


Figure 2-44: Tryon's Normalized Rotational Stiffness vs. Embedment Curve for W10 Family (Tryon 2016)

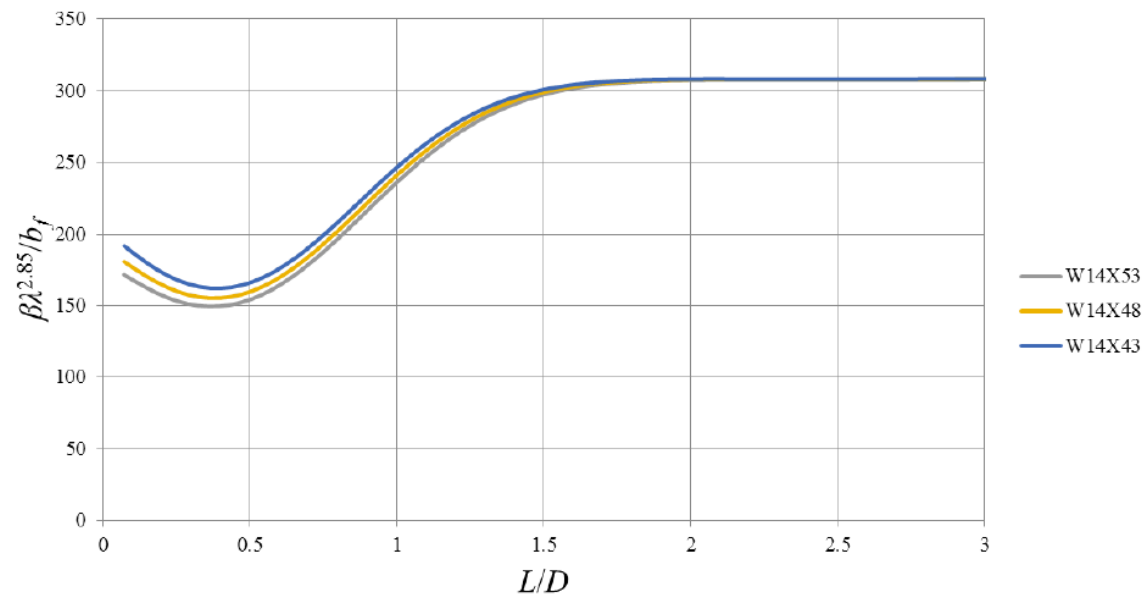


Figure 2-45: Tryon's Normalized Rotational Stiffness vs. Embedment Curve for W14 Family (Tryon 2016)

$$\frac{\beta\lambda^{2.85}}{b_f} = \begin{cases} 135 & \frac{L}{D} < 0.50 \\ 110 \cdot \frac{L}{D} + 80 & 0.5 \leq \frac{L}{D} < 2.0 \\ 300 & 2.0 \leq \frac{L}{D} \end{cases} \quad (2.5.10)$$

Where:

β = Rotational stiffness at the embedment concrete (kip·in/radians)

b_f = Width of column flange (in)

L = Embedment depth of the column (in)

D = Depth of the column (in)

λ = Factor that incorporates the material properties of both the embedment material and the column material.

$$= \sqrt[4]{\frac{k_0(2 \cdot b_f - t_w)}{4 \cdot E \cdot I_x}}$$

k_0 = modulus of reaction of the embedment material, assumed to be = 500 kip/in³

t_w = web thickness of column (in)

E = Modulus of Elasticity of column material = 29000 ksi

I_x = Moment of Inertia of the column about its strong axis (in⁴)

For reference, this equation will be applied to predict the rotational stiffness of a specimen from this thesis. Specimen F3 will be used for this reference (See the Test Matrix in section 3.2.3 for the pertinent information regarding this test specimen).

$$\frac{L}{D} = \frac{15 \text{ in}}{10.6 \text{ in}} = 1.415$$

$$\text{Since } 0.5 \leq \frac{L}{D} < 2.0$$

$$\frac{\beta \lambda^{2.85}}{b_f} = 110 \cdot (1.415) + 80 = 235.7$$

$$\lambda = \sqrt[4]{\frac{k_0(2 \cdot b_f - t_w)}{4 \cdot E \cdot I_x}} = \sqrt[4]{\frac{\left(500 \frac{\text{kip}}{\text{in}^3}\right)(2 \cdot (10.20 \text{ in}) - (0.53 \text{ in}))}{4 \cdot (29000 \text{ ksi}) \cdot (455 \text{ in}^4)}} = 0.1171 \text{ in}^{-1}$$

$$\beta = \left(\frac{\beta \lambda^{2.85}}{b_f} \right) \cdot \frac{b_f}{\lambda^{2.85}} = (235.7) \cdot \frac{(10.2 \text{ in})}{(0.117 \text{ in}^{-1})^{2.85}} = 1,084,336 = 1.08 \text{ E} + 06 \frac{\text{kip} \cdot \text{in}}{\text{radians}}$$

This predicted value, and the others associated with the rest of the specimens will be compared with actual test values in Section 5

3 METHODS

3.1 Overview

In order to test the effects of the block out on the rotation of a column base, a total of eight test specimens were designed and built at 2/3 scale. The tests were intended to replicate a common situation involving column bases under high lateral and bending moments: a moment frame designed with a “fixed” base. This type of moment frame is designed to resist design lateral forces applied at the top of the column. At the base of the column, large lateral forces and bending moments are generated. Special attention is required in the detailing and construction of the base of the column, and its attachment to the foundation below, to adequately resist those forces. Refer to Figure 3-1 for a simple model illustrating this concept.

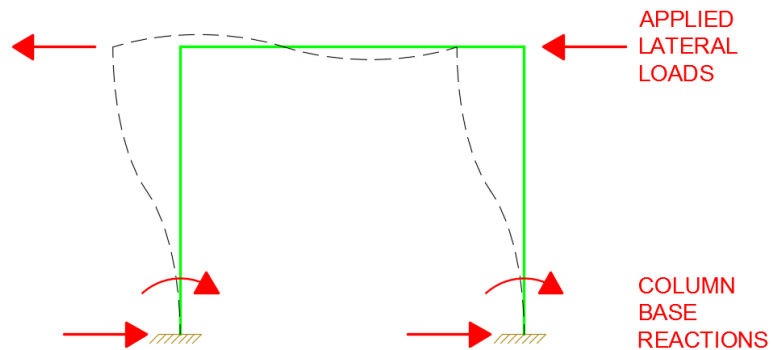


Figure 3-1: Model of Lateral Force-Resisting Moment Frame with a Fixed Base

The test specimens built represent one of the columns in the moment frame. The column itself was designed as a steel wide flange shape, oriented to bend about its strong axis. The applied lateral loads were imposed on the top of the column by means of a hydraulic actuator which, in turn, was anchored to a reaction frame. Both the reaction frame and the specimen base were anchored to the floor of the lab. The actuator was attached to the top of the column by means of a corbel. This corbel was bolted into a horizontal plate on top of the column, then bolted into the head of the actuator. This configuration allowed the pivot point of the corbel to be directly in line with the centerline of the column. A connection of this type ensured a consistent horizontal force on the column, regardless of the deflection experienced. Another reaction frame, perpendicular to the actuator, was attached to the side of the corbel to restrict motion out-of-plane. For a general layout of the test specimens and configurations, refer to Figure 3-2, Figure 3-3, and Figure 3-4.

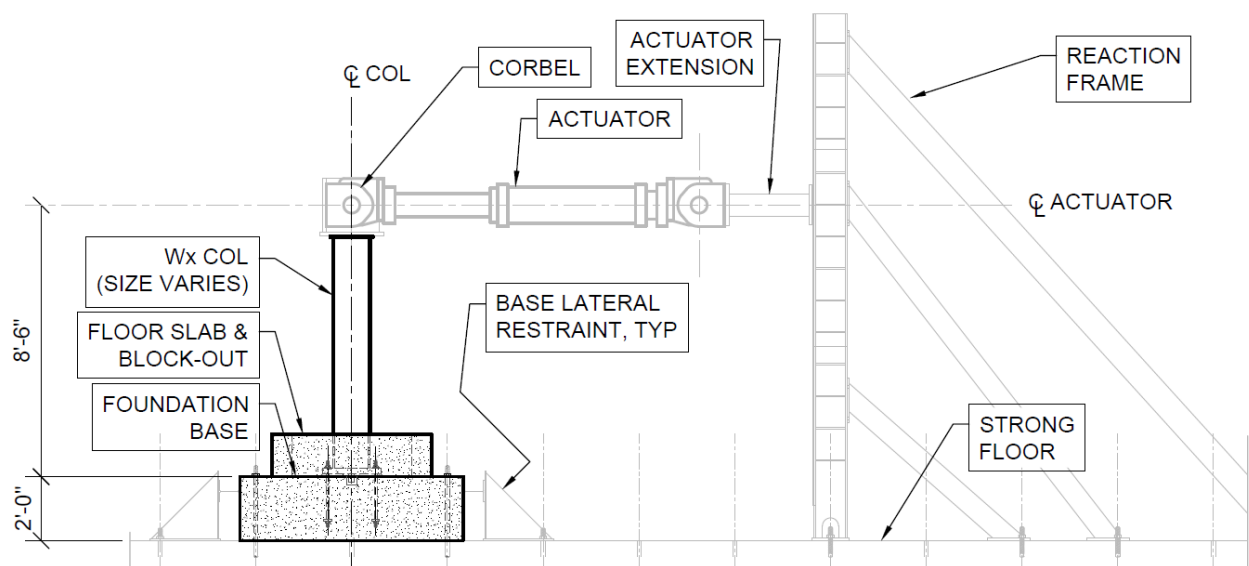


Figure 3-2: Test Setup General Layout - Elevation View Perpendicular to Loading

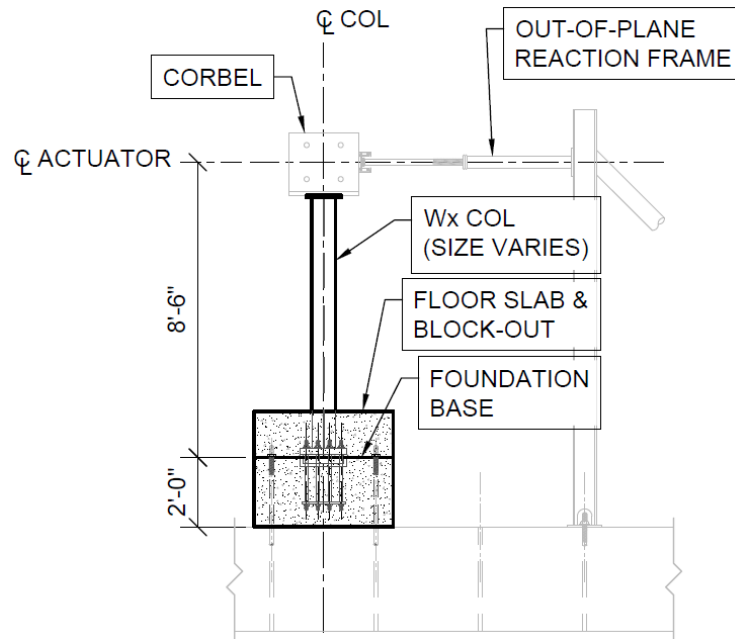


Figure 3-3: Test Setup General Layout - Elevation View Parallel to Loading

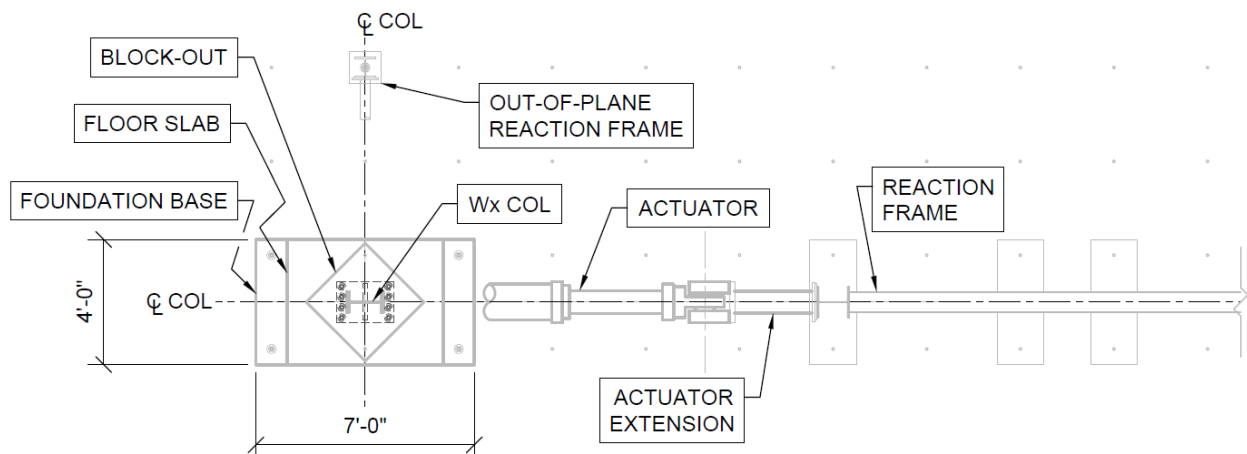


Figure 3-4: Test Setup General Layout - Plan View

3.2 Test Matrix

Refer to Table 3-1 for the test matrix used.

Table 3-1: Test Matrix

Specimen Name	Column	Base Plate		Shear Lug	Anchor Bolts			Base	Block out
	Size	Thickness (in)	ASTM grade		Qty	DIA (in)	Steel Grade	Depth (in)	Depth (in)
D1	W14x53	2.25	A36	Yes	8	1	F1554 Gr 36	24	0
D2	W14x53	2.25	A36	Yes	8	1	F1554 Gr 36	24	8
D3	W14x53	2.25	A36	Yes	8	1	F1554 Gr 36	24	16
D4	W14x53	1.5	A36	Yes	4	1	F1554 Gr 36	24	16
F1	W10x77	3	A36	Yes	8	1 1/8	F1554 Gr 36	24	0
F2	W10x77	3	A36	Yes	8	1 1/8	F1554 Gr 36	24	8
F3	W10x77	3	A36	Yes	8	1 1/8	F1554 Gr 36	24	16
F4	W10x77	2	A36	Yes	4	1 1/8	F1554 Gr 36	24	16

3.3 Specimen Design

Refer to (Appendix A: Test Specimen Design Drawings) for the complete drawings of each of the specimens. The eight specimens built and tested were divided into two test series. The two test series paralleled one another, and provided comparable results. Each of the test series had similar test objectives, and used different column shapes. The objectives of each test in the series were as follows:

Test 1: Acted as the control test, meaning a column base with no block out. This served as a benchmark to compare later tests with.

Test 2: Kept the base plate detail exactly the same, added a shallow block out, and served to observe any differences between this and test 1.

Test 3: Again, kept the base plate detail exactly the same, and added a deeper block out, and served to observe any differences between this and tests 1 and 2.

Test 4: Used a deep block out (similar to test 3), but this time the base plate detail was altered to be much less robust. Results of this test were compared to Test 3.

3.3.1 Member Size Selection

Two column sizes were chosen as the prototype members. The first group of four test specimens was intended to approximate a “shallow” column, or one whose ratio of depth to flange width (d/b_f) is near 1.0. The prototype column chosen was a W14x109, which has a d/b_f ratio of 0.98. A $2/3$ scale representation of this column is one whose depth and flange width are as near as possible to $2/3$ of the original column, while maintaining a similar d/b_f ratio. The test column size used was a W10x77.

The second group of four test specimens was intended to approximate a “deep” column, or one whose ratio of depth to flange width is nearer 1.75. The prototype column chosen was a W21x101, which has a d/b_f ratio of 1.74. A $2/3$ scale representation of this column that was used as the test column was a W14x53. A summary of the shapes chosen and their pertinent geometric data can be found in Table 3-2. The columns were designed assuming ASTM A992 steel.

Table 3-2: Summary of Member Size Selection

	Shallow Column			Actual Scale	Deep Column		
	Prototype Column W 14x109	→	Test Column W10x77		Prototype Column W21x101	→	Test Column W14x53
col depth d (in)	14.3		10.6	0.741	21.4		13.9
col flange width b _f (in)	14.6		10.2	0.699	12.3		8.06
<i>ratio d/b_f</i>	0.98	→	1.04		1.74	→	1.72

3.3.2 Design Methodology

3.3.2.1 Base Plate Design

The base plates were designed with the intent that they be strong enough to develop the bending strength of the column. This practice is common for columns in moment frames designed with “fixed” base connections. This method followed the requirements found in AISC 341 section 8.5c.(2).(a), (AISC 2010) which states that the required flexural strength of the base must be equal to equation (3.3.1).

$$M_u = 1.1 \cdot R_y \cdot F_y \cdot Z \quad (3.3.1)$$

Where:

R_y = ratio of the expected yield stress to the specified minimum yield stress, F_y . (See the

AISC “Seismic Design Manual” Table I-6-1. For ASTM A992 steel, $R_y = 1.1$)

F_y = specified minimum yield stress of the column (For ASTM A992 steel, $F_y = 50$ ksi)

Z = Plastic section modulus of the member, about the axis of bending. Note that in all test cases, columns are bent about their strong axis.

The base plates were designed assuming ASTM A36 steel.

Due to the nature of the tests, and since the anchor bolts were purposefully undersized (refer to section 3.2.2.3), the need to design the specimens to the full flexural strength given in equation (3.3.1) was unnecessary. Thus the additional 1.1 factor was ignored, and the equation was modified to that seen in equation (3.3.2).

$$M_u = R_y \cdot F_y \cdot Z \quad (3.3.2)$$

See Table 3-3 for a summary of the required flexural strengths that were used in designing the base plates. The exception to this value occurred when designing the base plates for the last test in each series (Specimens D4, and F4). The thickness of the base plates for these two specimens was reduced so that their modulus of elasticity (and thus its strength) was approximately ½ of the other specimens, concurrent with the reduction of the anchor bolts.

Table 3-3: Required Flexural Strength of Column Bases

Test No	Col Size	R_y	f_y (ksi)	Plastic Section Modulus, Z_x (in ³)	Required Flexural Strength (k-ft)
D1-D3	W14x53	1.1	50	87.1	399.2
F1-F3	W10x77	1.1	50	97.6	447.3

The base plates themselves were design in accordance with the AISC Steel Design Guide 1 (Fisher and Kloiber 2006). See Appendix B.1 Base Plate Design for Specimens D1, D2, D3, & D4, and Appendix B.5 Base Plate Design for Specimens F1, F2, F3, & F4, for the actual calculations that were used to design the base plates. The design followed the procedure outlined in that design guide in section 3.4 “Design of Column Base Plates with Large Moments”. See Figure 3-5 below for an example of the base plate design. See also Appendix A: Test Specimen Design Drawings, for the actual design drawings of each specimen’s steel assembly.

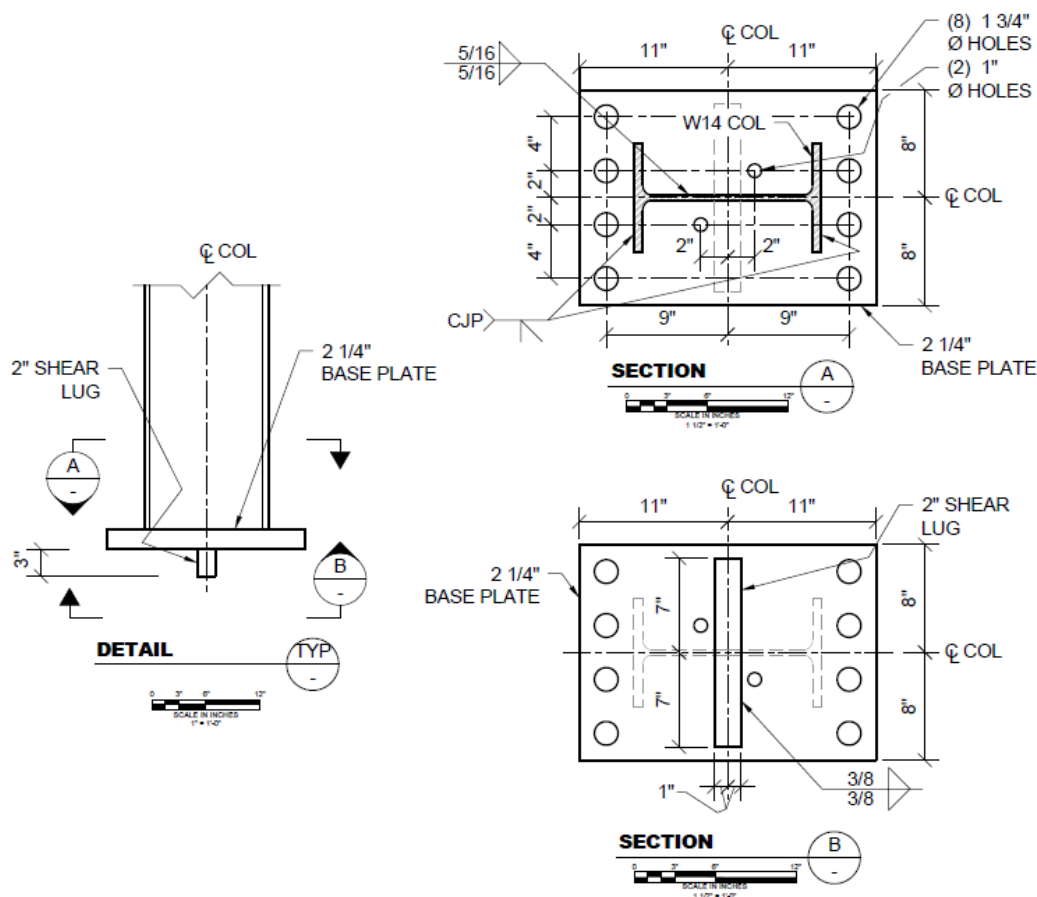


Figure 3-5: Example Base Plate Design (for D-Specimens)

3.3.2.2 Column-to-Base Plate Weld Design

The steel column was connected to the base plate with a weld. In an attempt to detail the specimens as closely as possible to details used in actual design, an ad hoc survey was made, determining how practicing engineers design this weld. The overwhelming consensus was that in cases such as this (A “fixed” column base in a moment frame), the column is nearly always connected to the base plate using a full-penetration weld. This was confirmed by (Myers, Kanvinde et al. 2009), when they stated that “the most common welds between the column flanges and the base plate are Complete Joint Penetration (CJP) groove welds or Partial Joint Penetration (PJP) groove welds with fillet reinforcing. The CJP details are considered to exhibit superior behavior...” They later concluded that both weld details are adequate for both strength and ductility. For the purposes of these tests and due to the ubiquity of this weld in current practice, a complete joint penetration (CJP) groove weld was used to connect the column flanges to the base plate. A small fillet weld was used at the column web/base plate interface. This is shown in Figure 3-5.

3.3.2.3 Anchor Bolt Design

The anchor bolts were designed to resist axial stress only. The required axial load on the anchor bolts was determined in accordance with the design procedure of section 3.4 AISC Steel Design Guide 1 (Fisher and Kloiber 2006). The design deviated from the design guide in one aspect: the resultant tensile force in the bolts was reduced by a factor of 1/2. The purpose of this deviation was to purposefully undersize the bolts, forcing failure of the connection into the anchor bolts. This was done due to the nature of the tests, where the interest lies in the effects of the block out on the strength and stiffness of the connection. By under-designing the bolts in this

fashion, the governing failure mode (neglecting any effects of the block out) was designed to be the failure of the anchor bolts.

The anchor bolts were designed using ASTM F1554 Gr. 36 steel. See Section 4.1.2 for the tests performed on the anchor bolts showing that the steel delivered exhibited a yield strength 40% higher than what was designed for and ordered. This increased strength played a role in the performance of the system as a whole, as discussed in Section 5.2.

For the last test in each series (D4 & F4), the number of anchor bolts was reduced by 1/2. As discussed previously, this was done to test the effects of the block out on a much less robust base connection. See B.2 Anchor Bolt Design for Specimens D1, D2, & D3, B.3 Anchor Bolt Design for Specimen D4, B.6 Anchor Bolt Design for Specimens F1, F2, & F3, and B.7 Anchor Bolt Design for Specimen F4 for the calculations used to design the anchor bolt embedment.

3.3.2.4 Shear Lug Design

As stated in the AISC Steel Design Guide 1 (Fisher and Kloiber 2006), there are three main methods of resisting shear in a base plate connection. These include: friction between the grout and the bottom of the base plate, bending of the anchor bolts, and bearing against concrete.

A common application for the third method is a shear lug, which has been used in practice with columns that are part of a lateral resisting system. The advantage to this method, is that by resisting lateral load through a shear lug, it effectively eliminates any transfer of lateral forces through the anchor bolts, which may then be designed for axial stresses only.

The shear lug, and its weld to the base plate were designed following the procedures from section 3.5.2 in the AISC Steel Design Guide 1 (Fisher and Kloiber 2006). The design lateral

load that the shear lug and its weld to the base plate were designed to resist is 100 kips. This was chosen as a conservative value, as both the column base and the column itself were expected to fail long before the lateral load imposed by the actuator reached this load. The steel material of the shear lug matched that used for the base plate. For the typical design of the shear plate and its connection to the base plate, see Figure 3-5. To see the calculation of the weld between the shear lug and the base plate, see Appendix B.9 Shear lug weld design for all Specimens.

3.3.2.5 Concrete Base Design

The concrete base simulated a footing pedestal, a grade beam, or other concrete base that would support the loads imposed by a moment frame column. The footprint was chosen to be as small as reasonable, while still maintaining adequate anchorage points to the strong floor of the lab. Anchorage points on the strong floor of the lab are laid in a 3 feet x 3 feet pattern ($\pm \frac{3}{4}$ inch). The footprint of the base was 4 feet x 7 feet, allowing anchorage points to the lab floor at each corner. The depth of the base was the minimum required to provide adequate depth for the embedment of the anchor bolts, and at 2 feet was sufficiently deep for the largest diameter (with the corresponding deepest required embedment) anchor bolt used. The base was designed to have a minimum 28-day compressive strength (f_c) of 4000 psi.

Reinforcement for the slab followed the requirements of ACI 318 (Committee, Institute et al. 2008) for minimum temperature and shrinkage reinforcement found in section 7.12.2.1.(b). Grade 60 bars were used. The minimum required reinforcement for a slab is given below in equation (3.3.3).

$$A_{s_min} = 0.0018 \cdot A_{conc} = 0.0018 \cdot (24 \text{ in} \cdot 12 \text{ in}/\text{ft}) = 0.518 \text{ in}^2/\text{ft} \quad (3.3.3)$$

The slab and its reinforcement were also checked for strength, under two conditions that imposed bending on the slab: 1) lifting and maneuvering in the lab, and 2) the bending moment transferred from the column to the slab during testing. It was determined that in the short direction, where little bending was expected to occur, the minimum reinforcement required for temperature and shrinkage was sufficient. Using #4 reinforcing bars spaced at 8 inches on center (OC), at the top and bottom of the slab provided a total of 0.6 in²/ft in the short direction. In the long direction, however, the moments imposed on the slab during testing governed the slab design and 2.4 times more reinforcing steel (1.47 in²/ft) was required in that direction. See Figure 3-6 for a typical base mat rebar configuration. See Appendix B.10 Base Slab Bending Capacity and Reinforcement Design for the calculations designing the rebar in the base slab. See also Appendix A: Test Specimen Design Drawings for the actual design drawings of each specimen's base slab.

3.3.2.6 Concrete Floor Slab Design

The concrete slab was meant to mimic an actual floor slab. In practice, these slabs vary in depth depending on various requirements. As such, the presence and depth of this slab was one of the main variables treated in this test. The distance from the top-of-slab to top-of-footing is typically between 12 inches and 24 inches. The specimens were designed to 2/3 scale of this depth, hence the depths of 8 inches and 16 inches. Reinforcement in this slab fulfilled the minimum requirements for temperature and shrinkage reinforcement. The minimum required steel for both slab depths is shown in Equation (3.3.4).

$$A_{s_min} = 0.0018 \cdot \left[\begin{array}{c} 8 \\ 16 \end{array} \right] \text{in} \cdot 12 \text{in}/\text{ft} = \left[\begin{array}{c} 0.173 \\ 0.346 \end{array} \right] \text{in}^2/\text{ft} \quad (3.3.4)$$

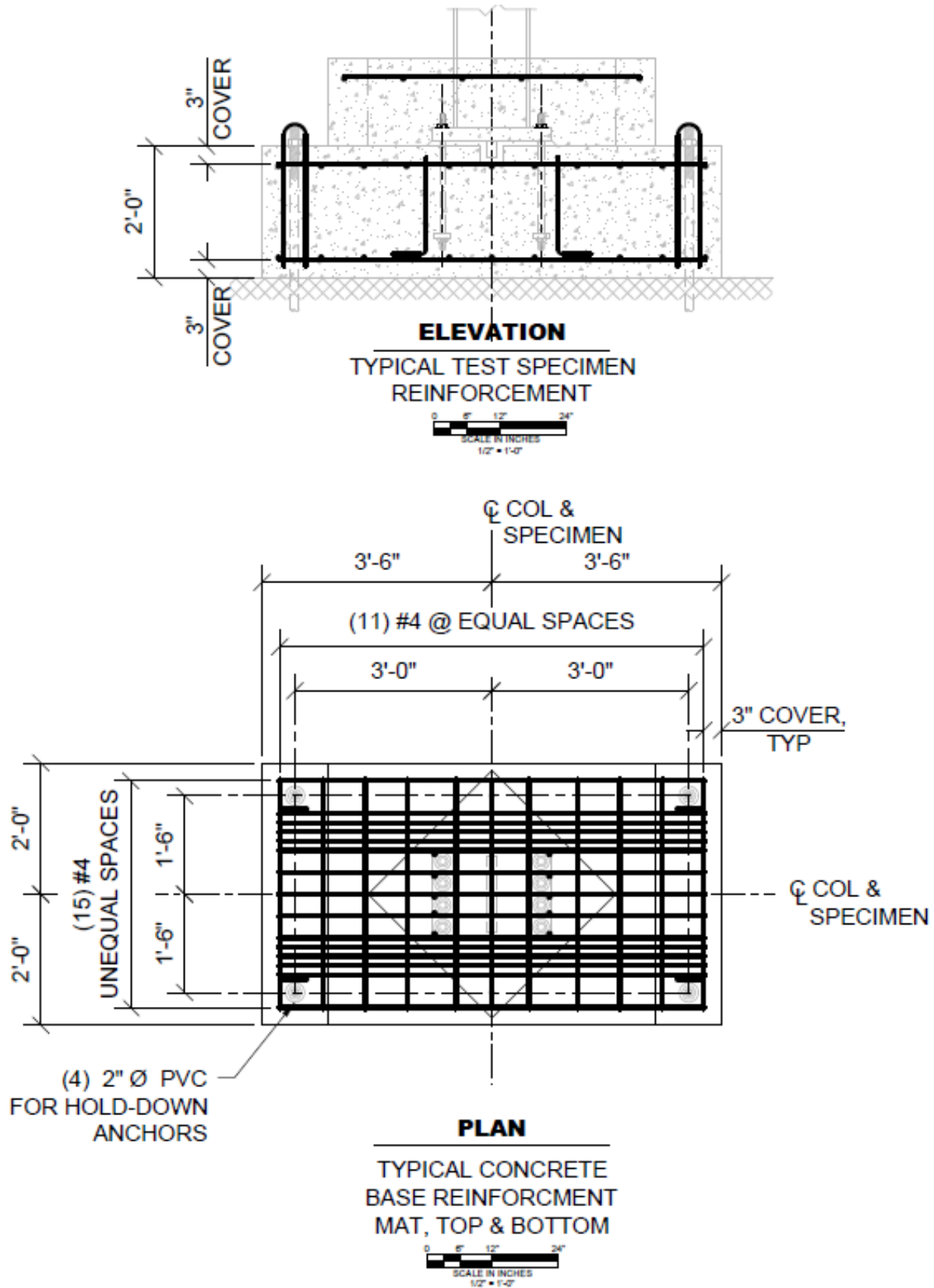


Figure 3-6: Typical Concrete Base Mat Reinforcement

The reinforcement was placed in the top slab in a single layer, using #4 bars at 12 inch spacing for the 8 inch-thick slab, and 6 inch spacing for the 16 inch-thick slab. This provides an actual steel area of $0.2\text{in}^2/\text{ft}$, and $0.4\text{in}^2/\text{ft}$. respectively. The slab was designed to have a minimum 28-day compressive strength (f'_c) of 4000 psi.

Regarding the interface between the top slab and the base slab: in order to mimic actual field conditions, the top surface of the base slab received a standard hand-trowel finish and received no other special treatment prior to placement of the top slab.

3.3.2.7 Concrete Block Out Design

The block out was designed to closely match details used in practice, and thus mimic actual conditions. The concrete block out matched the depth of the floor slab, and consisted of unreinforced concrete. The block out measured 32 inches square, and was rotated 45° from the principle axis of the column, giving it the distinctive diamond shape. The size was chosen to be as small as possible while still allowing sufficient space to fit the column base plates. The design concrete strength of the block out concrete matched that used for the floor slab. The concrete in the block out had no reinforcing steel, thus was unreinforced concrete.

3.4 Construction Process

3.4.1 Base Mat Construction

The first item built was the base mat for each specimen, Figure 3-7. Construction of the base mats began with the rebar mats, see Figure 3-8. The rebar was cut to length and bent (where required) by Clydeco Building Supplies, located in Mapleton, Utah. The rebar purchased was standard ASTM A615 (grade 60) steel bars and consisted entirely of #4 bars. The individual mats

were tied together atop a plywood template, cut to match the size of the actual specimens, to ensure that each bar was placed in its precise location and wouldn't interfere with the other elements in the mat. Grip-Rite bar ties, 6 inches long with a 16 gauge thickness, were used and were tied by hand using a Grip-Rite tie wire twister tool.

The next element built was a base plate template. This template served two purposes: 1) to hold the anchor bolts in the correct position and at the correct height, and 2) to provide a block that would create a pocket for the shear lug. The bottom of this template and all sides of the shear lug pocket block were liberally coated in concrete form release to prevent the poured concrete from bonding. Figure 3-9.

The base rebar mats were tied together on the ground, with the anchor bolt template in place, see Figure 3-10. The top mat was connected to the bottom mat at the correct elevation by tying it to the vertical "up-side down U" bars. Diagonal bars were added and tied at the corners for lateral stability. The anchor bolts were placed with their embedded plates, as well as the supplemental "L-shaped" reinforcing bars.

A pair of 2x4s was attached to the top edge of the anchor bolt template to allow for proper positioning during the concrete pour. As many elements as possible were put into position to minimize the amount of work done once the bar cages were placed into the forms, when it was considerably more difficult to access the interior of the cage.

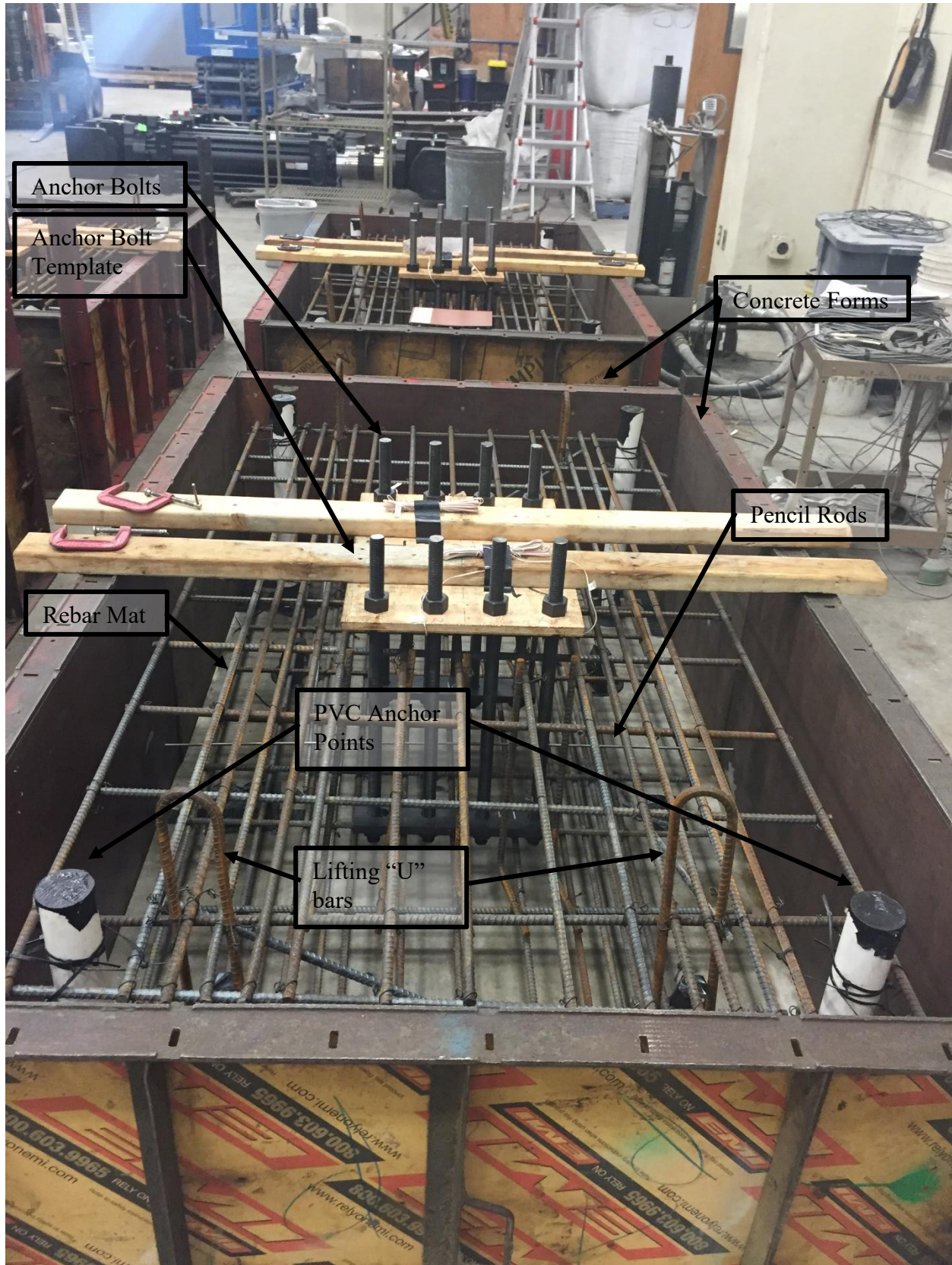


Figure 3-7: Typical Base Mat Prepared for Concrete Pour



(a)

(b)

Figure 3-8: Rebar Mats for the (a) Base Mat, and (b) Top Mat, Tied atop Templates

The concrete forms were set up next. These were Symon Steel-ply Concrete Forming System, donated by For-Shor, located in Salt Lake City, Utah. They are extremely strong and heavy steel forms. The forms came in 2ft tall sections, both 4ft and 3ft long. The short sides were made with the 4ft long sections, and the long sides were created by joining a 4ft and a 3ft length. The forms were joined together using nothing but wedge bolts. The sides of these forms and the lab floor were liberally greased with concrete form release. See Figure 3-11 for the concrete forms.

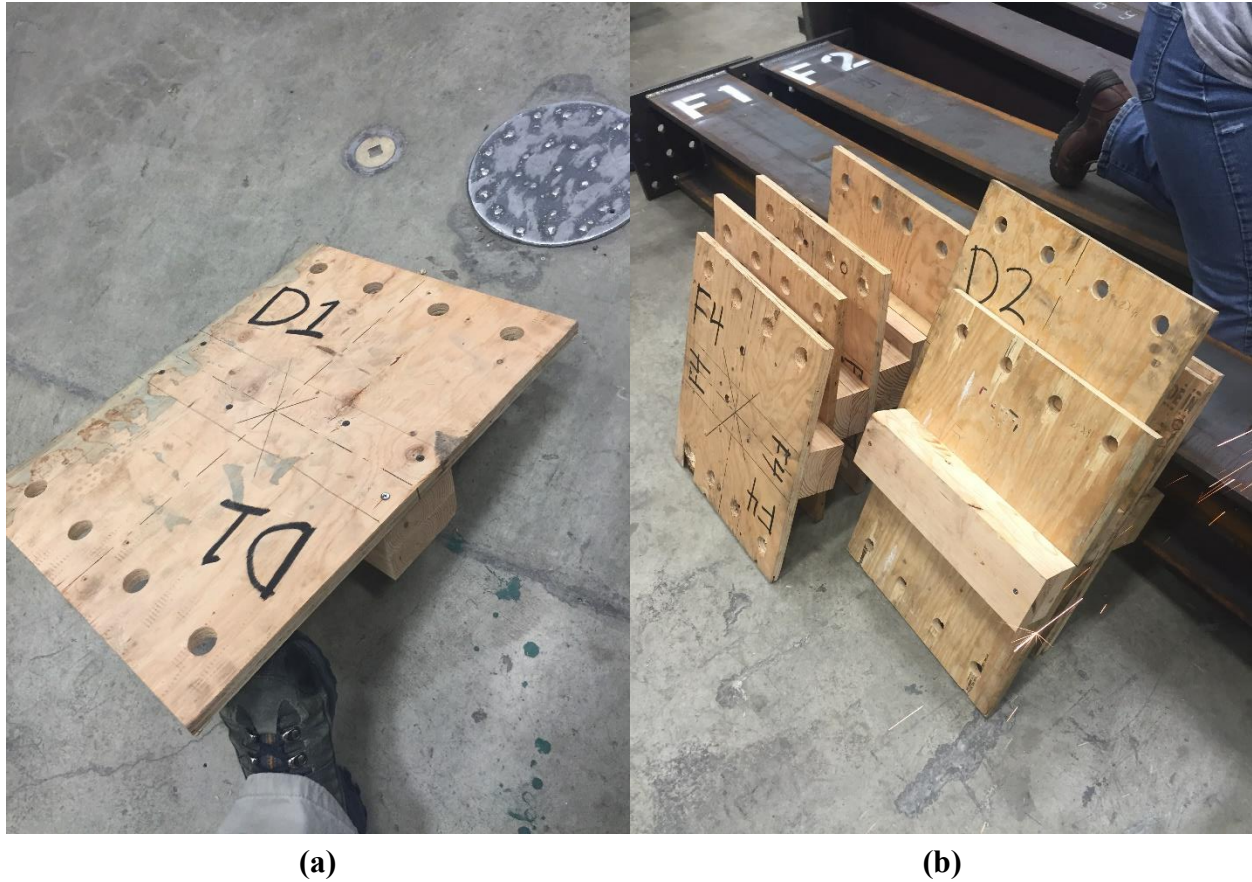


Figure 3-9: Anchor Bolt/Shear Lug Pocket Template (a) Top View, (b) Bottom View

The assembled rebar cages were lifted using a crane, and lowered into the prepared concrete forms. The cage was adjusted until it was in the correct position. Next, 3 inch diameter PVC pipes were cut to length, then capped with duct tape. These PVC pipes were placed at the corners and tied into place against the top & bottom rebar mats using 11 inch long black plastic cable zip ties, See Figure 3-12. The zip ties were doubled together where necessary. These PVC pipes created holes through the base mat that corresponded to holes in the lab floor where steel rods secured the base mat to the floor.

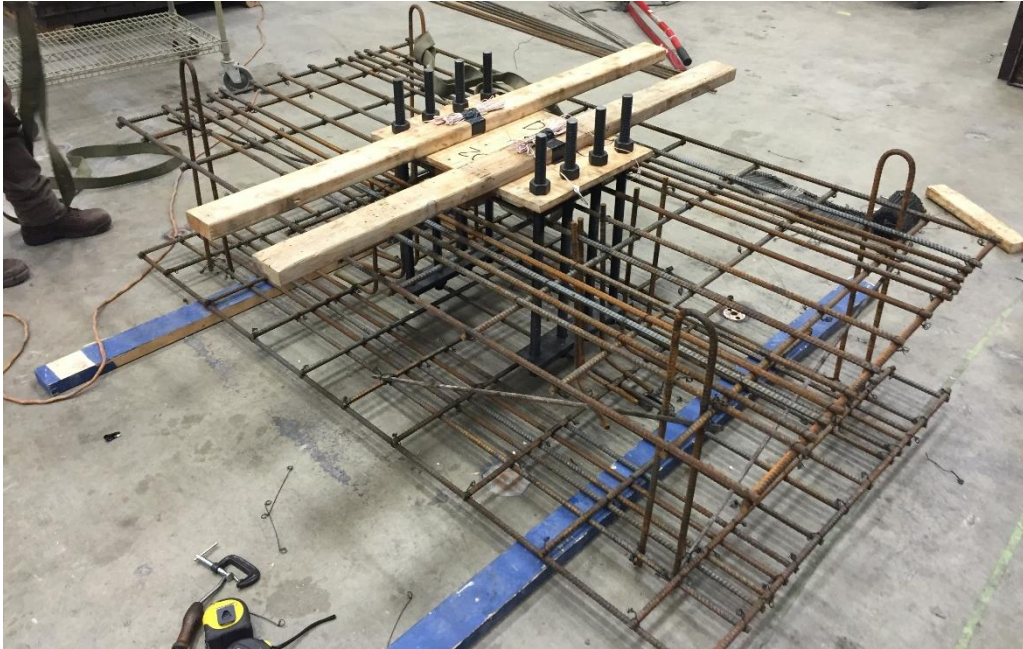


Figure 3-10: Fully Assembled Base Mat Rebar Cage



Figure 3-11: Concrete Symon Form Setup

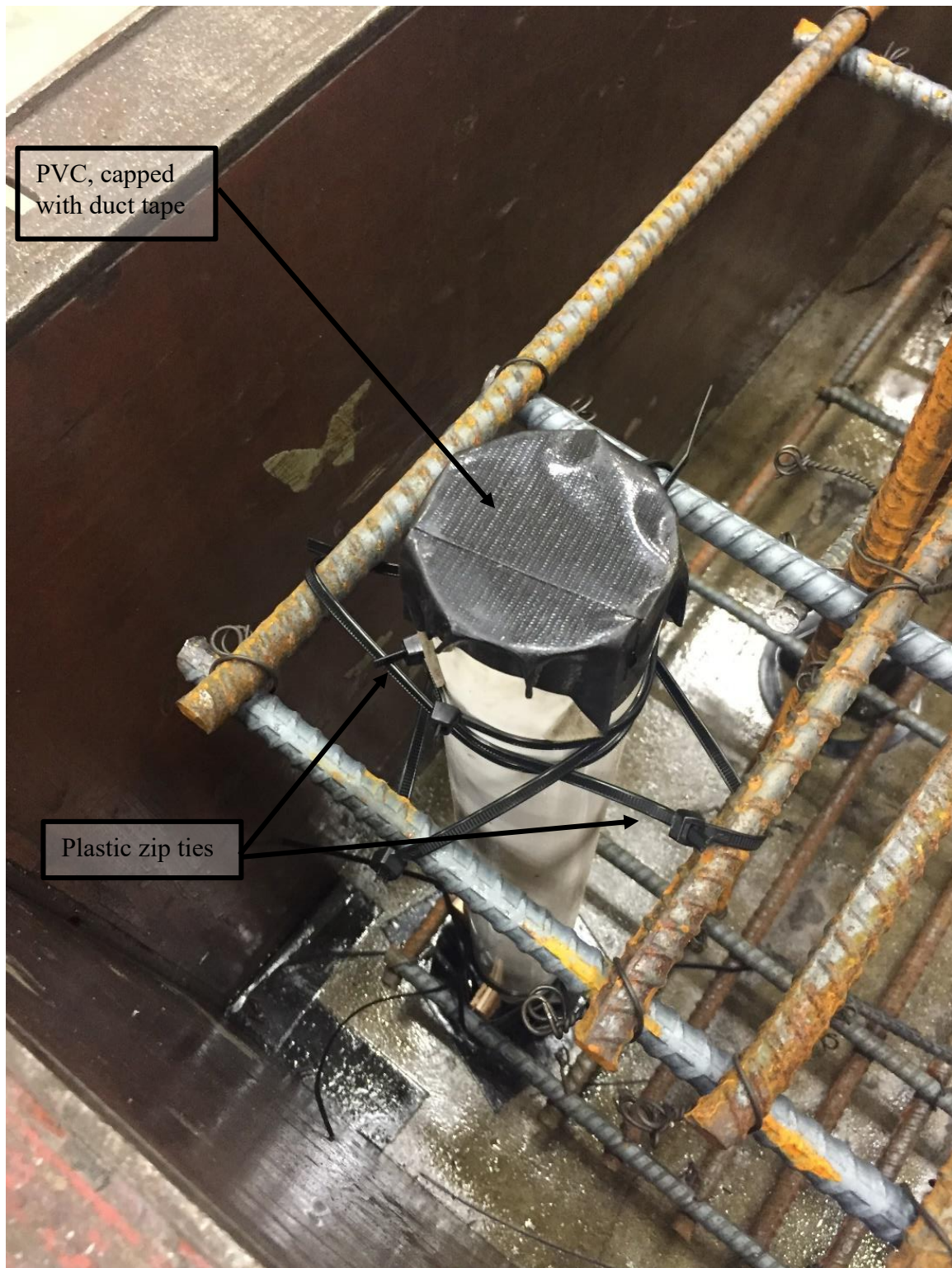


Figure 3-12: PVC in Place to Create Tie-Down Holes

To avoid excessive deflection on the long side where the two Symon forms were joined together under the pressure of the wet concrete, ¼ inch diameter steel rods or “pencil rods”, were placed through the form, and clamped on the outside of the forms. A total of three rods were placed at each of these locations, one on either side of the joint, and one directly on the joint itself. See Figure 3-13. Another pencil rod was placed perpendicular to these three rods, through the forms, in the long direction. This perpendicular pencil rod was most likely unnecessary as the form in the short direction did not have a joint and was strong enough to handle the force of the wet concrete without excessive deflection.

The final step in preparing the base mat for the concrete pour was double-checking dimensions of the form, the location of the anchor bolt/shear lug pocket template, and the height of the exposed anchor rods. The 2x4s holding that template in place were clamped to the edges of the concrete form.

The concrete for the base mats was mixed and delivered by Geneva Rock Products, Inc, out of Salt Lake City, Utah. The 17 yd³ of concrete was brought in two mixer trucks, spaced one hour apart. See the appendix for the delivery receipt with the mix design. The concrete was poured in two, 1 foot lifts. After each lift, an electrical concrete vibrator, or “stinger”, was used to consolidate the concrete, inserted at approximately 1 foot on center throughout the entire mat. A 5/8 inch diameter tamping rod was used underneath the anchor bolt template to ensure that concrete filled all of the voids underneath the template completely. The top was finished immediately after pouring the concrete by hand using trowels. See Figure 3-14 for the pouring process.

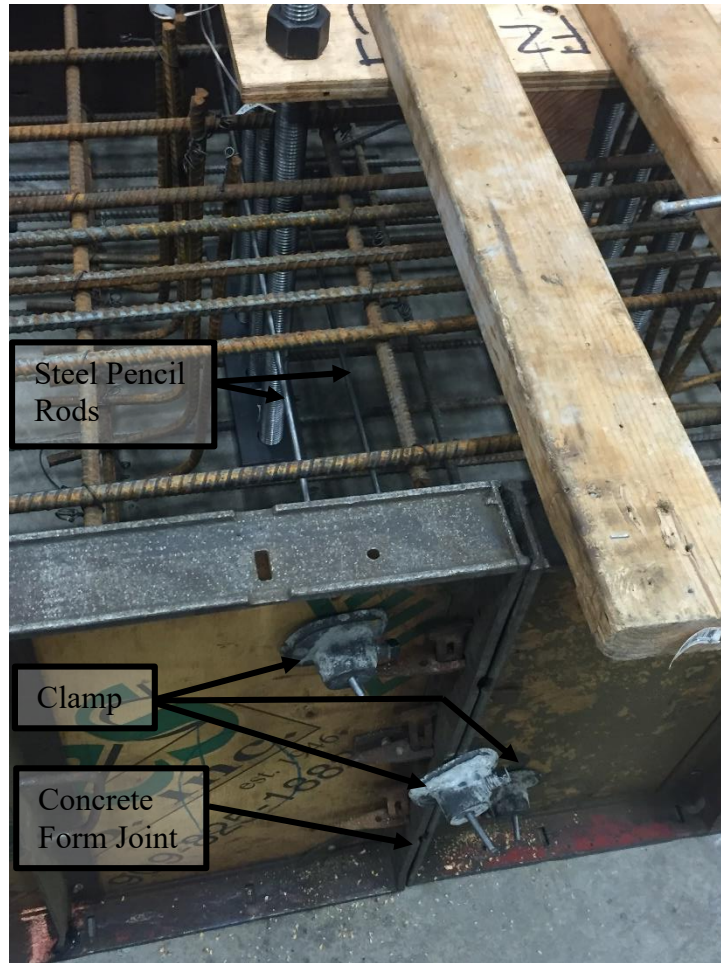


Figure 3-13: Steel Pencil Rods in Place to Hold the Sides of the Concrete Form

The base mat was allowed to cure overnight. See Figure 3-15. After that time, the wooden anchor bolt template was removed, to reveal the anchor bolts and the shear key pocket. See Figure 3-16.



Figure 3-14: Base Mat Concrete Pour



Figure 3-15: Completed Base Mat Pour



Figure 3-16: Exposed Anchor Bolts and Shear Key Pocket

3.4.2 Top Mat Construction & Column Installation

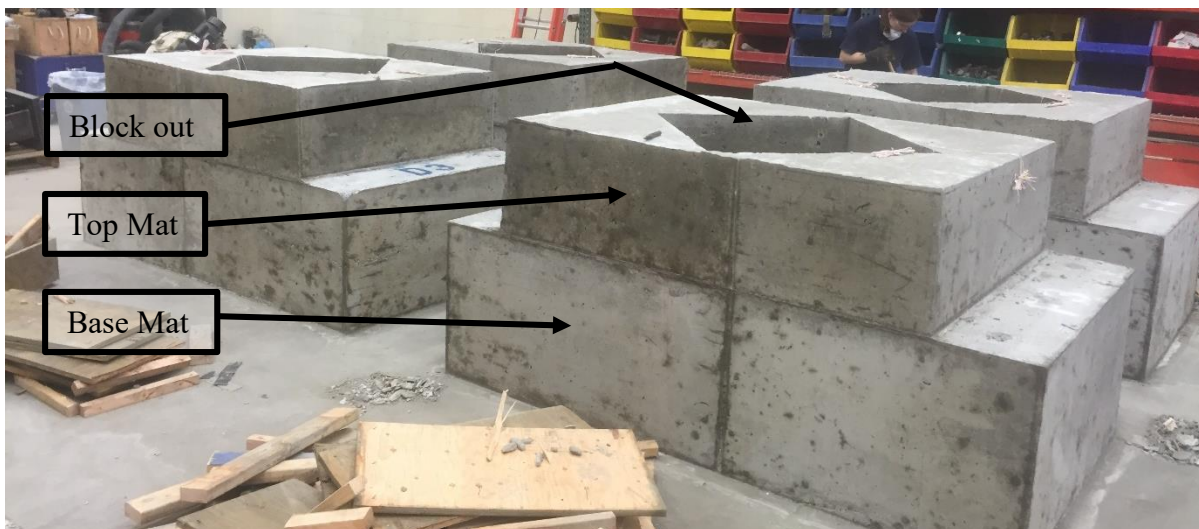


Figure 3-17: Finished Top Mat

Next, the form work for the upper floor slab was prepared, see Figure 3-17 for the finished specimen. Additional Symon forms were placed directly atop the base mat forms. 1ft tall forms were used for specimen D2 and F2, and 2ft tall forms were used for specimens D3, D4, F3, F4. A box was constructed using $\frac{3}{4}$ inch thick plywood to form the block out void, and was internally reinforced by 2x4s. This box was tied into place to the protruding anchor rods to ensure that, while pouring the wet concrete, it would not shift or move. The rebar mat for the floor slab was then set into place. For the shorter (8 inch) floor mat, the rebar mat was held at the correct height (3 inches of clear space below the top of the concrete) using small standees. For the taller (16 inch) floor mat, pencil rods were strung through the slab and clamped on either side of the formwork. The rebar mat was placed atop, then tied to these pencil rods, again at 3 inches below the top of the concrete. A plywood lid was placed atop the block out during concrete pouring to ensure the space remained free of any wet concrete. Concrete form release was applied to the sides of the formwork and the plywood box, taking care that the top surface of the base mat remained clean. See Figure 3-18 for the top floor mat preparations.

The concrete for the top floor mat was again mixed and delivered by Geneva Rock Products, Inc. This time, only a single mixer truck was needed. The 8 inch mat was poured in a single lift, while the 16 inch mats were poured in two equal lifts. For each lift, the electric concrete vibrator was used to consolidate the concrete, using similar methods as used in the base mat. The top of the concrete was finished using the same method used for the base mat. See Figure 3-19 for the concrete pour of the top floor mat.



(a)

(b)

Figure 3-18: Top Floor Mat Preparations (a) 8 inch Floor Slab, (b) 16 inch Floor Slab



(a)

(b)

Figure 3-19: (a) First Lift Complete for the Concrete Pouring of an 16 inch Top Floor Mat, (b) Completed Concrete Pouring for a 16 inch Top Mat

The top floor mat was allowed to cure overnight, after which all the concrete forms were removed, as well as the plywood block out forms. See Figure 3-20.



Figure 3-20: (a) 8 inch Top Floor Mat Specimen with Concrete Forms Removed (b) Close up of Block out for a 16 inch Top Floor Mat with Forms Removed

To prepare for the placement of the column, leveling nuts were placed on the 4 corner anchor bolts, with a small washer placed atop each leveling nut. The column/base plate assembly was then lowered into place on the anchor bolts, using the lab's overhead crane. Since oversized holes were used on the base plate, care was taken to ensure that the column was positioned and oriented appropriately. Care was taken to be sure that the anchor bolts didn't bear on the edge of the base plate hole, ensuring that for small deflections no lateral load was resisted by the anchor

bolts (see Figure 3-21(b)). The leveling nuts were used to ensure the column was plumb, then the heavy duty washers and nuts were placed on all anchor bolts above the base plate, securing the column in place, see Figure 3-21. The bolts were finger tightened first, then additionally tightened by hand using an 18 in. wrench and the full effort of one person.

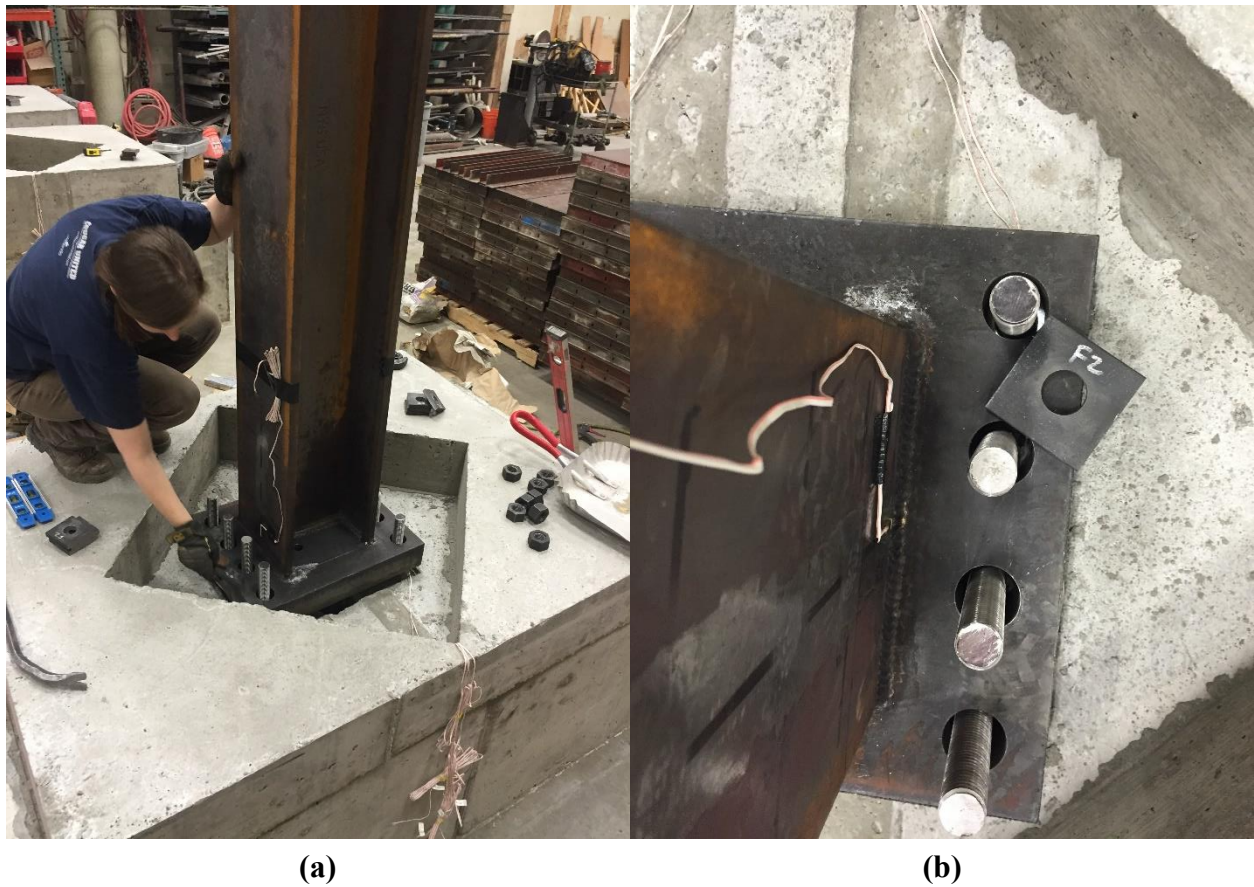


Figure 3-21: (a) Column Placement and Adjusting, (b) Anchor Bolts

The grout underneath the column base plate was added several days after the concrete pour. A small form was built out of wood 2x4s to surround the column base plate. Since the top surface of the concrete was not perfectly smooth, modeling clay was placed on the internal bottom corner of the form to ensure that the grout would not leak through below the 2x4s. See Figure 3-22.

The grout used was a high-strength structural non-shrink construction grout, made explicitly for column base applications (meets ASTM standard C 1107). The grout was produced by Sakrete, and came in 50 pound bags. To get the desired consistency, 1.1-1.2 gallons (9.18-10.01 lb) of clean water was added per bag of grout. For the first specimen (F1) the grout was mixed in a wheelbarrow using a shovel and hoe. The rest of the grout was mixed using a small electric 1.75 ft³ mixer, running for 5-7 minutes.

The grout was added via a funnel directing material into small grout access holes on either side of the column web in the column base plate. 5/8 inch diameter tamping rods were used to force the grout around the shear key, and under the entire base plate. Material was added, then tamped with the rod until material was observed coming up out of the opposite grout hole and out all sides of the base plate. Note that for the six specimens in a block out, the process was similar with the exception that a 2x4 form was not created. Instead the grout was allowed to simply fill up the bottom of the block out as required to ensure the grout filled all voids underneath the base plate. After the grout was allowed to cure overnight, the forms were removed. See Figure 3-23 for an example of the finished grout.



Figure 3-22: Column Base Prepped for Grout Pour



Figure 3-23: Finished Grout for Specimen D2

3.4.3 Block out Construction

Due to the relatively small amount of concrete needed for the block out, it was designed and mixed in-house, rather than delivered by a mixer truck. It was important that the quality and strength of the block out concrete be as consistent as possible between the specimens, so care was taken that the material quantities and method of mixing them remained consistent between pours. See Table 3-4 for the mix design, and Table 3-5 for the mixing procedure that was followed.

Table 3-4: Concrete Mix Design for Block Out Concrete

Specimen			D2	D3	D4	F2	F3	F4
Quantity	ft ³	27	5.12	10.24	10.24	5.12	10.24	10.24
	yd ³	1	0.190	0.379	0.379	0.190	0.379	0.379
Water	lbs	298	56.5	113.0	113.0	56.5	113.0	113.0
Cement	lbs	596	113.0	225.9	225.9	113.0	225.9	225.9
Coarse Agg.	lbs	1598	302.9	605.8	605.8	302.9	605.8	605.8
Fine Agg.	lbs	1228	232.8	465.5	465.5	232.8	465.5	465.5
Total	lbs	3720	705.1	1410.2	1410.2	705.1	1410.2	1410.2

An electric concrete mixer was used to mix the ingredients together. The mixer had a maximum concrete capacity of 0.2 yd³, so for the two smaller block outs (Specimens D2, and F2), only one batch was required. For the larger block outs (Specimens D3, D4, F3, & F4), the concrete had to be mixed in two batches. To ensure the two batches were done as quickly as possible, the material was measured out before hand in buckets, see Figure 3-24. Note that this

picture shows only aggregates measured out, but the water and cement were also pre-measured into buckets. The cement used was a Portland Cement (Type I, II, V) produced by Holcimm, and came in 92.6 lb bags

Table 3-5: Procedure Used to Mix Block Out Concrete

Step	Material Added	Quantity		Time mixed
1	Course Aggregate	All	302.9 lbs	1:00
	Cement	All	113.0 lbs	
	Water	1/4	14.1 lbs	
2	Fine Aggregate	All	232.8 lbs	2:00
	Water	1/4	14.1 lbs	
3	Water	1/4	14.1 lbs	4:00
4	<i>check slump</i>			
5	Water	1/8	7.1 lbs	3:00
6	<i>check slump</i>			
7	Water	1/32	1.8 lbs	1:00
8	<i>Repeat steps 6-7 until desired slump achieved</i>			

For each batch made, the concrete was transferred to a tilting bucket attached to a forklift. The four specimens with larger block outs required two batches; the first batch was poured into the tilting bucket while the second batch was mixed. The second batch was also poured into the bucket, then the entire quantity was poured all at once into the block out. See Figure 3-25.



Figure 3-24: (a) Electric Mixer Used to Mix Concrete in 0.2 yd³ Batches, (b) Material Measured out in Buckets

Note that other than cleaning out of the interior of the block out of dust and debris, no other preparations were done to the block out. The block out concrete was poured directly against the top floor mat concrete, and the top was finished using the identical method used on the base and top mat. See Figure 3-26 for the block out concrete pour.

See Figure 3-27 through Figure 3-30 for pictures of the finished and cleaned-up specimens.

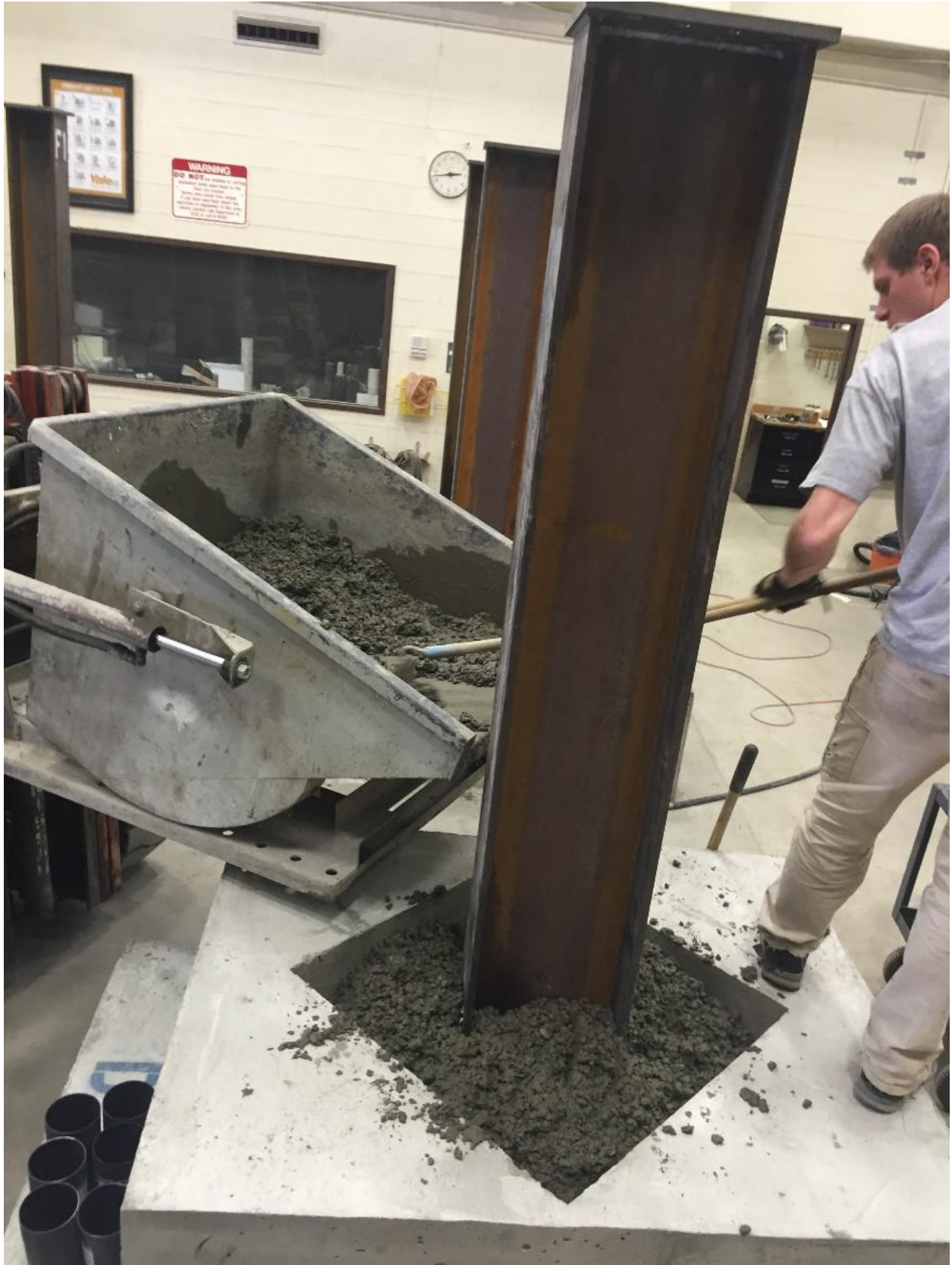


Figure 3-25: Block Out Concrete Placement



Figure 3-26: Placed Block Out Concrete



Figure 3-27: Finished Specimen D1, No Block Out



Figure 3-28: Finished Specimen F2, 8 inch Block Out



Figure 3-29: Finished Specimen F3, 16 inch Block Out

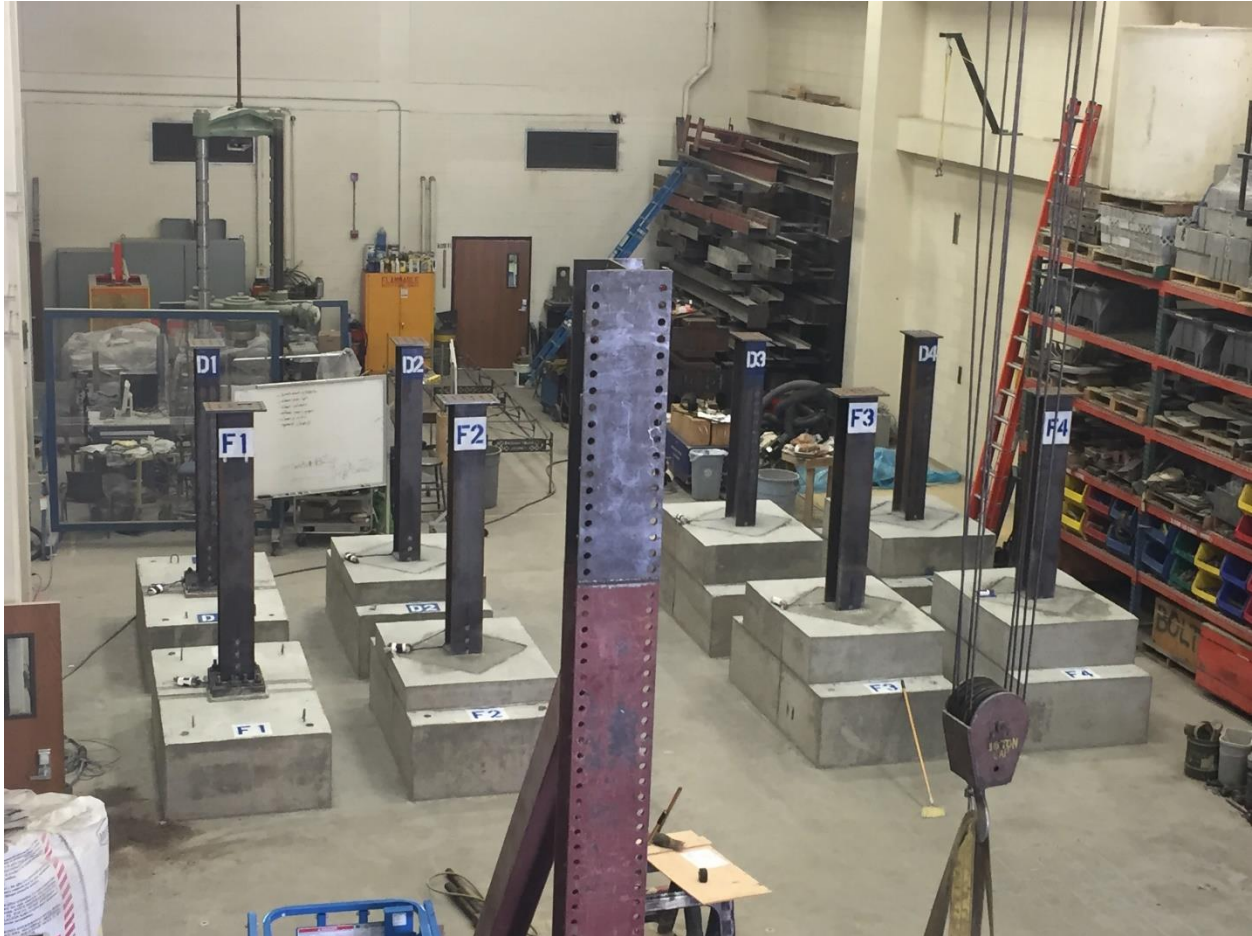


Figure 3-30: Bird's-Eye View of all Completed Specimens

3.4.4 Specimen Placement & Test Setup

Figure 3-31 shows a specimen completed and ready for testing.

The finished specimen was lifted and moved into place using the overhead lab crane, Figure 3-32. The lift points on specimens D1 & F1 were the protruding #4 bent rebar. These corresponding #4 bars had to be removed from the remainder of the specimens when the top mats were poured, as they were installed in the incorrect locations.

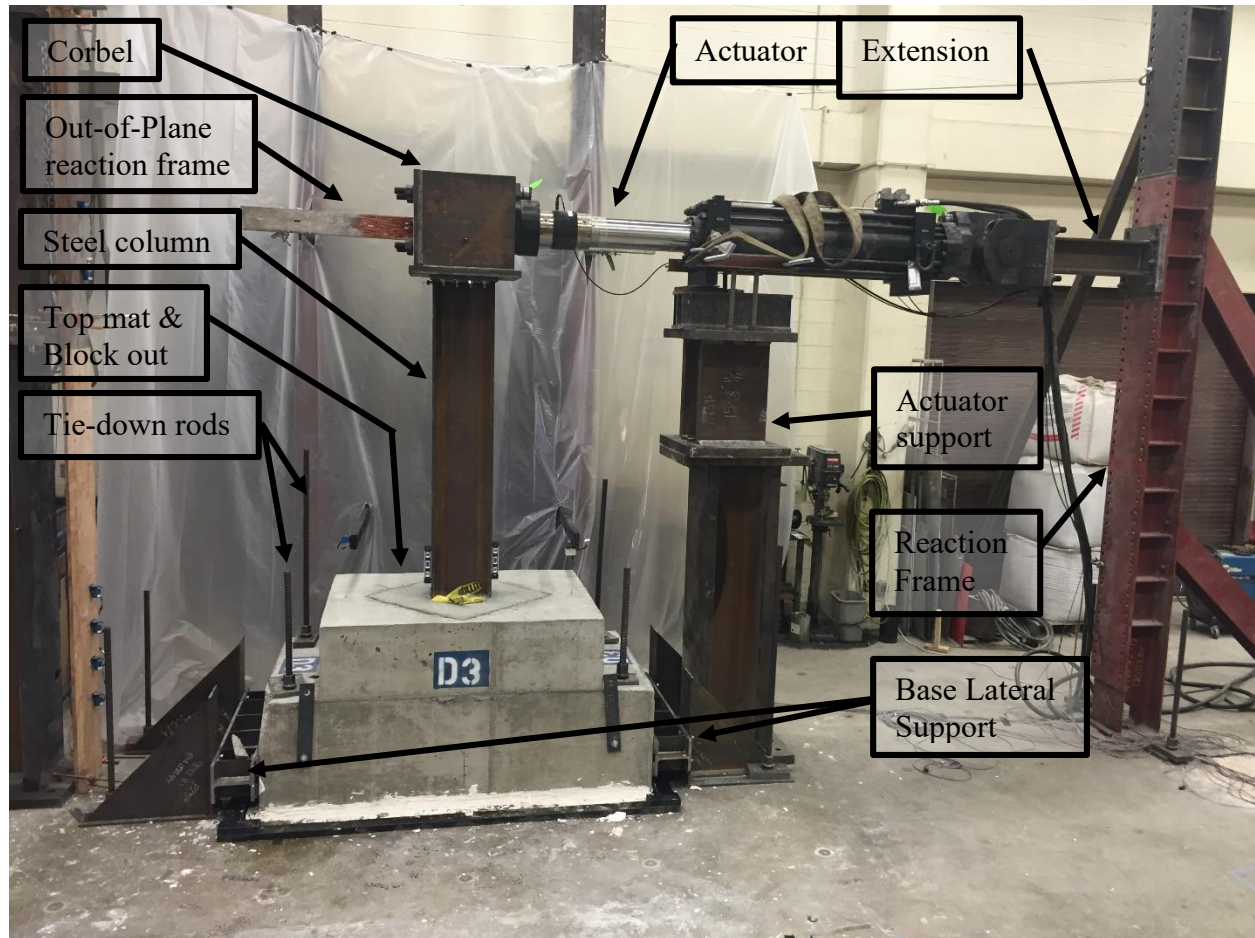


Figure 3-31: Specimen in Place and Ready for Testing

As such, lift points for these specimens were created after the concrete was poured. Four holes were drilled into the side of the base mat for $\frac{3}{4}$ inch x 7 inch long post-installed wedge anchors (Trubolt, by Redhead). These were embedded 4-5 inches into the hole, and used to bolt a 15 inch x 3 inch x $\frac{1}{2}$ inch thick steel plate to the side of the base mat. This plate had a $\frac{13}{16}$ inch diameter hole (for the wedge anchor) drilled into one end, and a 1 $\frac{1}{2}$ inch diameter hold (for a clevis) drilled into the other end. This plate provided a pick point for the crane, see Figure 3-33. This method worked well, but care was taken to check the anchor bolt after testing each

specimen: cracking in the base mat on one specimen caused one of the anchor bolts to lose its tensile capacity. The bolts were oriented so that they supported shear loads only, so they could still be used if cracks developed in the base mat during testing.

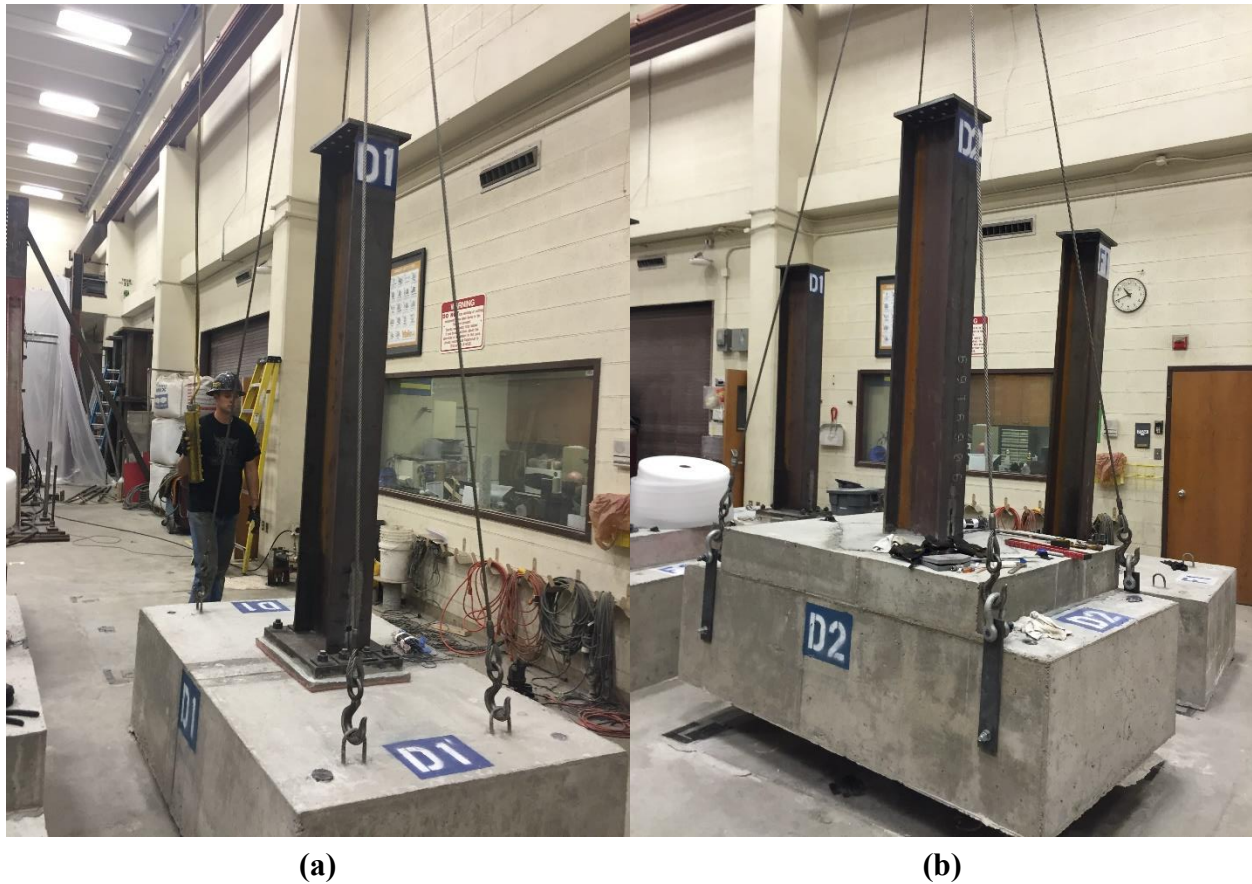


Figure 3-32: Moving Specimens Using the Lab Overhead Crane Using (a) Original Bent-Rebar Pick Points, and (b) Post-Installed Pick Points

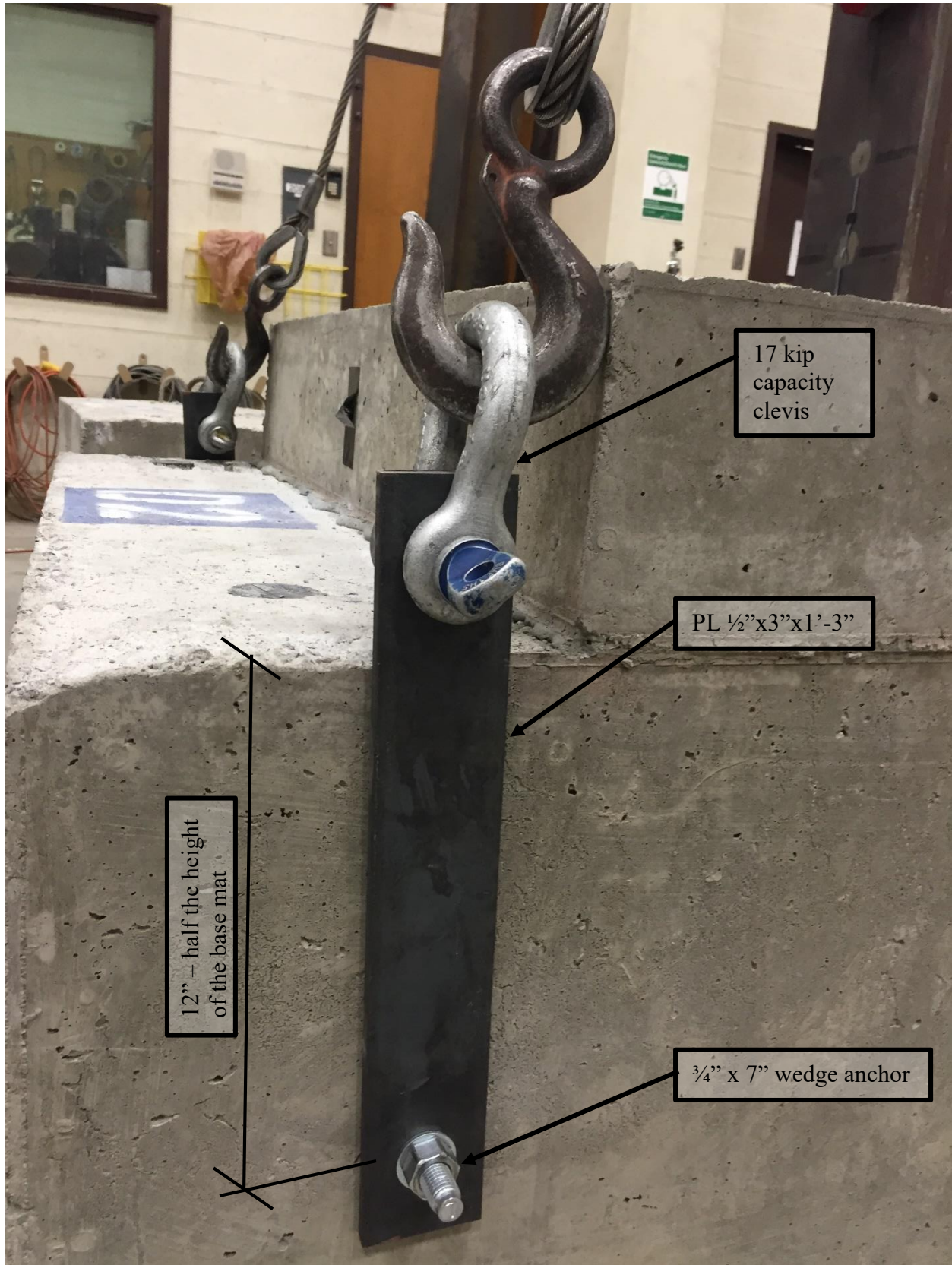


Figure 3-33: Post-Installed Crane Pick Points on Specimens D2, D3, D4, F2, F3, & F4

The specimen was set into place, with shims used to make the specimen level and ensure that it rested in the correct position on the floor. Then it was lifted back up off the ground to access the floor, which was then coated in concrete form release. A layer of hydrocal was placed between the lab floor and the concrete base. Hydrocal is a very low-viscosity cementitious mixture that cures and develops strength extremely fast. It was placed in between the lab floor and the base of the specimen to ensure proper bearing along the entire surface. To prevent the hydrocal mixture from spilling into the anchor holes and the basement beneath, small donuts were made using modeling clay, that formed a dam around the anchor holes.

The hydrocal comes in 100 lb bags, labeled “Hydrocal Gypsum Cement” manufactured by USG, and was mixed by hand in buckets. Each bucket contained the following ingredients: 32.0 lbs of hydrocal, and 12.5 lbs of clean water. The hydrocal was added to the water and allowed to sit and hydrate for 60 seconds, after which it was vigorously mixed using a paint-paddle attached to a cordless drill, for 90 seconds. It was then immediately poured underneath the concrete onto the floor, into an area framed out using 2x4s duct-taped to the ground (Figure 3-34).

The specimen was immediately lowered back down onto the floor covered with hydrocal, ensuring that the hydrocal mixture was forced out on all sides as the weight of the specimen rested onto the floor. The first specimen tested, F1 used four buckets, while the remaining seven each used only three buckets.

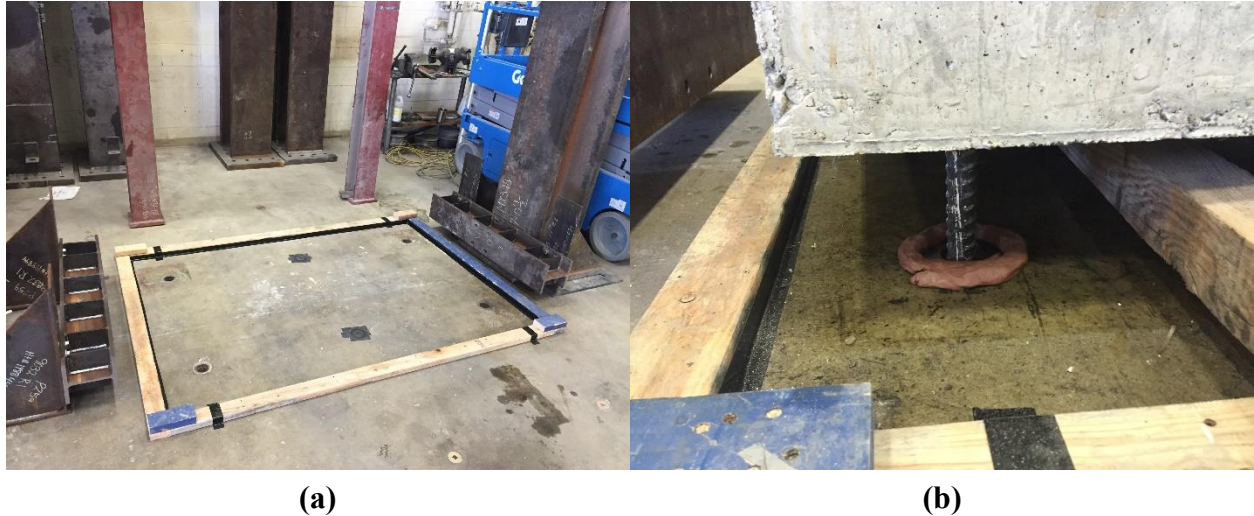


Figure 3-34: Base Preparations, (a) 2x4 Frame Built to Contain Hydrocal Mixture, (b) Floor Prepared with Form Release and Clay Donuts

After two hours, the hydrocal develops over 6000 psi strength, so at that time the four anchors at the specimen corners were each post-tensioned to approximately 50 kips of tension. The base lateral restraints were also pushed tight up the specimen base, and their respective anchor rods were also post-tensioned to the same force to hold them in place. The corbel was then attached to the top of the column using sixteen – $\frac{3}{4}$ inch x 3 $\frac{1}{2}$ inch bolts. Due to the nature of the connection, it was critical that this connection remain tight so that during high loads from the actuator, the corbel would not slip against the column. To accomplish this, the bolts were post-tensioned with an impact wrench using direct tension indicator (DTI) washers to ensure the bolts were tensioned sufficiently to create a slip-critical connection. These bolts were re-used for a maximum of three tests, then replaced with new bolts.



Figure 3-35: Corbel-to-Column Connection, Seen from Above with Actuator Arm Ready to Move into Place

The actuator arm was extended until it made contact with the back face of the corbel, then it was bolted directly to the corbel using four, 2 inch diameter bolts. A small steel extension piece was manufactured that connected the back end of the actuator to the reaction frame, so that when the actuator arm was bolted to the corbel, the arm was at its approximate mid-span allowing the actuator to move freely in both directions. The actuator was then adjusted as needed so that it reported zero force resistance from the specimen.

The corbel was braced out-of-plane using a reaction frame, see Figure 3-36. A steel box was fabricated to fit around a rail, and to restrict movement perpendicular to the actuator movement path. This box allowed very little clearance on the sides (1/8 inch -1/4 inch), but allowed for plenty of clearance on the top and bottom (>6 inches). The rail was liberally greased to reduce the friction between the box and the rail.

The rail was attached to two arms that were adjustable, to ensure the rail was parallel to the actuator travel path. These adjustable arms, were in turn attached to W8 columns bolted to the floor and laterally braced against movement. Care was taken before the tests began to get the rail as close to possible to parallel. During testing and during the very high deflection cycles, testing was occasionally paused to make adjustments to the adjustable arms.

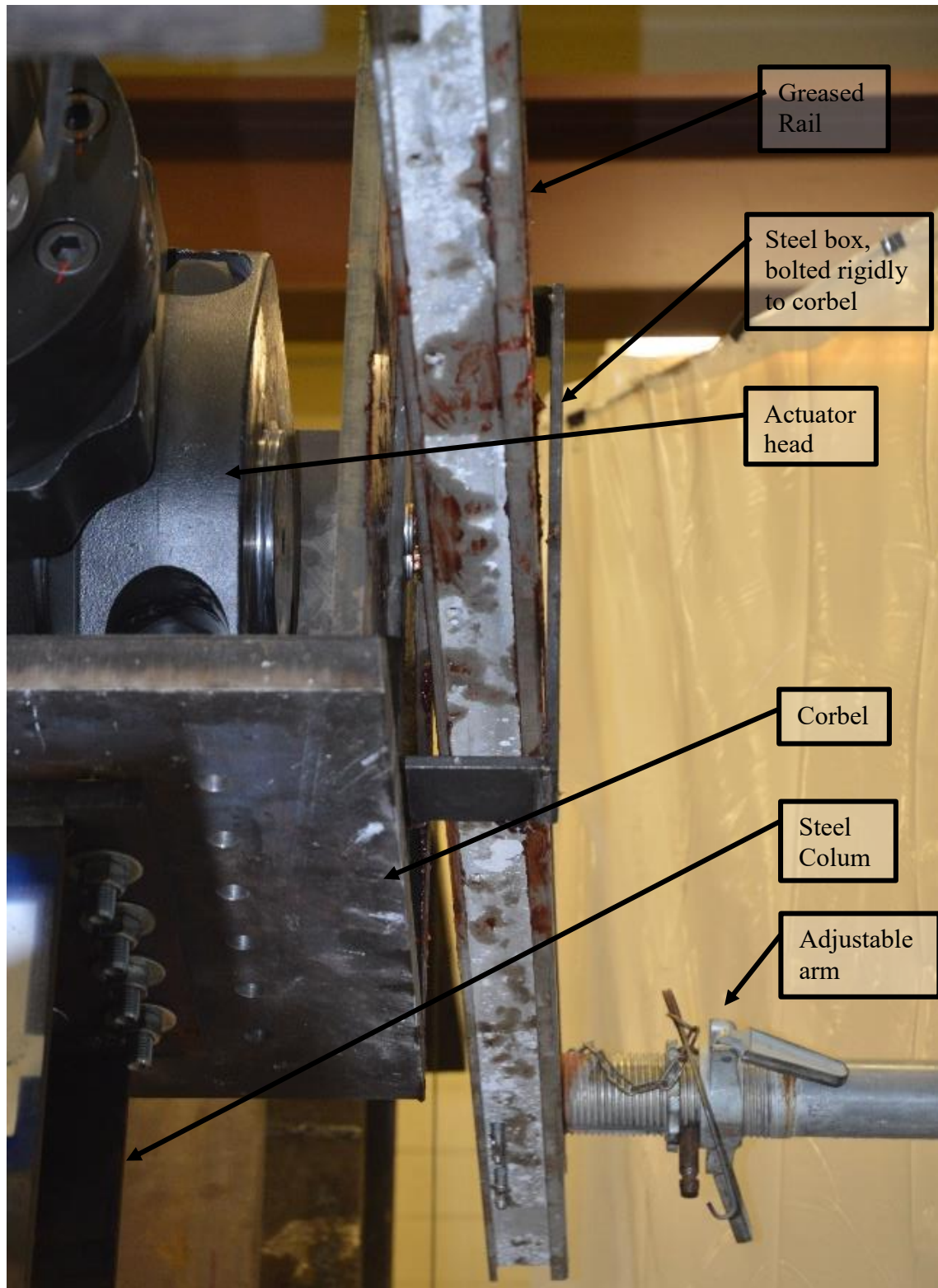


Figure 3-36: Out-of-Plane Reaction Frame

3.5 Testing Equipment and Instrumentation

3.5.1 Actuator

The actuator used to produce the loads and displacements in the column was a hydraulic actuator, model number 201.70, manufactured by MTS Systems Corporation, headquartered in Eden Prairie, Minnesota. See (Appendix C.7 Actuator Schematic) for a drawing of this actuator. The rated capacity of the actuator was 216 kip (tension) and 328 kips (compression). It had a total stroke length of 40 inches, 20 inches in each direction. The program used to control the actuator was called “MTS TestStar II_m”.

3.5.2 String Potentiometers

Deflections at various locations were measured using string potentiometers (string pots). These were read using an NI-9206 Analog Input Fuel Cell module. String pots were placed at identical locations on the different samples, to allow for useful comparisons between tests.

The string pots consisted of an actual unit that was attached to a stable object (Figure 3-38) opposite the location on the test specimen where the deflections would be measured. The string pot then had a length of fishing line, made from braided Dyneema fiber (for its no-stretch characteristics) made by SpyderWire. This line was then attached to the specimen at desired locations. The movement of the line in the string pot unit is what measured the deflection of the test specimen.

The lines attached to steel were done so using magnets. The string pots attached to concrete were done so by drilling small holes into the concrete and using construction adhesive to secure small eye-hooks. Refer to Figure 3-37 and Figure 3-38 for pictures of these attachment

methods. See Figure 3-39 for the string pot locations and names. Note that all measurements were taken at the centerline of the specimen. During testing, the program recorded a data point for each string pot five times per second.



Figure 3-37: String Potentiometer Attachment Methods into (a) Steel Locations, and (b) Concrete Locations



Figure 3-38: String Potentiometers Attached Onto Wooden Plank

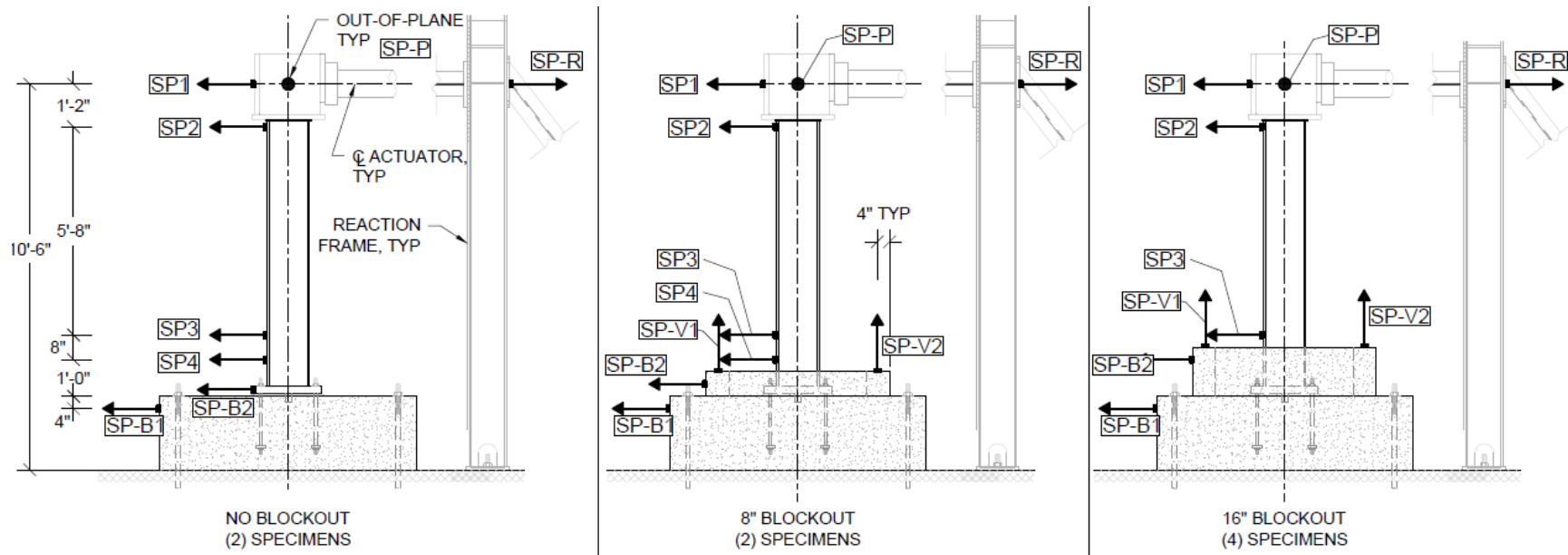


Figure 3-39: String Potentiometer Locations and Names

3.5.3 Strain Gages

Strains at various locations on the steel were measured using strain gages manufactured by Tokyo Sokki Kenkyujo Co., Ltd. Two types of strain gages were used. Gages at locations not embedded in the concrete were type: FLA-6-11-5LT, with a gauge length of 6mm, a gauge factor of $2.12 \pm 1\%$, a gauge resistance of $120 \pm 0.5 \Omega$, and a lead wire length of 5m. The gages at locations embedded in concrete were waterproof type: WFLA-6-11-5LT, with a gauge length of 6mm, a gauge factor of $2.12 \pm 1\%$, a gauge resistance of $120 \pm 0.5 \Omega$, and a lead wire length of 5m. The leads were connected to the main block, NI cDAQ-9172. The data acquisition system used was made by National Instruments, and was analyzed using LabView 2013 software.

The strain gages require a flat, clean surface to function properly. Where gages were placed on the column steel, the steel was prepared by grinding off the outer layer (mill steel), then was sanded using increasingly fine sand paper: 80, 200, and 440 grit. It was then wiped clean with acetone. The gage itself was attached to the steel using special adhesive manufactured by the same company that produced the gages. It was general purpose type CN adhesive, composed of cyanoacrylate. The adhesive was attached to the gage, and the gage was held in place using “thumb pressure” on the steel for 60 seconds, after which the adhesive had cured.

Attaching the gages to the anchor bolts required that the threads be ground away at the desired location to create a flat surface. To minimize the strength reduction to the bolt caused by reducing the steel area of the shaft, care was taken to grind off only enough of the threads for adhesion of the gages. It is noted that even with this preparation, when the bolts did break during testing, they (without exception) fractured at these locations, indicating that this preparation did indeed create a weak point in the bolts. Like the column steel, this flat surface was sanded with

80, 200, and 440 grit sandpaper, then cleaned with acetone. It was attached to the bolt steel using similar adhesive and procedure as was described above for the column steel. Refer to Figure 3-40 for a picture of an anchor bolt prepped for a strain gage. During testing, the computer program recorded a data point (in micro strain) for each instrument five times per second.

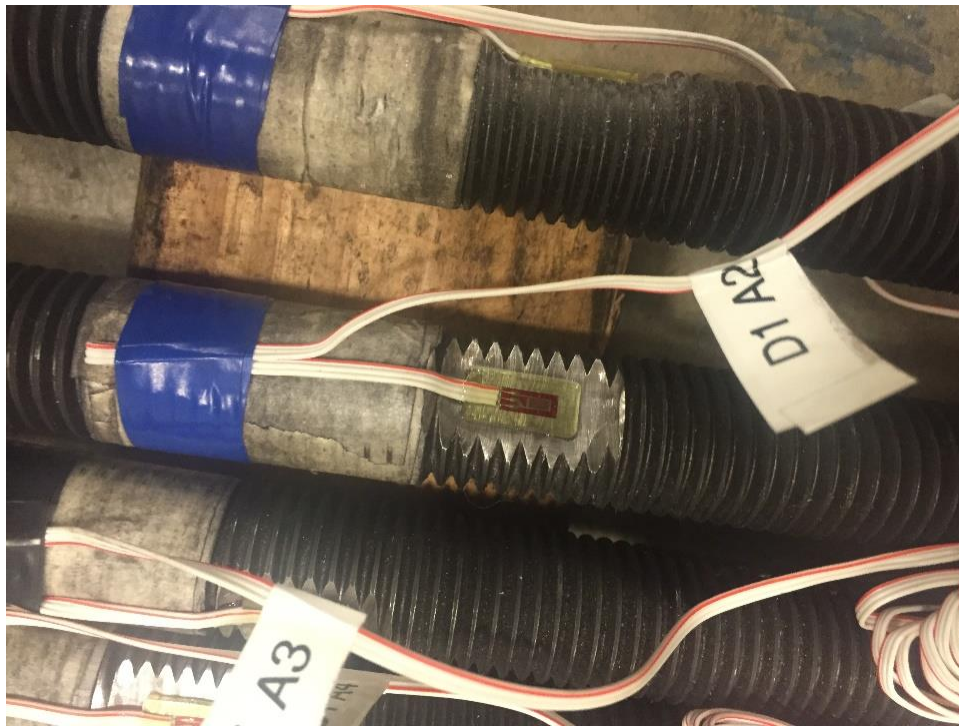


Figure 3-40: Threaded Rod Anchor Bolt Prepared for Strain Gage

Twelve total strain gages were attached to each test specimen, four on the anchor bolts and eight on the column itself. Locations were kept consistent for the different specimens to allow for useful comparison of the data. For the two test specimens with only four anchor bolts, a gage

was attached to each bolt. For those specimens having 8 anchor bolts, the gages were placed on alternating interior & exterior anchor bolts. Refer to Figure 3-41 for the strain gage locations.

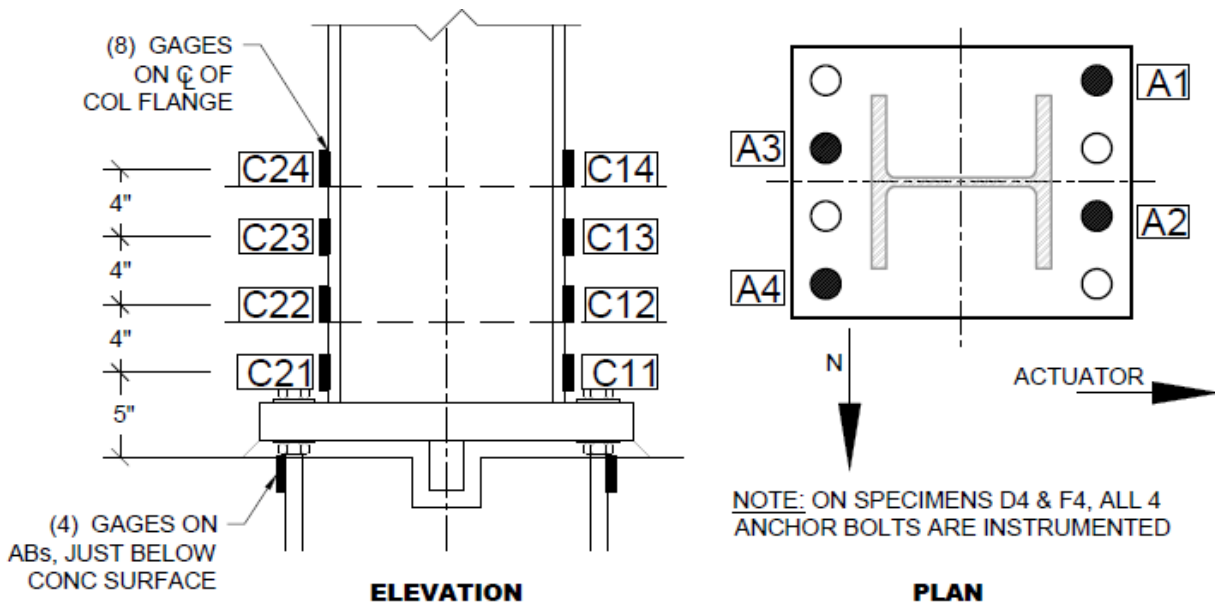


Figure 3-41: Strain Gage Locations and Names, Typical for Each Specimen

Gages were placed with redundancy in mind, accounting for the possibility that some gages could fail. The gages or their lead wires could become inadvertently damaged during construction, concrete placement, or specimen movement and placement. Therefore, immediately before testing a specimen, each strain gage was tested with a resistance meter to determine if it was functioning and sending data. Table 3-6 shows which gages were functioning and which were non-functioning (marked “BAD”).

Table 3-6: Report of Functioning and Non-Functioning Strain Gages

Strain Gages		Specimen							
		D1	D2	D3	D4	F1	F2	F3	F4
Column	C11	-	-	-	BAD	-	-	-	-
	C12	-	-	-	-	-	-	-	-
	C13	-	-	-	-	-	-	-	-
	C14	-	-	-	-	-	-	-	-
	C21	-	-	-	-	-	-	-	-
	C22	-	-	-	-	-	BAD	-	-
	C23	-	-	BAD	-	-	-	-	-
	C24	-	-	-	-	-	-	-	-
Anchor Bolts	A1	BAD	-	-	-	-	-	-	-
	A2	BAD	BAD	-	-	-	-	-	-
	A3	BAD	-	BAD	-	BAD	-	BAD	-
	A4	BAD	BAD	BAD	-	-	-	-	-

3.6 Loading Protocol

The loading protocol was based on story drift, translated into a displacement at the top of the column (CL of the actuator). Translating story drift into a displacement at the actuator multiplies the story drift by the floor height, per EQ (3.6.1).

$$\Delta_{actuator} = h_{story} \cdot \%_{drift} \quad (3.6.1)$$

For this test, the floor height was taken as the distance from the top of the base mat to the centerline of the actuator, and was kept constant for every test. For example, the first cycle's actuator distance was calculated using EQ (3.6.2).

$$\Delta_{actuator} = (8.5 \text{ ft}) \cdot (0.00375) = 0.3825 \text{ in} \quad (3.6.2)$$

The actuator was programmed to exert the force necessary to obtain the desired displacement. The loading protocol used is listed below in Table 3-7. A graphical representation of the loading protocol is shown in Figure 3-42. All specimens were loaded according to this protocol until the maximum story drift was achieved, or until enough anchor bolts had fractured to make the specimen unstable.

Table 3-7: Loading Protocol

Deflection (% Story Drift)	# of Cycles	Actuator Movement	Movement Rate		Time per Segment		Total Time
		(in)	(in/min)	(in/sec)	(min)	(sec)	(min)
0.375 %	1	0.3825	0.300	0.0050	1.275	76.5	5.10
0.375 %	5	0.3825	1.500	0.025	0.255	15.3	5.10
0.5 %	6	0.510	1.500	0.025	0.340	20.4	8.16
0.75 %	6	0.765	3.00	0.05	0.255	15.3	6.12
1.0 %	4	1.020	3.00	0.05	0.340	20.4	5.44
1.5 %	2	1.530	6.00	0.10	0.255	15.3	2.04
2.0 %	2	2.040	6.00	0.10	0.340	20.4	2.72
3.0 %	2	3.060	12.0	0.20	0.255	15.3	2.04
4.0 %	2	4.080	12.0	0.20	0.340	20.4	2.72
5.0 %	2	5.100	12.0	0.20	0.425	25.5	3.40
6.0 %	2	6.120	12.0	0.20	0.510	30.6	4.08
7.0 %	2	7.140	24.0	0.40	0.298	17.9	2.38
8.0 %	2	8.160	24.0	0.40	0.340	20.4	2.72
9.0 %	2	9.180	24.0	0.40	0.383	23.0	3.06
10.0 %	2	10.200	24.0	0.40	0.425	25.5	3.40
11.0 %	2	11.220	24.0	0.40	0.468	28.1	3.74
Total Testing Time (min)							62.22

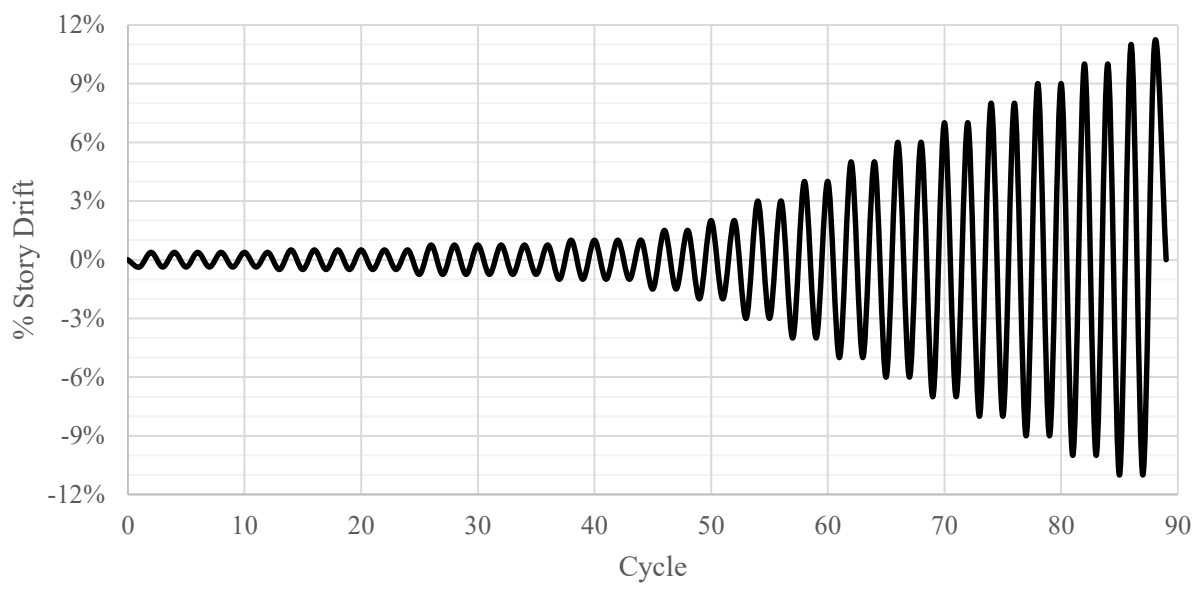


Figure 3-42: Loading Protocol - Graphical Representation

4 RESULTS

4.1 Material Tests

4.1.1 Concrete Tests

Slump tests were performed according to the procedures found in ASTM (C143 2015) “Standard Test Method for slump of hydraulic-cement concrete”. A slump test was performed for each truck that delivered concrete. For the block out concrete that was mixed in the lab, a slump test was performed for each 0.2 yd³ batch. The goal, when mixing the concrete, was to achieve a slump between 4 – 5 inches.

In addition to the slump test, concrete cylinders were made following the procedures of ASTM (C192 2015), “Standard practice for making and curing concrete test specimens in the laboratory”. The cylinders created were 4 inch diameter cylinders, 8 inches tall. A total of sixty-six concrete test cylinders were created.

For the base mat concrete, a total of three cylinders for each specimen were created that would be tested on the same day that the specimen itself was tested. An additional three cylinders were created from the base mat concrete that were used to test the 28-day strength.

For the top mat concrete, a total of three cylinders were made, and these were tested after 28 days.

For the block out concrete, a total of six cylinders per test specimen were created. three of these were tested after 28 days, and the other three were tested on the same day that the specimen was tested. For several of the test specimens, these occurred on the same day.

The cured concrete cylinders were tested in accordance with ASTM (C39 2001), “Standard Test Method for Compressive Strength of Cylindrical Concrete Specimens”. The design 28-day strength (f'_c) of all of the concrete used was 4000 psi. All of the concrete that was delivered by Geneva Rock consistently showed strength well above 5000 psi, and the concrete that was mixed in the lab consistently broke with strengths between 5500 psi and 6500 psi, with a few outliers above that range. See Table 4-1 through Table 4-3 for a summary of the test results.

Table 4-1: Summary of Concrete Cylinder Tests for the Base Mat

Specimen	Cylinder	Date Poured	Date Tested	Days	Force (lbs)	f'_c (psi)	f'_c ave (psi)
D1	D1-BM-1	Mon, 05/02/16	Tue, 06/07/16	36	68,340	5,438	5,534
	D1-BM-2				68,795	5,475	
	D1-BM-3				71,505	5,690	
D2	D2-BM-1	Mon, 05/02/16	Wed, 06/08/16	37	69,975	5,568	5,626
	D2-BM-2				71,215	5,667	
	D2-BM-3				70,890	5,641	
D3	D3-BM-1	Mon, 05/02/16	Thu, 06/09/16	38	73,115	5,818	5,678
	D3-BM-2				69,295	5,514	
	D3-BM-3				71,650	5,702	
D4	D4-BM-1	Mon, 05/02/16	Fri, 06/10/16	39	67,070	5,337	5,569
	D4-BM-2				71,755	5,710	
	D4-BM-3				71,115	5,659	

Table 4-1: Continued

Specimen	Cylinder	Date Poured	Date Tested	Days	Force (lbs)	f'_c (psi)	f'_c ave (psi)
F1	F1-BM-1	Mon, 05/02/16	Mon, 06/06/16	35	71,435	5,685	5,304
	F1-BM-2				66,550	5,296	
	F1-BM-3				61,970	4,931	
F2	F2-BM-1	Mon, 05/02/16	Tue, 06/14/16	43	70,870	5,640	5,775
	F2-BM-2				72,800	5,793	
	F2-BM-3				74,025	5,891	
F3	F3-BM-1	Mon, 05/02/16	Wed, 06/15/16	44	76,900	6,120	5,960
	F3-BM-2				74,430	5,923	
	F3-BM-3				73,345	5,837	
F4	F4-BM-1	Mon, 05/02/16	Thu, 06/16/16	45	72,140	5,741	5,894
	F4-BM-2				75,965	6,045	
	F4-BM-3				74,105	5,897	
ALL (28-day)	28-BM-1	Mon, 05/02/16	Tue, 05/31/16	29 *	69,225	5,509	5,451
	28-BM-2				65,525	5,214	
	28-BM-3				70,765	5,631	

** the 28th day fell on a national holiday, and the lab was closed, but the specimen was tested within the ± 20 hr time tolerance permitted in ASTM C39 section 7.3, thus still qualifies as "28-day strength".*

Table 4-2: Summary of Concrete Cylinder Tests for the Top Mat

Specimen	Cylinder	Date Poured	Date Tested	Days	Force (lbs)	f'_c (psi)	f'_c ave (psi)
ALL	28-TM-1	Mon, 05/09/16	Mon, 06/06/16	28	65,925	5,246	5,128
	28-TM-2				63,645	5,065	
	28-TM-3				63,740	5,072	

Table 4-3: Summary of Concrete Cylinder Tests for the Block Out

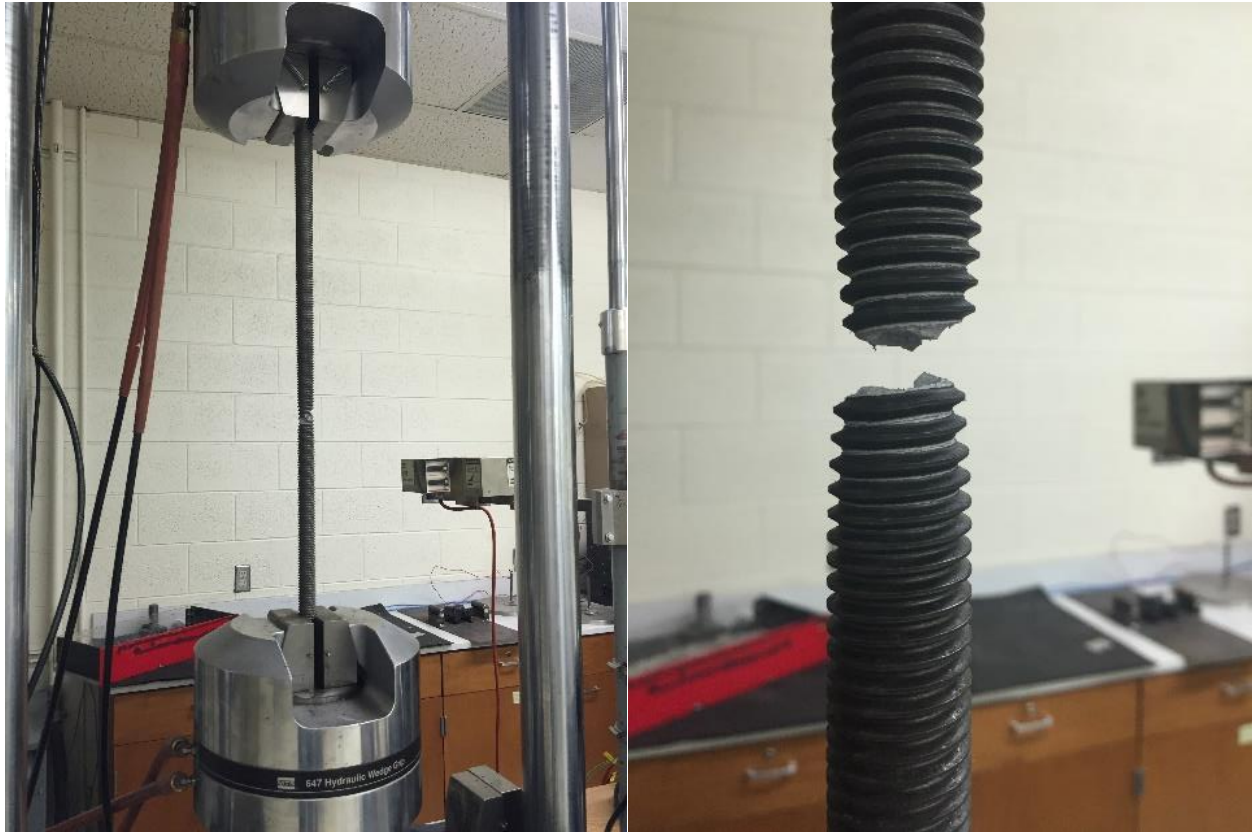
Specimen	Cylinder	Date Poured	Date Tested	Days	Force (lbs)	f_c (psi)	f_c ave (psi)
D2	D2-BO-1	Thu, 05/12/16	Thu, 06/09/16	28	74,260	5,909	5,559
	D2-BO-2				62,460	4,970	
	D2-BO-3				72,865	5,798	
	D2-BO-4	Thu, 05/12/16	Wed, 06/08/16	27	68,790	5,474	5,699
	D2-BO-5				73,595	5,857	
	D2-BO-6				72,455	5,766	
D3	D3-BO-1	Thu, 05/12/16	Thu, 06/09/16	28	69,165	5,504	5,716
	D3-BO-2				75,540	6,011	
	D3-BO-3				70,800	5,634	
	D3-BO-4	Thu, 05/12/16	Thu, 06/09/16	28	68,570	5,457	5,575
	D3-BO-5				74,680	5,943	
	D3-BO-6				66,905	5,324	
D4	D4-BO-1	Fri, 05/13/16	Fri, 06/10/16	28	81,050	6,450	6,362
	D4-BO-2				76,570	6,093	
	D4-BO-3				82,225	6,543	
	D4-BO-4	Fri, 05/13/16	Fri, 06/10/16	28	78,820	6,272	6,499
	D4-BO-5				79,410	6,319	
	D4-BO-6				86,760	6,904	
F2	F2-BO-1	Wed, 05/18/16	Wed, 06/15/16	28	72,970	5,807	6,213
	F2-BO-2				80,885	6,437	
	F2-BO-3				80,360	6,395	
	F2-BO-4	Wed, 05/18/16	Tue, 06/14/16	27	82,245	6,545	6,548
	F2-BO-5				82,775	6,587	
	F2-BO-6				81,830	6,512	
F3	F3-BO-1	Wed, 05/18/16	Wed, 06/15/16	28	71,590	5,697	5,717
	F3-BO-2				70,260	5,591	
	F3-BO-3				73,675	5,863	
	F3-BO-4	Wed, 05/18/16	Wed, 06/15/16	28	80,795	6,429	6,172
	F3-BO-5				73,875	5,879	
	F3-BO-6				78,025	6,209	
F4	F4-BO-1	Wed, 05/18/16	Wed, 06/15/16	28	88,275	7,025	6,966
	F4-BO-2				86,310	6,868	
	F4-BO-3				88,025	7,005	
	F4-BO-4	Wed, 05/18/16	Thu, 06/16/16	29	89,095	7,090	7,098
	F4-BO-5				86,935	6,918	
	F4-BO-6				91,550	7,285	

4.1.2 Steel Tests

Two sizes of anchor rods were used: 1 1/8 inch, and 1 inch diameters. The rods were fully threaded, and were composed of ASTM F1554 Gr. 36 steel. The material type was verified by the invoice sent along with the anchor rods. Since the anchor bolts played such a crucial role in the behavior of the connection, one extra rod of each size was obtained for testing to verify the material properties. A simple tensile test was performed on each rod (see Figure 4-1), and the results of the test are presented in Figure 4-2 and Figure 4-3.

There is some uncertainty from these tests regarding the modulus of elasticity, due to the testing procedure. The most accurate method of performing a tensile test on material is by using a prepared steel coupon, and measuring the deflection using an extensometer or strain gage on the steel itself. Since a steel coupon for the material was not available, the threaded steel rod itself was tested, and the deflection was measured from the testing machine itself. This method has been noted to produce results for the modulus of elasticity that are lower than what would be determined using a prepared coupon sample and the more sophisticated deflection instruments. The method used, however, more closely matched the conditions found in the test specimens, therefore the results gained were still used for analysis purposes.

The key information from these tensile tests is shown below in Table 4-4. The expected values are shown alongside the values obtained from testing. Very importantly, the expected values are what were used when designing the test specimens. The observed values for the yield stress of the material were approximately 40% greater than what was expected and used in design.



(a) (b)
Figure 4-1: Tensile Test on Threaded Anchor Rod

Table 4-4: Key Information from Tensile Tests

Rod DIA	Specimens	Steel Grade**	Expected*		Observed		E
			$f_{y_expected}$ (ksi)	$f_{u_expected}$ (ksi)	f_{y_tested} (ksi)	f_{u_tested} (ksi)	
1 in.	D1, D2, D3, D4	F1554 Gr 36	36	58-80	51.68	90.01	18000
1 1/8 in.	F1, F2, F3, F4	F1554 Gr 36	36	58-80	49.36	76.47	17400

*From AISC Steel Construction Manual, 14th Ed. Table 2-6

**As reported on the invoice from the company that the steel rods were ordered from: Fastenal

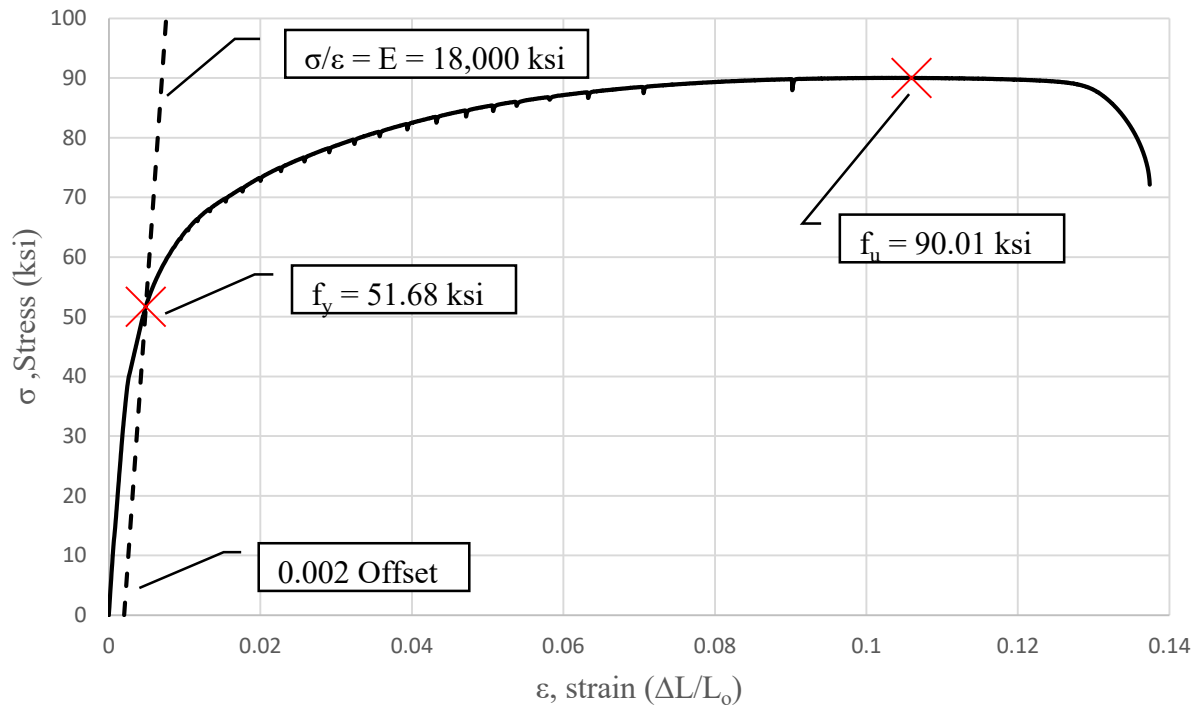


Figure 4-2: Tensile Test, 1 inch DIA Threaded Rod, ASTM F1554 Gr. 36 Steel

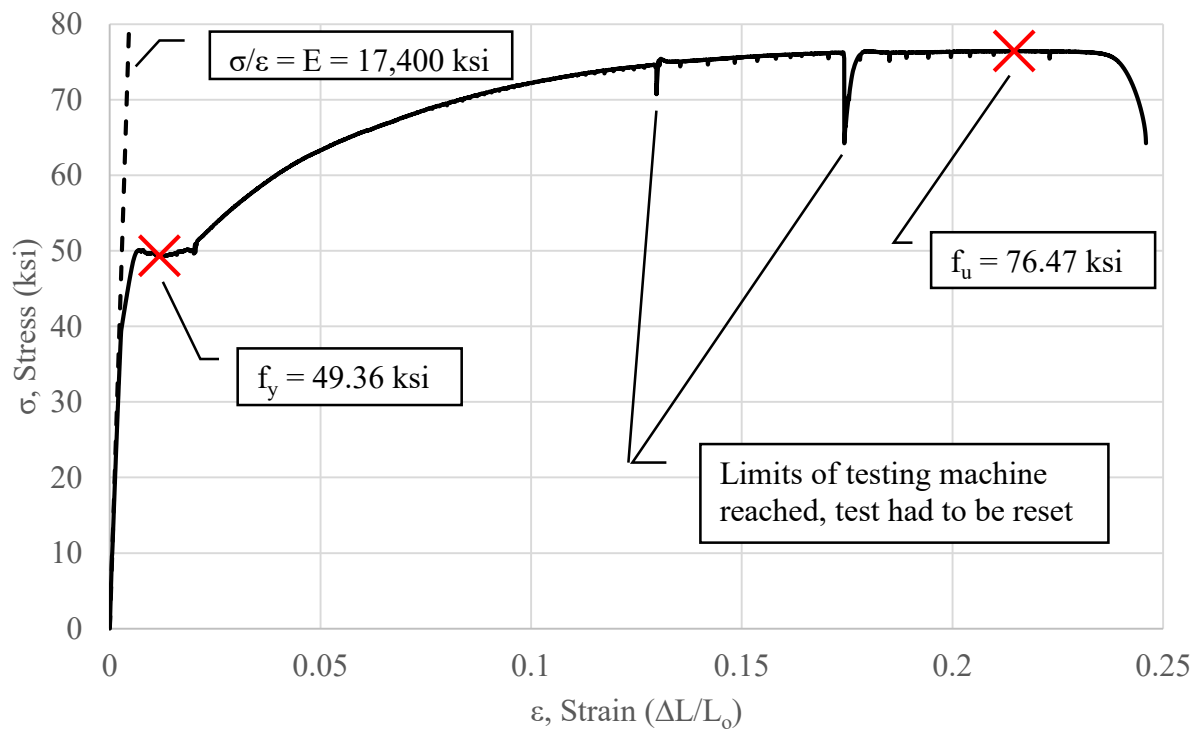


Figure 4-3: Tensile Test, 1 1/8 inch DIA Threaded Rod, ASTM F1554 Gr. 36 Steel

4.2 Test Observations

4.2.1 Test Observations - Specimen D1

The specimen at the base of the column immediately before and after testing is shown below in Figure 4-4.

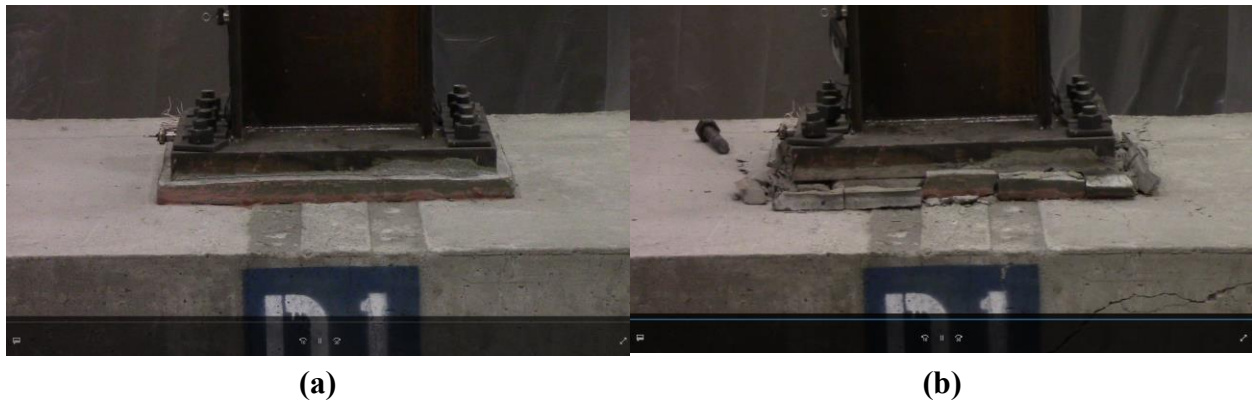


Figure 4-4: Specimen D1 (a) Start of Testing, and (b) End of Testing

During testing at the low deflection cycles (0.375% to 1.0 % story drift), there was no visible damage or movement at the base of the column.

At story drifts between 1.0% and 3.0%, movement at the base was noted. The base plate was visibly seen rocking back and forth, and the anchor bolts were being stretched as the base plate moved. There was still no discernable damage to either the grout beneath the base plate, or the concrete base.

During testing at higher deflections (3.0% story drifts and above) damage was observed to the grout and the concrete base. The grout began to fail under compressive loads, and began to spall off the sides of the base plate, revealing the grout underneath the base plate, which also showed signs of destruction. At a story drift of 4.0%, a diagonal crack appeared in the base mat. This crack started at the approximate location of the anchor bolt embedded plate and proceeded at a roughly 45° angle to the top of the mat (Figure 4-5). This crack widened slightly with each progressive increase in story drift, but the reinforcing steel remained intact and the base mat retained its strength throughout the test. Small amounts of surface damage to the top of the concrete base was observed in the form of small cracks. It was also observed that there was a difference in the way the exterior anchor bolts behaved relative to the interior anchor bolts. Under tension, all four anchor bolts on a side of the column were engaged and stretched. When the movement was reversed, the two interior bolts remained at their stretched length, while the two exterior bolts were engaged in compression and very obviously shrunk in height, see Figure 4-6. This was consistent with all anchor bolts on both sides of the column.

Two anchor bolts fractured nearly simultaneously at the 6.0% story drift cycle. The third anchor bolt fractured at the first 7.0% story drift cycle. The fourth anchor bolt fractured spectacularly at 49:19.85 into the test (the 2nd 7.0% story drift cycle). The bolt fractured under tensile stress and launched itself vertically, only stopping as it impacted the bottom of the corbel. Its associated square washer also launched vertically but was stopped and held by one of the magnets holding a string pot wire in place. The test was ended after the 4th anchor bolt failed. It was noted afterwards that the 4 bolts that fractured (out of 8 total) were the same 4 bolts that were instrumented with strain gages, and that fractures occurred at reduced sections where threads had been ground down to prepare a flat surface to mount the strain gage (Figure 3-40).

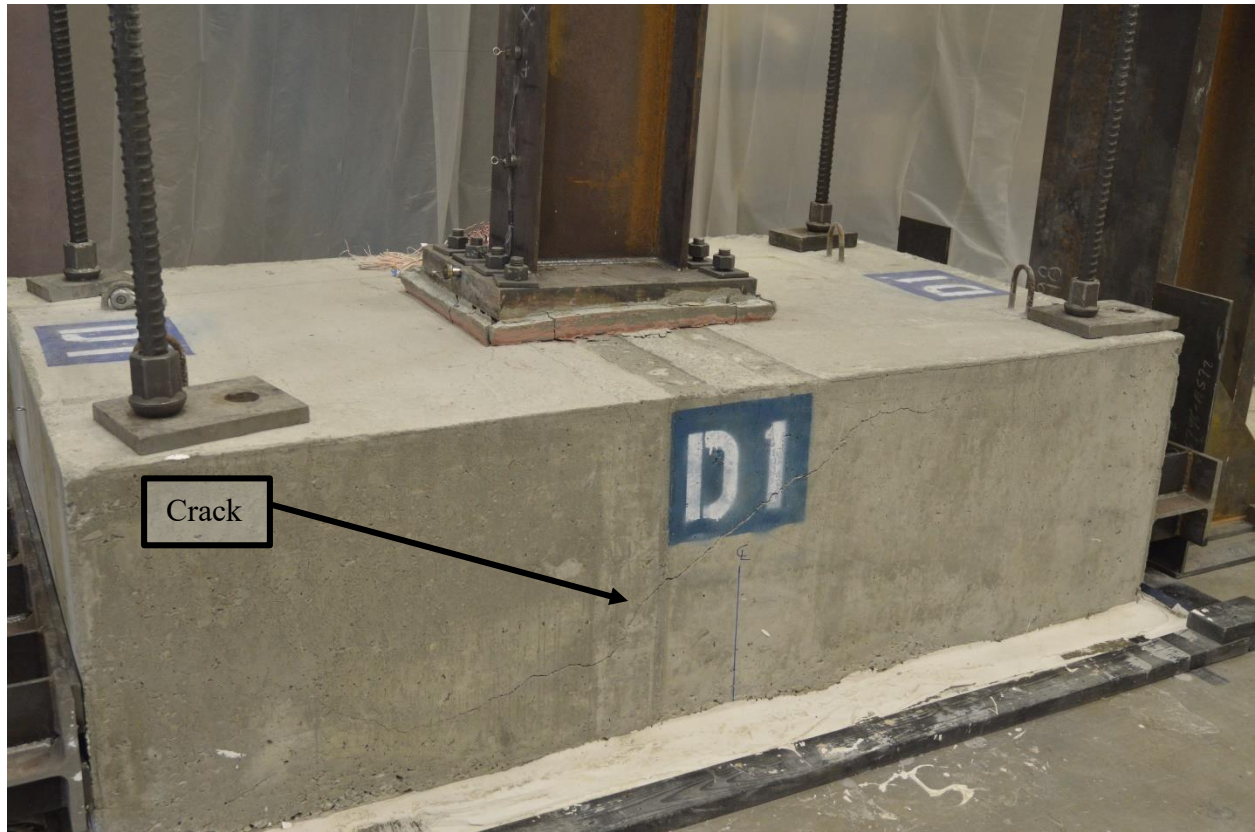


Figure 4-5: Specimen D1, Crack in the Base Mat



Figure 4-6: Specimen D1, Anchor Bolts Under Tensile and Compressive Stresses

4.2.2 Test Observations - Specimen D2

The specimen at the base of the column immediately before and after testing is shown below in Figure 4-7.



Figure 4-7: Specimen D2 (a) Start of Testing, and (b) End of Testing

During testing at the low deflection cycles (0.375% to 1.0% story drift), there was no visible damage or movement at the base of the column. At the 2nd and 3rd peaks of the 0.5% story drifts, an audible popping noise indicated a breaking of the bond at the cold joint between the slab and base concrete. This resulted in no visible damage to the specimen, and was only discernible during the test audibly (and later verified by analyzing the string pot data).

During testing at the 1.0% to 3.0% story drifts, the gap between the top and bottom mats became noticeable and became larger with each successive increase in deflection. No visible damage was detected to the top mat, block out, or the base mat until the first peak of the 3.0% story drift. At this time, a small vertical crack was noticed in the top mat (Figure 4-8) that began

at the bottom of the mat and propagated about halfway through the mat. The width of this crack grew through subsequent story drifts, but never extended upwards past the location of the rebar mat (see Appendix A.2 Design Drawings for Specimen D2) for the location of this rebar mat.

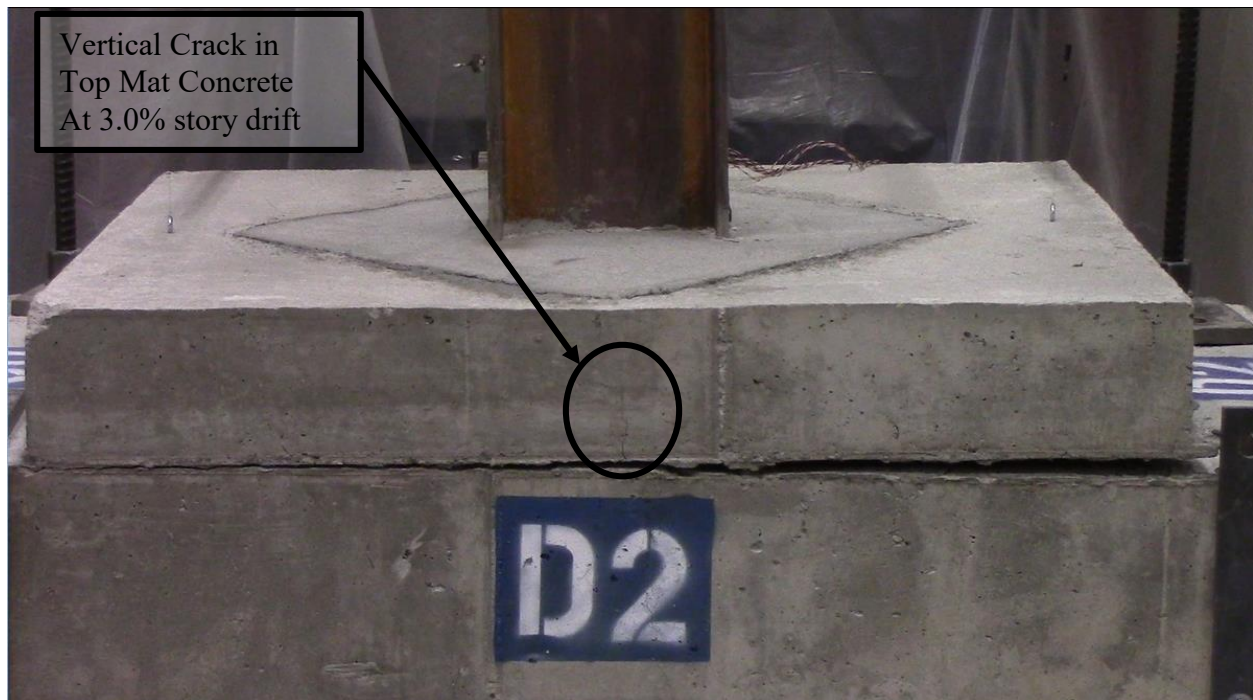


Figure 4-8: Specimen D2, Vertical Crack in Top Mat

Soon thereafter, starting with the 4.0% story drift, cracks began to appear in the base mat. There were two main cracks that extended diagonally from about mid-height of the base, intersecting in an X formation, then extending to the top of the base mat. See Figure 4-9. These cracks grew in size as the test progressed to higher deflections, but the reinforcement inside remained intact, and the concrete never failed beyond these cracks.



Figure 4-9: Specimen D2, Cracks in Base Mat

During the larger displacements, it was also observed that the gap between the base mat and the top mat increased. As the specimen rocked back and forth, the actual elevation of the steel column and top mat increased about 1.5-2 inches. This can be clearly seen in the final specimen photo, Figure 4-7(b).

It was observed that very little damage was visible to the top of the top mat and the block out. Small amounts of concrete spalled off immediately next to the column steel, but other than that small amount of damage, no crack or other distress was visible. See Figure 4-10.

The first anchor bolt fractured at the first peak of the 7.0% story drift cycle, and the second bolt broke at the next peak. The test was stopped after the second bolt broke.

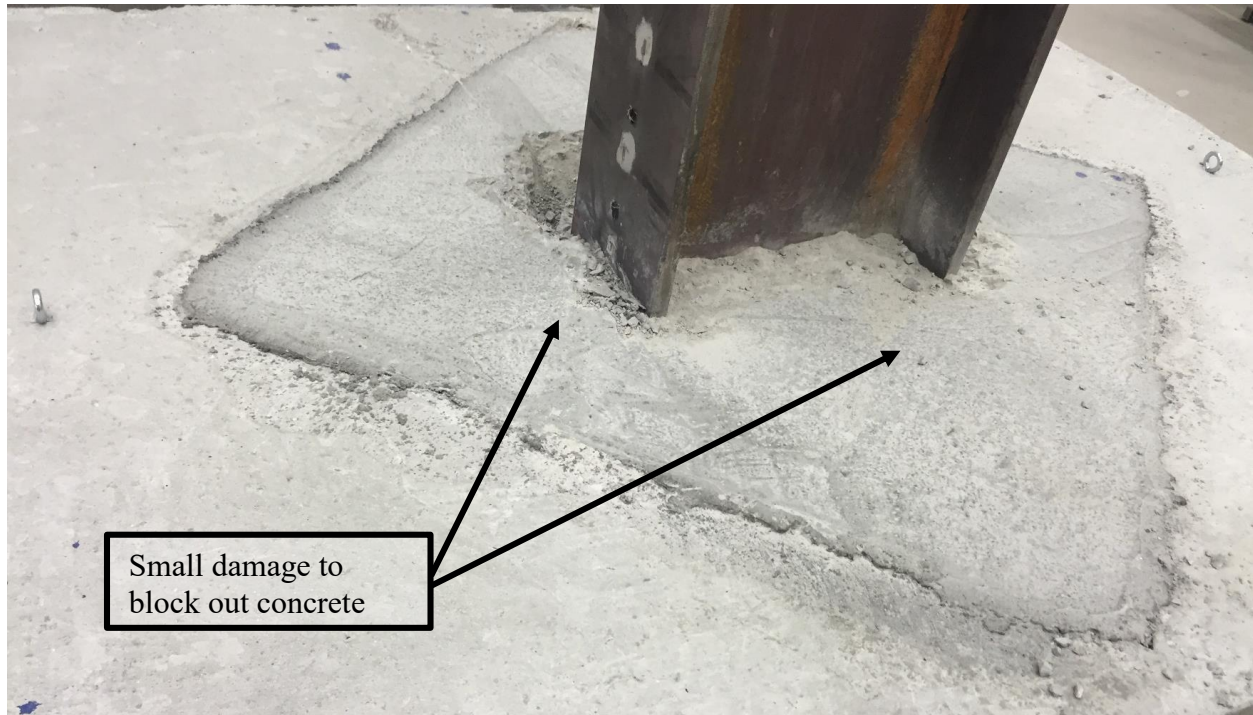


Figure 4-10: Specimen D2, Top of Concrete at Conclusion of Testing (7% Drift)

4.2.3 Test Observations - Specimen D3

The specimen at the base of the column immediately before and after testing is shown below in Figure 4-11.

During testing at the low deflection cycles (0.375% to 1.0% story drift), there was no visible damage or movement at the base of the column. There was a separation at the cold joint between the base mat concrete and the top mat concrete. This resulted in no visible damage to the specimen, and was only discernible audibly during the test (and later verified by analyzing the string pot data). The cold joint broke at the 1st and 2nd peaks of the 0.75% story drift movements.



Figure 4-11: Specimen D3 (a) Start of Testing, and (b) End of Testing

During testing at the 1.0% to 3.0% story drifts, the gap between the top and bottom mats became noticeable and became larger with each successive increase in deflection. No visible damage was detected to the top mat, block out, or the base mat until the first peak of the 3.0% story drift. At this time, two small vertical cracks were noticed in the top mat (Figure 4-12) that began at the bottom of the mat and propagated upwards until about 4 inches from the top of the mat. The width of these cracks grew through subsequent story drifts, but never extended upwards past the location of the rebar mat, again about 4 inches from the top of the mat.

Starting with the 4.0% story drift, cracks began to appear in the base mat. There were two main cracks that extended diagonally from about mid-height of the base, intersecting in an X formation, then extending to the top of the base mat. See Figure 4-13. These cracks grew in size as the test progressed to higher deflections, but the reinforcement inside remained intact, and the concrete never failed beyond these cracks. It was observed after the completion of all the tests that the base mat for this specimen exhibited the largest amount of distress and damage compared to all other specimens.

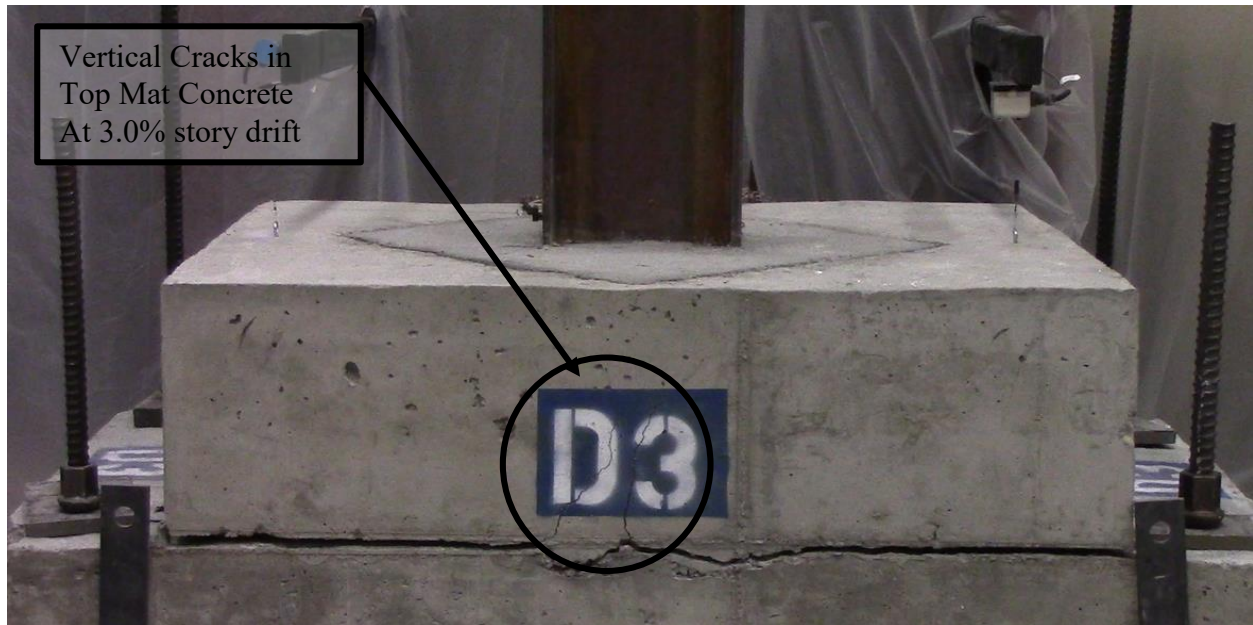


Figure 4-12: Specimen D3, Vertical Crack in Top Mat

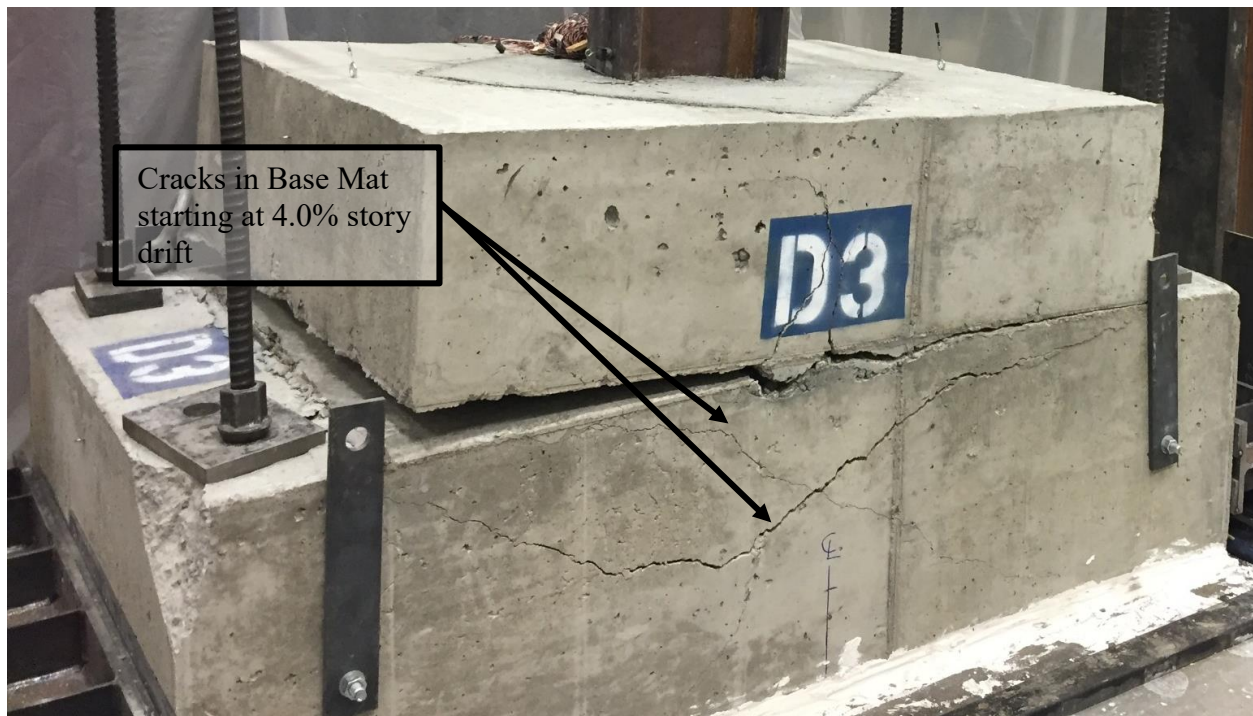


Figure 4-13: Specimen D3, Cracks in Base Mat

During the larger displacements, it was also observed that the gap between the base mat and the top mat increased. As the specimen rocked back and forth, the actual elevation of the steel column and top mat increased about 2-3 inches. This can be clearly seen in the final specimen photo, Figure 4-11(b).

It was observed that very little damage was visible to the top of the top mat and the block out. Small amounts of concrete spalled off immediately next to the column steel, but other than that small amount of damage, no crack or other distress was visible. Also observed was that at the higher deflections, small bits of the mill steel flaked off the column flanges near the interface with the block out concrete. Figure 4-14.

The first anchor bolt fractured at the first peak of the 6.0% story drift cycle. The second anchor bolt broke at the second peak for the 7.0% story drift cycle. The third broke at the first 8.0% story drift cycle peak. The fourth broke at the last 10.0% story drift cycle peak. When anchor bolts began breaking, it became apparent that because of the location of the broken anchor bolts, when the top of the column experienced large deflections, there was uneven resistance at the base, and the top of the column tended to skew to one side. This put significant force on the out-of-plane reaction frame. The test was paused several times to adjust this reaction frame and relieve the pressure. When it became apparent that the top of the column was moving out of plane due to this problem and exerting large loads on the reaction frame, the test was stopped. This occurred after the fourth anchor bolt fractured.

Post-test visual analysis indicated that the 4 anchor bolts that fractured were the 4 bolts that were instrumented with strain gages, and that they broke at the sections that had been ground down to create a flat surface to attach the strain gage (Figure 3-40).

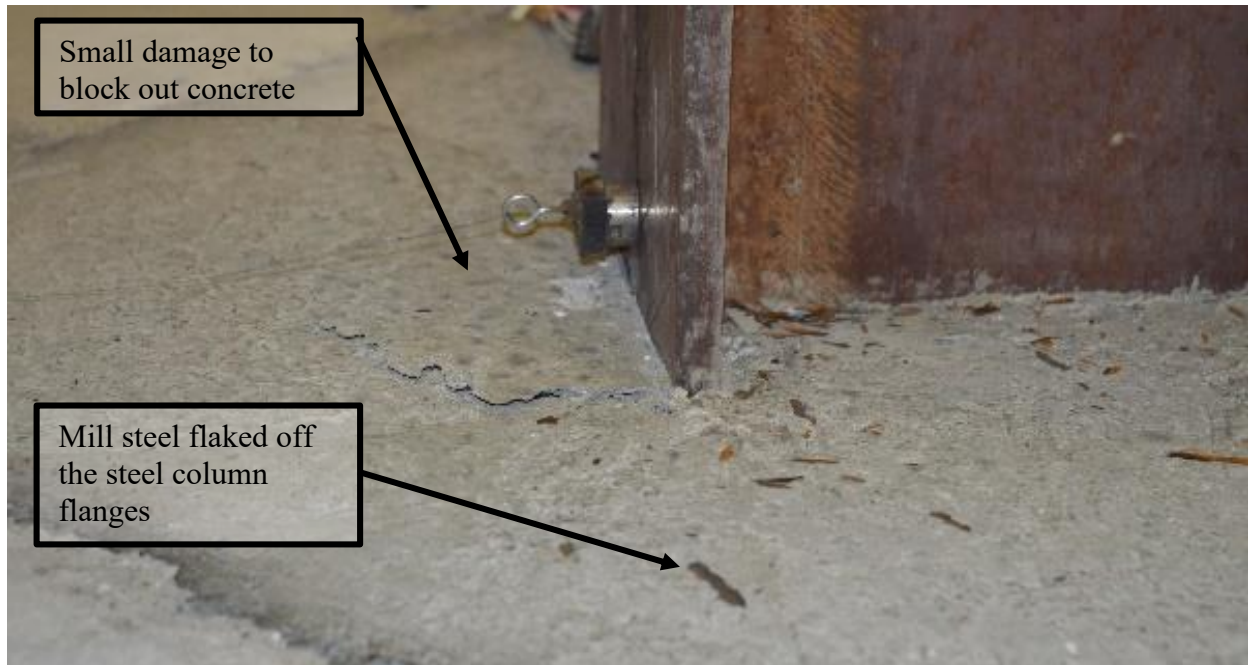


Figure 4-14: Specimen D3, Top of Concrete at Conclusion of Testing (10% Drift)

4.2.4 Test Observations - Specimen D4

The specimen at the base of the column immediately before and after testing is shown below in Figure 4-15.

During testing at the low deflection cycles (0.375% to 1.0% story drift), there was no visible damage or movement at the base of the column. There was a separation at the cold joint between the base mat concrete and the top mat concrete. This resulted in no visible damage to the specimen, and was only discernible audibly during the test (and later verified by analyzing the string pot data). The cold joint broke at the 2nd and 3rd peaks of the 0.75% story drift movements.

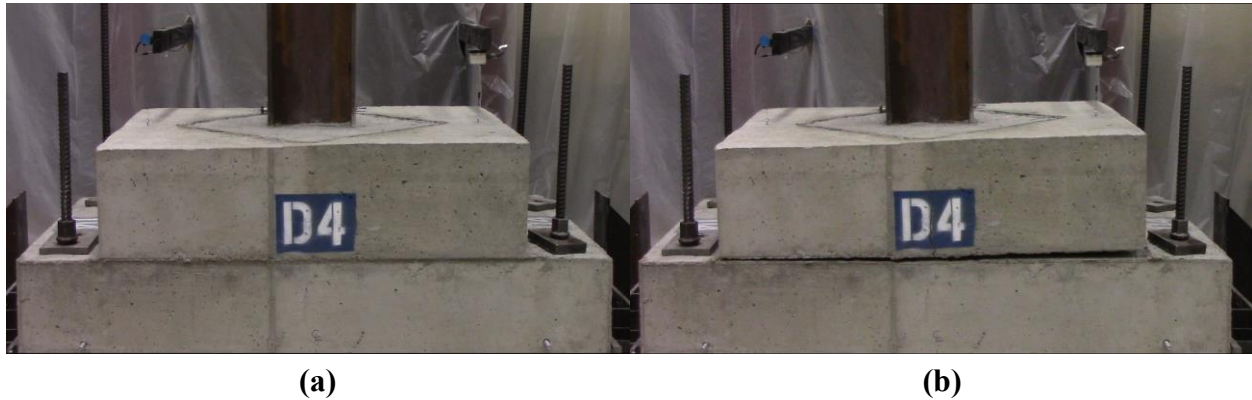


Figure 4-15: Specimen D4 (a) Start of Testing, and (b) End of Testing

During testing at the 1.0% to 3.0% story drifts, the gap between the top and bottom mats became noticeable and became larger with each successive increase in deflection. No visible damage was detected to the top mat, block out, or the base mat until the first peak of the 1.5% story drift. At this time, a small vertical crack was noticed in the top mat (see Figure 4-16) that began at the bottom of the mat and propagated upwards until about 4 inches from the top of the mat. The width of these cracks grew through subsequent story drifts, but never extended upwards past the location of the rebar mat, again about 4 inches from the top of the mat.

At no time in the test were any cracks observed in the base mat. See Figure 4-17, and note that with all four anchor bolts broken, the top mat and column were easily removed, leaving only the base mat shown.



Figure 4-16: Specimen D4, Vertical Cracks in Top Mat



Figure 4-17: Specimen D4, Base Mat at the Conclusion of Testing

During the larger displacements, it was also observed that the gap between the base mat and the top mat increased. As the specimen rocked back and forth, the actual elevation of the steel column and top mat increased about 0.5-1 inches. This can be clearly seen in the final specimen photo, Figure 4-15(b).

It was observed that very little if any damage was visible to the top of the top mat and the block out. Other than the tiniest of spalling next to the column steel, no cracks or distress of any kind was visible. See Figure 4-18.

The first anchor bolt fractured at the first peak of the 4.0% story drift cycle. The second and third bolts broke nearly simultaneously at the second peak of the 4.0% story drift cycle, and the last bolt broke at the third peak of the 4.0% story drift cycle. After all four bolts had fractured, the test was ended.

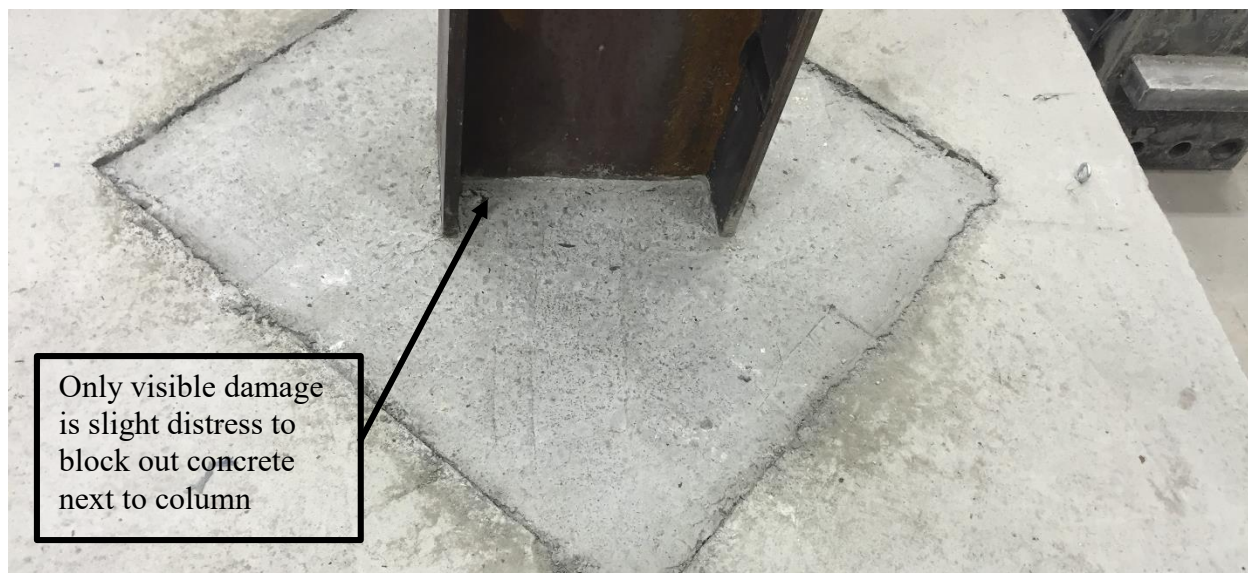


Figure 4-18: Specimen D4, Top of Concrete at Conclusion of Testing

4.2.5 Test Observations - Specimen F1

The specimen at the base of the column immediately before and after testing is shown below in Figure 4-19.

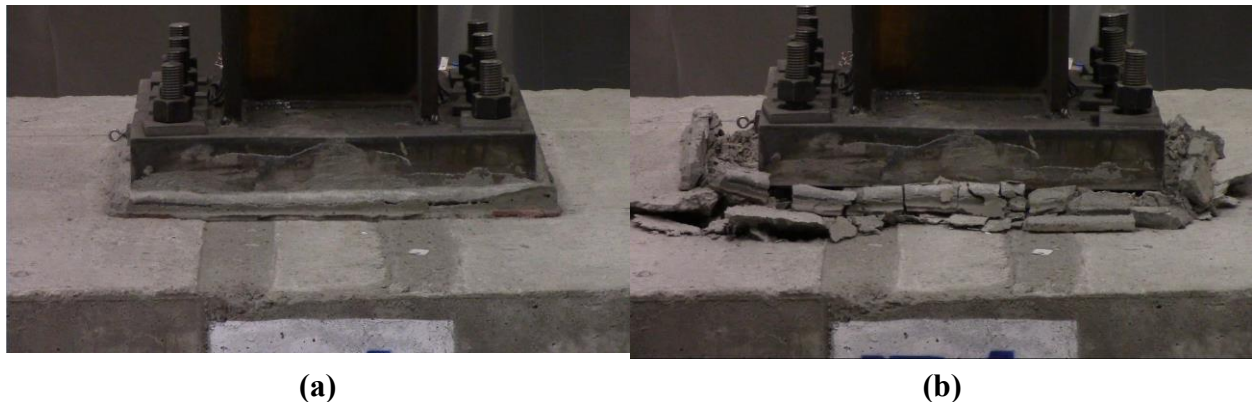


Figure 4-19: Specimen F1 (a) Start of Testing, and (b) End of Testing

During testing at the low deflection cycles (0.375% to 1.0% story drift), there was no visible damage or movement at the base of the column.

At story drifts between 1.0% and 2.0%, movement at the base was noted. The base plate was visibly seen rocking back and forth, and the anchor bolts were being stretched as the base plate moved. There was still no discernable damage to either the grout beneath the base plate, or the concrete base.

During testing at higher deflections (2.0% story drifts and above) damage was observed in the grout and top surface of the base mat. The grout began to fail under compressive loads, and

then to spall off the sides of the base plate, revealing the grout underneath the base plate, which also showed signs of destruction. At this time, the top of the base mat showed distress underneath the compression end of the column base plate, see Figure 4-20.



Figure 4-20: Specimen F1, Grout and Top Surface of Concrete Failing

At no time in the test was any damage (other than the surface distress noted above) observed in the base mat. No cracks or other failures were seen. It was also observed that there was a difference in the way the exterior anchor bolts behaved relative to the interior anchor bolts. Under tension, all four anchor bolts on a side of the column were engaged and stretched. When the movement was reversed, the two interior bolts remained at their stretched length, while the

two exterior bolts were engaged in compression and very obviously shrunk in height, see Figure 4-21. This was consistent with all anchor bolts on both sides of the column.

An anchor bolt fractured at the last peak of the 9.0% story drift cycle, and the test was ended.



Figure 4-21: Specimen F1, Anchor Bolts Under Tensile and Compressive Stresses

4.2.6 Test Observations - Specimen F2

The specimen at the base of the column immediately before and after testing is shown below in Figure 4-22.



Figure 4-22: Specimen F2 (a) Start of Testing, and (b) End of Testing

During testing at the low deflection cycles (0.375% to 1.0% story drift), there was no visible damage or movement at the base of the column. There was a separation at the cold joint between the base mat concrete and the top mat concrete. This resulted in no visible damage to the specimen, and was only discernible during the test audibly (and later verified by analyzing the string pot data). The cold joint broke at the 2nd and 3rd peaks of the 0.75% story drift movements.

During testing at the 1.0% to 3.0% story drifts, the gap between the top and bottom mats became noticeable and became larger with each successive increase in deflection. No visible damage was detected to the top mat, block out, or the base mat until the end of the 2.0% story drift. At this time, a small vertical crack was noticed in the top mat (see Figure 4-23) that began at the bottom of the mat and propagated about halfway through the mat. The width of this crack remained very small through subsequent story drifts, and never extended upwards past the location of the rebar mat. The width of the crack appeared to remain static once the block out concrete began to show signs of distress. This began to occur at the second peak of the 4.0% story drift. The block out concrete began to crack and show signs of distress that grew

throughout the test. These cracks extended through the block out to the top of the base plate. Several large chunks of concrete were removed by hand at the conclusion of the test, see Figure 4-24. At no time were any cracks or distress observed in the top surface of the top mat.

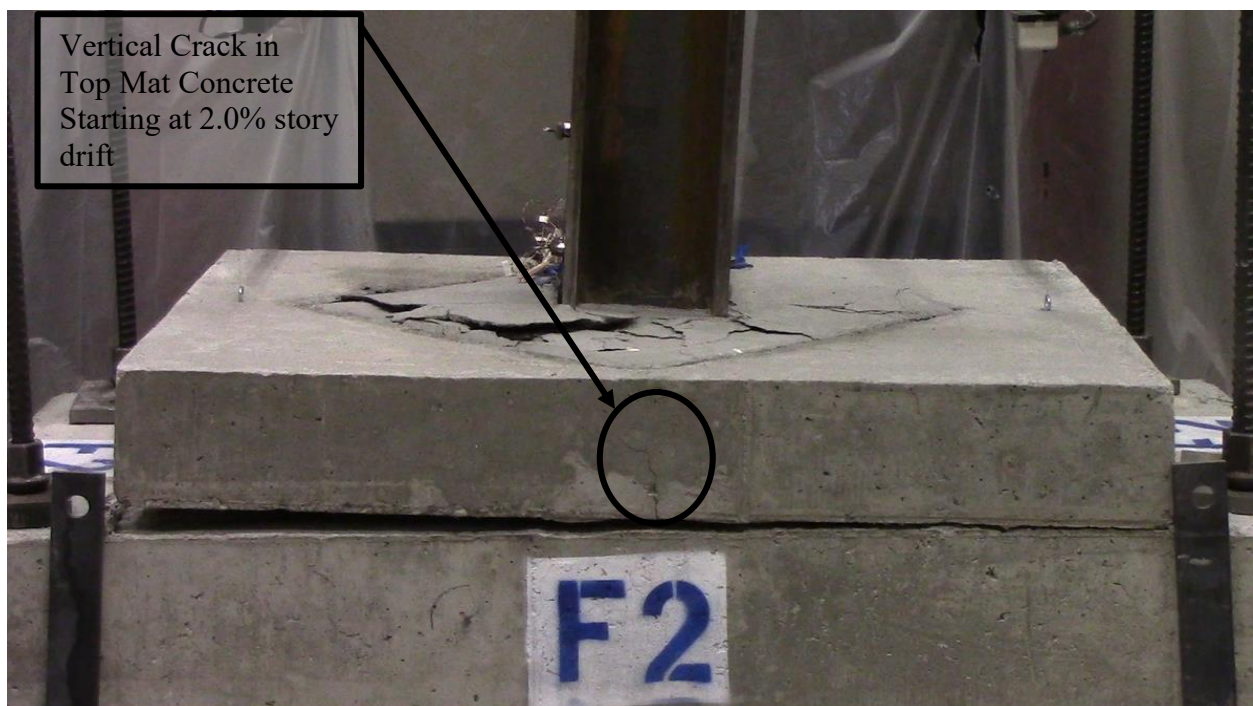


Figure 4-23: Specimen F2, Vertical Crack in Top Mat

At no time during the tests were any cracks or distress of any kind observed in the base mat.

During the larger displacements, it was also observed that the gap between the base mat and the top mat increased. As the specimen rocked back and forth, the actual elevation of the

steel column and top mat increased about 1.5-2 inches. This can be clearly seen in the final specimen photo, Figure 4-22(b).



Figure 4-24: Specimen F2, Block Out Distress at Conclusion of Testing

The first anchor bolt fractured at the first peak of the 11.0% story drift cycle, and the second bolt broke at the next peak. The test ran through the remainder of the 11.0% story drift cycles, and was ended at the end of the loading protocol.

4.2.7 Test Observations - Specimen F3

The specimen at the base of the column immediately before and after testing is shown below in Figure 4-25.



Figure 4-25: Specimen F3 (a) Start of Testing, and (b) End of Testing

During testing at the low deflection cycles (0.375% to 1.0% story drift), there was no visible damage or movement at the base of the column. There was a separation at the cold joint between the base mat concrete and the top mat concrete. This resulted in no visible damage to the specimen, and was only discernible audibly during the test (and later verified by analyzing the string pot data). The cold joint broke at the 2nd and 3rd peaks of the 1.0% story drift movements.

During testing at the 1.0% to 3.0% story drifts, the gap between the top and bottom mats became noticeable and became larger with each successive increase in deflection. No visible damage was detected to the top mat, block out, or the base mat until just after the second peak of

the 2.0% story drift. At this time, a small vertical crack was noticed in the top mat (see Figure 4-26) that began at the bottom of the mat and propagated upwards until it was a little higher than the halfway point of the top mat. The width of this crack grew through subsequent story drifts, and developed into a Y shape, with one end extending up through to the top of the mat, as seen in Figure 4-25(b), and Figure 4-27.

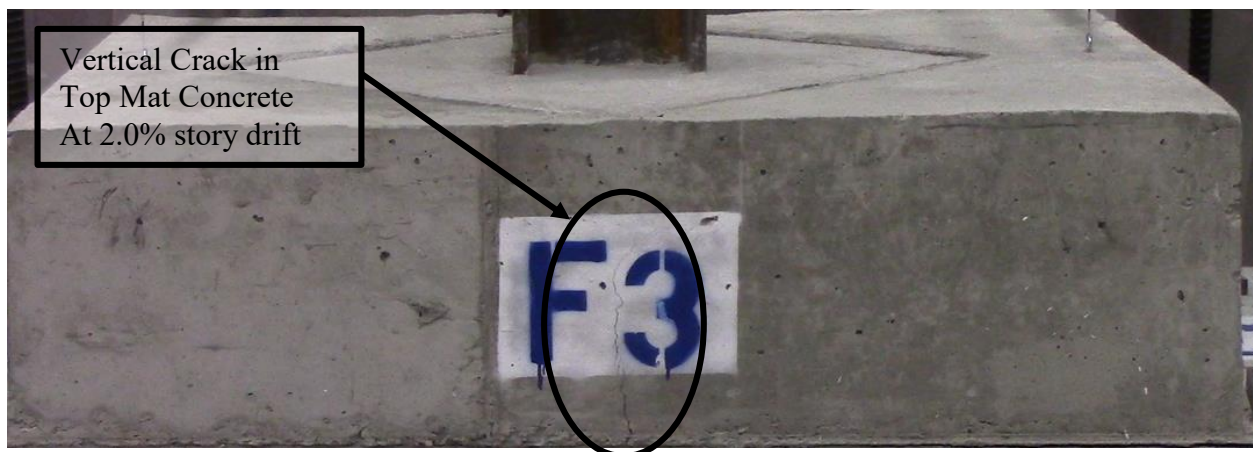


Figure 4-26: Specimen F3, Vertical Cracks in Top Mat

The block out concrete surface began to show cracks after the first peak of the 6.0% story drift cycle. These cracks started near the column flange and grew through subsequent test cycles. See Figure 4-28.



Figure 4-27: Specimen F3, Vertical Crack in Top Mat at Conclusion of Testing, Back Side



Figure 4-28: Specimen F3, Block Out Concrete at Conclusion of Testing (9% Drift)

During the larger displacements, it was also observed that the gap between the base mat and the top mat increased. As the specimen rocked back and forth, the actual elevation of the steel column and top mat increased about 2-3 inches. This can be clearly seen in the final specimen photo, Figure 4-25(b).

The base mat showed no signs of cracking or distress of any kind during the tests.

A single anchor bolt fractured at the second peak of the 9.0% story drift cycle. The test proceeded to the end of the 9.0% story drift cycles and then ended.

4.2.8 Test Observations - Specimen F4

The specimen at the base of the column immediately before and after testing is shown below in Figure 4-29.

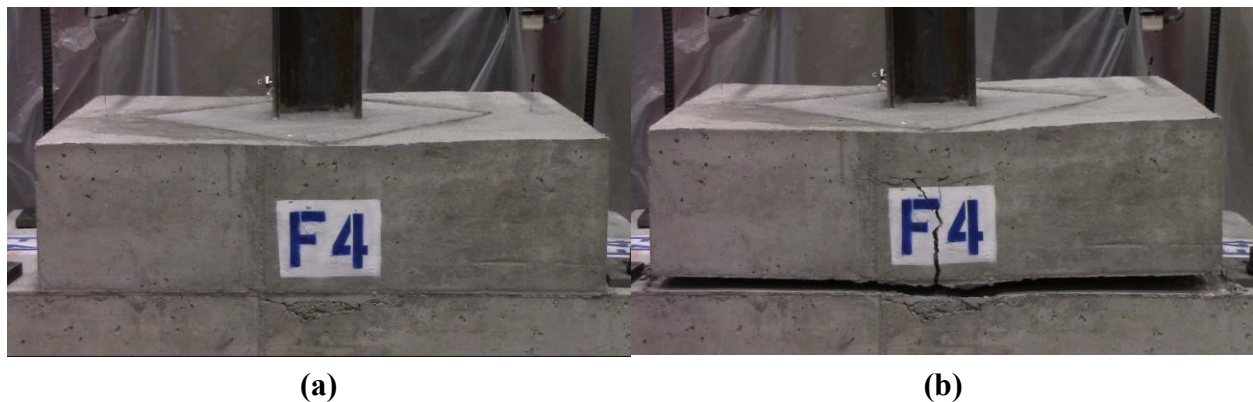


Figure 4-29: Specimen F4 (a) Start of Testing, and (b) End of Testing

During testing at the low deflection cycles (0.375% to 1.0% story drift), there was no visible damage or movement at the base of the column. There was a separation at the cold joint between the base mat concrete and the top mat concrete. This resulted in no visible damage to the specimen, and was only discernible audibly during the test (and later verified by analyzing the string pot data). The cold joint broke at the 6th and 7th peaks of the 1.0% story drift movements.

During testing at the 1.0% to 3.0% story drifts, the gap between the top and bottom mats became noticeable and became larger with each successive increase in deflection. No visible damage was detected to the top mat, block out, or the base mat until the second peak of the 1.5% story drift. At this time, a small vertical crack appeared in the top mat (see Figure 4-30) that began at the bottom of the mat and propagated upwards until about 4 inches from the top of the mat, where the crack spread into a Y pattern. The width of these cracks grew through subsequent story drifts, but never extended upwards past the location of the rebar mat, as seen in Figure 4-31.

The surface of the block out concrete showed signs of distress at very large deflections near the end of the testing. This cracking and damage remained very minimal. See Figure 4-32.

During the larger displacements, it was also observed that the gap between the base mat and the top mat increased. As the specimen rocked back and forth, the actual elevation of the steel column and top mat increased about 1-2 inches. This can be clearly seen in the final specimen photo, Figure 4-29(b).



Figure 4-30: Specimen F4, Vertical Crack in Top Mat



Figure 4-31: Specimen F4, Vertical Crack in Top Mat at Conclusion of Testing



Figure 4-32: Specimen F4, Surface of Block out at Conclusion of Testing (10% Drift)

The base mat showed no signs of cracking or distress of any kind during the tests.

The first two anchor bolts broke nearly simultaneously at the second peak of the 8.0% story drift cycle. The third anchor bolt broke at the first peak of the 9.0% story drift cycle. The final anchor bolt held out until the 10.0% story drift cycle, at which point it, too, fractured. After this occurred, the test was ended.

4.3 Backbone Curve

The backbone curve for each specimen was created using the data from the peak deflection at the first positive and negative peak for each story drift in the test protocol. The backbone curves for all the D-series and F-series tests are shown together for comparison in section 4.3.1. In sections 4.3.2 through 4.3.9, the curves for each individual test are shown in detail. The entire curve is shown first, with locations indicated where anchor bolts had broken. The second graph shows the same curve, but zoomed in to show only up to the 1% story drift cycles.

To provide a useful comparison, the individual specimen graphs also show the theoretical backbone curve for a column with a truly fixed connection, ie. a base connection with an infinite rotational stiffness. This line was determined based on basic Bernoulli beam theory, and the deflection of a cantilevered beam, see Figure 4-33 & EQ (4.3.1).

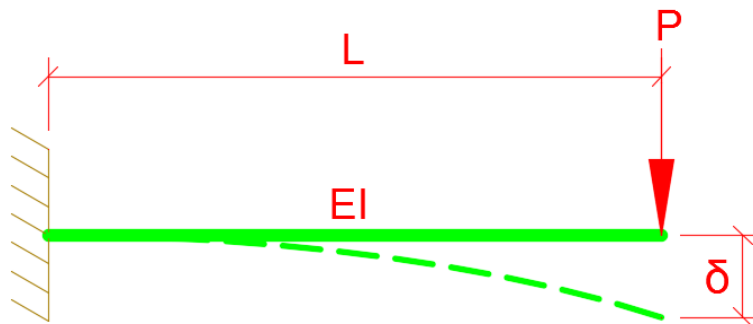


Figure 4-33: Model for Deflection of a Cantilevered Beam

$$\delta = \frac{PL^3}{3EI} \quad (4.3.1)$$

Where:

δ = deflection of cantilevered beam at its end point (the column at the center line of the actuator)

P = the applied load at the end point of the cantilevered beam (the load applied to the column by the actuator)

L = the length of the cantilevered beam from its support location to its end point (the length from the centerline of the actuator to either the top of the base mat concrete, 102 inches, or the top of the block out concrete, 94 inches or 86 inches)

E = modulus of elasticity of the beam material (29,000 ksi for steel)

I = moment of inertia for the beam along its axis of bending (moment of inertia for the column along its strong axis: D-series tests, W14x53 = 541 in³; F-series tests, W10x77 = 455 in³)

4.3.1 Backbone Curve – All

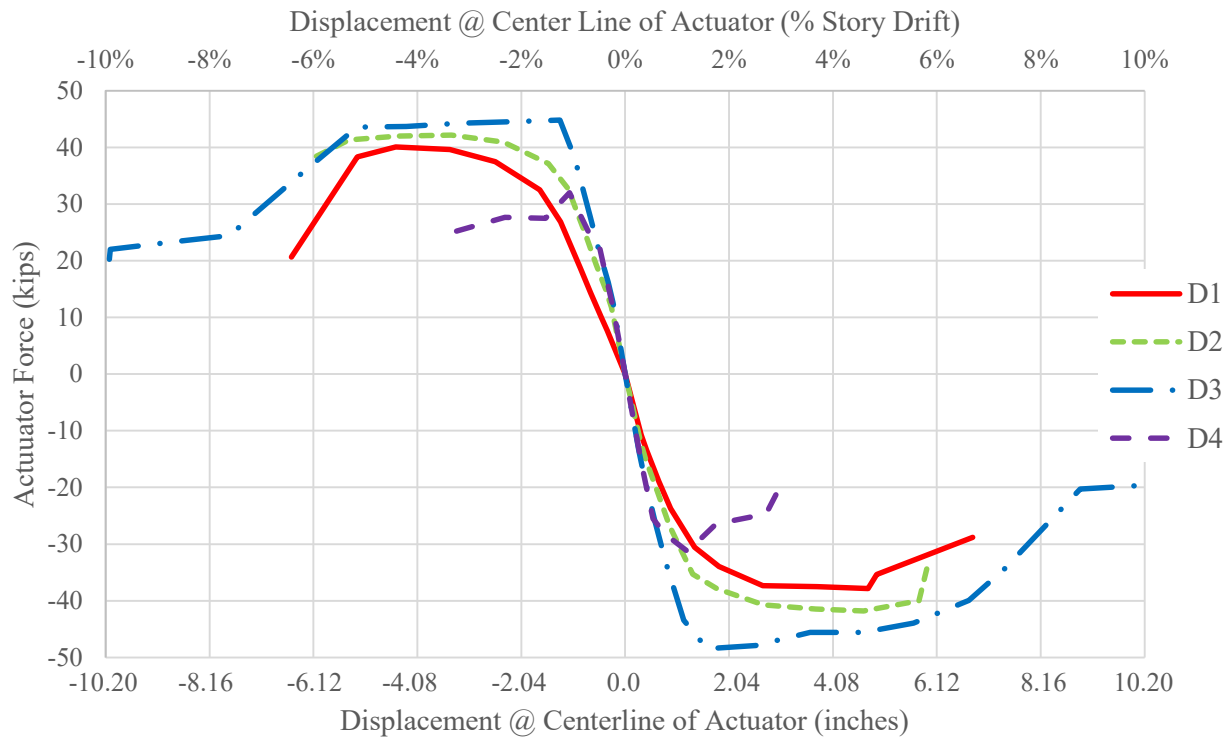


Figure 4-34: Backbone Curve - All D-Series Tests

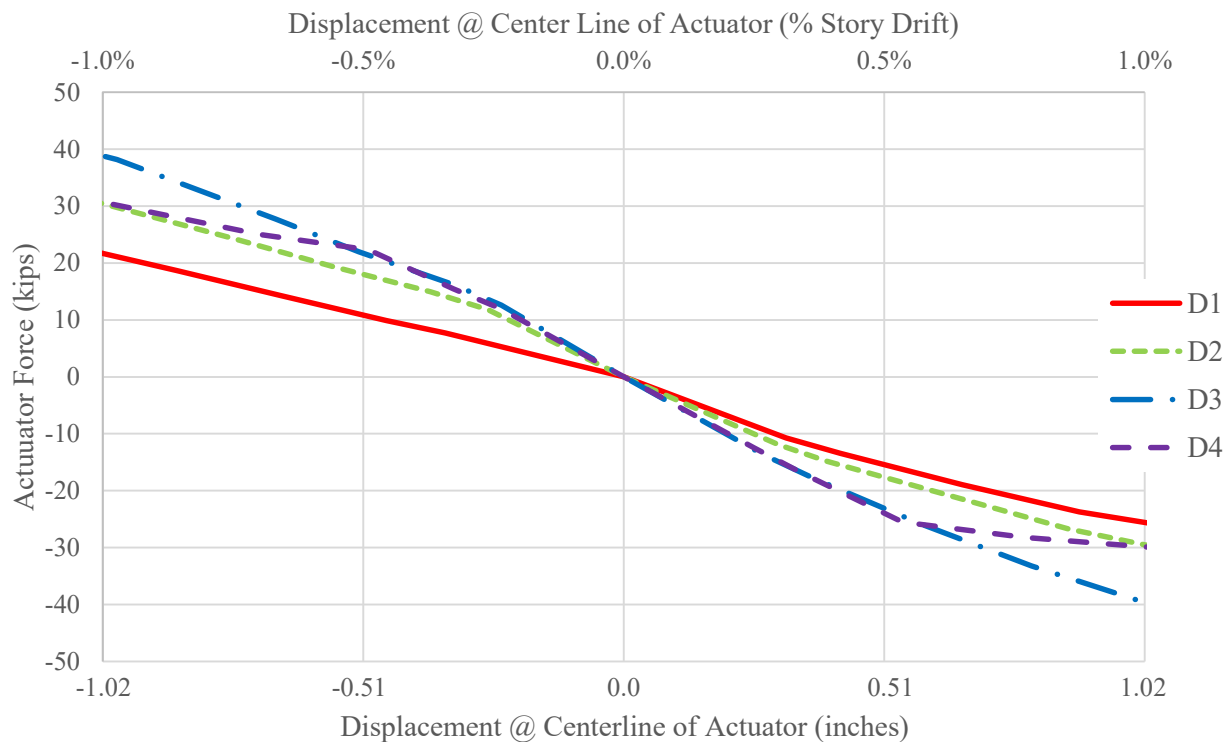


Figure 4-35: Backbone Curve – All D-Series Tests, up to 1%

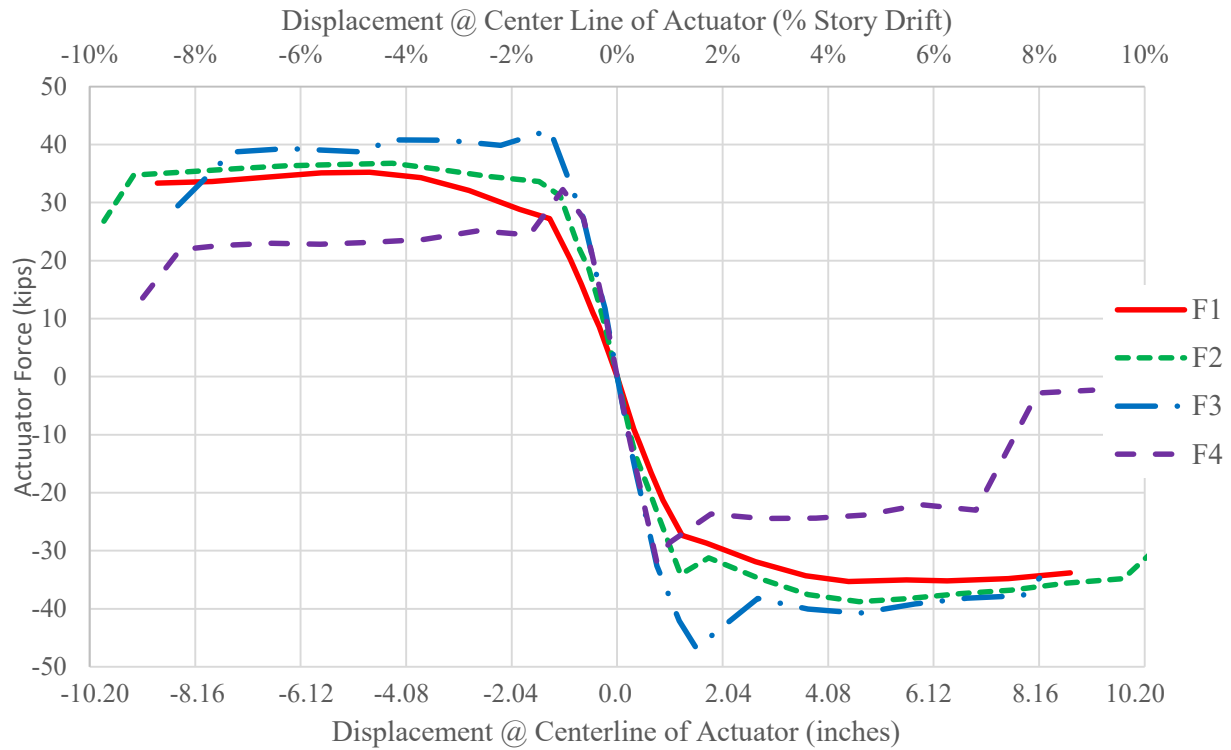


Figure 4-36: Backbone Curves - All F-series Tests

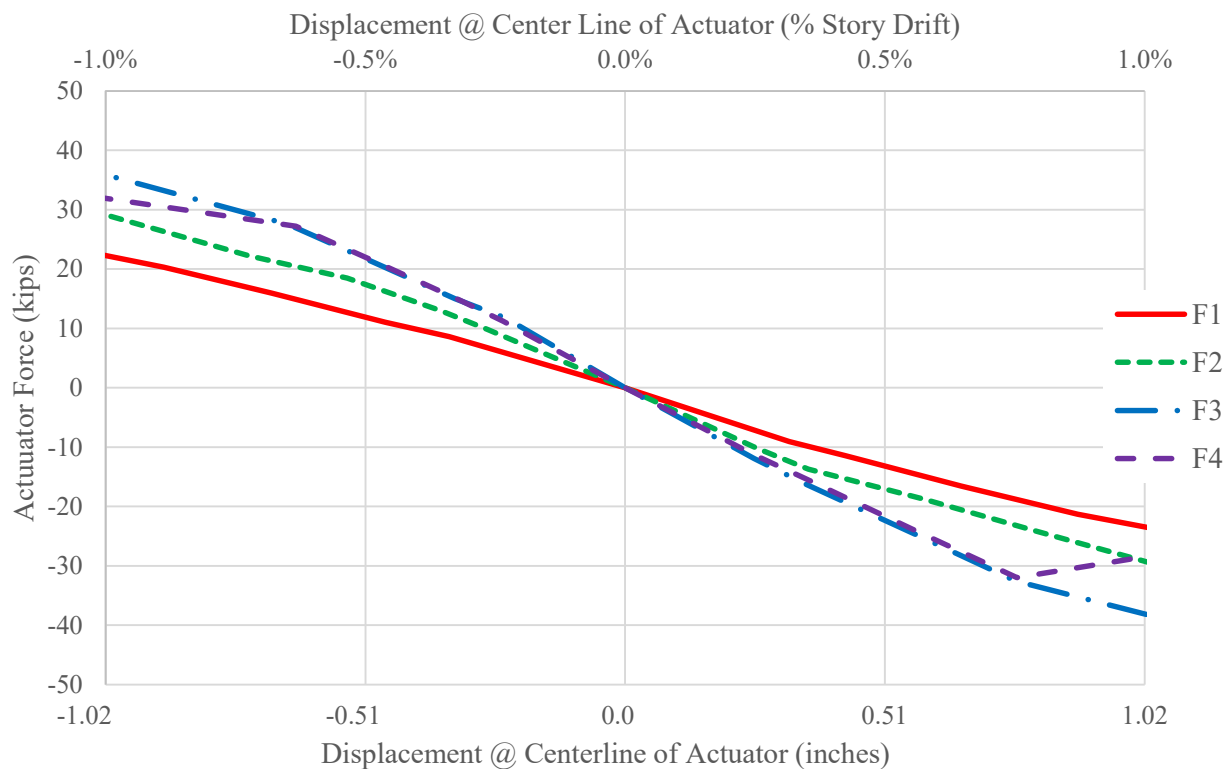


Figure 4-37: Backbone Curve - All F-Series Tests, up to 1% Drift

4.3.2 Backbone Curve - D1

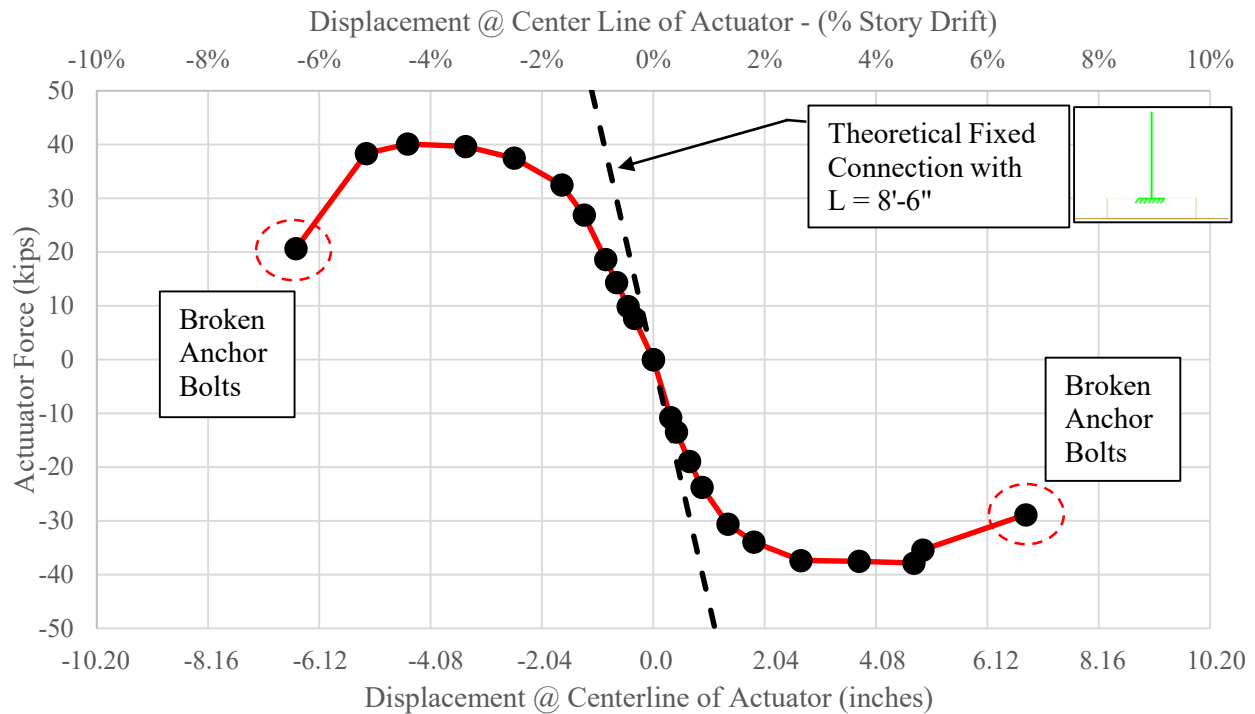


Figure 4-38: Specimen D1 - Backbone Curve; Entire Testing Protocol

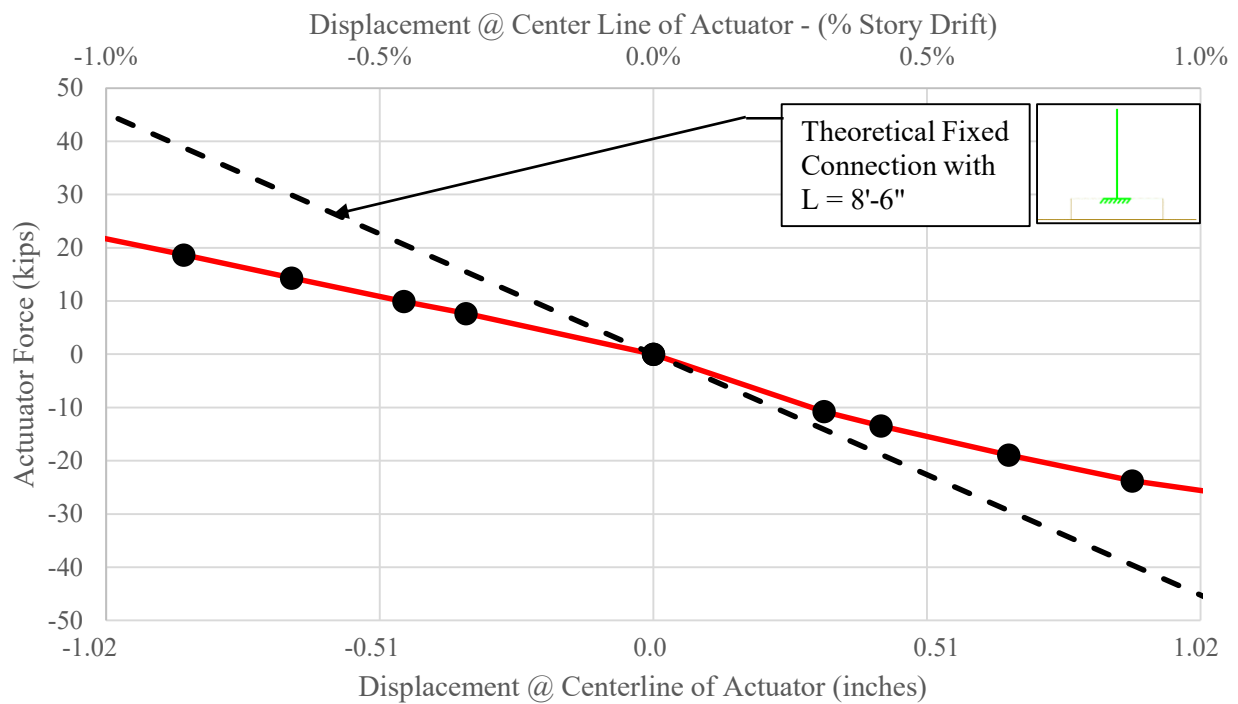


Figure 4-39: Specimen D1 - Backbone Curve; up to 1% Story Drift

4.3.3 Backbone Curve - D2

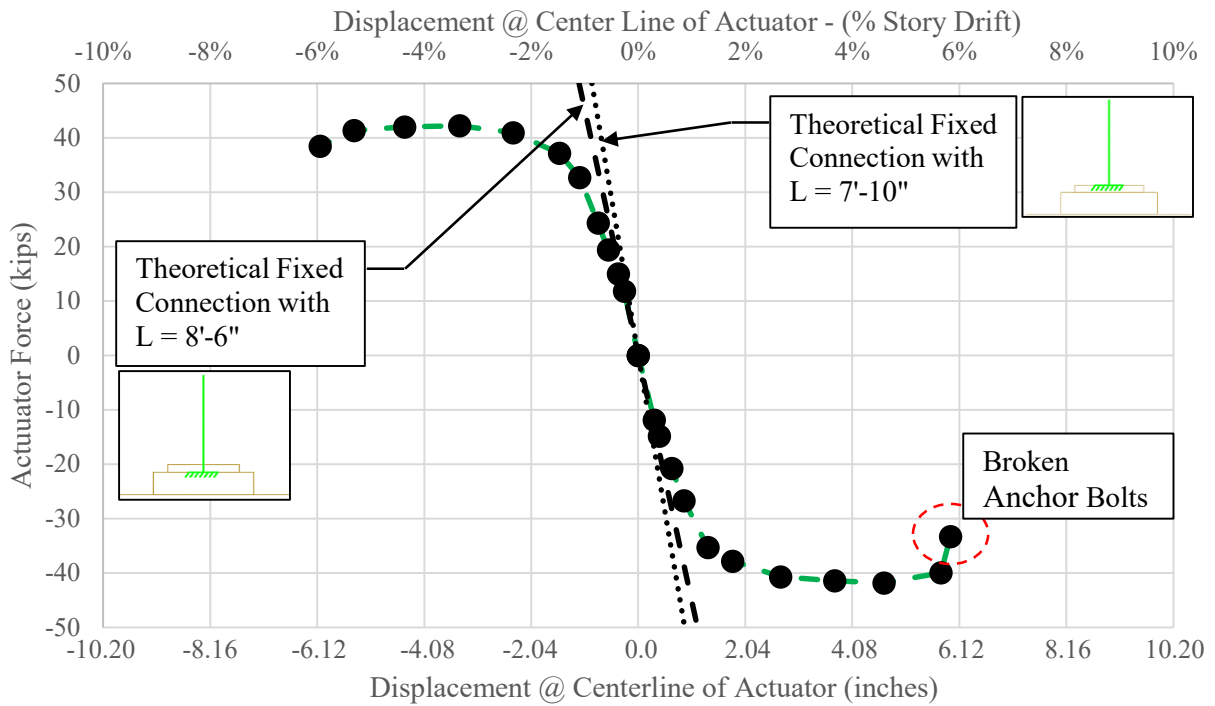


Figure 4-40: Specimen D2 - Backbone Curve; Entire Testing Protocol

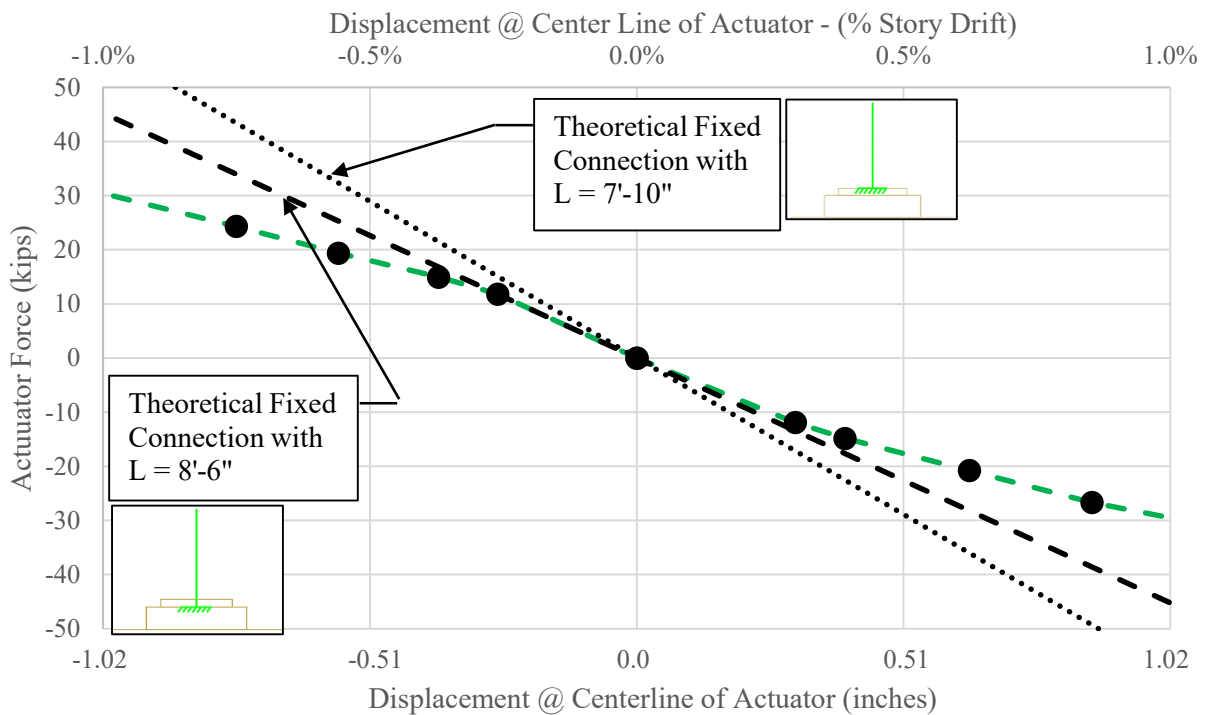


Figure 4-41: Specimen D2 - Backbone Curve; up to 1% Story Drift

4.3.4 Backbone Curve - D3

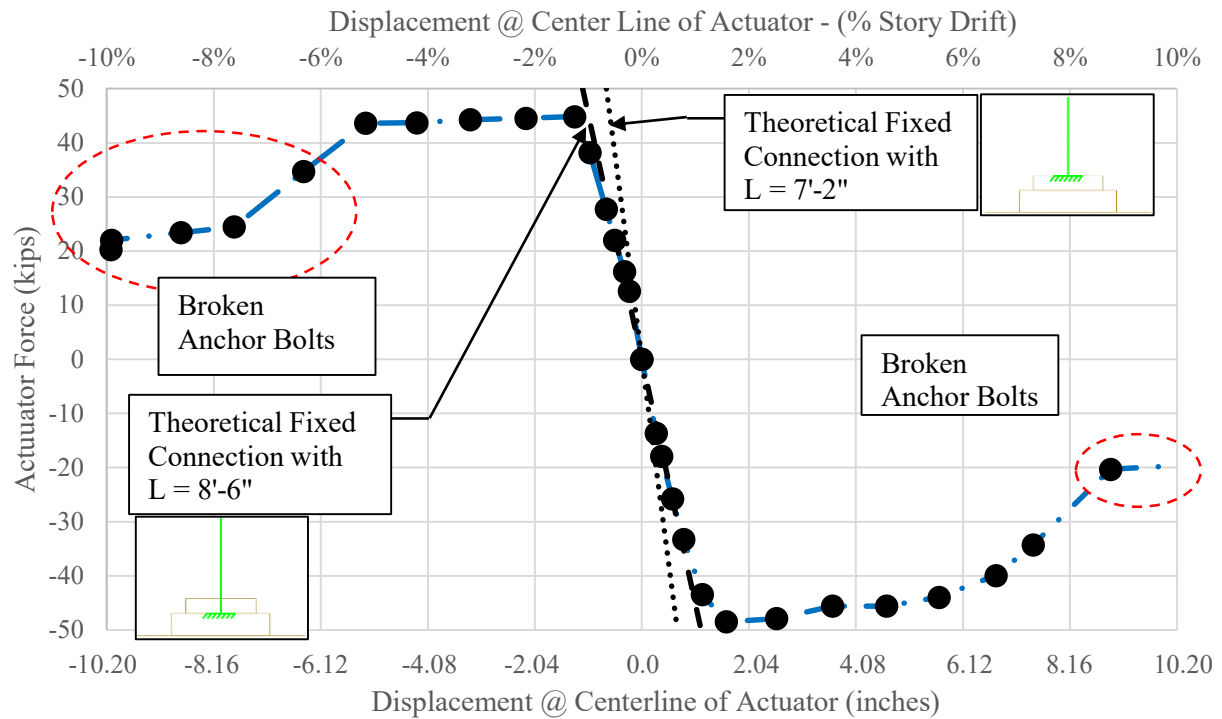


Figure 4-42: Specimen D3 - Backbone Curve; Entire Testing Protocol

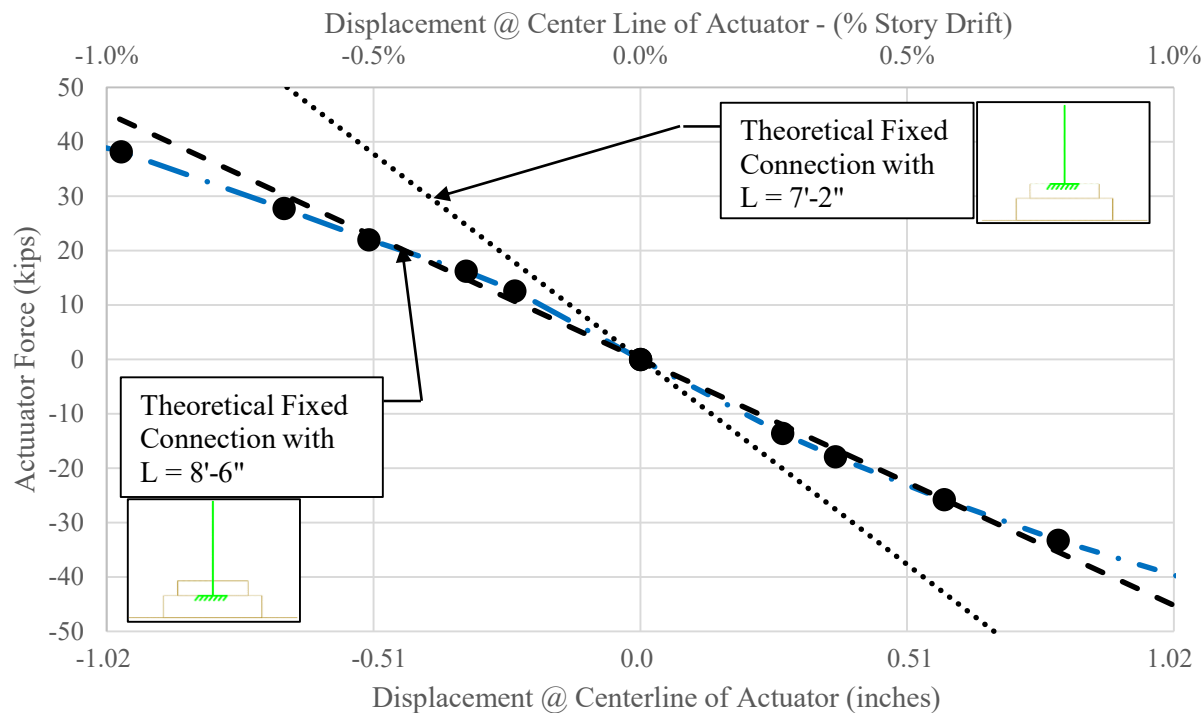


Figure 4-43: Specimen D3 - Backbone Curve; up to 1% Story Drift

4.3.5 Backbone Curve - D4

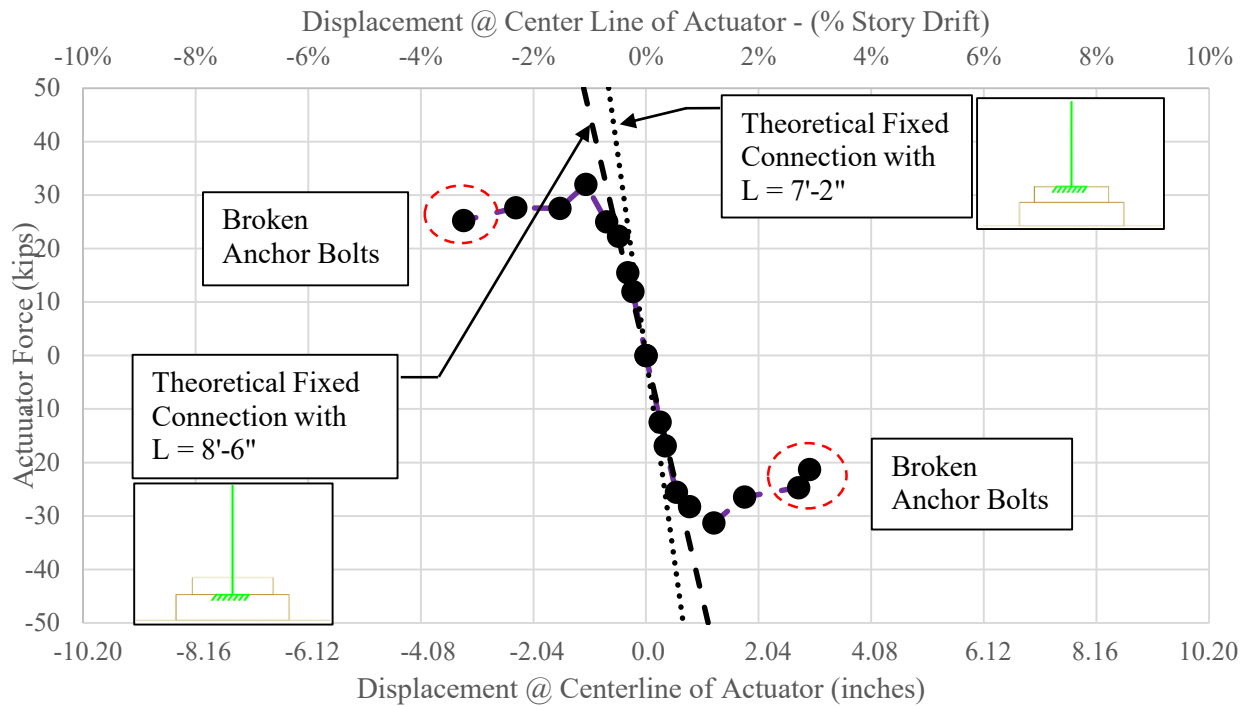


Figure 4-44: Specimen D4 - Backbone Curve; Entire Testing Protocol

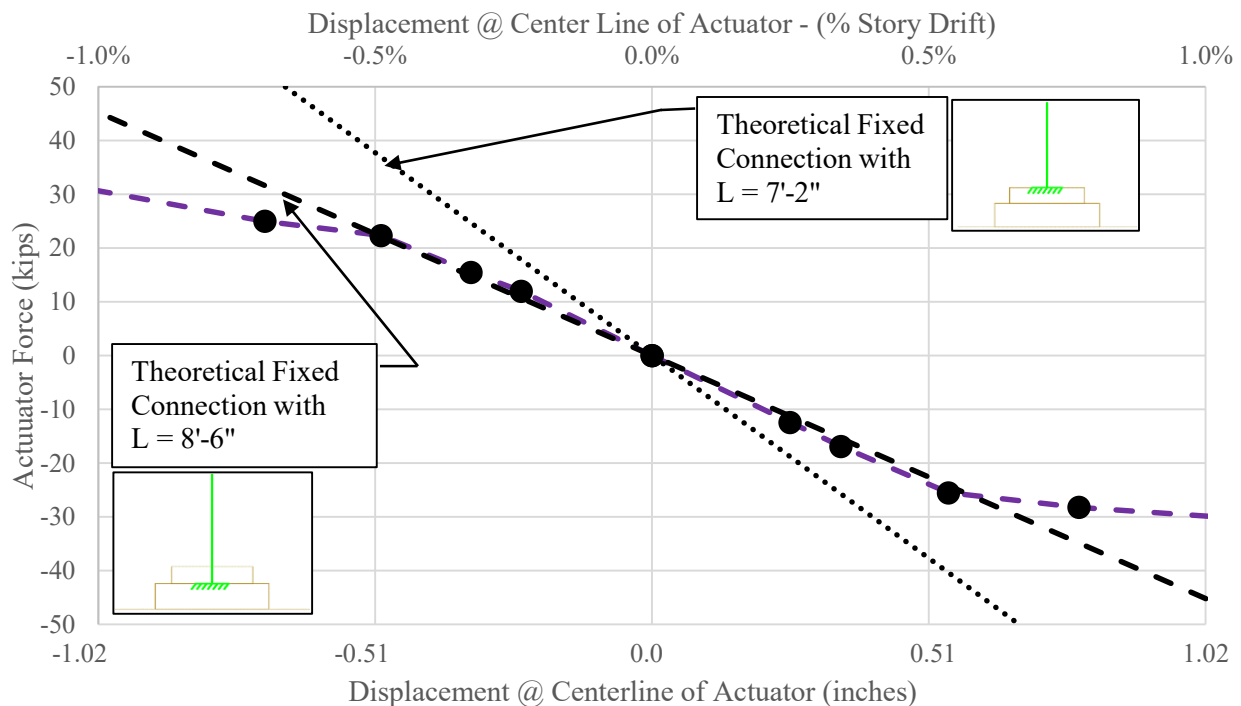


Figure 4-45: Specimen D4 - Backbone Curve; up to 1% Story Drift

4.3.6 Backbone Curve - F1

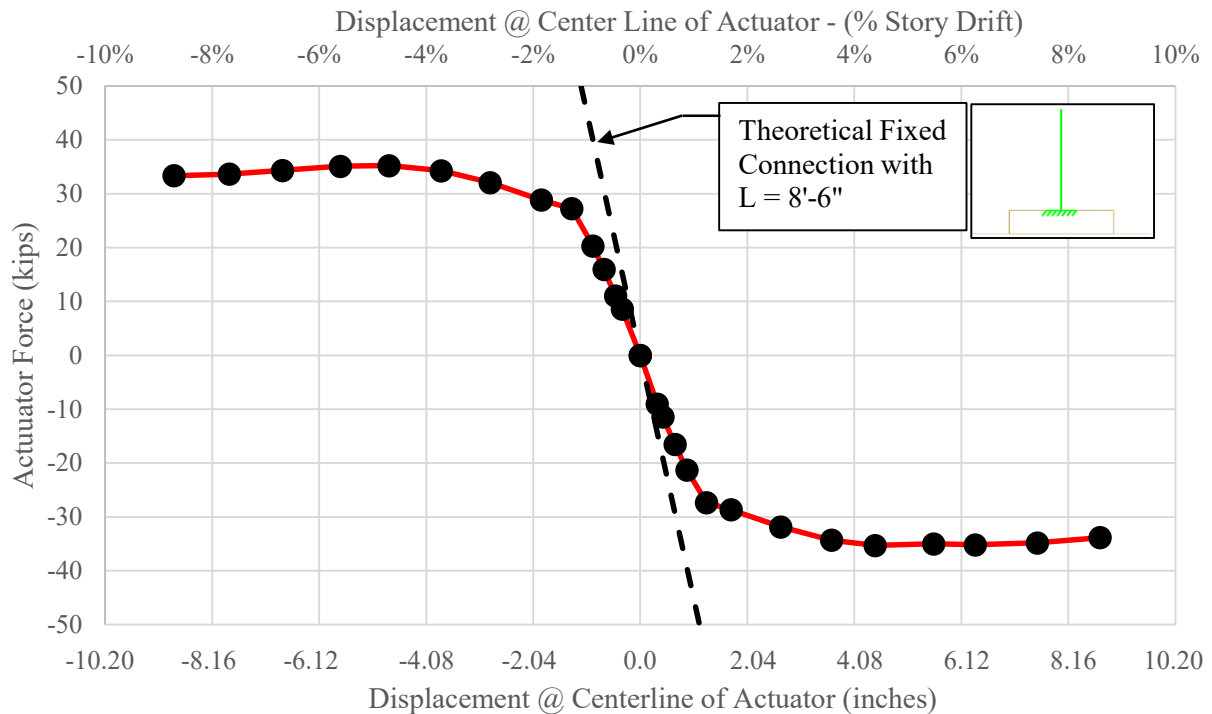


Figure 4-46: Specimen F1 - Backbone Curve; Entire Testing Protocol

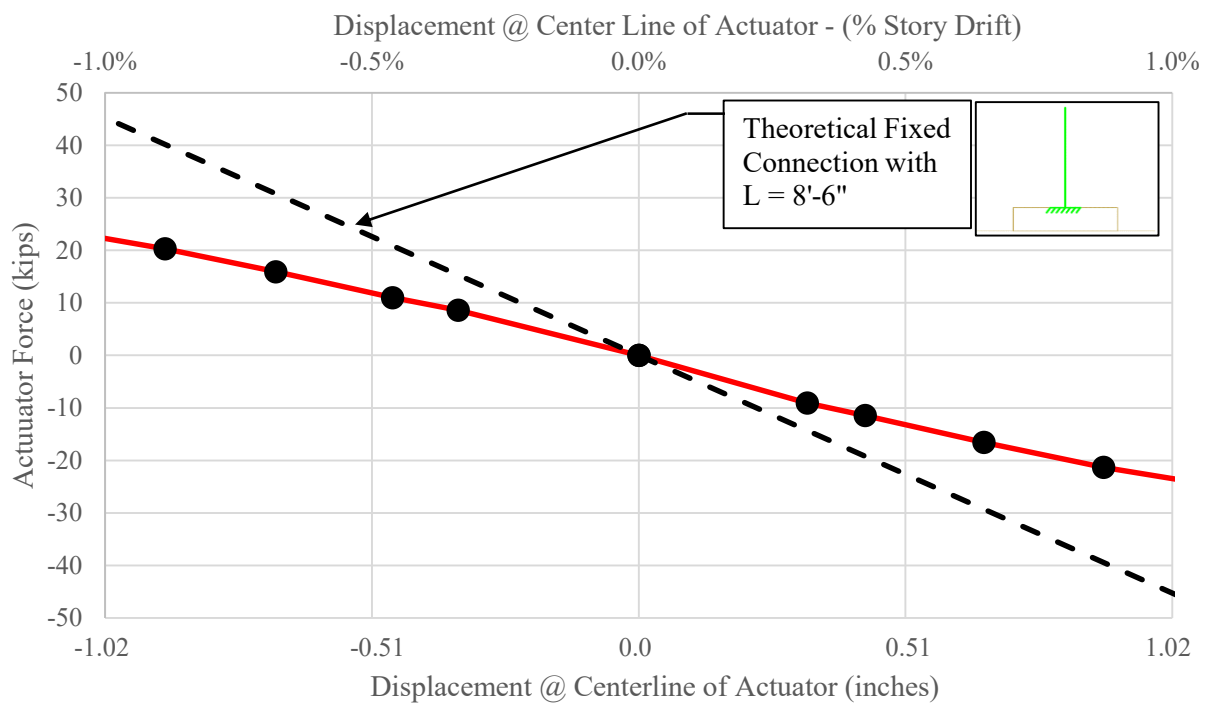


Figure 4-47: Specimen F1 - Backbone Curve; up to 1% Story Drift

4.3.7 Backbone Curve - F2

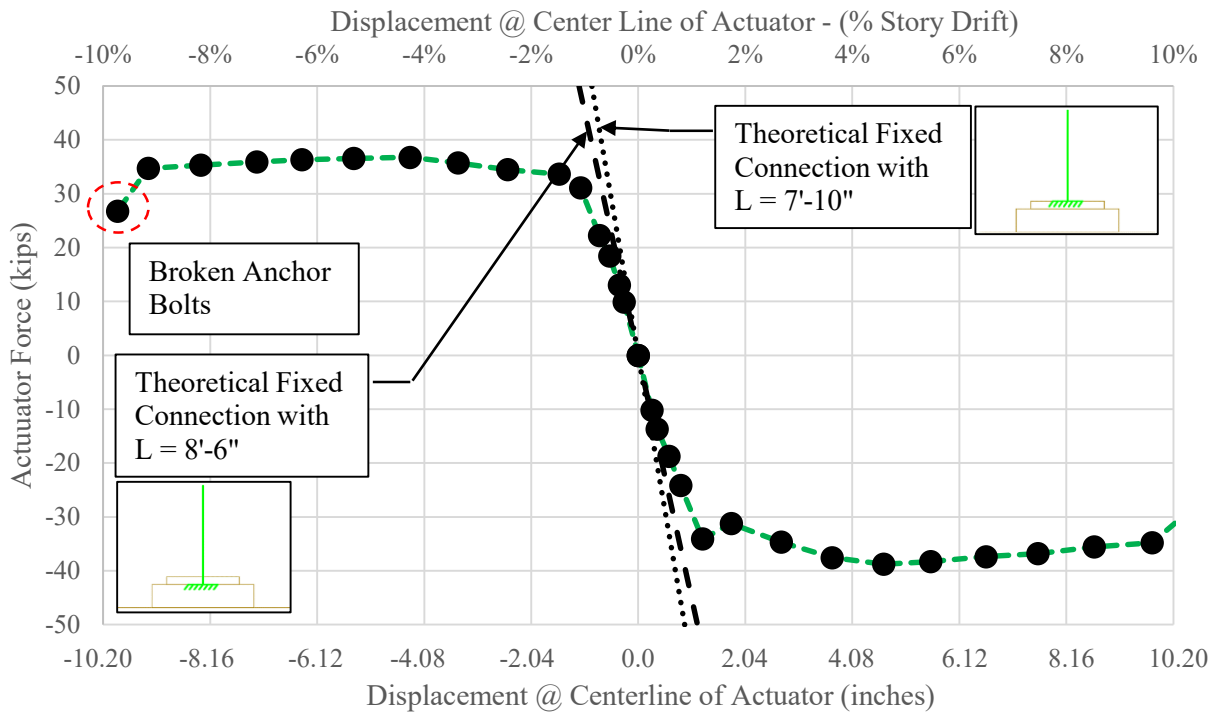


Figure 4-48: Specimen F2 - Backbone Curve; Entire Testing Protocol

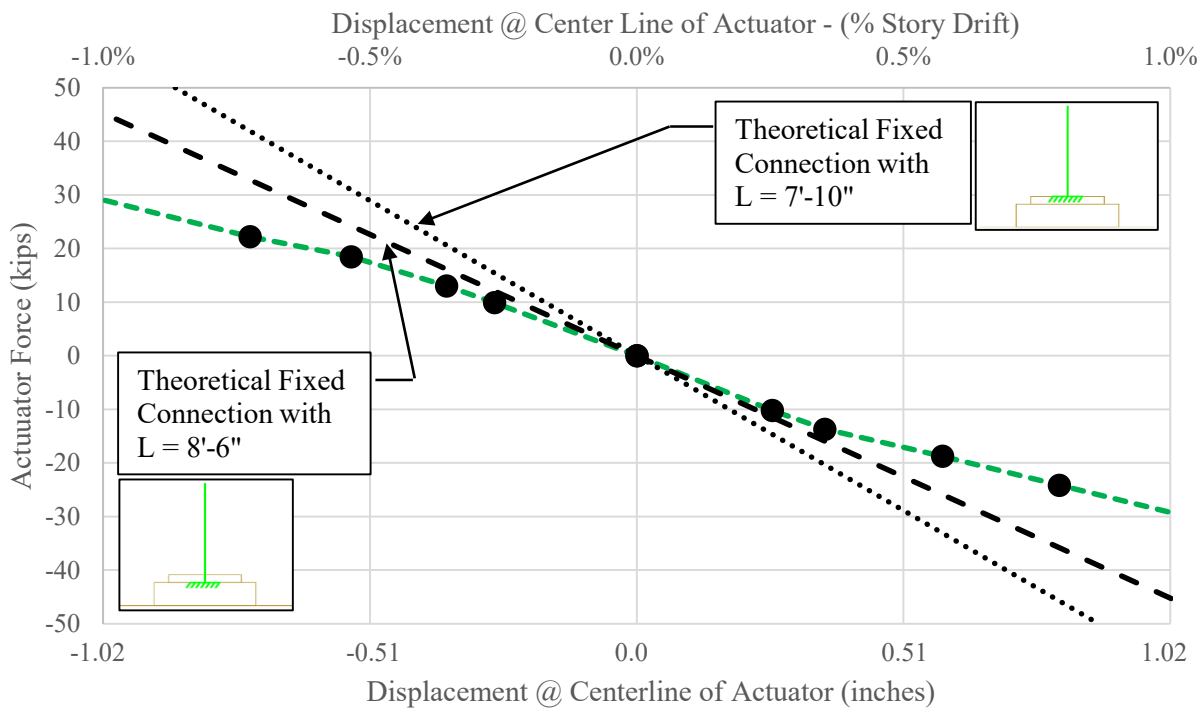


Figure 4-49: Specimen F2 - Backbone Curve; up to 1% Story Drift

4.3.8 Backbone Curve - F3

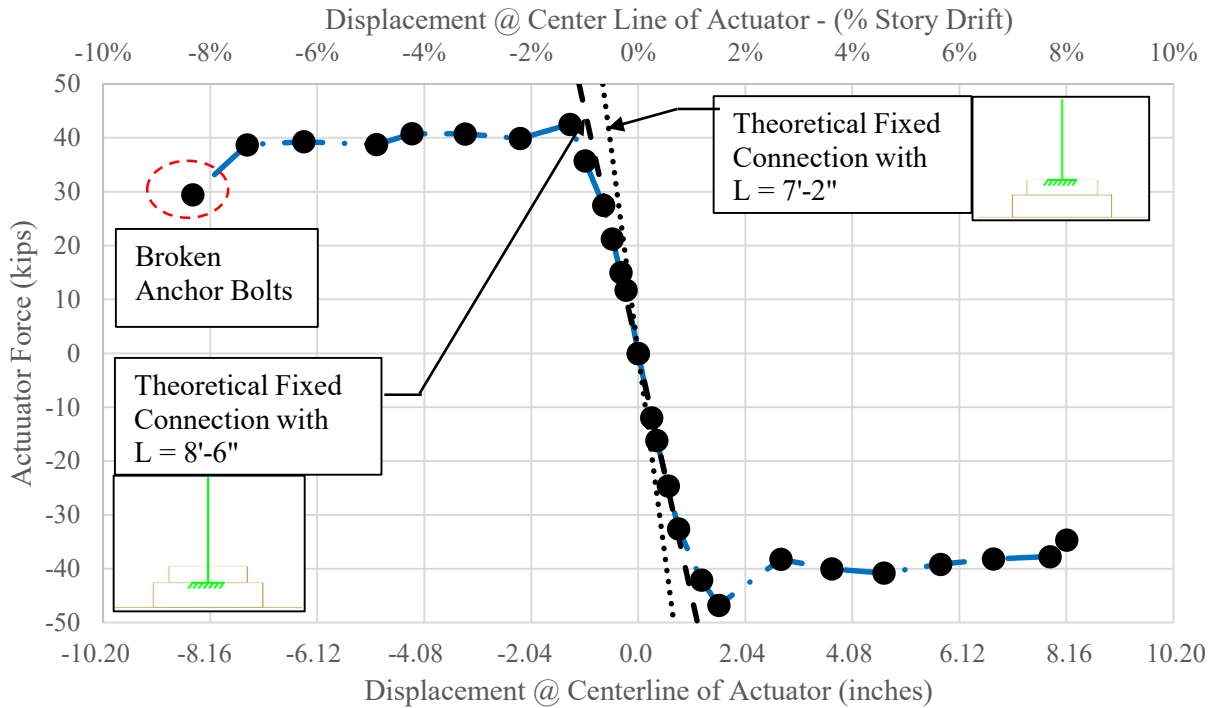


Figure 4-50: Specimen F3 - Backbone Curve; Entire Testing Protocol

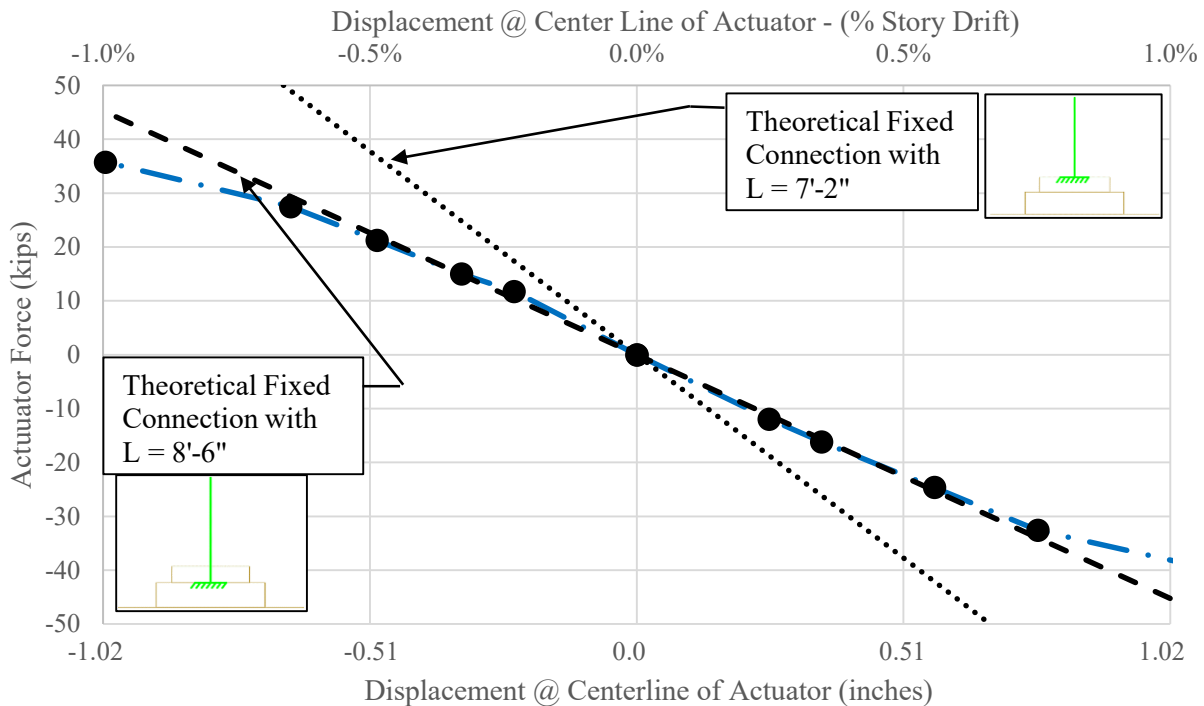


Figure 4-51: Specimen F3 - Backbone Curve; up to 1% Story Drift

4.3.9 Backbone Curve - F4

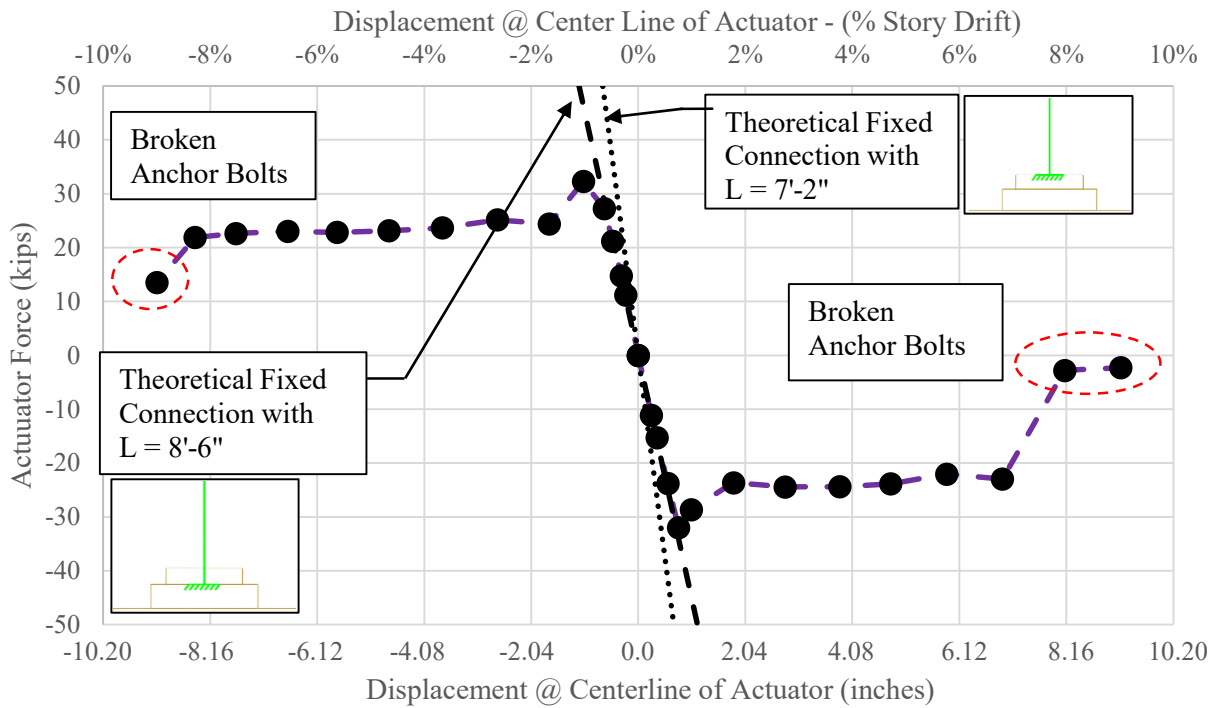


Figure 4-52: Specimen F4 - Backbone Curve, Entire Testing Protocol

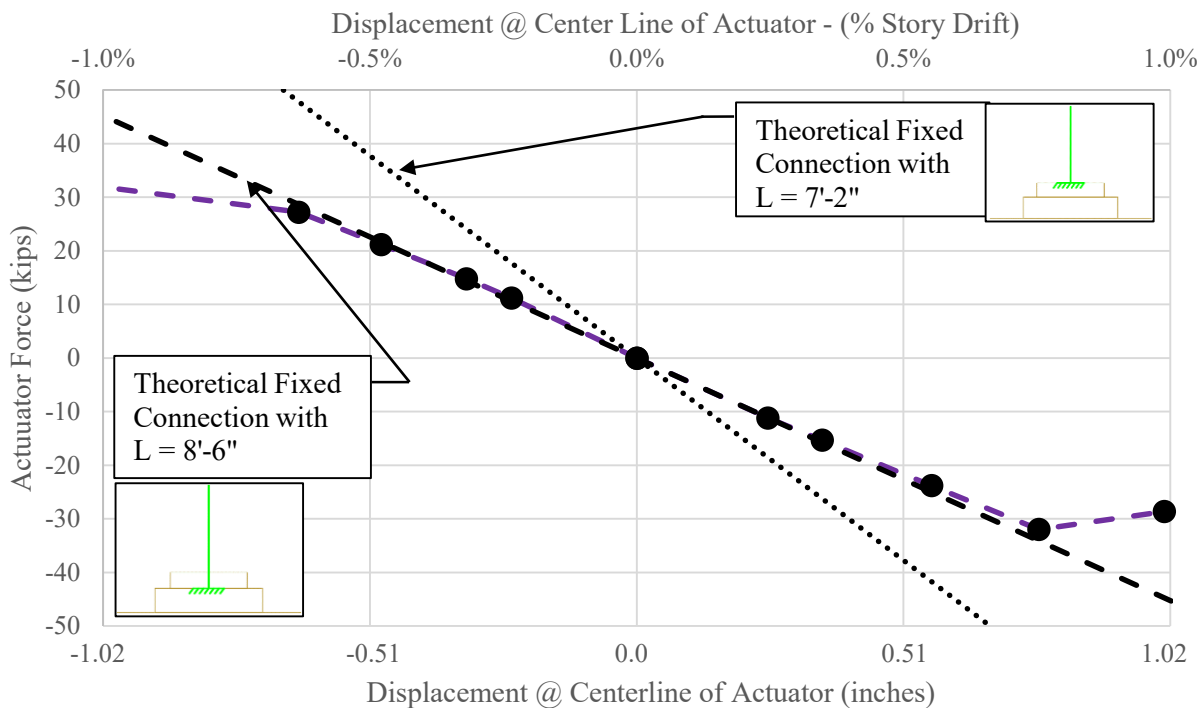


Figure 4-53: Specimen F4 - Backbone Curve; up to 1% Story Drift

4.3.10 Backbone Curve – Discussion

The backbone curves reveal behavior that is expected for column base connections of this type. The curve for the low-deflection cycles is a steep line, whose slope indicates the stiffness of the connection. Soon after the anchor bolts yield, the slope of the line flattens out, then experiences a sudden decrease whenever an anchor bolt fractures.

The initial slope (at low deflection cycles) of the backbone gives important information regarding the stiffness of the connection. The two exposed base connections (D1 & F1) show shallower lines than the theoretical “fixed” connection line, as shown in Figure 4-39 and Figure 4-47. The shallower line indicates that the connection is not “fixed”, but has a measureable rotational stiffness. Therefore, it would be inadvisable to model a connection like this as a “fixed” connection with infinite rotational stiffness.

The backbone curve for the two specimens with 8 inches of block out concrete are compared to two separate lines, corresponding to theoretical “fixed” connections at the top of the block out and the bottom of the column base. See Figure 4-41, and Figure 4-49. These slopes are steeper than those for specimens D1 and F1, indicating a stiffer connection than the exposed base connections. Therefore, adding even a small amount of block out concrete had a positive impact on the stiffness of the connection. The slopes of these backbone curves were still shallower than both theoretical lines, indicating that the 8 inches of block out concrete was not enough to create a “fixed” connection, either at the top of the block out concrete, or the base of the column. Like the exposed base connection, it would be inadvisable to model this connection as a “fixed” connection with infinite rotational stiffness.

The backbone curve for the 4 specimens with 16 inches of block out concrete (D3, D4, F3, & F4) display a steeper line than those with 8 inches of block out concrete. See Figure 4-43,

Figure 4-45, Figure 4-51, & Figure 4-53. These steeper curves indicated that the additional block out concrete did indeed contribute to an even stiffer connection. Interestingly, these 4 graphs have a slope that straddles the line approximating a theoretical fixed connection at the base of the column. This indicates that the block out concrete is stiffening the base of the connection enough that it exhibits behavior similar to that of a connection with a theoretical “fixed” base. Therefore, it would be appropriate to model these specimens as having a “fixed” base with infinite rotational stiffness at the base of the column. This will be discussed further in Section 5.4.

The backbone curve also reveals information regarding the ultimate strength of the specimens. The ultimate strength of the specimen is defined as the highest possible load supported by the system. This can be easily identified from the backbone curve as the highest point on the curve. As expected, the additional block concrete gave the connection a higher ultimate strength, on the order of 8% increase for the 8 inch block out, and 29% increase for the 16 inch block out. Specimens D4 and F4 also had, on average an ultimate strength that was 30% lower than their counterpart specimens, D3 and D4. This indicates that while the block out concrete plays a critical role in adding strength to a connection, the anchor bolts still play a large role in the ultimate strength of the connection.

4.4 Hysteresis Curve

A Hysteresis curve for each test specimen was created using the data reported from the actuator (load) and the string pot at the top of the column, SP1 (deflection). The hysteresis curve is similar to the backbone curve, except that it contains all of the data during the entire test rather than just the data points at the cycle peaks. The testing program recorded a data point for each instrument five times every second.

4.4.1 Hysteresis Curve - D1

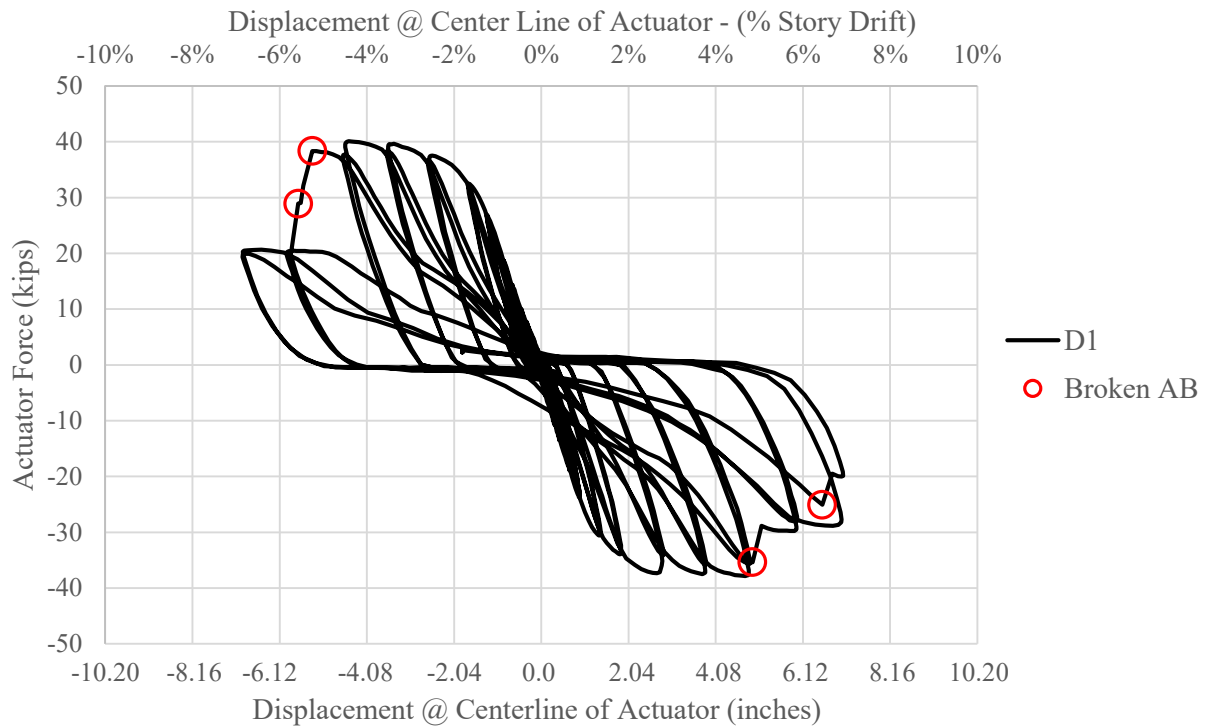


Figure 4-54: Specimen D1 - Hysteresis; Entire Testing Protocol

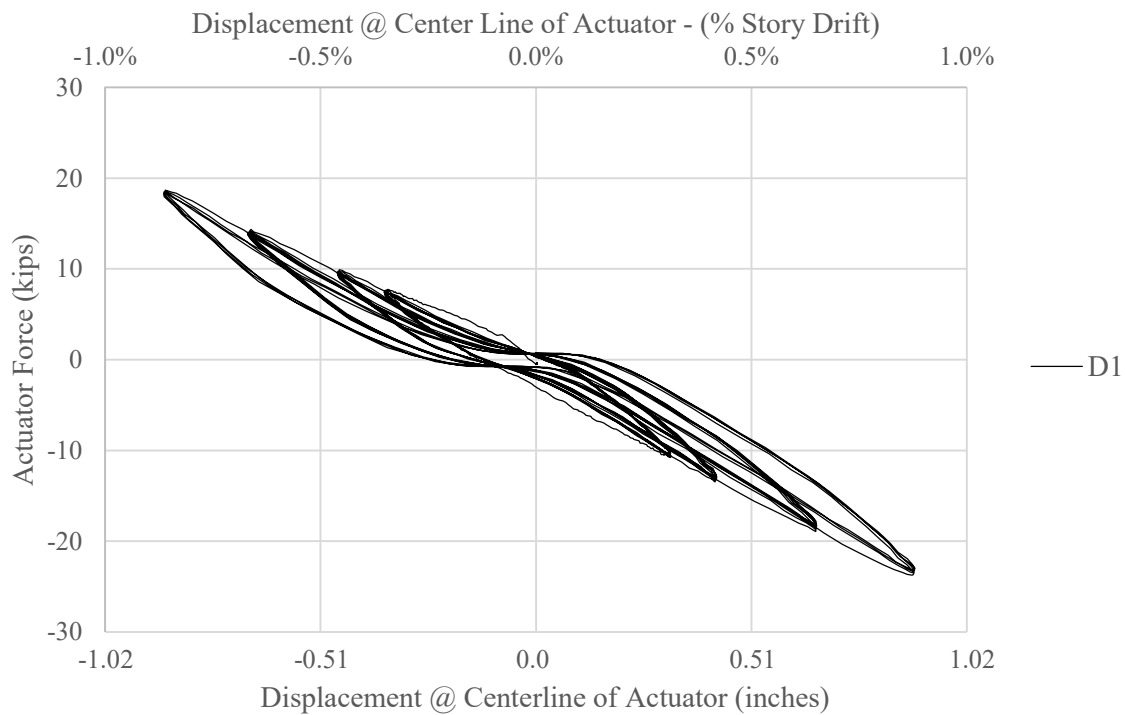


Figure 4-55: Specimen D1 – Hysteresis; up to 1% Story Drift

4.4.2 Hysteresis Curve – D2

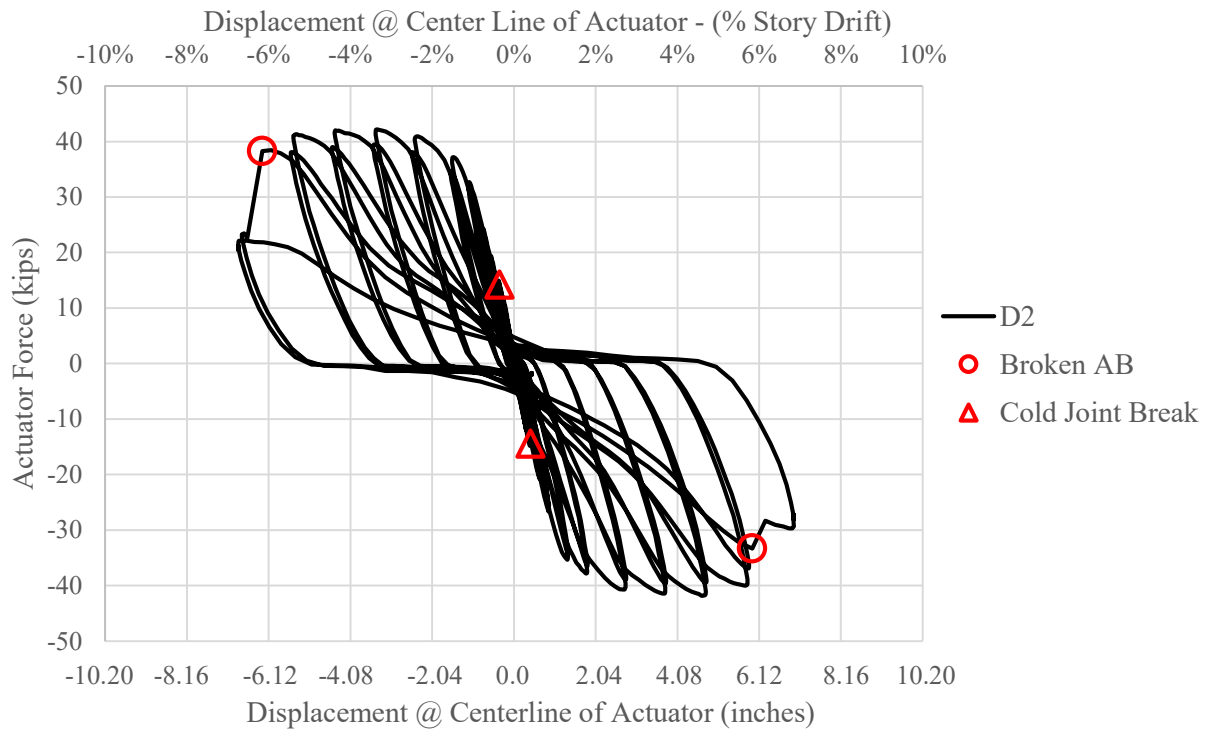


Figure 4-56: Specimen D2 - Hysteresis; Entire Testing Protocol

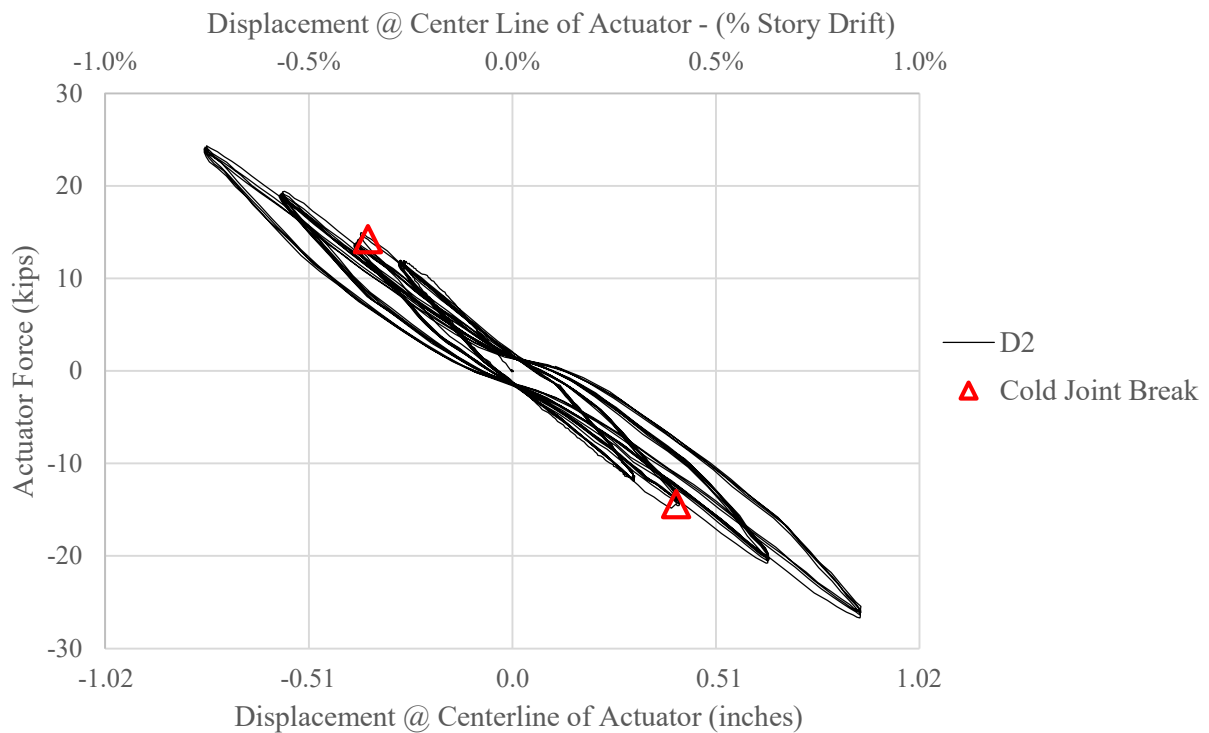


Figure 4-57: Specimen D2 - Hysteresis; up to 1% Story Drift

4.4.3 Hysteresis Curve – D3

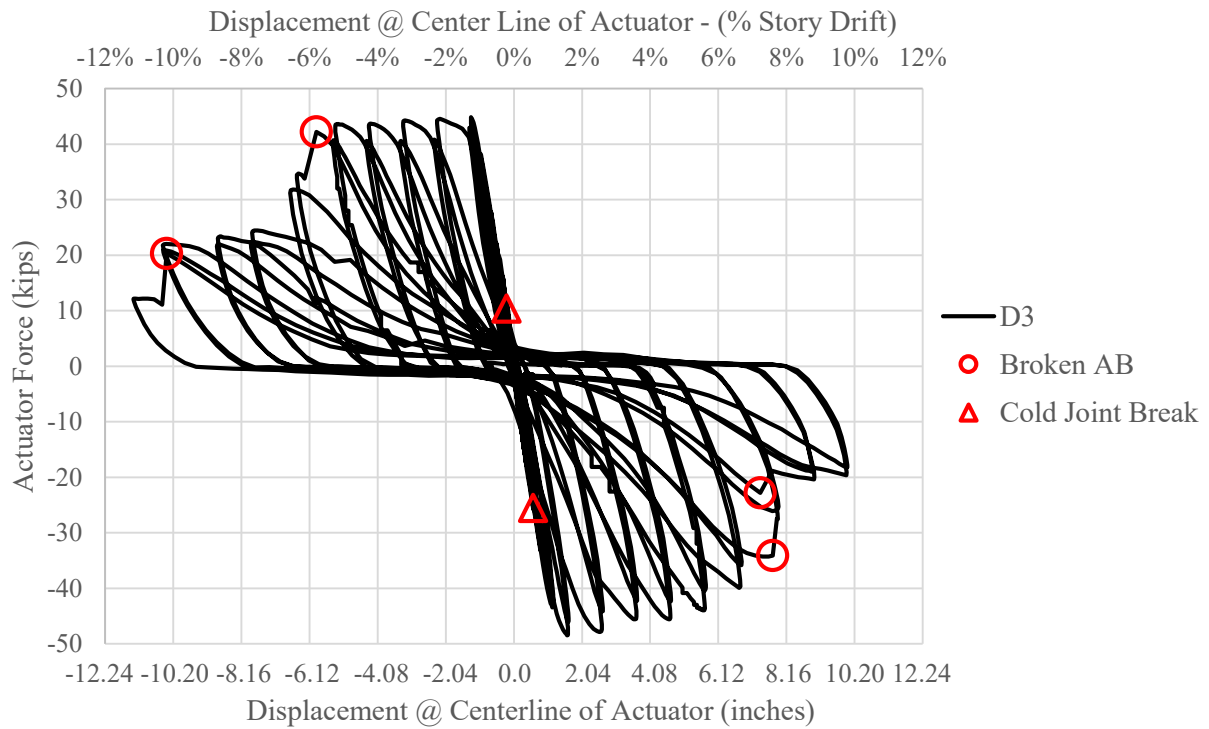


Figure 4-58: Specimen D3 - Hysteresis; Entire Testing Protocol

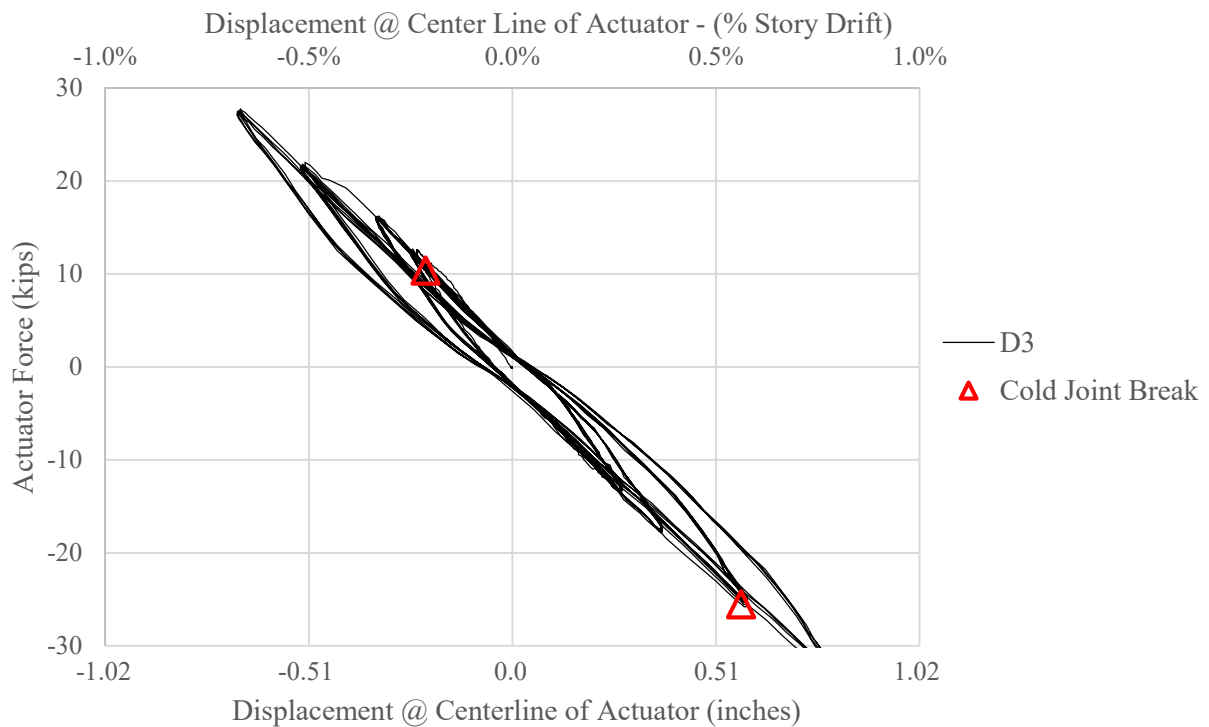


Figure 4-59: Specimen D3 - Hysteresis; up to 1% Story Drift

4.4.4 Hysteresis Curve – D4

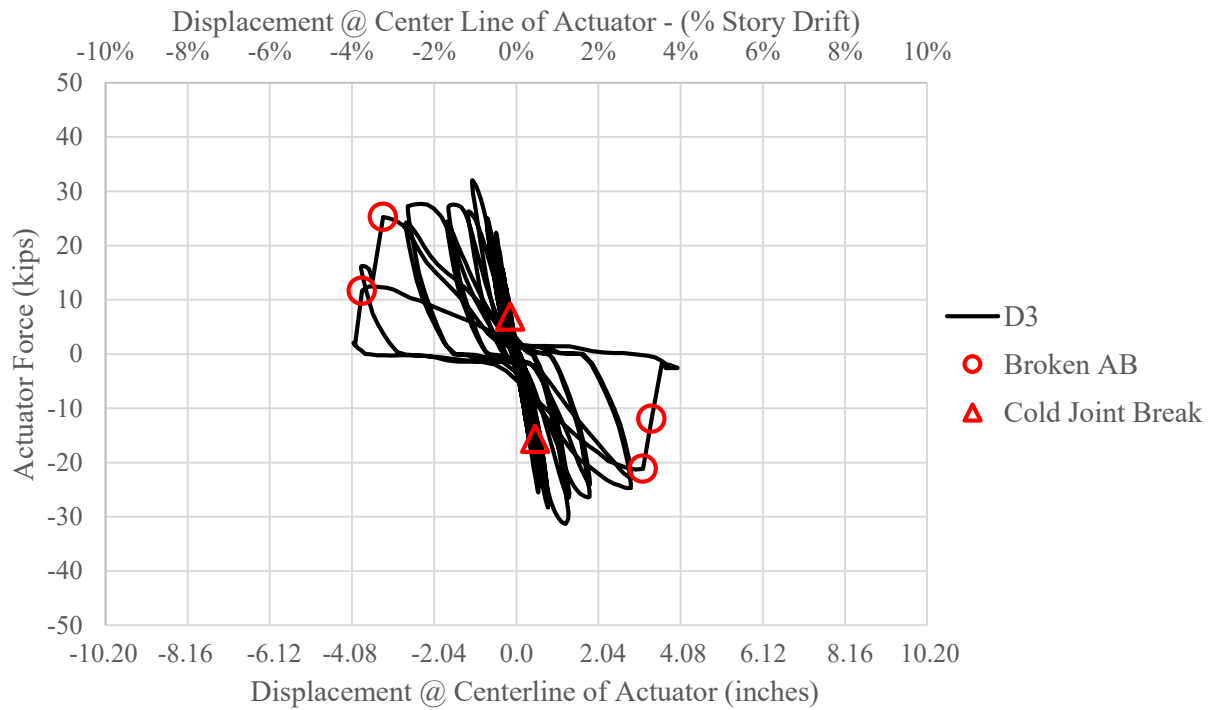


Figure 4-60: Specimen D4 - Hysteresis; Entire Testing Protocol

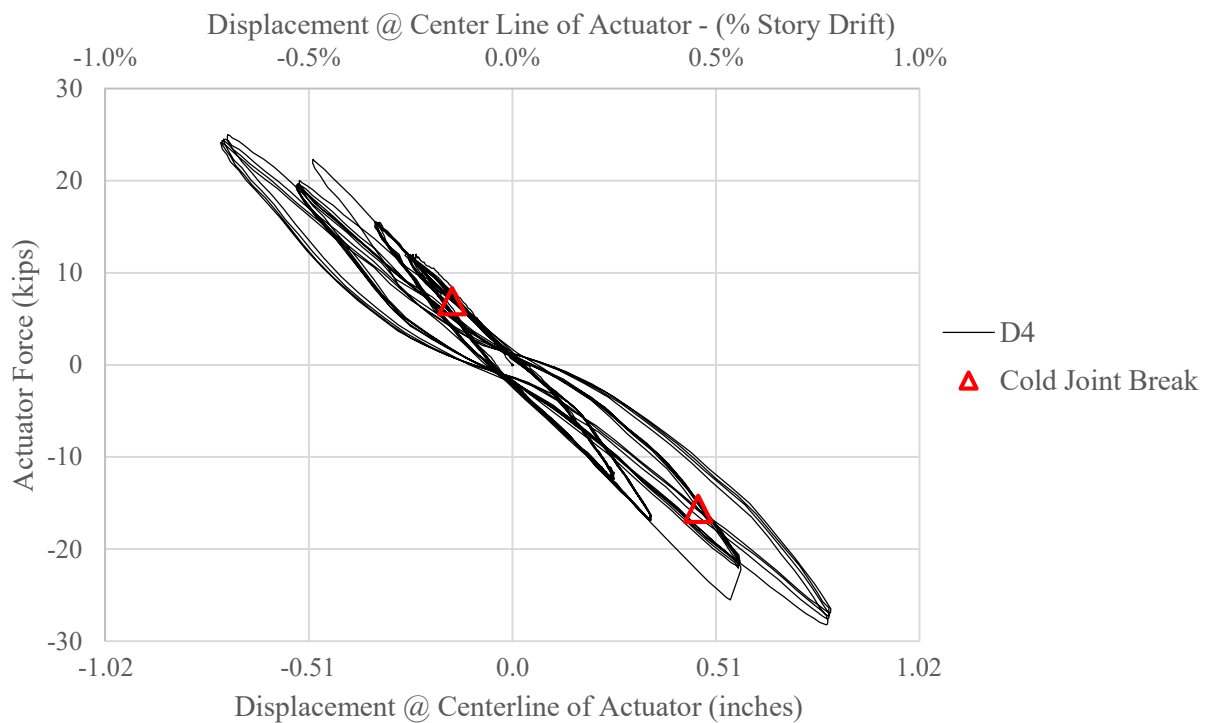


Figure 4-61: Specimen D4 - Hysteresis; up to 1% Story Drift

4.4.5 Hysteresis Curve – F1

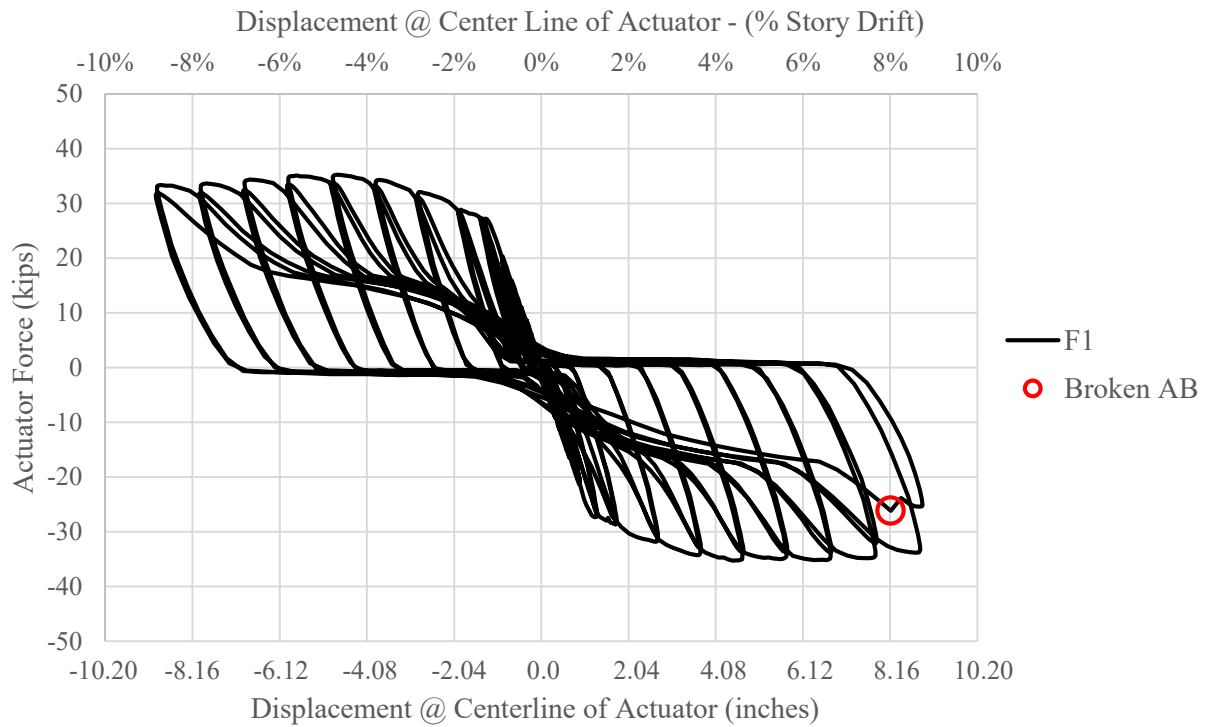


Figure 4-62: Specimen F1 - Hysteresis; Entire Testing Protocol

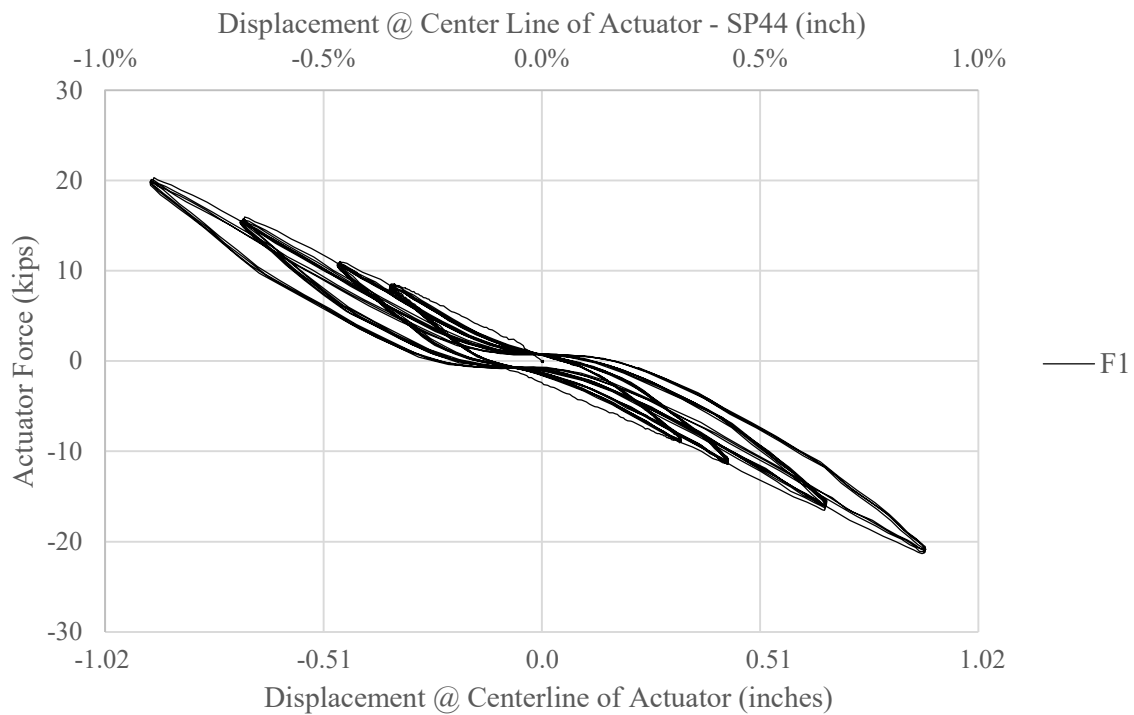


Figure 4-63: Specimen F1 - Hysteresis; up to 1% Story Drift

4.4.6 Hysteresis Curve – F2

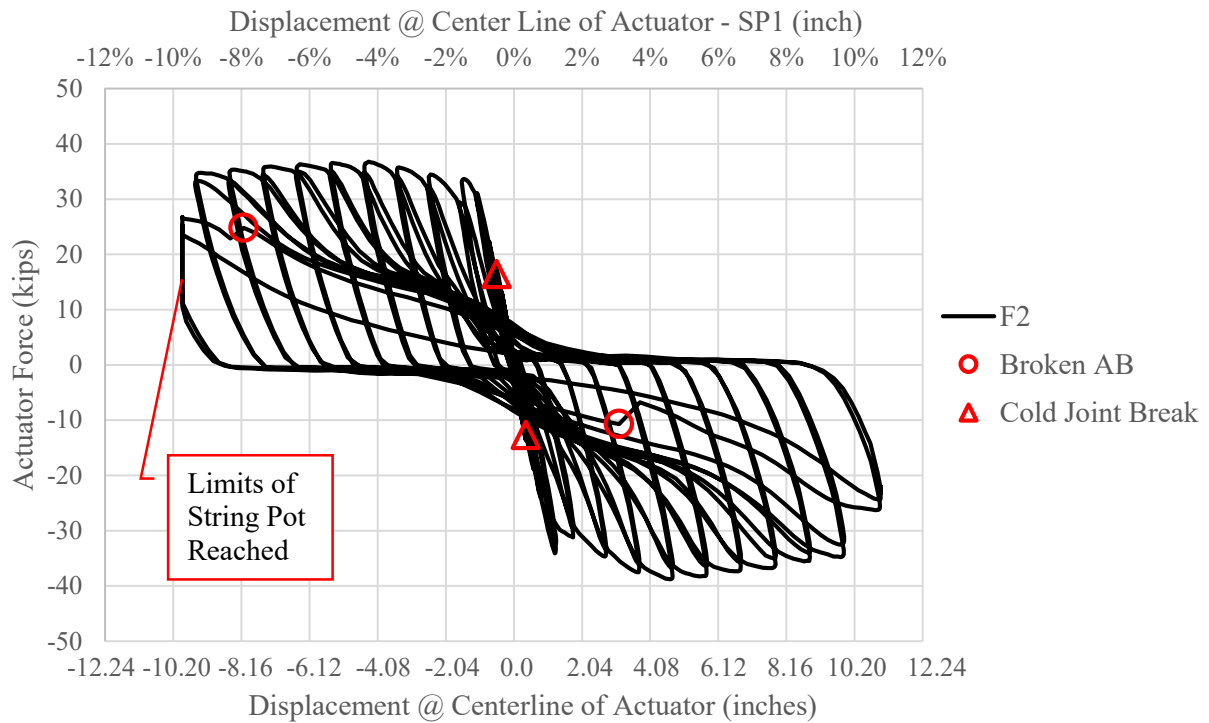


Figure 4-64: Specimen F2 - Hysteresis; Entire Testing Protocol

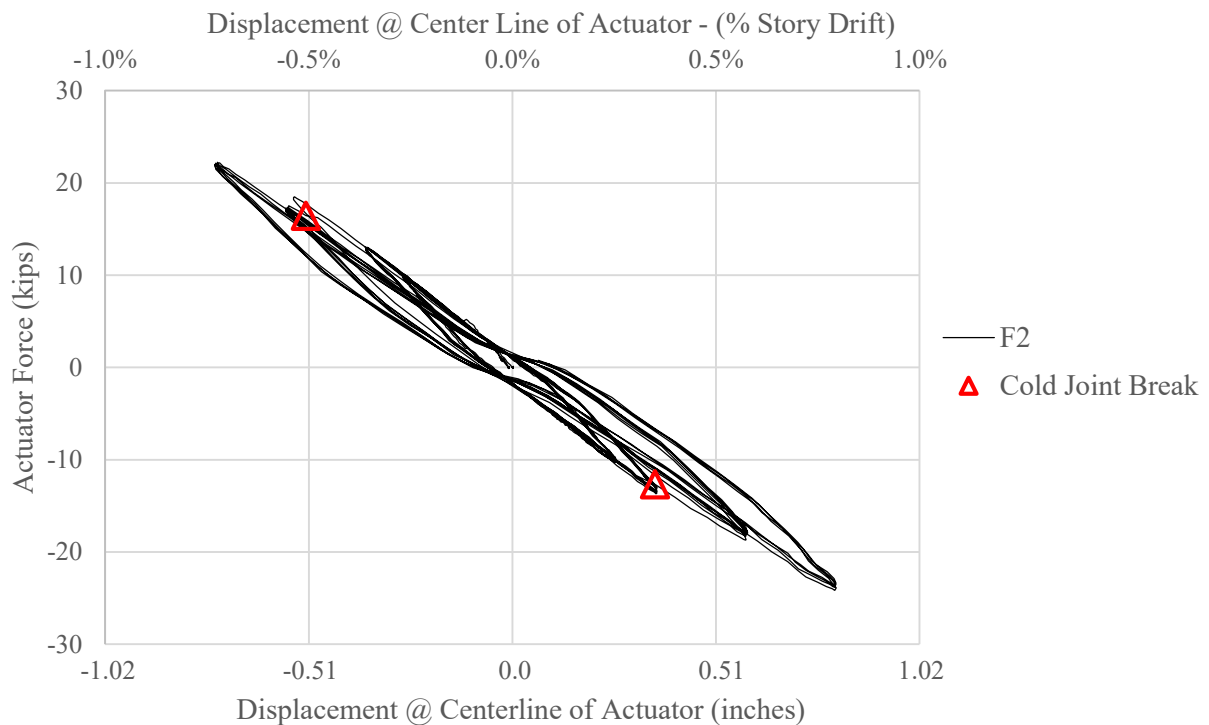


Figure 4-65: Specimen F2 - Hysteresis; up to 1% Story Drift

4.4.7 Hysteresis Curve – F3

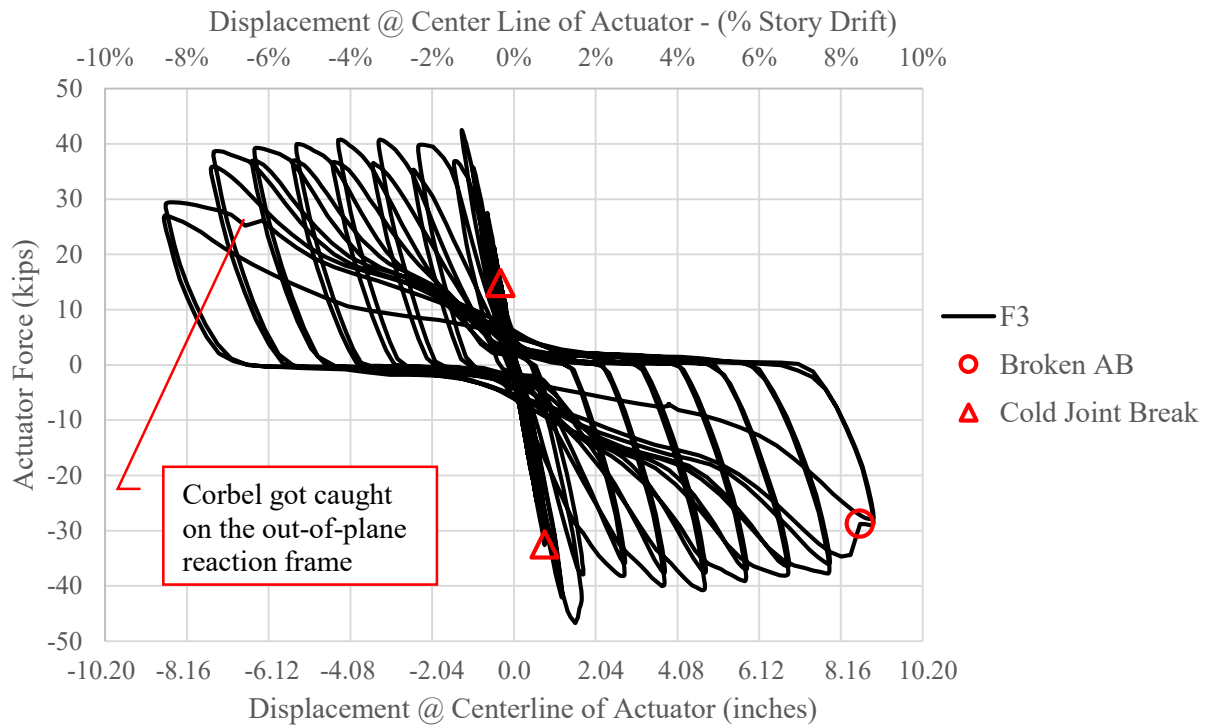


Figure 4-66: Specimen F3 - Hysteresis; Entire Testing Protocol

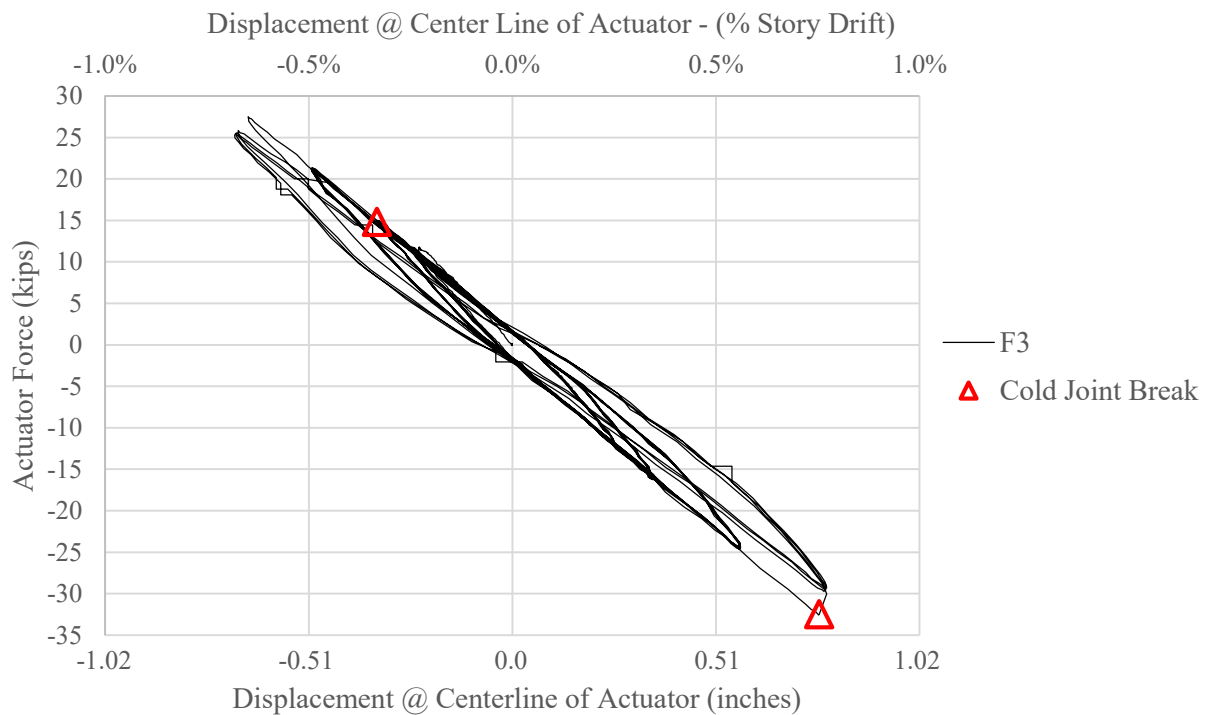


Figure 4-67: Specimen F3 - Hysteresis; up to 1% Story Drift

4.4.8 Hysteresis Curve – F4

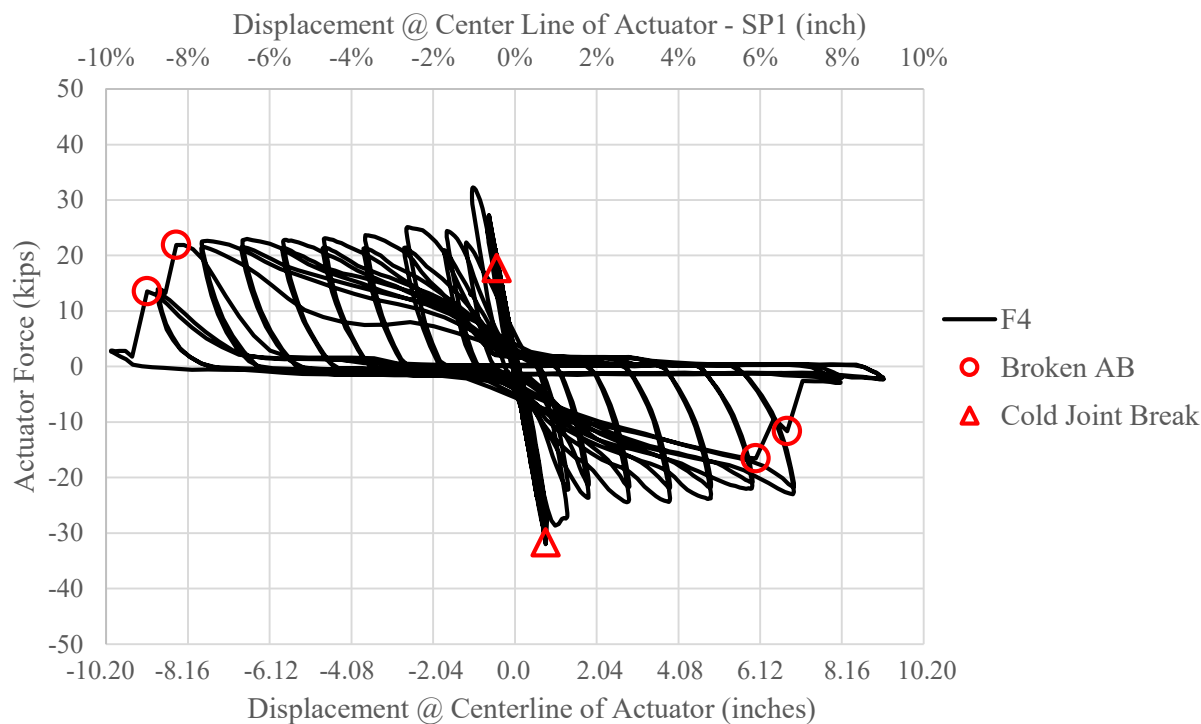


Figure 4-68: Specimen F4 - Hysteresis; Entire Testing Protocol

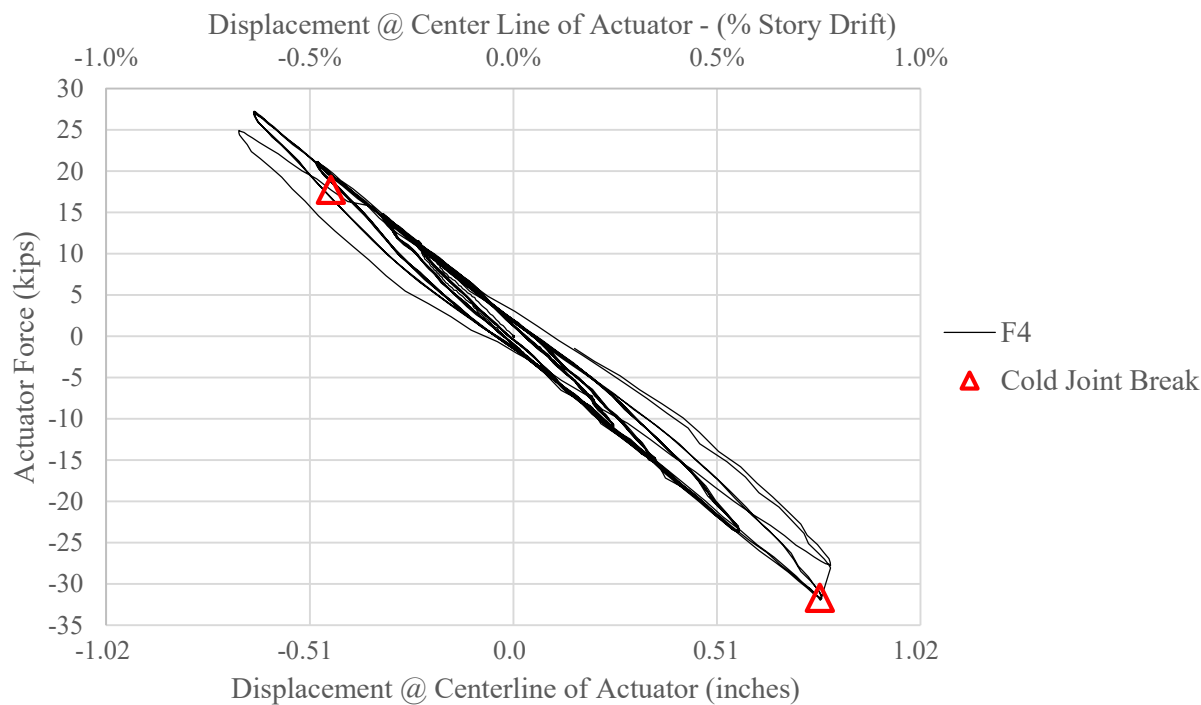


Figure 4-69: Specimen F4 - Hysteresis; up to 1% Story Drift

4.4.9 Hysteresis Curve – Discussion

The backbone curves and the hysteresis plots are very similar and yield similar information. Like the backbone curves, the hysteresis curves indicate that the additional block out concrete gives the specimens greater stiffness and ultimate strength.

The hysteresis curves give additional information on the critical role of the anchor bolts in the performance of the specimens. The location on the graphs when the various anchor bolts break is clearly marked. It can be clearly seen that with a broken anchor bolt comes an accompanying large drop in strength of the connection. This furthers the conclusion that the anchor bolts play a very critical role in the ultimate strength of the connection. This is true for the large deflection cycles, when the ultimate strength of the connection became a critical component in the behavior of the specimen.

These curves also indicate the role that the breaking of the concrete bond at the cold joint between the top mat and base mat had. For specimens 1 through 3 of both series, the breaking of the cold joint had little effect on the overall stiffness of the specimen, as indicated by the hysteresis curve being mostly linear before and after the break. When the cold joint broke, the resultant tensile force was transferred from the cold joint to the anchor bolts. When there was a sufficient amount of anchor bolts resisting the tensile load (as is the case with the first 3 specimens in each series), the anchor bolt strength was sufficient to maintain the stiffness of the connection. In specimens D4 and F4 however, the breaking of the cold joint had a much greater effect, as evidenced by the change in the slope and shape of the hysteresis graph after the cold joint break. The reduced number of anchor bolts means that there was much less steel available to resist the tensile resultant of the connection, and the stiffness and strength were reduced. This is clearly evident in Specimen F4, Figure 4-68.

4.5 Rotational Stiffness

The rotational stiffness at the top of the concrete for each specimen is shown in the idealized model below in Figure 4-70. It is often expressed in models as a “rotational spring”.

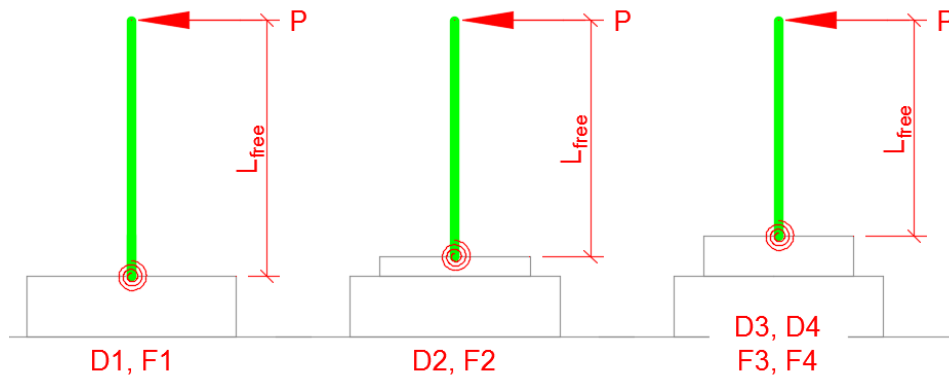


Figure 4-70: Rotational Spring Model and Location at Each Specimen

The rotational stiffness is expressed as β , and is expressed in terms of the moment required to rotate a point by a given angle, in this case, kip-in/radians. The rotational stiffness is determined from EQ (4.5.1) below.

$$\beta = \frac{M}{\theta} \quad (4.5.1)$$

Where:

M = Moment applied at the point of interest (kip-in)

θ = Angle of rotation at the point of interest (radian)

The Moment (M) is determined simply by using EQ (4.5.2).

$$M = P \cdot L_{free} \quad (4.5.2)$$

Where:

P = load applied to the top of the column by the actuator

L_{free} = Length of the column between the point of the load and the top of concrete, depending on the specimen, 102 inches, 94 inches, or 86 inches.

The angle of rotation at the point of interest (θ), was not directly measured and must be calculated from the available data. This angle was determined using the small angle approximation illustrated below in Figure 4-71, and given in EQ (4.5.3).

$$\theta = \frac{\delta_{connection}}{L_{free}} \quad (4.5.3)$$

Where

$\delta_{connection}$ = deflection at the top of the column due only to the rotation at the point of interest, ie. assuming a perfectly rigid column.

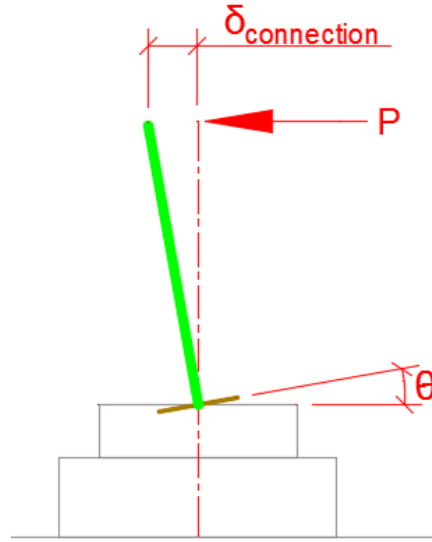


Figure 4-71: Angle of Rotation at Point of Interest

Determining this value involved the movement at the top of the column (as reported by string pot SP1) under load and has three contributing influences: The bending/flexibility of the column, the rotational flexibility of the column base connection, and the lateral movement of the base. This relationship is expressed in EQ (4.5.4), and visually in Figure 4-72.

$$\delta_{total} = \delta_{column} + \delta_{connection} + \delta_{base} \quad (4.5.4)$$

For small deflections, the deflection due to the lateral movement of the base (δ_{base}) was assumed to be negligible and was ignored. This assumption was validated by analyzing the deflections at the base of the columns as reported by string pots. Thus the deflection at the top of the column due only to rotation was determined from EQ (4.5.5).

$$\delta_{connection} = \delta_{total} - \delta_{column} \quad (4.5.5)$$

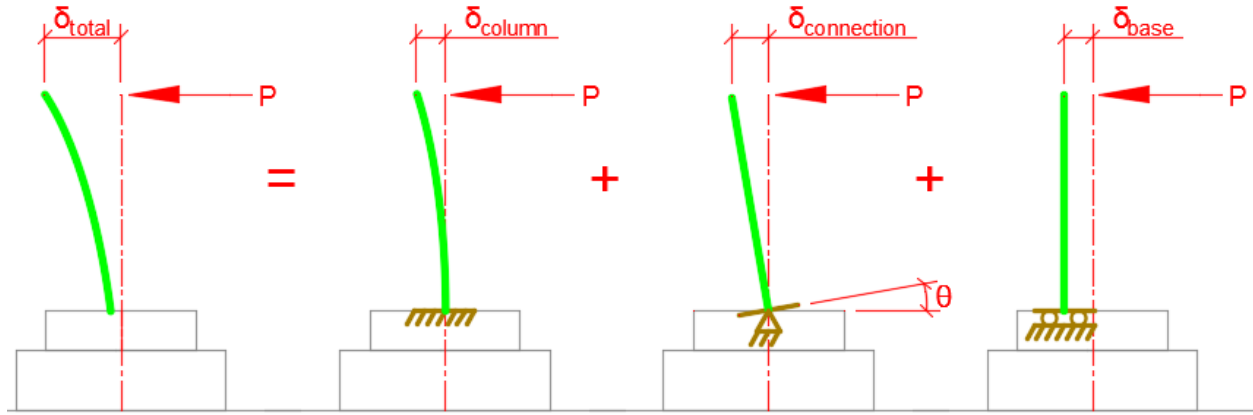


Figure 4-72: Model for Contributions to Total Deflection

The total deflection (δ_{total}) was reported during testing from string pot SP1. The contribution of the total deflection caused by the bending of the column (δ_{column}) was determined numerically from the Bernoulli beam equation discussed previously in section 4.2, and repeated here for convenience as EQ (4.5.6). Refer to section 4.2 for further information on this equation.

$$\delta_{column} = \frac{PL_{free}^3}{3EI} \quad (4.5.6)$$

The load applied to the column (P) was simply recorded from the actuator. The length used here (L_{free}) was the distance from the centerline of the actuator to the top of the block out concrete (or the top of the base mat concrete in the case of specimens D1 & F1) and varied with each specimen. The material and shape properties of the column (EI) are known constants.

Combining EQs (4.5.6), (4.5.5), (4.5.3), & (4.5.2), into EQ (4.5.1) gives us EQ (4.5.7).

$$\beta = \frac{M}{\theta} = \frac{P \cdot L_{free}}{\frac{\delta_{connection}}{L_{free}}} = \frac{P \cdot L_{free}^2}{\delta_{total} - \delta_{column}} = \frac{P \cdot L_{free}^2}{\delta_{total} - \frac{P \cdot L_{free}^3}{3 \cdot E \cdot I}} \quad (4.5.7)$$

For reference, this formula was applied to each specimen at the first peak of the 0.75% story drift cycle. See Table 4-5 for the results of this analysis. In addition to the rotational stiffness at the first peak of the 0.75% story drift cycle, the stiffness was also calculated at the first positive peak immediately after the concrete cold joint broke. This can be seen in Table 4-6.

Table 4-5: Rotational Stiffness at First Peak of 0.75% Story Drift Cycle

Specimen	Actuator Force P (kip)	Column Length L_{free} (in)	Column Deflection, SP1 δ_{total} (in)	Modulus of Elasticity E (ksi)	Moment of Inertia I (in ⁴)	Rotational Stiffness β (kip-in/radian)
D1	14.3605	102	0.6746	29000	541	4.26E+05
D2	14.8407	94	0.3981	29000	541	9.63E+05 *
D3	19.2394	86	0.4156	29000	541	9.14E+05 *
D4	15.4897	86	0.3339	29000	541	9.20E+05
F1	15.9385	102	0.6943	29000	455	6.21E+05
F2	18.4793	94	0.5461	29000	455	10.31E+05
F3	21.2373	86	0.4964	29000	455	10.12E+05
F4	21.1794	86	0.4886	29000	455	10.56E+05

* The concrete cold joint broke before the first 0.75% story drift cycle peak, so this point is taken just before the cold joint breaks.

In Sections 4.5.1 through 4.5.9, graphs are shown for each of the test specimens. These show the rotational stiffness during the run from zero displacement to max displacement for the first cycle of the first four story drift cycles.

For those specimens with a block out, the rotational stiffness dropped when the cold joint between the base mat and the top mat/block out broke. When this occurred prior to the first cycle of the 1.0% story drift, it is indicated on the graph.

Table 4-6: Rotational Stiffness Before and After Concrete Cold Joint Break

Specimen	Rotational Stiffness	
	pre-cold joint break	post-cold joint break
	β (kip-in/radian)	β (kip-in/radian)
D1	4.26E+05	-
D2	9.63E+05	8.52E+05
D3	9.14E+05	6.97E+05
D4	9.20E+05	5.64E+05
F1	6.21E+05	-
F2	10.31E+05	7.73E+05
F3	10.12E+05	7.04E+05
F4	10.56E+05	6.41E+05

4.5.1 Rotational Stiffness – D1

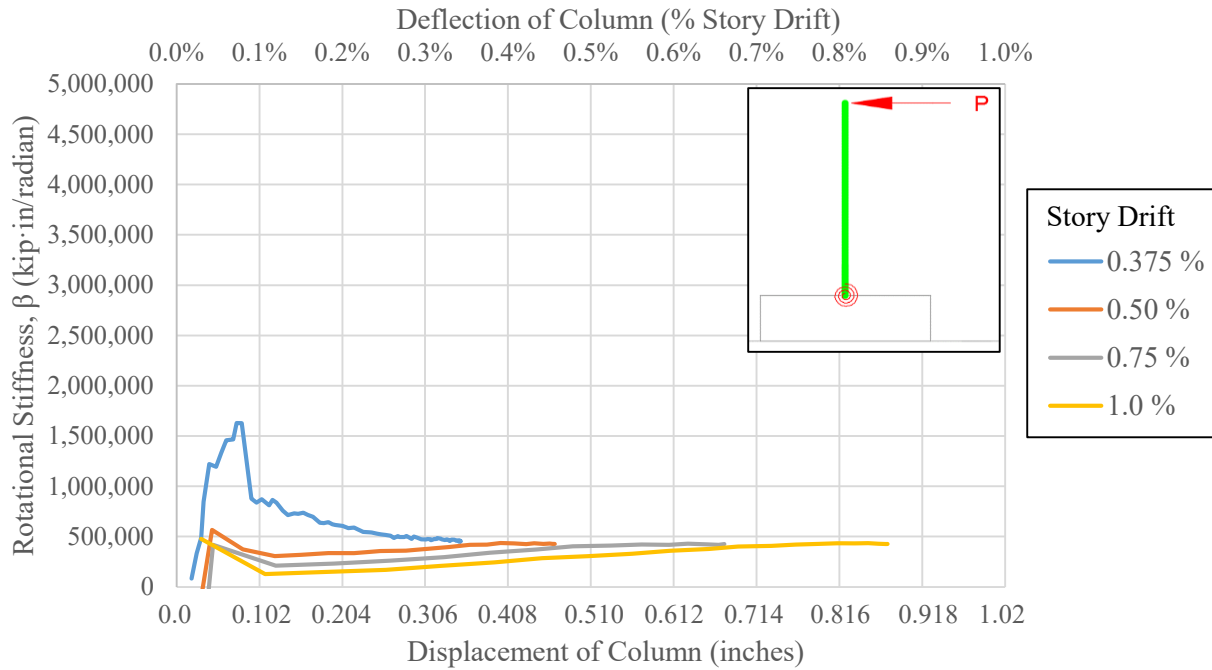


Figure 4-73: Rotational Stiffness for Test Specimen D1

4.5.2 Rotational Stiffness – D2

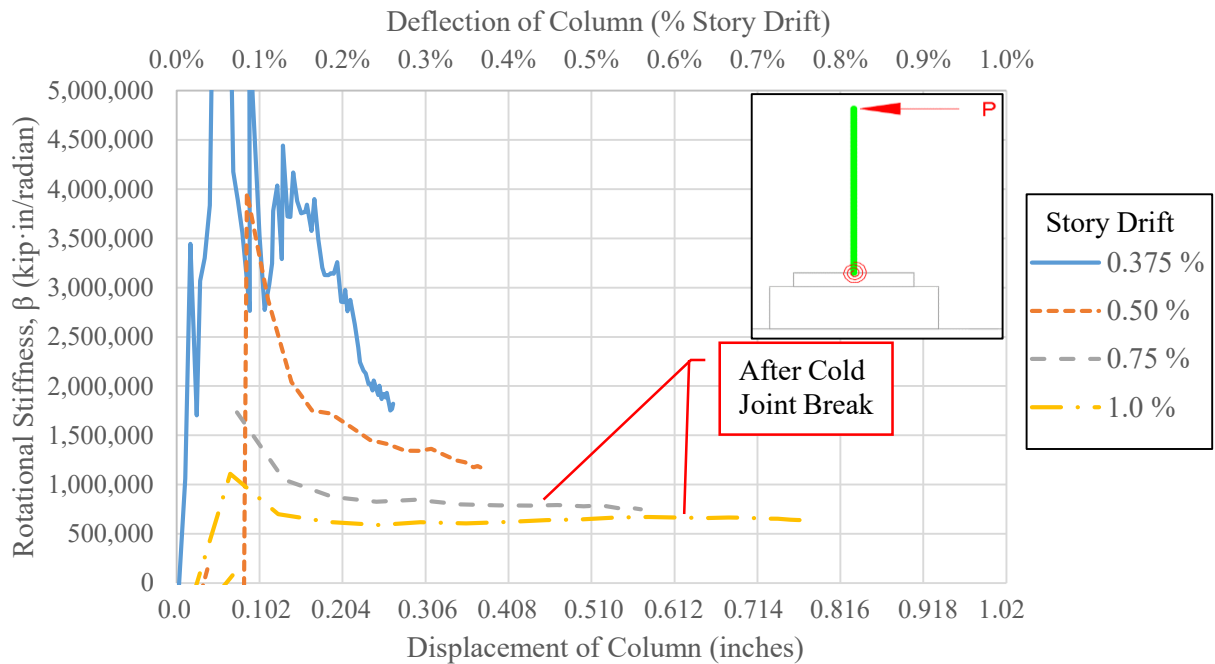


Figure 4-74: Rotational Stiffness for Test Specimen D2

4.5.3 Rotational Stiffness – D3

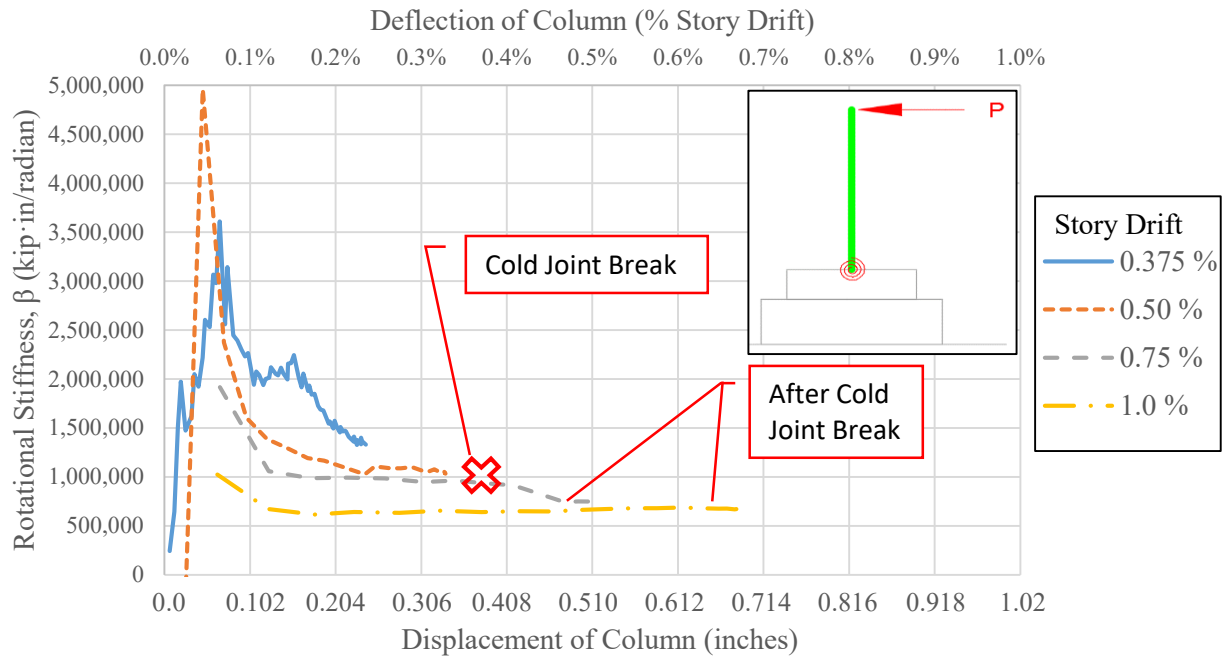


Figure 4-75: Rotational Stiffness for Test Specimen D3

4.5.4 Rotational Stiffness – D4

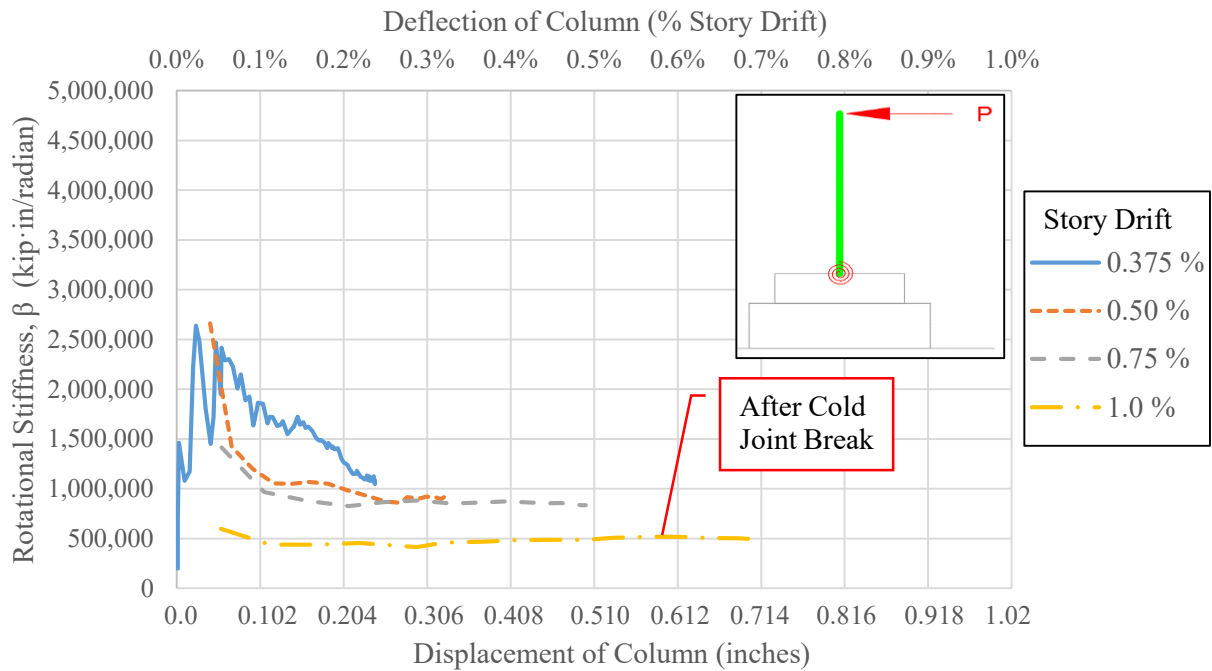


Figure 4-76: Rotational Stiffness for Test Specimen D4

4.5.5 Rotational Stiffness – F1

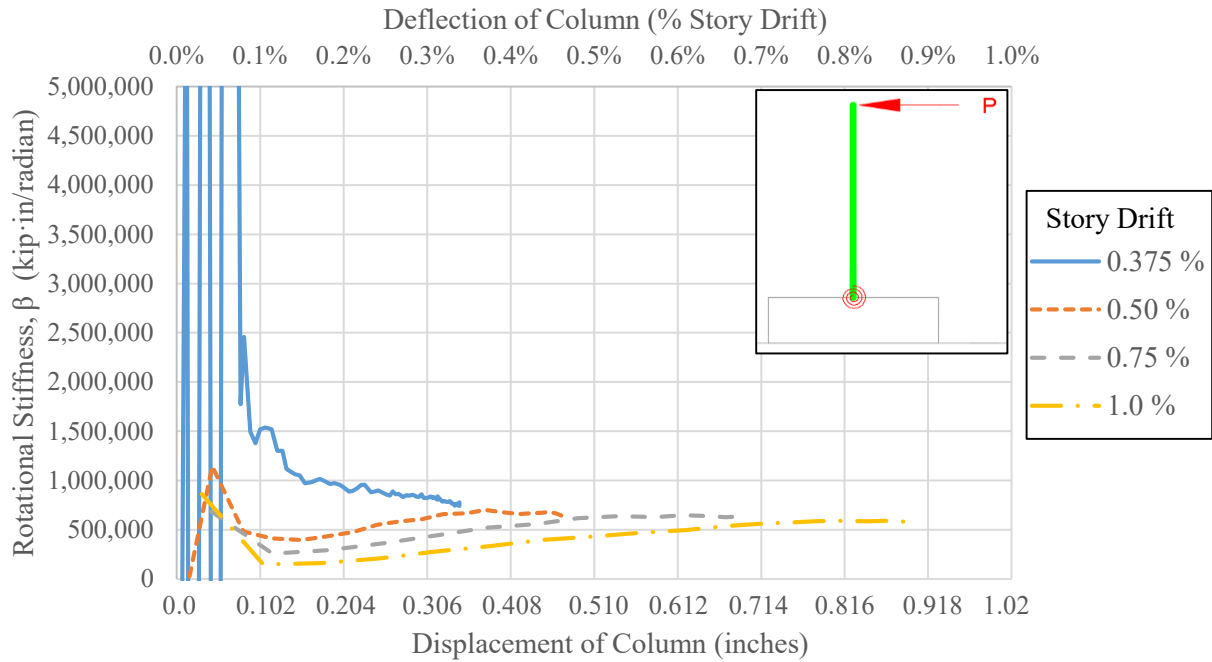


Figure 4-77: Rotational Stiffness for Test Specimen F1

4.5.6 Rotational Stiffness – F2

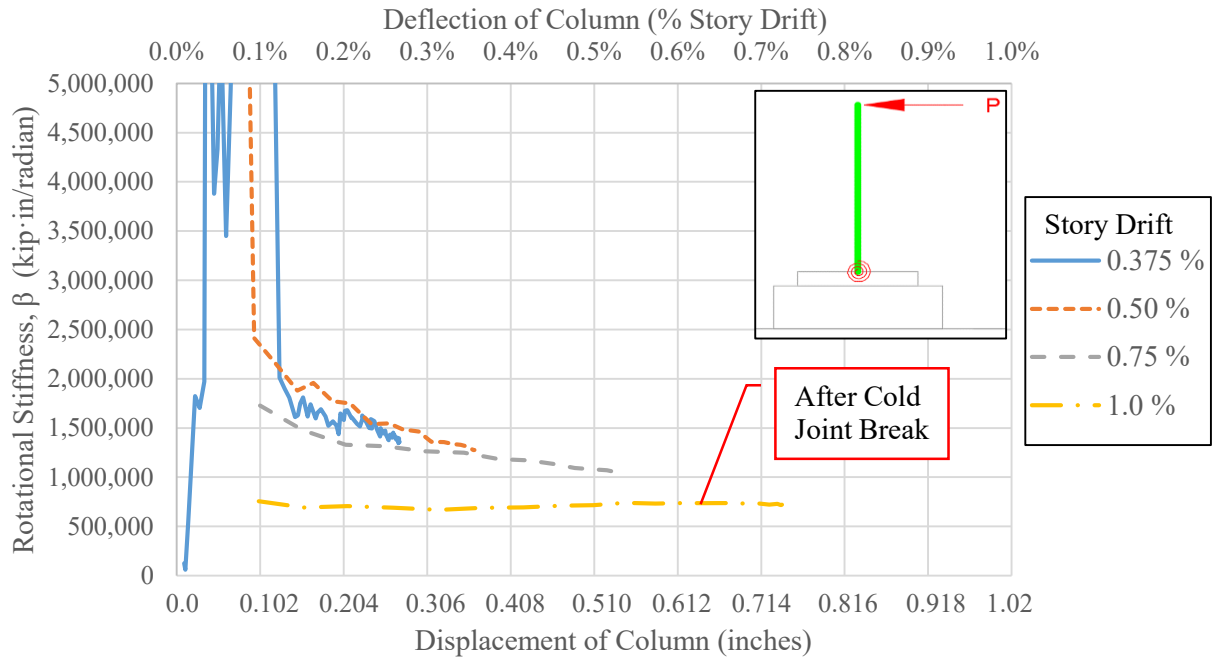


Figure 4-78: Rotational Stiffness for Test Specimen F2

4.5.7 Rotational Stiffness – F3

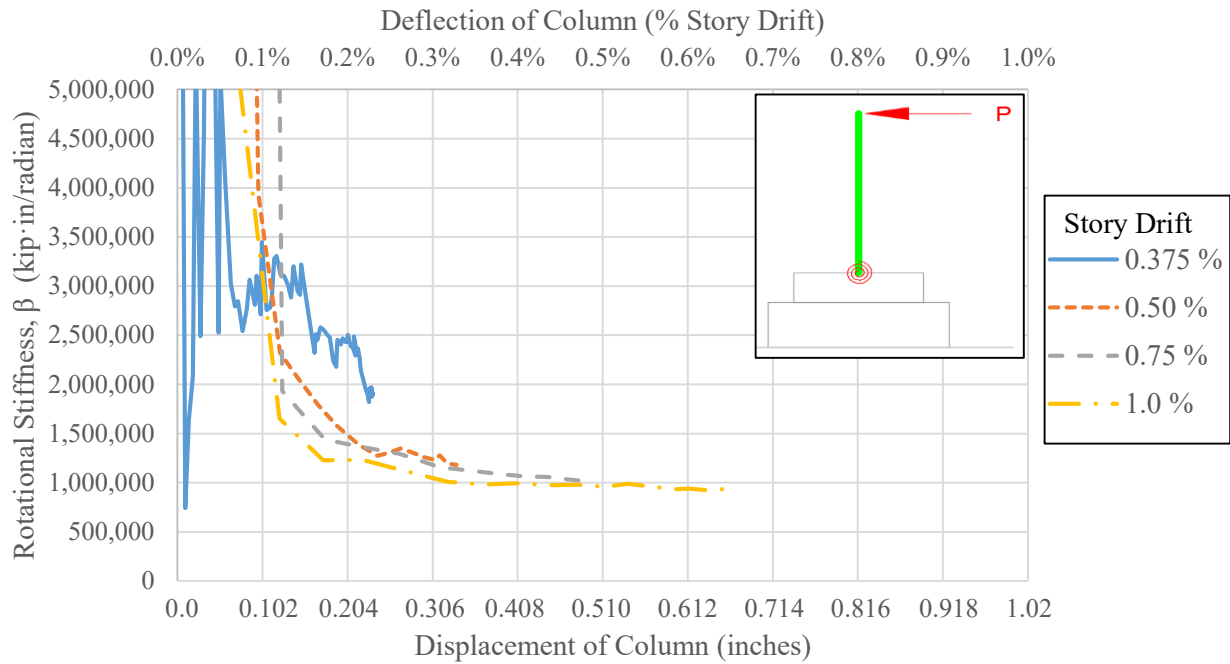


Figure 4-79: Rotational Stiffness for Test Specimen F3

4.5.8 Rotational Stiffness – F4

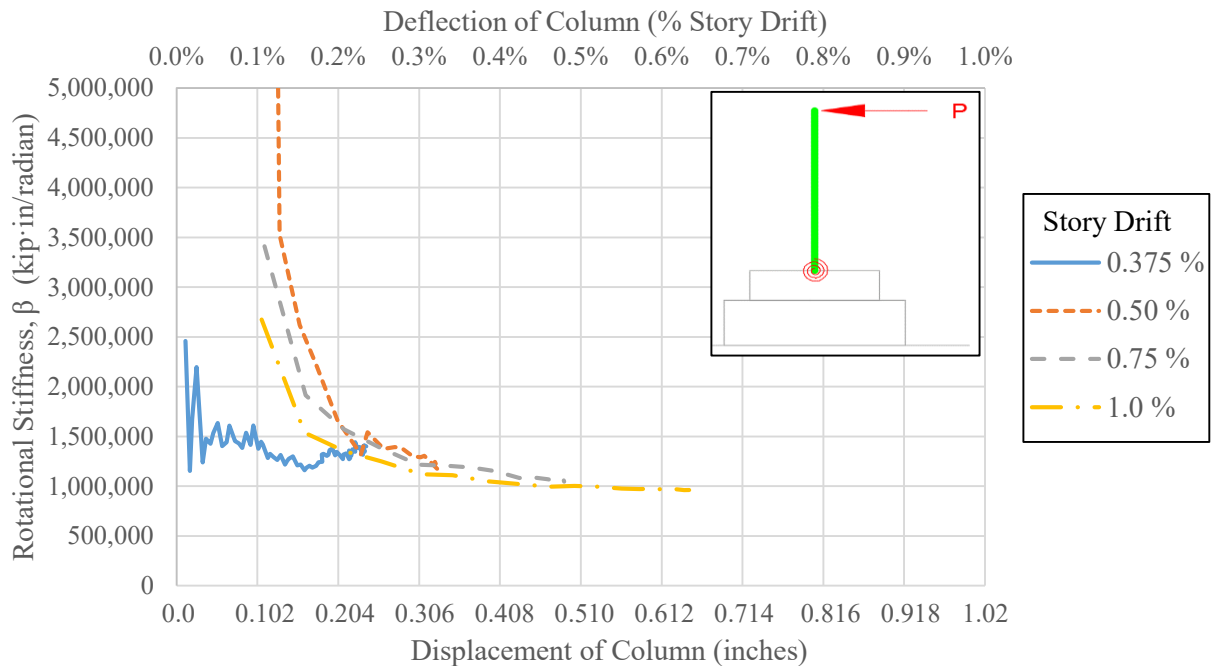


Figure 4-80: Rotational Stiffness for Test Specimen F4

4.5.9 Rotational Stiffness – Discussion

The rotational stiffness data plotted in the previous sections indicate that the addition of the block out concrete added an average 119% (D series), and 66% (F series) rotational stiffness to the connection at the top of the block out. Interestingly, the amount of block out concrete did not have a significant effect on the rotational stiffness at low deflections.

Once the cold joint between the top mat and the bottom mat broke, the rotational stiffness dropped an average 28%. This is evidenced in the graphs for all specimens with a block out (except Specimens F3 and F4, whose cold joint broke after of the 1.0% story drift cycle, and thus is not shown on this graph), and is seen the most clearly with specimen D3 (Figure 4-75). This graph clearly shows that after the cold joint has broken, the stiffness drops dramatically. This seemingly contradicts the finding discussed in Section 4.4.9 that the breaking of the cold joint had little effect on the slope of the hysteresis curve and thus the stiffness of the connection.

Regarding this apparent contradiction, there is a main difference between the stiffness of the overall connection as denoted by the slope of the hysteresis curve (and the backbone curve, Section 4.3), and the rotational stiffness investigated here. The stiffness of the connection denoted by the backbone curve is the stiffness of the connection as a whole, and takes into account the flexure of the column. It can be thought of as the stiffness of the connection at the base the column, whereas the rotational stiffness investigated in this section is at the top of the block out concrete, and has been corrected for the flexure of the column.

4.6 Anchor Bolt Strain

After the cold joint between the base mat and top mat/bock out concrete broke, the anchor bolts provided the primary resistance to the tensile forces that resisted rotation at the column base and provided both strength and rotational stiffness to the entire system. The anchor bolts were instrumented with strain gages (see Section 3.5.3). The strain gage data was used to evaluate the accuracy of the two models shown in Figure 4-81.

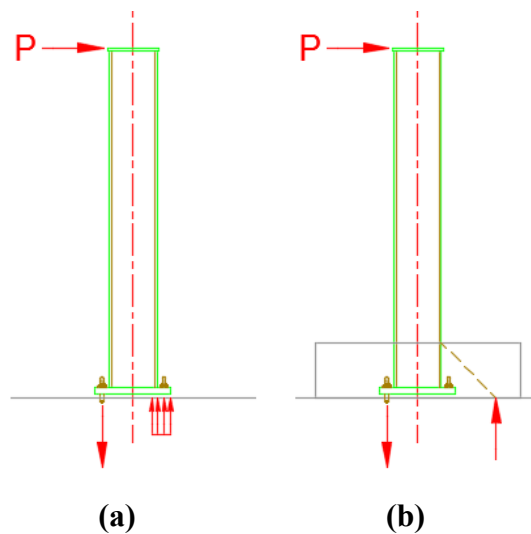


Figure 4-81: Predictive Models as Proposed by: (a) (DeWolf and Sarisley 1980), and (b) (Barnwell 2015)

The first, proposed by (DeWolf and Sarisley 1980), was intended for use with an exposed base plate. The base resists rotation through tension in the anchor bolts on one side, and a

compression block in the concrete on the other side. Note that this method is used in the AISC Design Guide #1.

The second, proposed by (Barnwell 2015) is meant specifically for a column base embedded in block out concrete. The base resists rotation through tension in the anchor bolts on one side, and a compression resultant acting at the block out/concrete base interface at a location 45° down from the face of the column flange.

Both methods provided a useful comparison, and both are included with the graphs. For the exposed base plate model (Figure 4-81(a)), the procedure for determining the load (P) that will cause failure (yielding in the anchor bolts) can be found in section 0. The actual yield strength of the bolts (f_y) as determined by the testing of the rods (see section 4.1.2) was used, and summarized below. The compressive strength of the concrete base (f'_c) used is 5.5 ksi. The latter value is taken as an average of the actual strength of the concrete used for the tests, as determined by the concrete tests (see section 4.1.1). For the embedded base plate model (Figure 4-81(b)), the procedure for determining the load (P) that will cause failure (yielding in the anchor bolts) can be found in Section 2.5.2. One line is shown for a column with an 8 inch block out, and one line is shown for a column with a 16 inch block out. Note that both models assume the use of eight total bolts. The condition with four total bolts (as is the case with specimen D4 and F4) is not shown on the graphs.

Testing of the anchor bolts (see section 4.1.2) revealed that they have the following properties:

1 inch diameter bolts:

yield strength, $f_y = 51.68$ ksi

effective modulus of elasticity, $E = 18,000$ ksi

yield strain, $\epsilon_{\text{strain}} = f_y/E = 2871$ microstrain

1 1/8 inch diameter bolts:

yield strength, $f_y = 49.36$ ksi

effective modulus of elasticity, $E = 17,400$ ksi

yield strain, $\epsilon_{\text{strain}} = f_y/E = 2837$ microstrain

After yielding, the anchor bolts are considered to provide no additional resistance, and the line depicting the theoretical anchor bolt strain in the following graphs is flat.

In the following sections, only anchor bolts A1 and A2 were analyzed. Not enough of the strain gages attached to bolts A3 and A4 functioned to provide useful comparisons. The graphs plot the micro strain in the bolts at the first peak of each of the story drift cycles. Frequently, even if a strain gage was functioning at the start of testing, as soon as the specimen began experiencing large deflections, the strain gage or its cable would get damaged, so many of the gages only show data for the lower deflection story drift cycles. Only the story drift cycle peaks that resulted in tension in the anchor bolts are shown.

4.6.1 Anchor Bolt Strain, Anchor Bolt A1

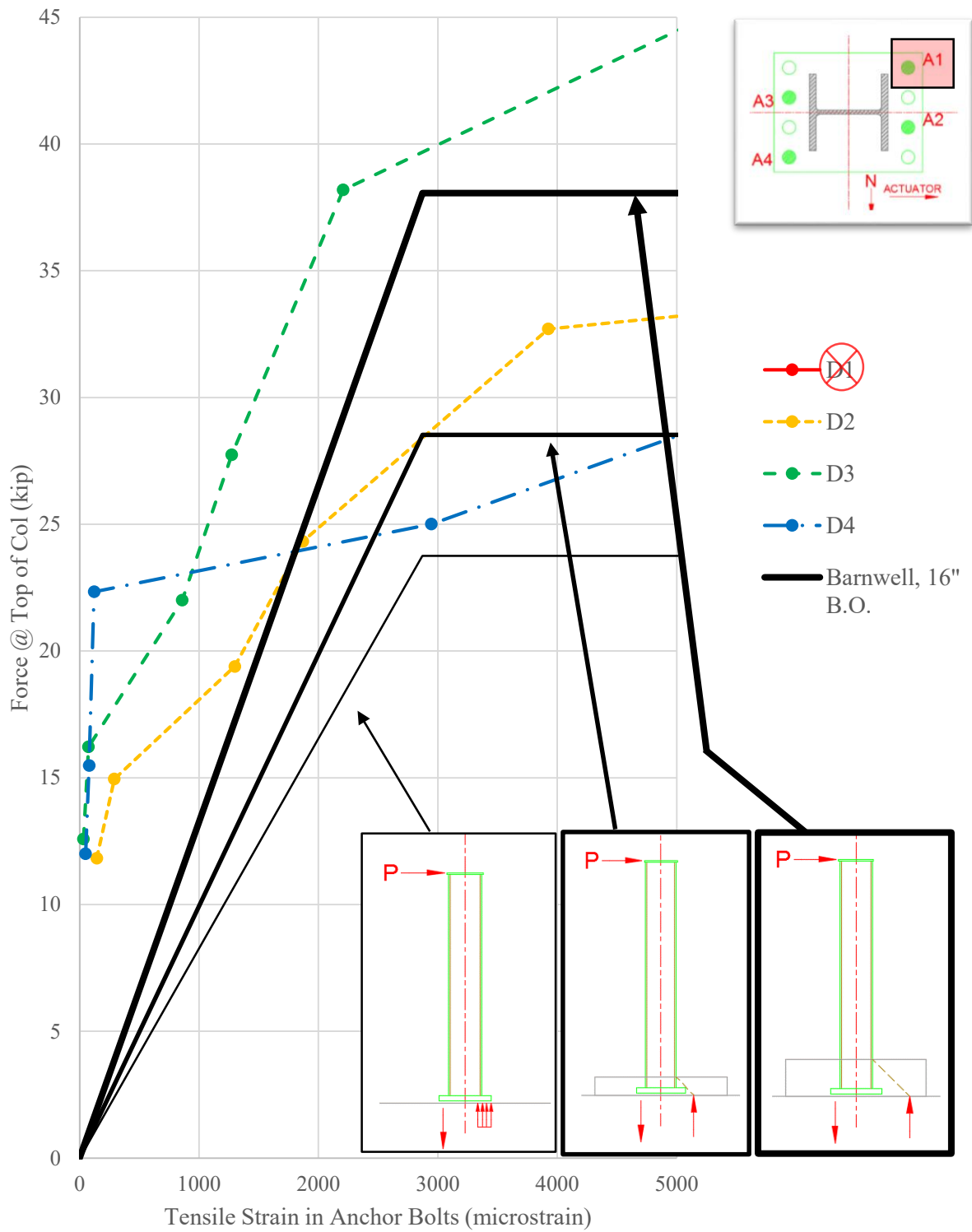


Figure 4-82: Strain in Anchor Bolt A1, D-Series Tests

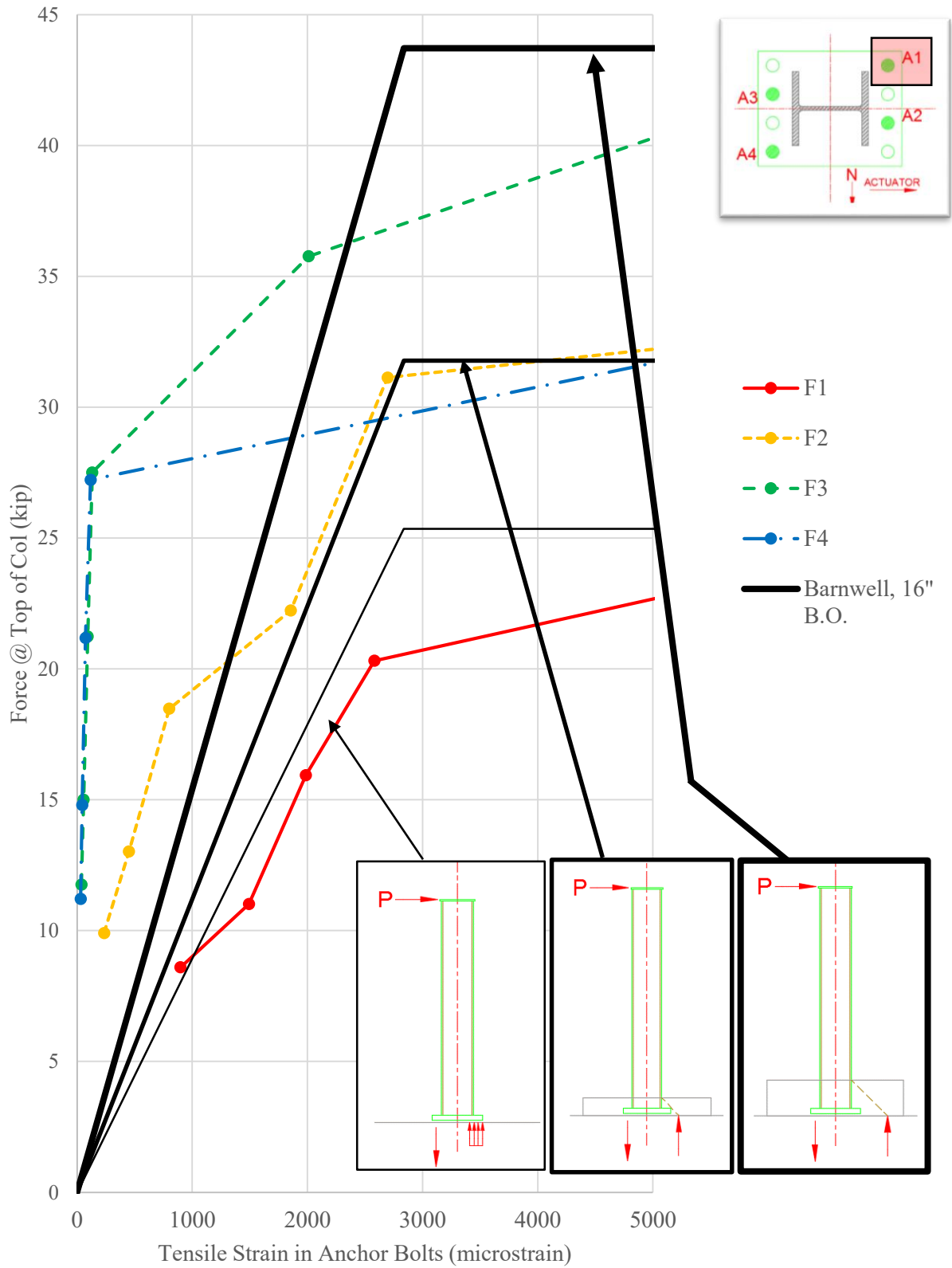


Figure 4-83: Strain in Anchor Bolt A1, F-Series Tests

4.6.2 Anchor Bolt Strain, Anchor Bolt A2

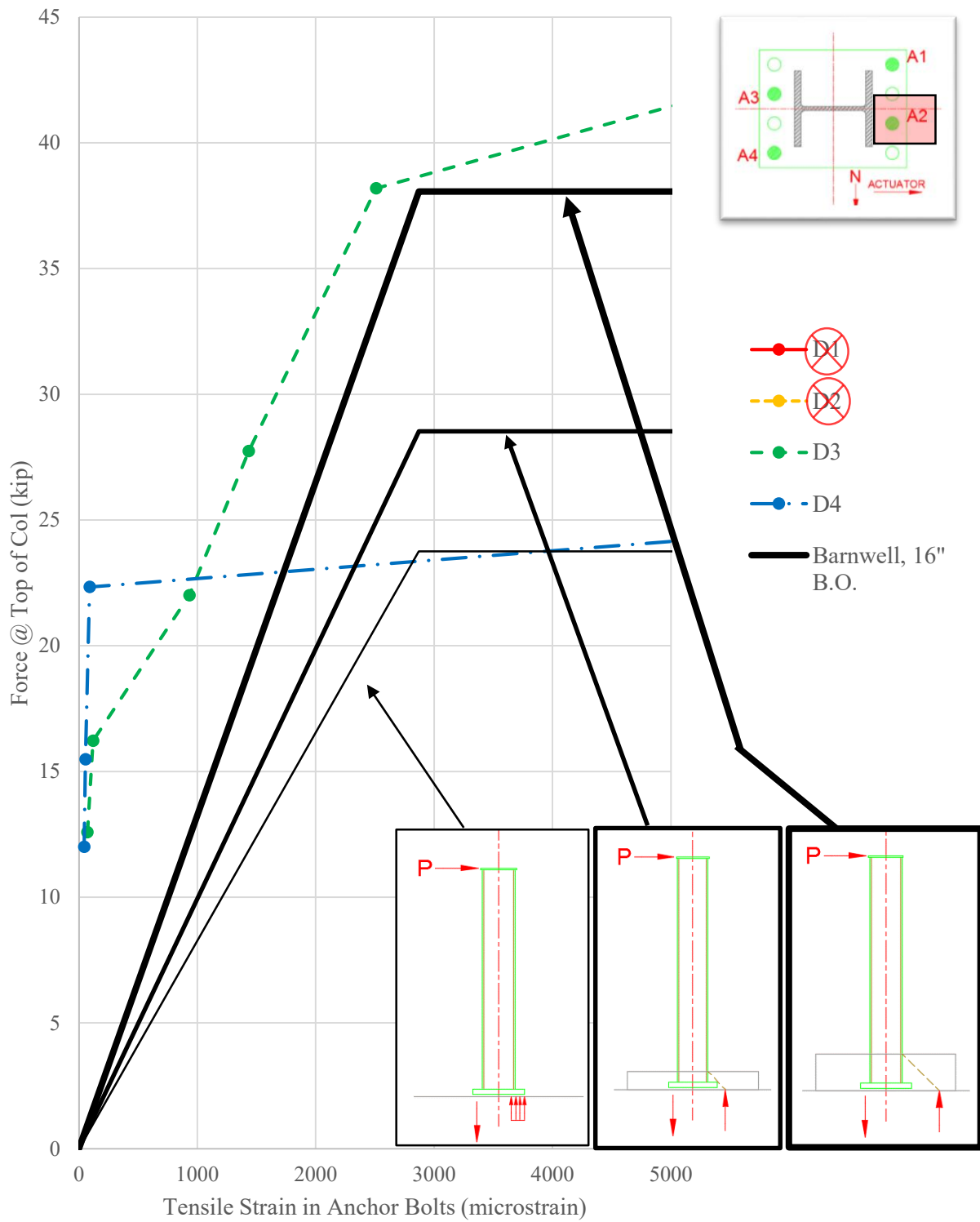


Figure 4-84: Strain in Anchor Bolt A2, D-Series Tests

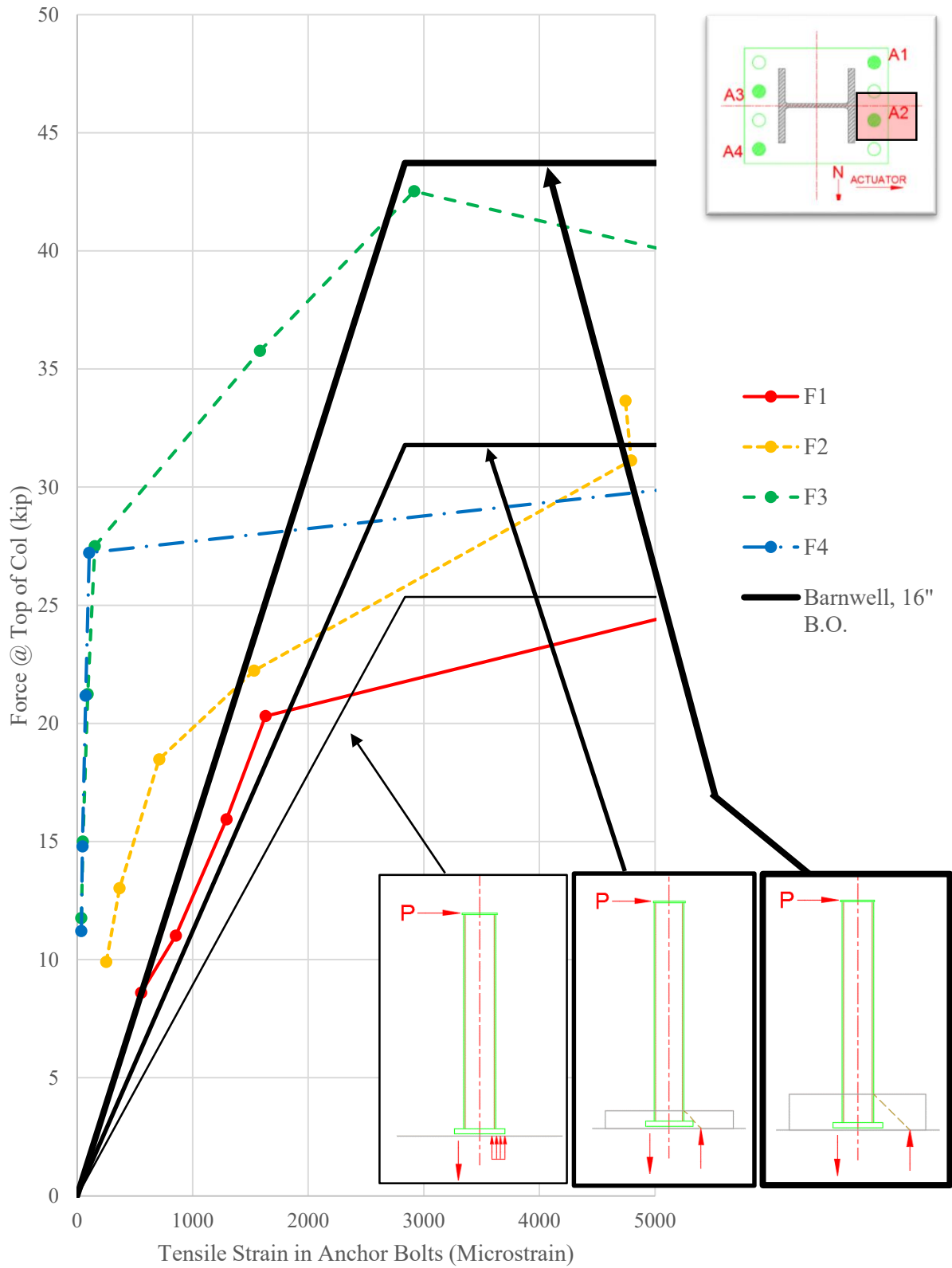


Figure 4-85: Strain in Anchor Bolt A2, F-Series Tests

4.6.3 Anchor Bolt Strain – Discussion

The strain data on the anchor bolts clearly shows that the increase in the depth of the block out concrete resulted in a decrease in the strain in the anchor bolts for the same load on top of the column. This validates the concept behind the model proposed by Barnwell, who predicted that the block out would extend the compression resultant away from the column, lowering both the compression and tensile resultant loads, and thus the amount of strain in the anchor bolts.

Comparing the data to the model as found in the AISC Steel Design Guide (DeWolf), shows that the anchor bolts experienced significantly less strain than predicted by this method. This suggests that the current practice of ignoring the block out concrete and designing the base as an exposed connection, using the design method found in the AISC Steel Design Guide #1 is a conservative method and overly predicts the strain in the anchor bolts.

Comparison of the data to the model proposed by Barnwell suggests that this method is much more accurate. It should be noted that the graphs indicate that prior to the breaking of the cold joint (low deflection cycles) the anchor bolts experienced less strain than even Barnwell's model predicted. This suggest that before the bond breaks, the tensile resultant of the moment force is resisted mainly by this concrete bond. After the cold joint break, however, the anchor bolt strain increases and more closely matches Barnwell's model.

4.7 Column Strain

Eight strain gages were placed on the column flanges of each specimen, following the procedure found in Section 3.5.3. The locations and placement of the strain gages can be found in Figure 3-41.

The strain reported from each of these gages is shown in the following figures, for the first peak displacement at each story drift cycle. Similar to the anchor bolt strain gages, even if the strain gage was functioning at the start of the test, during large deflections and in several instances, the gage or its lead wire became damaged. There are several gages that report information during small deflection cycles, but not during large deflections, indicating that they were damaged or destroyed when the specimen began to experience larger deformations. Gages that were not functioning at all are marked on the graphs with an “X”.

For reference, the theoretical yield strain is shown on the graph as a dashed line. This line serves as a reference point at which the column steel should theoretically yield. Since the exact properties of the column steel are not known (a destructive test of the steel was unfeasible, and a coupon of the steel material was not available for testing), the properties of the column steel were taken from the AISC Steel Design Guide, table 2-4 and AISC 360 “Symbols” section. With a column steel yield strength (f_y) of 50 ksi, and a modulus of elasticity (E) of 29,000 ksi, the column flanges will yield at a strain of 0.001724, or a micro strain of 1,724.

4.7.1 Column Strain – D1

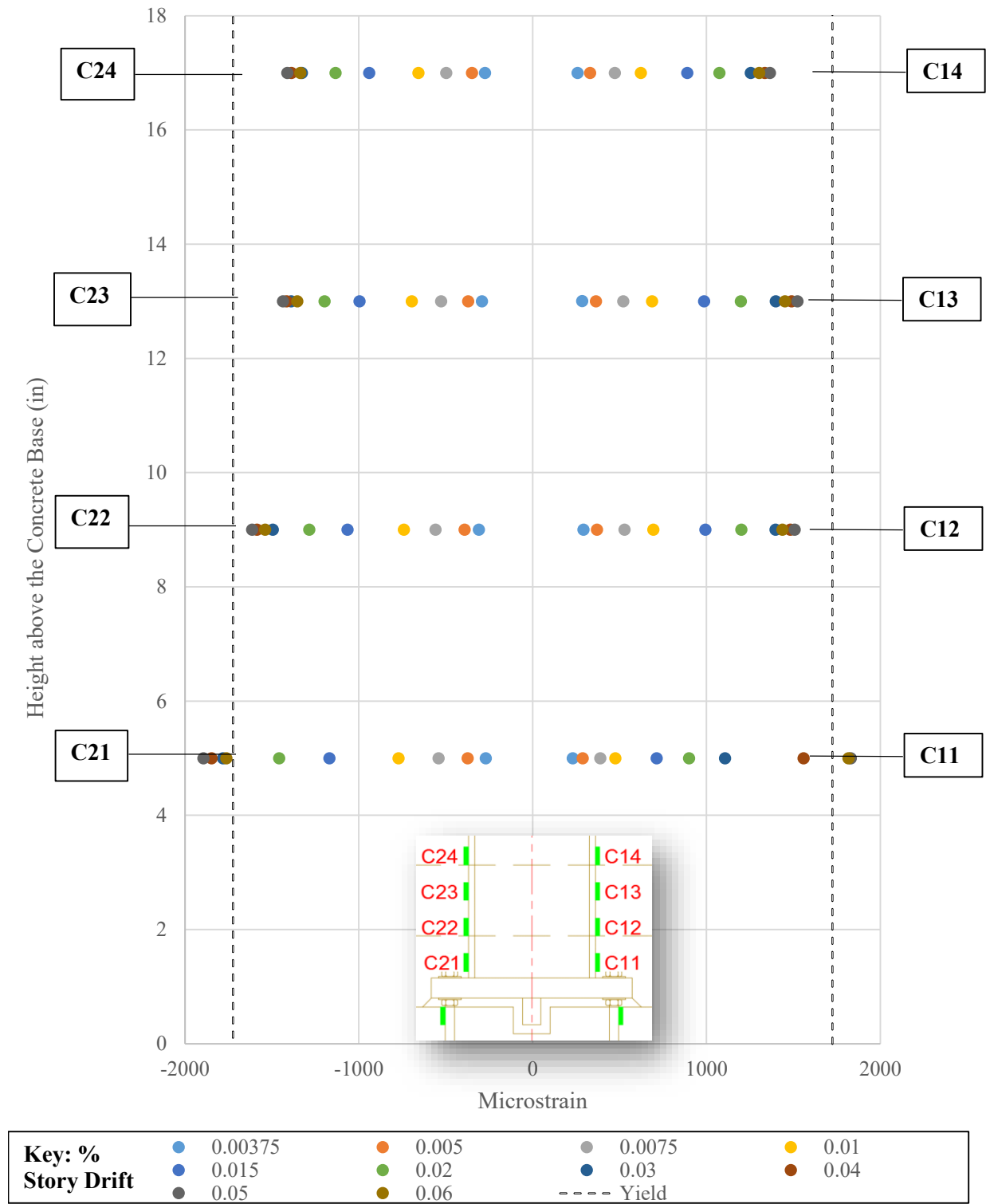


Figure 4-86: Strain in Column Flanges, Specimen D1

4.7.2 Column Strain – D2

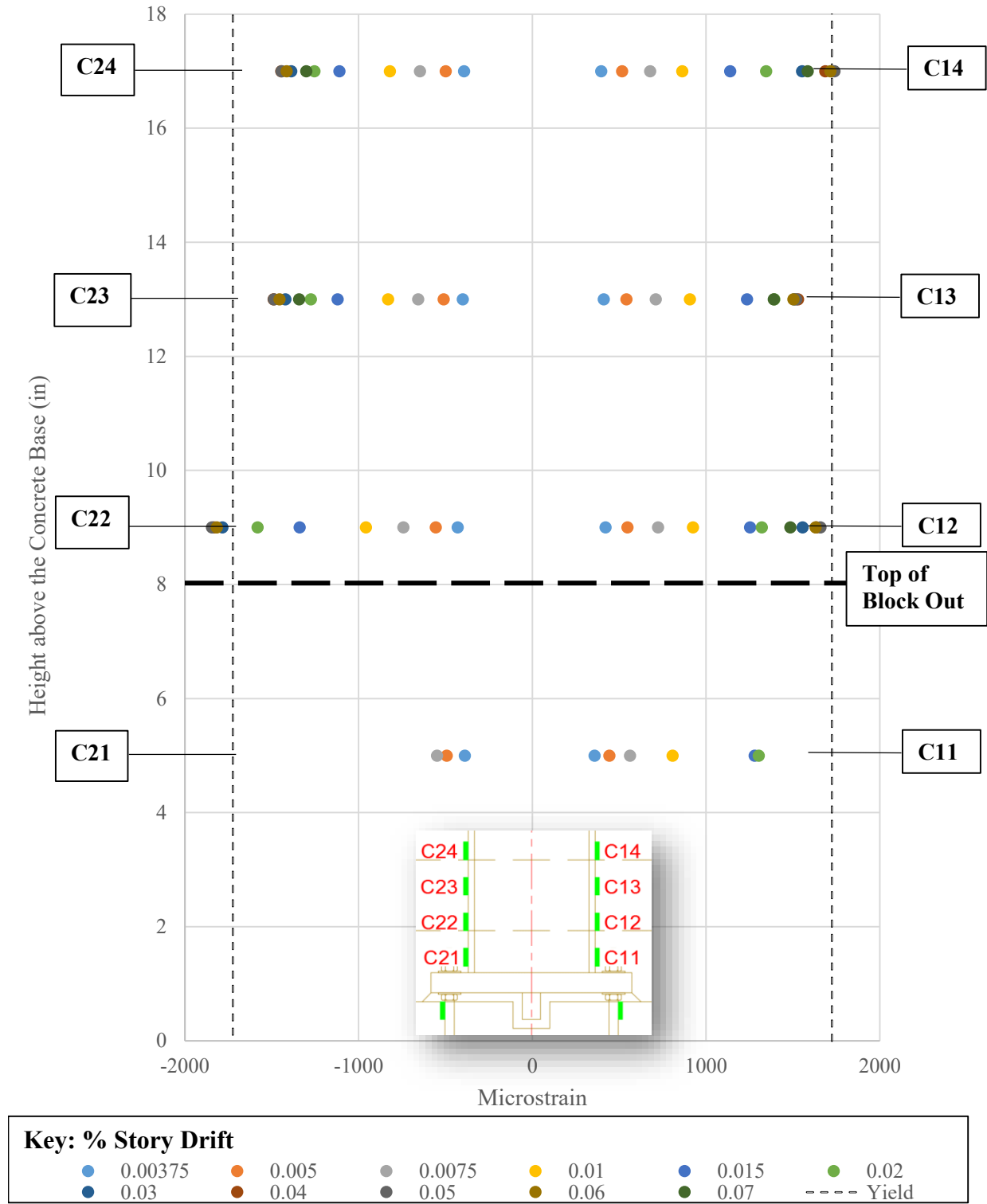


Figure 4-87: Strain in Column Flanges, Specimen D2

4.7.3 Column Strain – D3

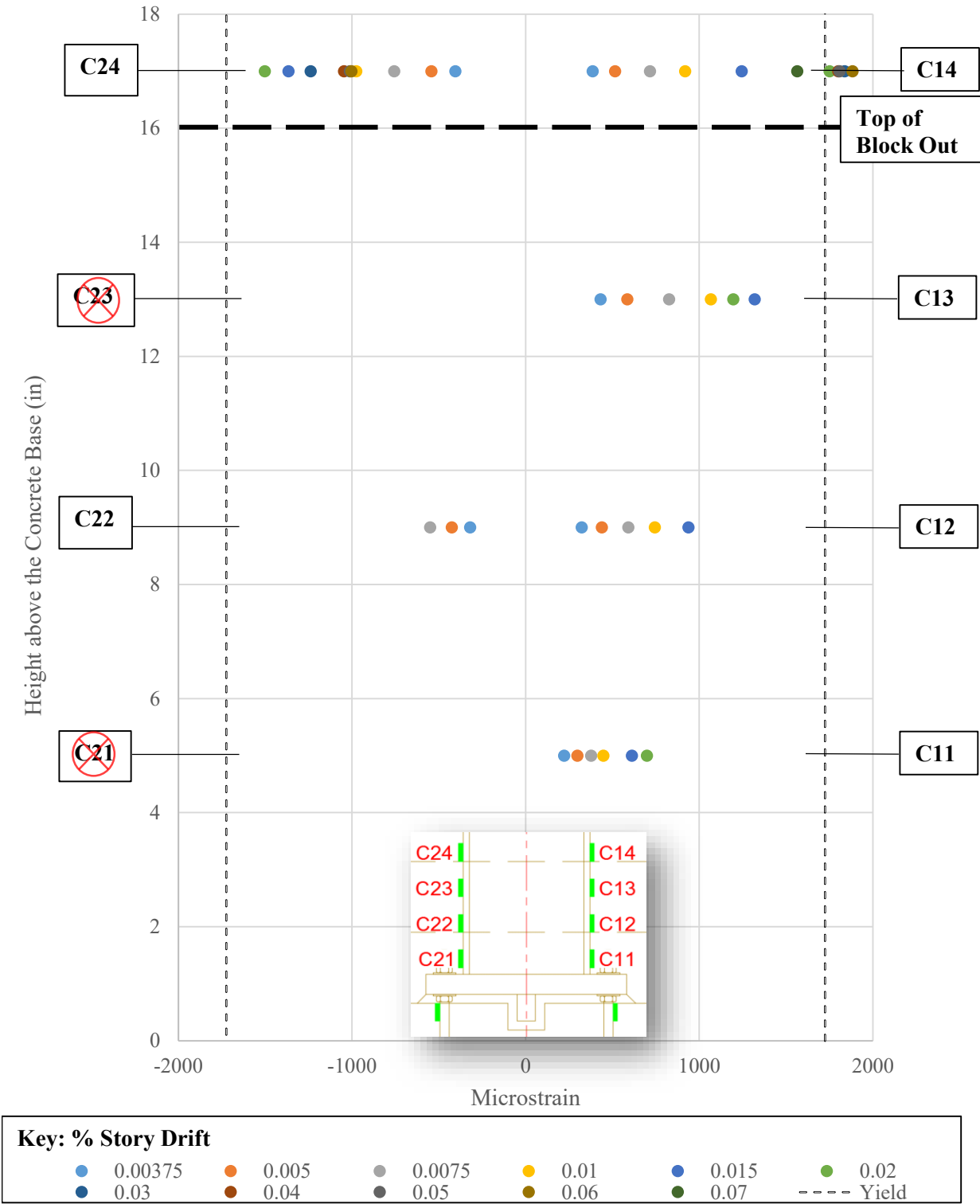


Figure 4-88: Strain in Column Flanges, Specimen D3

4.7.4 Column Strain – D4

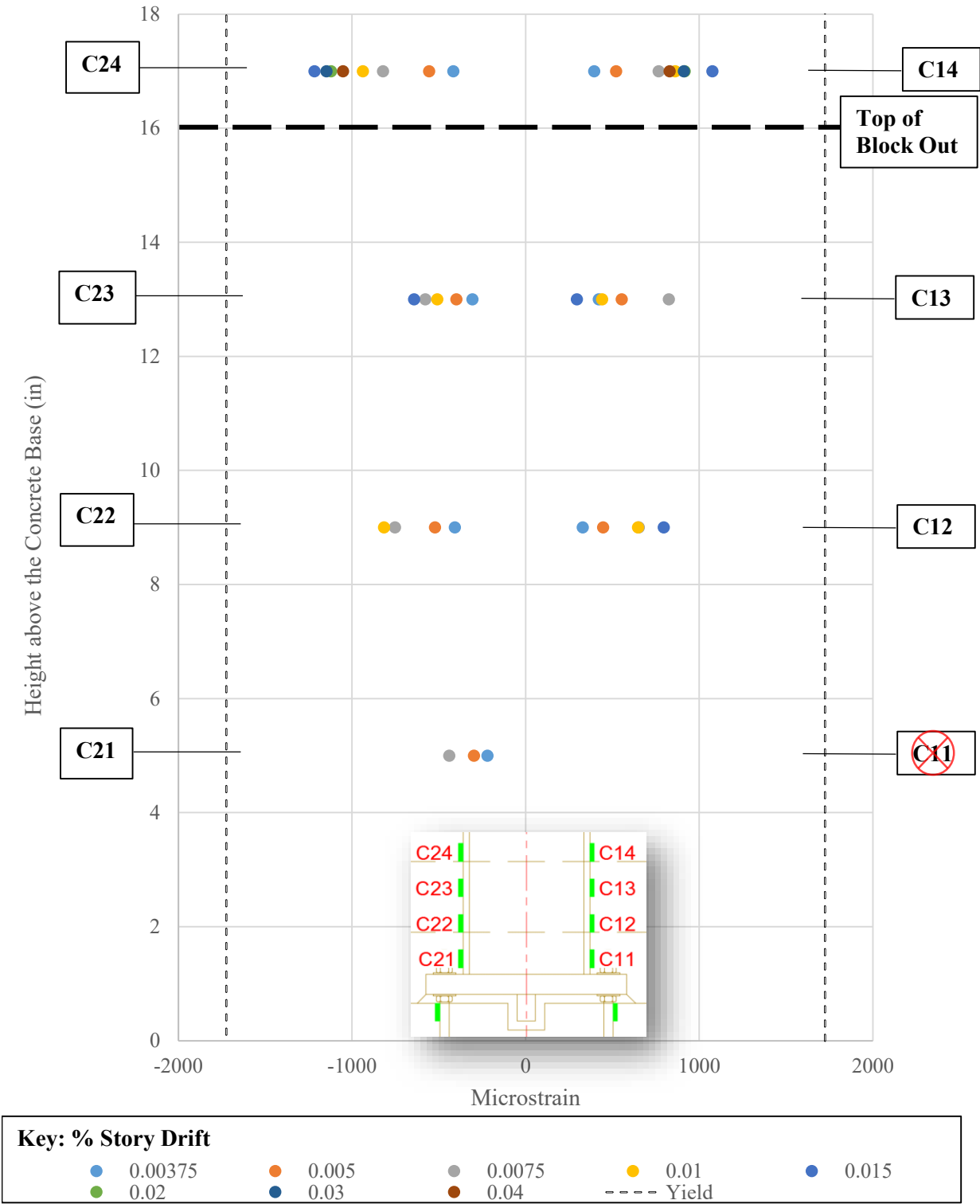


Figure 4-89: Strain in Column Flanges, Specimen D4

4.7.5 Column Strain – F1

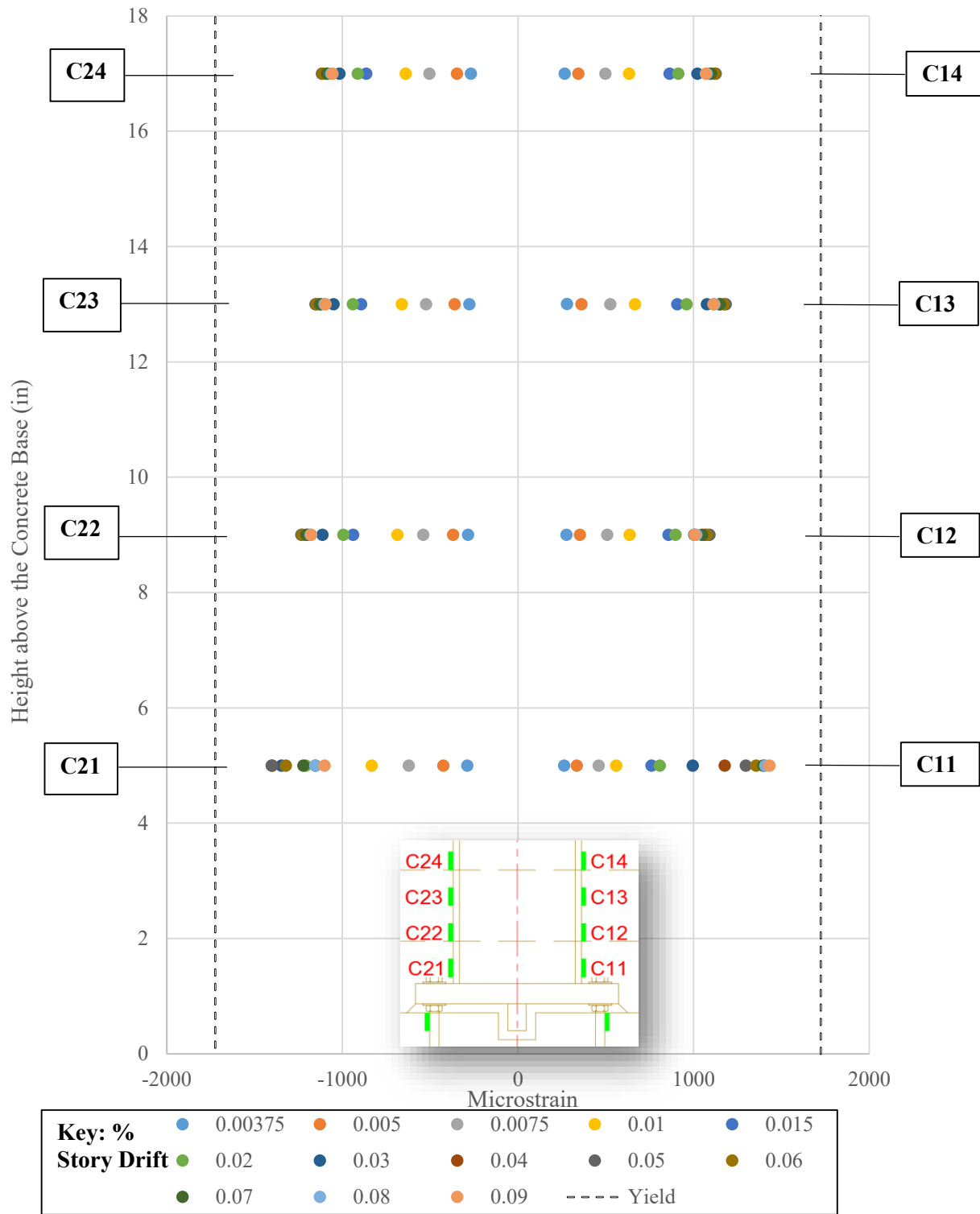


Figure 4-90: Strain in Column Flanges, Specimen F1

4.7.6 Column Strain – F2

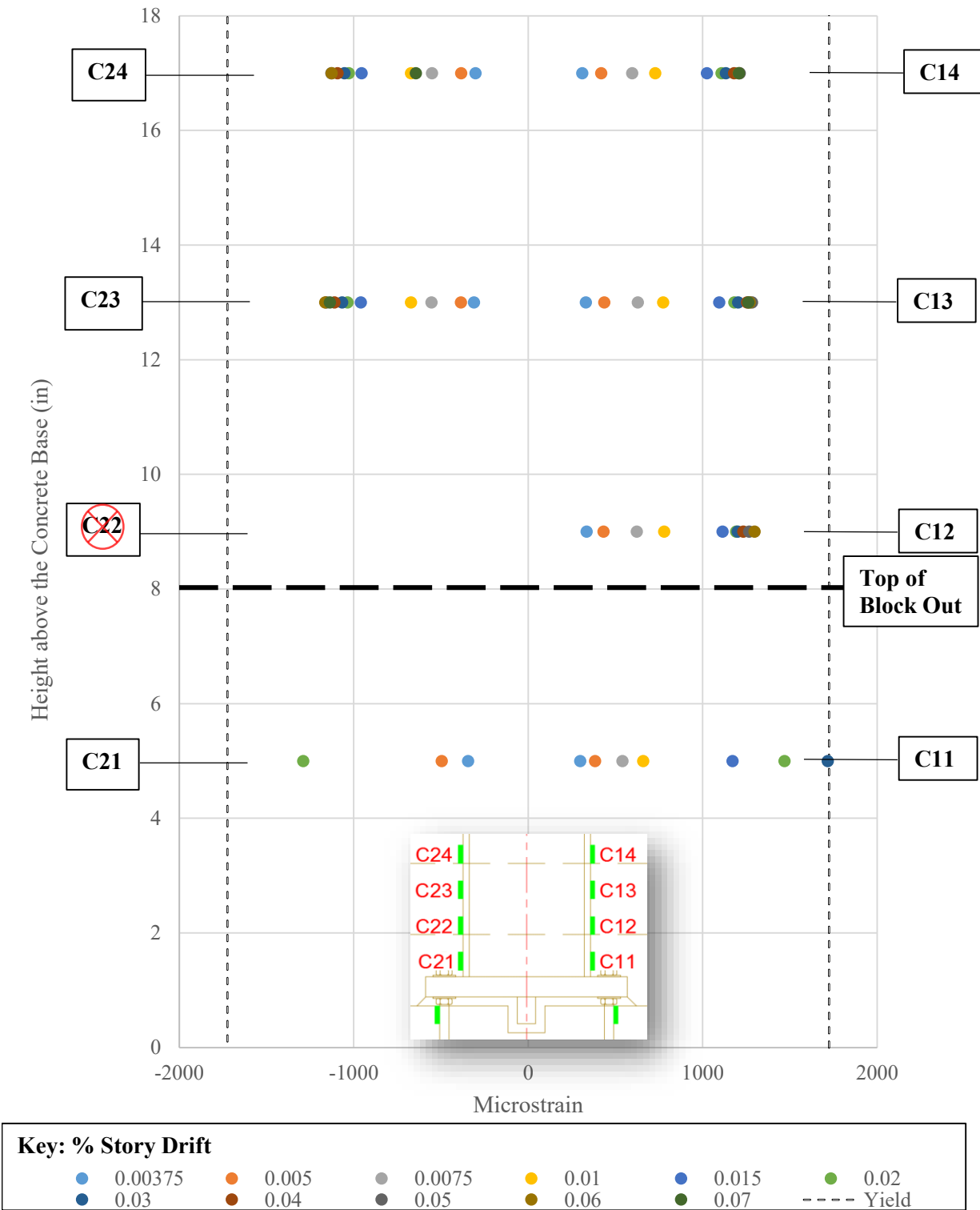


Figure 4-91: Strain in Column Flanges, Specimen F2

4.7.7 Column Strain – F3

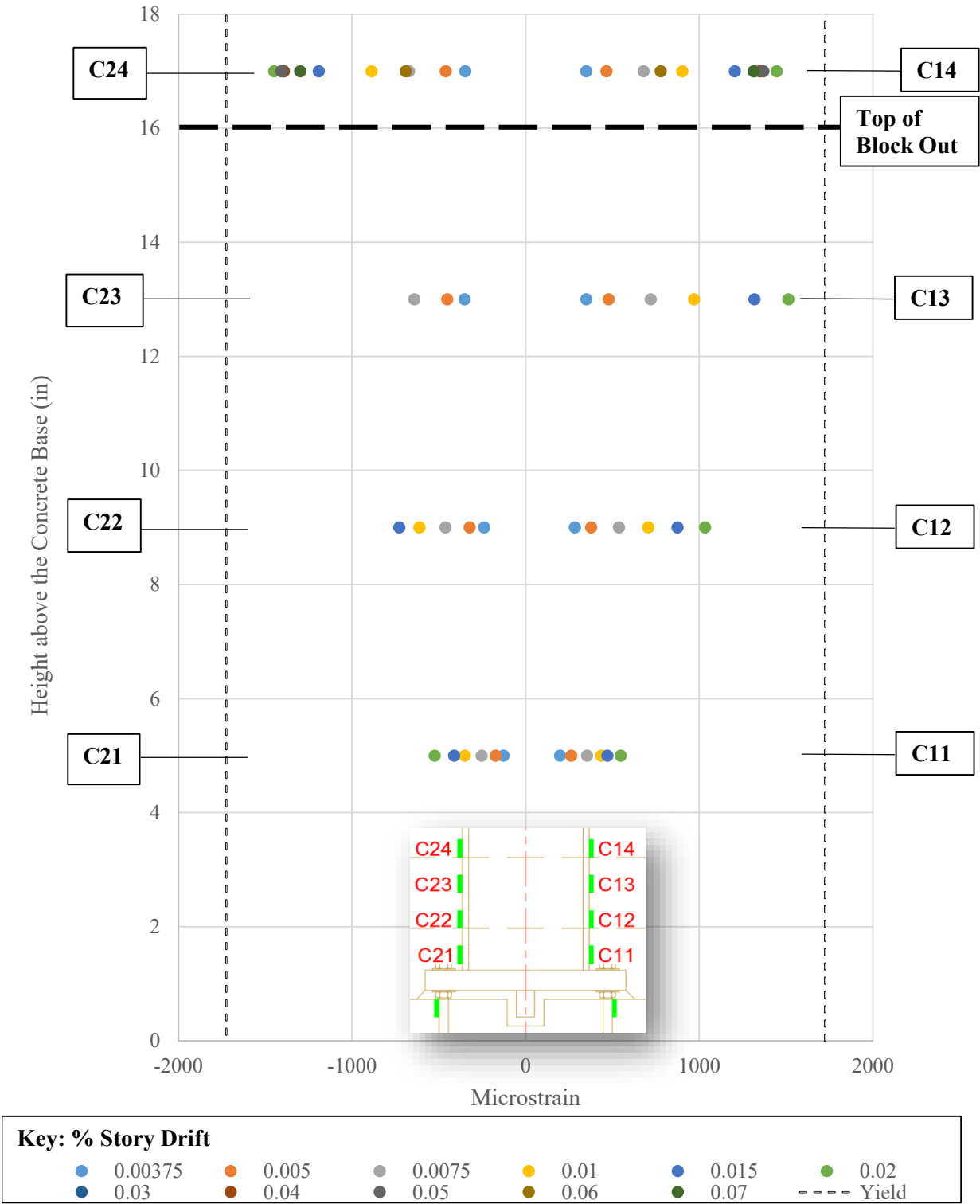


Figure 4-92: Strain in Column Flanges, Specimen F3

4.7.8 Column Strain – F4

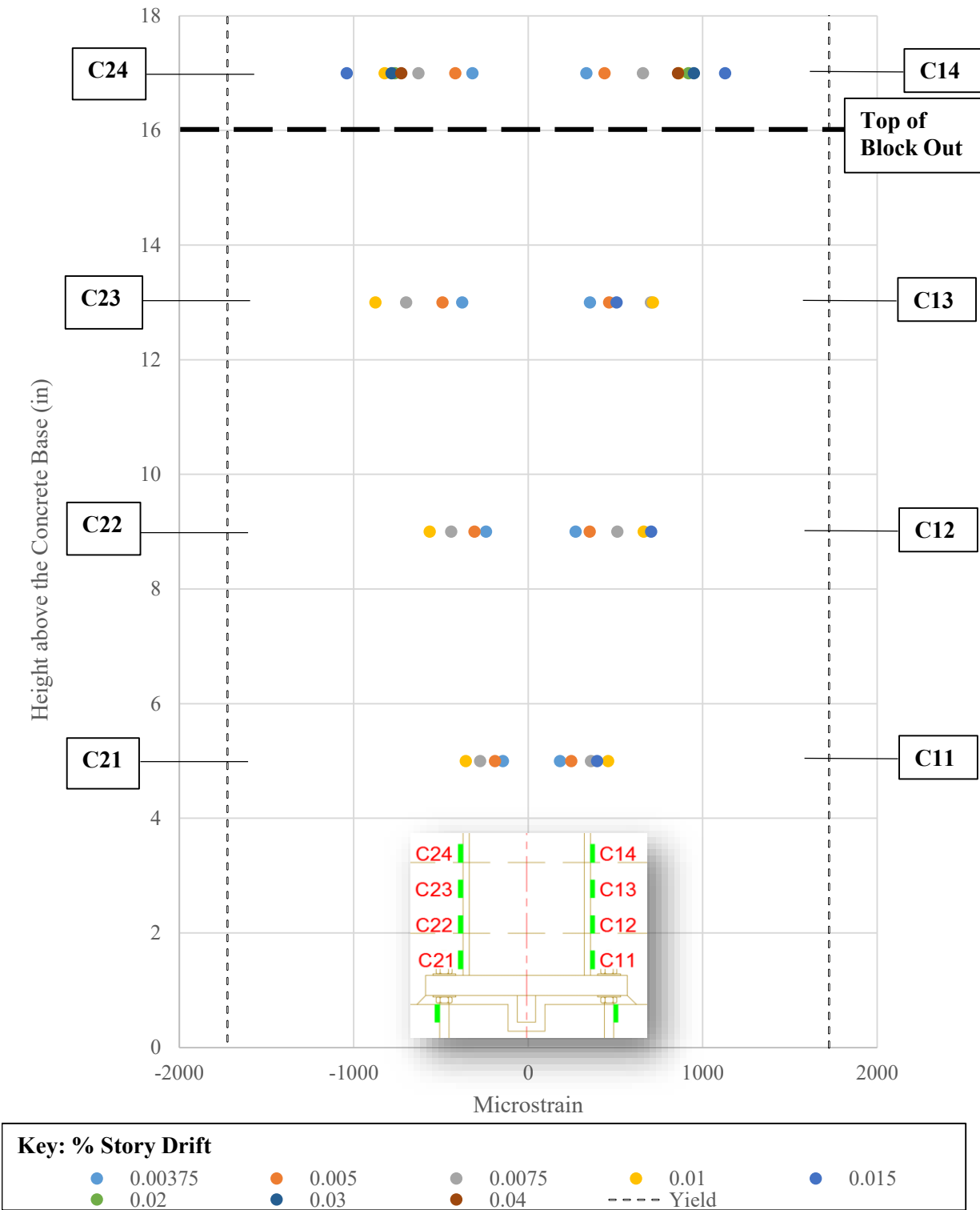


Figure 4-93: Strain in Column Flanges, Specimen F4

4.7.9 Column Strain – Discussion

It is helpful to begin a discussion on the column strain by determining what the strain should be in an ideal situation. The strain in the column flanges is directly related to the moment force in the column, which increases linearly towards the base, where it reaches its maximum. Therefore, it would be expected to see the strain in the column reflect this and increase linearly towards a maximum at the base of the column. This can be seen in specimens D1 and F1 (Figure 4-86 and Figure 4-90).

The specimens with the deeper embedment show behavior that is opposite this. The largest strain is located at the top of the block out, and gradually decreases to near zero at the base of the column. See Figure 4-88, Figure 4-89, Figure 4-92, and Figure 4-93. This suggests that the moment demand in the column was the largest at the top of the block out concrete and decreased as the column extended into the concrete. This supports the conclusion mentioned in Section 4.5.9, that the base of the column could be modelled as a “fixed” connection. If the column itself experiences zero moment at its base because of the presence of the block out concrete, it is effectively “fixed” by the block out concrete.

5 DISCUSSION

5.1 Performance of Test Setup

5.1.1 Reaction Frame

After the first test was completed, it became obvious that the reaction frame provided for use with these tests was roughly three times more stiff in one direction than the other. This possibility was anticipated, and a string pot (SP1) was placed at the top of the column at the centerline of the actuator. This string pot provided data on the actual displacement of the top of the column, negating the need to rely on the deflection reported by the actuator. With a perfectly rigid reaction frame, it would be expected that the reported displacements from the actuator and string pot SP1 be exactly the same throughout the test. They were not, which is evidence of the flexible nature of the reaction frame. String pot SP-R (reaction frame at the centerline of the actuator) was also placed to analyze movement of the actuator.

During repeated drift cycles, the actuator consistently reported uneven forces during positive and negative movements. These differences were consistently between 2% and 15% larger negative loads than positive loads for similar story drift movements in each direction. Also, while the actuator itself would report consistent positive and negative story drift movements, the string pot SP1 would report comparatively larger displacements when extending

in the positive direction than in the negative direction. Further evidence of this phenomenon is shown in the hysteresis plot in Figure 4.1.9-1.

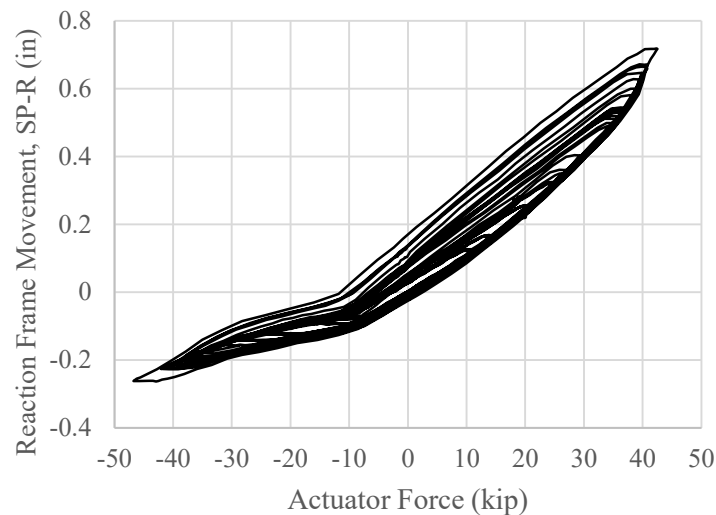


Figure 5-1: Typical Hysteresis Plot of Reaction Frame During Testing; Specimen F3

If the reaction frame had similar stiffness in both directions, the hysteresis would have similar-sloped lines of equal length straddling the origin. Figure 5-1 shows this is not the case, and indicates that the reaction frame is 3 times stiffer in the negative direction. When looking at Figure 3-2, a positive load would “push” on the reaction frame to the right, while a negative load would “pull” on the frame to the left.

Visual investigation of the reaction frame during testing revealed where the “soft spot” was in the assembly: the base of the main column. Under large positive loads from the actuator, the

reaction frame resisted this load with compression loads in the diagonal braces and a tensile load in the column base, see Figure 5-2.

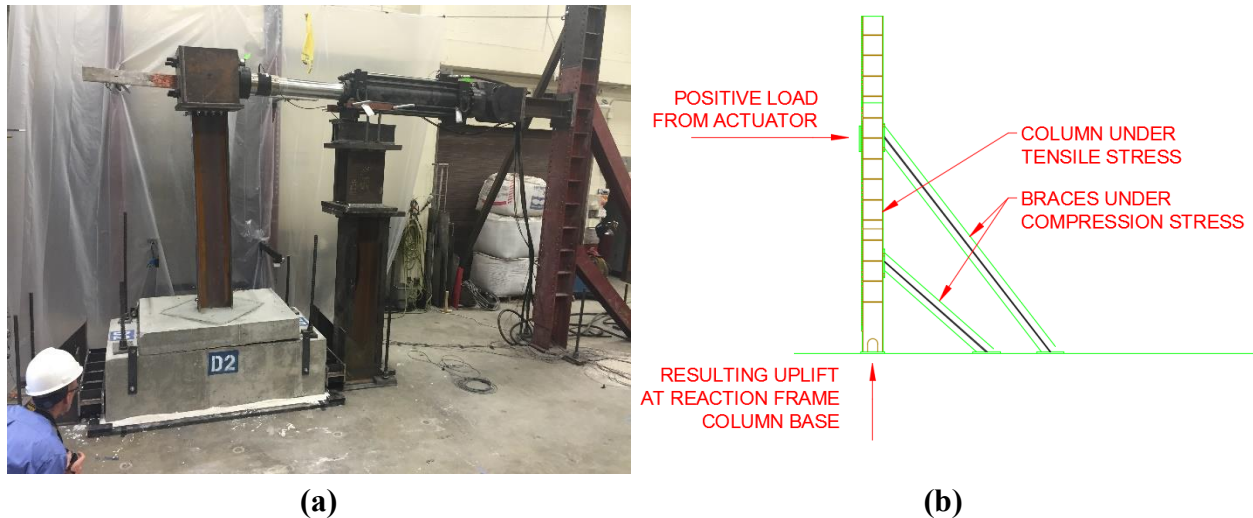


Figure 5-2: Reaction Frame (a) Test Setup, and (b) Resultant Forces

The reaction frame column base was secured to the lab floor using two tie rods, post-tensioned to roughly 50 kips, in a similar fashion as the tie-rods securing the specimen to the lab floor. The holes in the lab floor that these tie rods were attached to were spaced at 3 feet on center in each direction. Long before these tests occurred, the reaction frame was designed and built to sit directly atop one of these holes (when the centerline of a specimen would be in line with these anchorage holes). In preparation for other tests (again, before this research), the frame was modified to allow the reaction frame (and consequently a test specimen) to straddle these holes. Small 1 inch thick steel extension plates were welded to the side of the column base plate

with holes for the tie down rods. See Figure 5-3 Note that similar methods were used at the bases of the two diagonal braces. This extension plate configuration was adequate when the column was under compression or lateral loads (which was the case when the actuator exerted a negative force on the reaction frame), but not in the case of uplift at the column base. During testing, and higher positive loads (40+ kips), the base of the column was observed flexing and rising off the ground as much as $\frac{1}{2}$ or more inches. This translated into the large lateral movement at the height of the actuator that was seen during testing.



Figure 5-3: Reaction Frame Base

The string pot at the top of the column, SP1, gave the true lateral movement of the column top, and ensured that it was not necessary to rely on the deflection data reported by the actuator. Since the information from this string pot was used for all data, graphs and calculations, no modifications to the data were necessary due to this imbalance of stiffness from the reaction frame.

5.1.2 Base Lateral Support

The specimen base (base mat), was secured to the floor as described in section 3.4. It was also secured against lateral movement using steel lateral support frames on either side of the base tied to the lab floor, as seen in Figure 3-31. It was crucial that the base of the specimen be kept as stable as possible to isolate deformation in the steel column base. To ensure that this was the case, a string pot (SP-B1) was set up to measure lateral movement of the base mat concrete.

Analysis of the data from string pot SP-B1 shows that the base mat experienced extremely small lateral movements, see Figure 5-4. Most specimens (five of the eight) experienced lateral movements not exceeding 0.03 inches. Three specimens (D1, D2, & D3) showed slightly larger displacements, and the maximum displacement recorded was 0.103 inches (Specimen D3). These relatively larger movements reported by the string pot can be attributed to the deformation and cracking that occurred in the base mat of these specimens, and not movement of the base mat itself. In these 3 specimens, no movement over 0.01 inches was recorded until after the 2.0% story drift movements (around 2000 seconds into testing), which was the time when cracking began to appear in the base mat concrete. Thus the movement reported is due to the cracking of the concrete, not lateral movement of the base.

Overall, the base lateral support performed adequately and the base mat was restrained from movement sufficiently to force all deformation to occur at the connection.

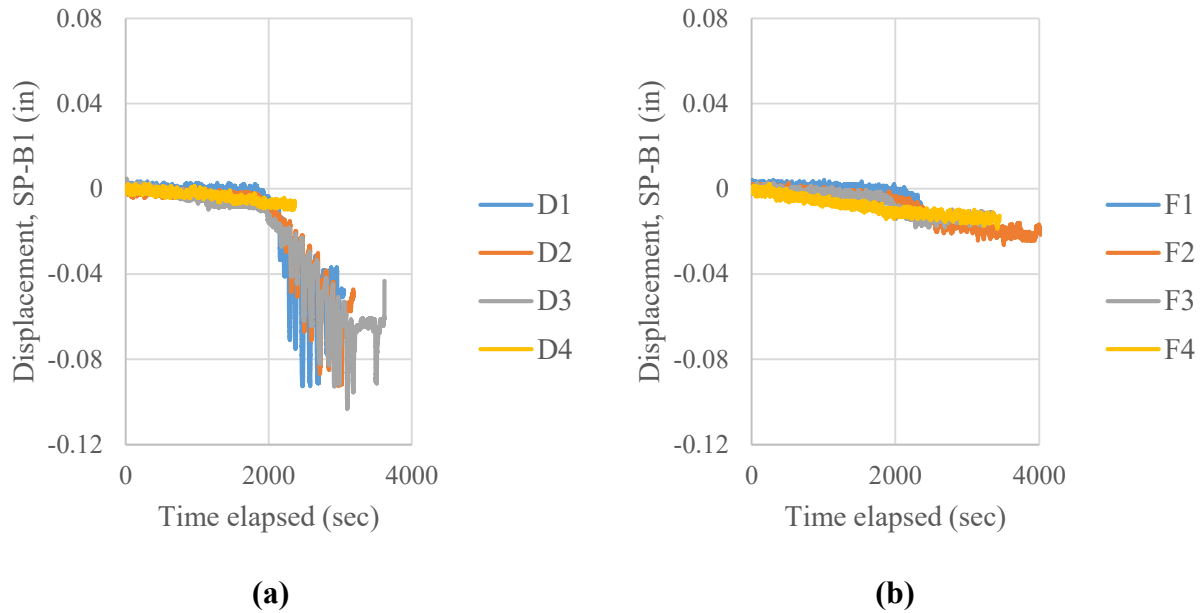


Figure 5-4: Lateral Movement of Base Mat for (a) D-Series Specimens and (b) F-Series Specimens

5.1.3 Out-of-Plane Reaction Frame

The top of the column, at the corbel, was restrained from lateral movement by means of the out-of-plane reaction frame, as explained in Section 3.3.4 and shown in Figure 3.3.4-6. In order to ensure the column did not move excessively out-of-plane, the string pot SP-R was set to measure this movement. Because the string pot measures movement perpendicular to the movement of the actuator, the string pot itself was set up as far away as possible from the actual specimen, approximately 25 feet away on the far wall of the lab. This large distance limited the amount of movement recorded by the string pot when the actuator moved the top of the column along its intended path, as shown in Figure 5-5(a).

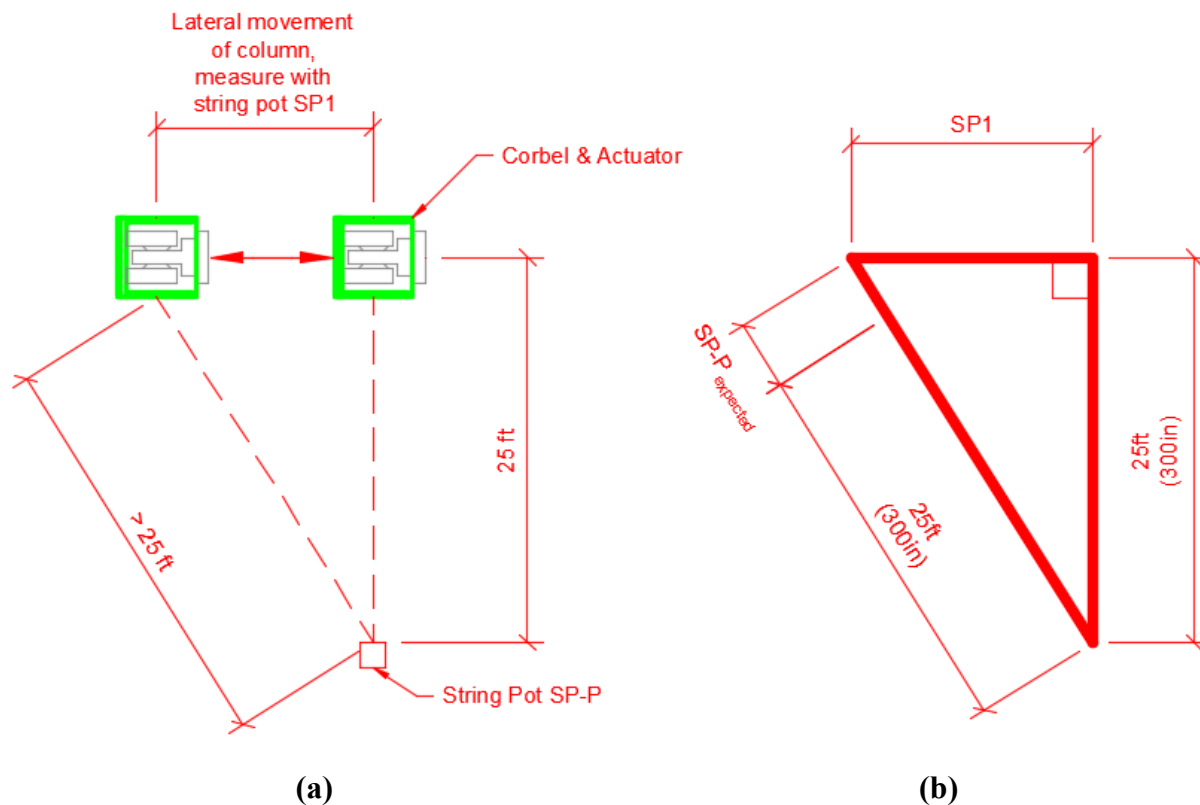


Figure 5-5: (a) Plan View of the Out-of-Plane String Pot Setup [Not To Scale], and (b) Model of Relative Distances

To correct for this expected error, a simple trigonometric relationship can be set up between the movements reported by string pots SP1 and SP-P, see Figure 5-5(b). The equation used to make this correction is shown in EQ (5.1.1).

$$(SP - P_{adjusted}) = (SP - P_{reported}) - (SP - P_{expected}) \quad (5.1.1)$$

Where:

$(SP - P_{adjusted})$ = The adjusted (actual) out-of-plane deflection of the top of the column

$(SP - P_{reported})$ = The out-of-plane deflection of the top of the column as reported by string pot SP-P

$(SP - P_{expected})$ = The expected out-of-plane deflection reported by the strong pot SP-P for a given lateral deflection. $= \sqrt{SP1^2 + (300 \text{ in})^2} - 300 \text{ in}$

SP1 = The lateral movement of the top of the column, as reported by string pot SP1

For reference, this calculation is shown for specimen D3, at the peak displacement for the 8.0% story drift cycle, when instruments reported the following data:

Lateral Movement at the top of the column, SP1: -8.7880 inch

Lateral out-of-plane movement, SP-P: 0.2639 inch

Applying the formulas above, the expected out-of-plane deflection reported by string pot SP-P is seen in EQ (5.1.2).

$$(SP - P_{expected}) = \sqrt{(-8.7880 \text{ in})^2 + (300 \text{ in})^2} - 300 \text{ in} = 0.1287 \text{ in} \quad (5.1.2)$$

Then applying these values to EQ (5.1.1), the adjustment to the lateral out-of-plane deflection:

$$(SP - P_{adjusted}) = (0.2639 \text{ in}) - (0.1287 \text{ in}) = 0.1352 \text{ in}$$

Using this formula, the data reported from string pot SP-P was adjusted, and is shown below in Figure 5-6.

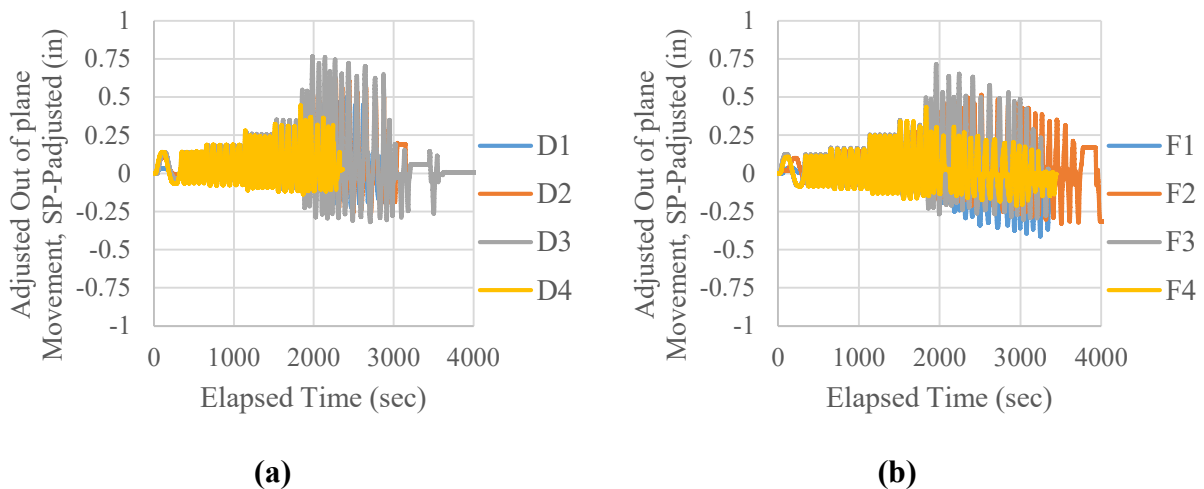


Figure 5-6: Adjusted Out-of-Plane Movement (a) D-Series Tests and (b) F-Series Tests

5.2 Performance of Specimen Design

The overall objective of the specimen design was to reduce the variables associated with testing the connection. Consequently, limiting movement and deformation during testing to the column base connection was key during the design, construction, and setup of the test specimens. To accomplish this purpose, the base mat needed to resist the large loads transferred to it from the column without failure and be restrained to the lab floor adequately to restrain movement. The shear lug was intended to limit the lateral movement of the column base during testing and eliminate the lateral loads imposed on the anchor bolts. The anchor bolts were designed to resist

axial loads only, and their embedment into the concrete was designed according to seismic recommendations, which state that the failure mode of the anchor bolts be tensile fracture. Data shows that these goals were accomplished and that the specimens all performed as intended.

Sections 5.2.1 through 5.2.4 will elaborate.

5.2.1 Performance of Base Mat

In order to isolate the column base connection elements during testing, the base mat needed to be strong, rigid, and adequately secured to the lab floor. Evidence indicates that the base mat performed its role adequately.

As discussed in section 3.3.2.5, the largest load imposed on the base mat during testing was the bending moment transferred to the base from the column as the actuator pushed/pulled on the top of the column. To resist this moment load, the base mat was reinforced with a top and bottom mat of reinforcement. Failure in the base mat from this load would have been preceded by vertical cracks visible in the side of the mat. During testing of all eight specimens, no vertical cracks of this kind were observed, and no bending failures occurred. The base mat remained intact and performed as expected.

It was also intended that the base mat be securely attached to the lab floor and not move. It was tied to the floor with four post-tensioned rods, one at each corner. As discussed in section 5.1.2, it was also secured laterally by means of steel support frames, also tied to the lab floor with post-tensioned rods. By visual inspection of video taken of each test, and data from the string potentiometers attached to the base mat for just this purpose, it was concluded that the base mat remained adequately secured during testing for each specimen.

Another purpose of the base mat was to provide an embedment for the anchor bolts and ensure that the anchor bolts failed in a desirable manner. Of the many failure modes of an embedded anchor bolt discussed in ACI 318 Appendix D (anchor bolt pullout, concrete breakout, side-face blowout, etc.), the desired failure mode was failure of the anchor rod in tension. Supplemental reinforcement was added to the base mat concrete to prevent concrete breakout when the anchor rods resisted large tensile loads. It was observed during testing that specimens D1, D2, and D3 showed cracking in the base mat that began at the location of the embedded anchor bolt plate and extended upward at an approximate 45° angle, consistent with a concrete breakout cone. The presence of cracks, however, does not imply failure of the concrete base. If this were the case, the anchor bolts would have lifted out of the base, taking an inverted cone of concrete with them. Even on these three specimens, the ultimate failure of the connection occurred when the anchor bolts fractured. This indicates that even though the concrete cracked, the supplemental reinforcement did its job and prevented a catastrophic concrete failure.

There was an obvious difference in the performance of the base mat of the D-series tests versus the F-series tests. As noted above, diagonal cracks were observed in the first three D-series tests, while no such cracks were observed in the F-series tests. One difference in the design of these two series was that the anchor rods in the F-series tests had an embedment length of 19 inches while those in the D-series tests were embedded 16 inches. The available strength of the concrete resisting the pullout of an anchor rod in tension is highly dependent on the embedment depth of the anchor rod itself. Therefore, the shallower embedment of the D-Specimens could explain why the base mats of these specimens exhibited more cracking and distress than the F-specimens (with deeper embedment).

Also, as was noted in section 4.1.2, the anchor rod steel used in the D-specimens (1 in. diameter) had a yield and fracture strength that were 44% and 55% higher, respectively, than was expected. This higher-than-expected bolt strength would explain why the base mats for the D-specimens showed more cracks and distress than the F-specimen's base mats, as the anchor bolts transmitted much more load than was expected into the base mat concrete before fracturing.

It is assumed that a combination of these two factors led to the difference in performance between the D and F Series base mats.

5.2.2 Performance of Top Mat and Block Out

The purpose of the top mat and the block out was to simulate a floor slab and block out. It was anticipated that these two elements would experience significant cracking and deformation.

When the specimen was loaded, the top mat contributed to the resistance of that load through beam action, meaning the top mat and block out acted as a beam. The rotation of the column base caused a compression resultant at one end and a tensile resultant at the other end.

The first effect of the beam action of this concrete was the tension resultant, resisted by the cold joint between the base mat and top mat concrete. This cold joint had an effect on the strength and stiffness of the connection, and will be discussed further in Section 5.4.

The second effect was that it caused the top mat to behave, and crack, as a beam. Vertical cracks in the side of the top mat at its bottom were observed in each and every specimen indicating positive bending moments. These cracks consistently began at the bottom and extended upwards until they reached the location of the horizontal reinforcement which was placed at around 4 inches from the top surface in every specimen. An example of this is shown in

Figure 4-26 for specimen F3. The reinforcement in the top mat was designed based on minimum amounts for temperature and shrinkage only, and placed near the top of the slab as is common for flooring systems. As such, the floor was not designed nor reinforced specifically for this beam action. Doing so may involve additional reinforcement near the bottom of this slab to resist the tensile forces evident by the cracks observed. It would be valuable in future research to do so, and investigate whether this could have a positive impact on the strength and stiffness of the connection.

Damage to the surface of the top mat and block out were observed in some, but not all specimens. This damage was caused by bearing of the concrete flange against the block out concrete. The D-series specimens consistently showed very little, if any, surface damage. In contrast, the F-series specimens consistently showed significant damage to the top surface at drifts greater than 5%. Of interest is that in those specimens which experienced large damage to the base mat (D series), little damage was noted at the top surface, while those specimens that experienced little to no damage in the base mat concrete (F series) showed much larger cracks and distress in the top surface of the block out concrete. When the concrete in the base mat began cracking and showing distress in the D specimens, it is speculated that this caused a “soft spot” in the system, in effect protecting the block out concrete from experience higher loads and cracking at its surface. The base mat concrete for the F specimens never saw this cracking (as explained in Section 5.2.1), and thus the block out concrete experienced much higher bearing forces from the column flange, leading to the cracking that was seen.

The cold joint between the top mat and the base mat played a role in the behavior of the specimens. This cold joint resisted tension loads for very small deflections. The joint eventually broke in each specimen, as noted in the Test Observations (section 4.2). When it broke, the

tension resultant was then transferred entirely to the anchor bolts. This is evident from the graphs depicting anchor bolt strain in section 4.6. These graphs (especially those of specimens D3, D4, F3, & F4) clearly show that the anchor rods exhibit very minimal strain until the larger displacements when the cold joint has broken. The breaking of the cold joint did have an effect on the rotational stiffness of the connection at the top of the block out. This is evidenced from the rotational stiffness data, that indicates a significant drop in stiffness once the cold joint broke. See the rotational stiffness graphs for specimens D3, and D4 (Figure 4-75 & Figure 4-76).

One phenomenon noted during testing was the tendency of the entire top mat, block out, and column assembly to lift up off the base mat during testing. This only occurred at the very large displacements and led to the column rising up to 2 inches. This occurred in all six specimens that had a top mat and block out. Post-test analysis of the specimens revealed that there was a significant amount of damage to the grout and concrete directly beneath the column base plate. It is believed that under very large deflections, this grout and concrete was crushed and deposited underneath the base plate as it rocked back and forth. As the anchor bolts stretched, this crushed material accumulated underneath the base plate and acted as a fulcrum around which the column base rotated raising up the column base plate. This distance grew larger and larger as the anchor bolts continued to stretch and more crushed material accumulated underneath the base plate.

5.2.3 Performance of Shear Lug

The purpose of the shear lug was to resist the lateral movement of the column base at small deflections. This was done to eliminate any lateral shear forces on the anchor bolts, which were designed to resist axial loads only. As explained in Section 0, care was taken during placement of

the column so that at the time of installation, none of the anchor bolts were bearing on the side of its hole on the base plate. This ensured that all lateral resistance to movement was by either friction between the base plate and grout, or by the bearing of the shear lug. Again, the shear lug was designed ignoring any contribution of friction between the base plate and underlying grout. Examination of the specimens after testing revealed that none of the shear lugs experienced any noticeable deformations, and that the welds attaching the shear lug to the base plate all remained intact. At the smaller deflections (less than 2% story drift), data from the string pots on the column bases reveals no significant lateral movement of the column base (less than 0.04 in), indicating that the shear lugs did indeed provide adequate lateral resistance to movement.

It wasn't until the larger deformations (greater than 4% drift) that the shear lug became ineffective. As noted previously, it was discovered in post-test analyses that there was a significant amount of damage to the grout underneath the base plate and surrounding the shear lug. At these higher deflections, the grout was crushed, removing any bearing surface for the shear lug, and the shear lug became ineffective. Large lateral movements were observed at the base of the column at the later end of the test cycles as the lateral resistance of the base shifted from the shear lug to the anchor bolts. This will be discussed further in the following section.

5.2.4 Performance of Anchor Bolts

The purpose of the anchor bolts was to secure the column base plate to the concrete base mat and resist rotation. As noted in section 3.3.2.3, the anchor bolts were specifically designed so that the anchor bolts would be the weakest element in the connection. Without exception, the anchor bolts performed as intended and failure of each of the specimens was the result of anchor bolt tensile fracture. Without exception, when the anchor bolts failed, it was due to the rupture of

the anchor bolt steel, as was intended. This occurred even though the anchor bolt material had a much higher yield and rupture strength than was designed for (see Section 4.1.2).

One phenomenon of note occurred to the anchor bolts during large deflection cycles. When the column was placed onto the base mat concrete, leveling nuts were used to correctly position and level the column base plate. For the six specimens that had eight anchor bolts, only the four exterior bolts (at the extreme corners) had these leveling nuts. This is a common method used by steel erectors to correctly position the column. Any compressive axial loads transferred from the steel column to the concrete foundation are assumed to transfer through the stiffer grout, rather than the more-flexible anchor rod, with a leveling nut. However, as noted above, during the large deflection cycles, the grout underneath the base plate was crushed and lost its stiffness and bearing capacity. When this occurred, the resultant compressive axial loads from the rotation of the base plate were transferred to the base concrete through the anchor rods with leveling nuts. Since only the exterior anchor rods had these leveling nuts, these rods were strained in both tension and compression, while the interior anchor rods were strained only in tension. This is the cause of the differing anchor bolt heights noted in the test observations (see Figure 4-6 and Figure 4-21), also see Figure 5-7, below. Post-test visual analysis of the specimens indicated a significant amount of deformation occurred in the exterior anchor bolts with leveling nuts, while this was absent from the interior bolts, as shown in Figure 5-8.

The anchor rods were also subjected to large lateral loads and deformations, but again this occurred only at the very large deformation cycles (greater than 4% drift). As noted previously, the shear lug became ineffective at resisting the lateral movements at these higher deflections, and this load was, instead, resisted by the anchor bolts.



Figure 5-7: Anchor Bolts with Differing Strains; Specimen F2 After Testing and With Block out Concrete Removed

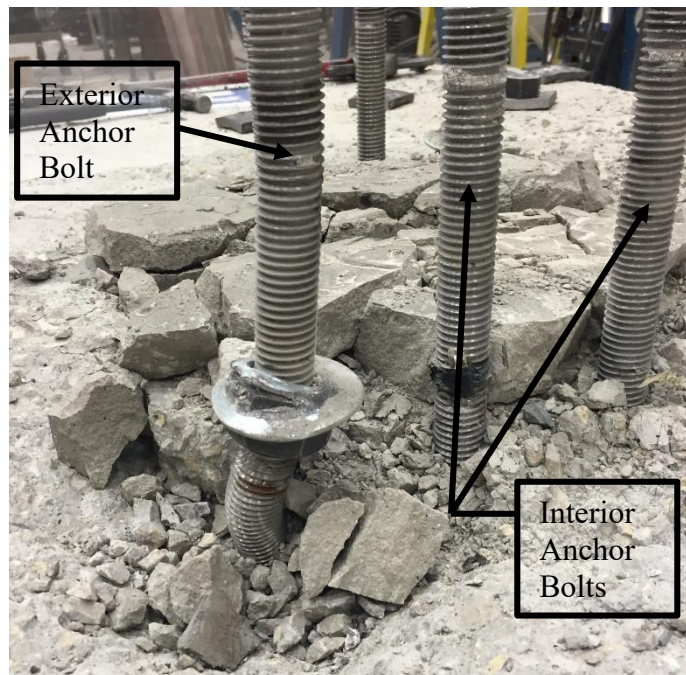


Figure 5-8: Anchor Bolts Post Test, Specimen D2

5.3 Connection Strength

Strength is an important characteristic of a column base connection. The available yield strength of a connection is defined as the upper limit at which all the elements of the connection remain in an elastic state. A connection is designed generally to its yield strength. The ultimate strength of a connection is defined as the maximum load that a connection can sustain before a catastrophic failure.

Yield failure of the connections was defined as the minimum force exerted on the specimen that caused the anchor bolts to yield, thus moving the entire connection into inelastic behavior. As explained in Section 3.3, care was taken during design to ensure that the yielding of the anchor bolts would govern the performance of the connection.

Determining the yield failure strength of each specimen is done by analyzing the information from the anchor bolt strain gage data. This process is demonstrated for specimen D3. Refer to Figure 4-82, and Figure 4-84 for the strain information for anchor bolts A1 and A2. As shown below in Figure 5-9, this specimen is analyzed by isolating the information for Specimen D3 from these graphs. Along with the anchor bolt strain data, the yield strain line is shown for the 1 inch diameter anchor bolts (As determined in Section 4.1.2). When the strain from the anchor bolts has passes this line, the anchor bolts have yielded. After this, the connection demonstrates inelastic behavior. Since we have the information from the two anchor bolts shown, the strength of the connection is taken as the average of these two anchor bolts, rounded to the nearest 1 kip.

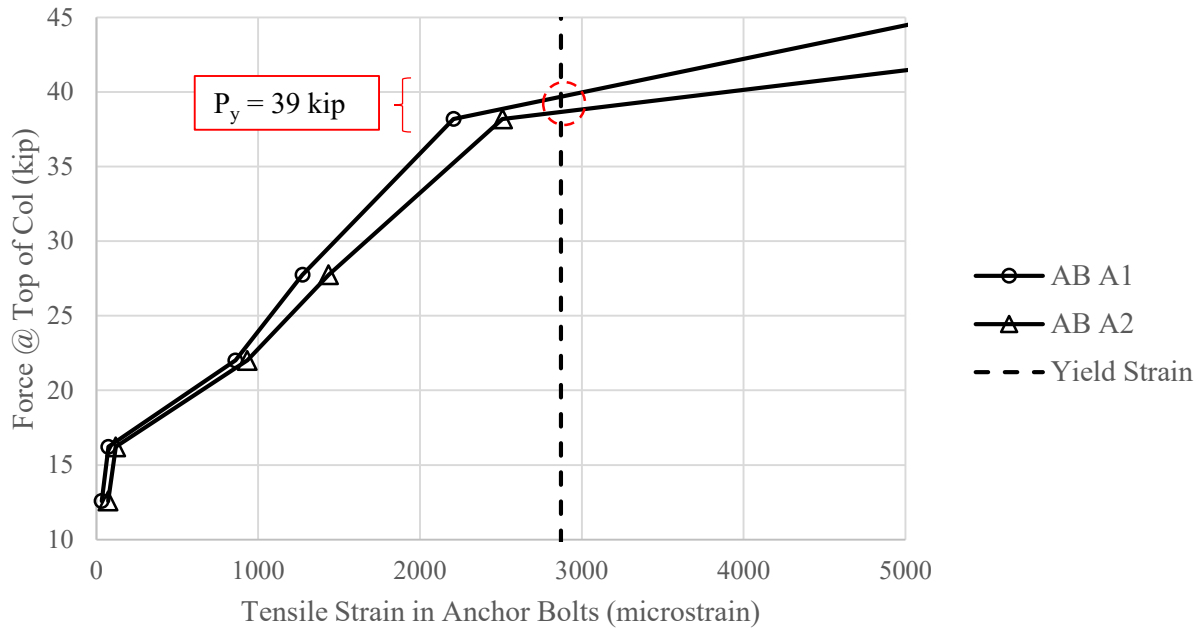


Figure 5-9: Anchor Bolt Strain Data for Specimen D3

Determining the ultimate strength of each specimen is done by analyzing the backbone curve of each specimen (see Section 4.3), and simply determining the maximum load that was allowed by the system. This procedure is shown below in Figure 5-10 for specimen F2. The ultimate strength of the specimen is determined by averaging the maximum load and the absolute value of the negative load, rounded to the nearest 1 kip.

This procedure was done for each specimen, and the results are listed below in Table 5-1. The maximum load is also translated into a maximum moment at the base of the column, simply by multiplying the load (P) by the height of the column (102 inches). This information is also shown graphically in Figure 5-11 and Figure 5-12.

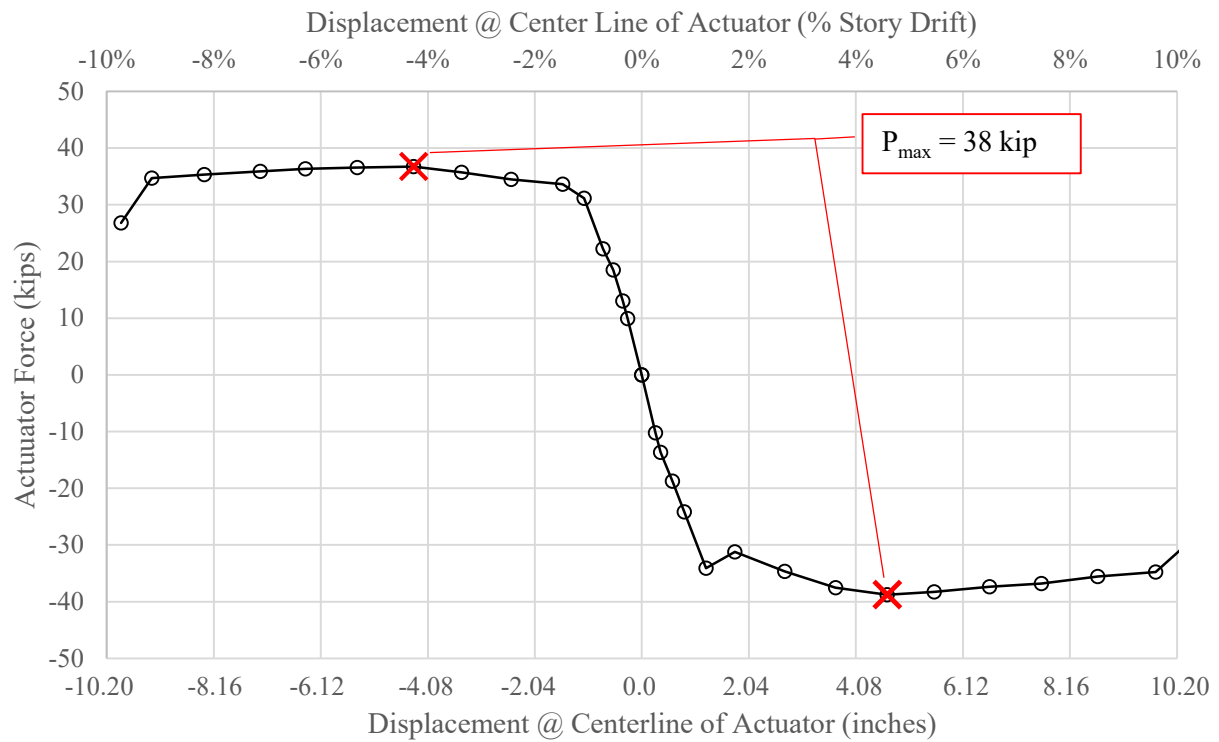


Figure 5-10: Backbone Curve for Specimen F2 (Copy of Figure 4-48)

Table 5-1: Observed Strength of Each Test Specimen

Specimen	Yield		Ultimate	
	P_y (kips)	M_y (kip·ft)	P_u (kips)	M_u (kip·ft)
D1	23	196	39	332
D2	28	238	42	357
D3	39	332	47	400
D4	24	204	32	272
F1	22	187	35	298
F2	32	272	38	323
F3	42	357	45	383
F4	30	255	32	272

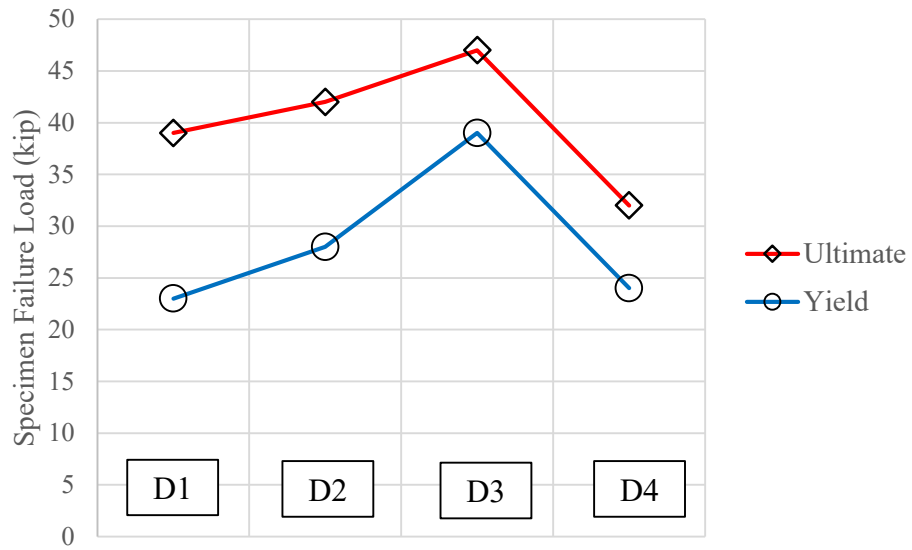


Figure 5-11: Observed Strength of D-Series Specimens

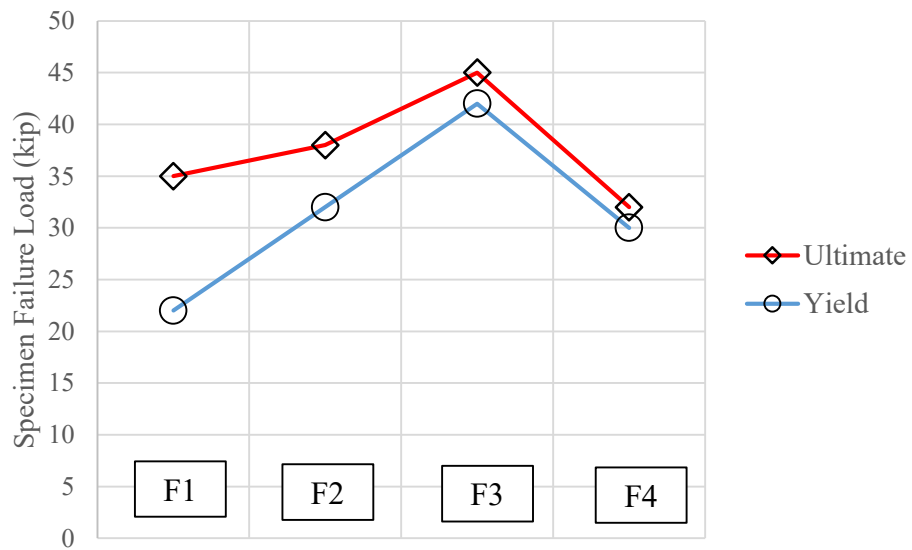


Figure 5-12: Observed Strength of F-Series Specimens

Comparing the specimens to each other yields valuable insight into the connection. The addition of the block out concrete to the connection increases its yield strength. Without altering the details of the design in any way, adding merely 8 inches of block out concrete to the connection increases the available yield strength 22% (D2) and 45% (F2). Adding 16 inches of concrete increases the yield strength 70% (D3) and 91% (F3).

Comparison of the specimens also indicates the critical role the anchor bolts continued to play in the strength. By looking at specimens 3 and 4 of both series, a significant drop in strength occurs when the number of anchor bolts is reduced. By cutting the number of anchor bolts in half, the strength of the connection is reduced by 40% (D4) and 29% (F4). Note that reducing the number of anchor bolts by $\frac{1}{2}$ does not decrease the strength of the connection by $\frac{1}{2}$. This indicates that there is not a linear relationship between the amount of anchor bolt steel resisting tension, and the strength of the connection. It is possible that with specimens D4 and F4, the compression resultant of the connection is far enough away from the column base that the tension resultant of the connection is partly resisted by all of the anchor bolts, not just the anchor bolts on the tension end of the column. While this could explain the non-linearity of the strength discussed above, further research is required to confirm this.

Comparison of the strength of the specimens to prediction models also yields valuable information. Two predictive methods are used for comparison. The first represents current, conventional practice: ignoring the block out concrete altogether and determining the strength treating the connection as an exposed base plate using the AISC Design Guide #1 (Fisher and Kloiber 2006). The second is the model proposed by (Barnwell 2015), meant specifically for this precise situation: a column base connection shallowly embedded into block out concrete. His model predicts that the lateral load imposed at the top of the column is resisted by two coupled

vertical forces. The tensile force is resisted by the anchor bolt(s), and the compression force is resisted by the base concrete with the location of the resultant found by extending an imaginary line 45° down from the face of the compression column flange. A simple statics analysis can be used to predict the maximum load (P) that can be supported by the connection before the anchor bolts yield. Refer to Section 2.5.2 for more details on this method.

The observed strength of each specimen was compared with the predictions of both of these methods, and is shown below in Table 5-2. This data is also shown graphically in Figure 5-13 and Figure 5-14.

Table 5-2: Observed Specimen Yield Strength vs. Predicted Strengths

Specimen	Traditional Method AISC Design Guide 1 (kips)	Barnwell's Model (kips)	Observed Strength P_y (kips)
D1	16.61	*	23
D2	16.61	29.40	28
D3	16.61	39.22	39
D4	8.43	19.61	24
F1	18.60	*	22
F2	18.60	31.47	32
F3	18.60	43.29	42
F4	9.50	21.65	30

** D1 & F1 had no block out concrete, thus Barnwell's model is not applicable*

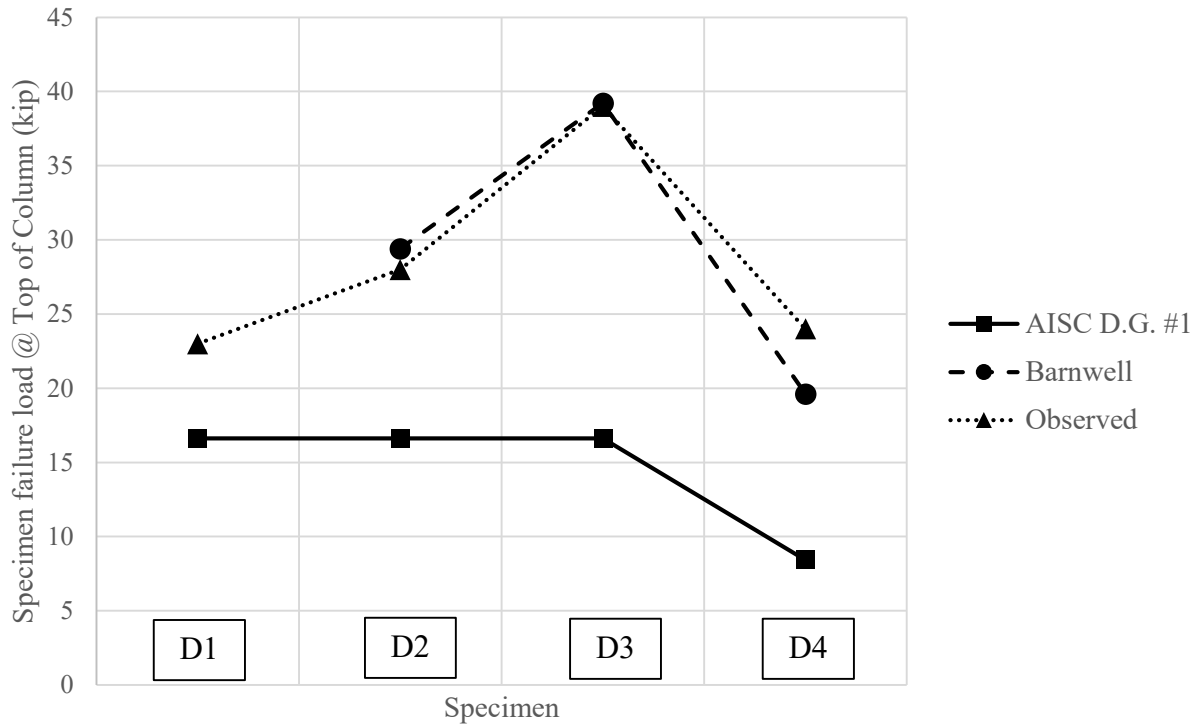


Figure 5-13: Observed Specimen Strength vs. Predicted Strengths, D-Specimens

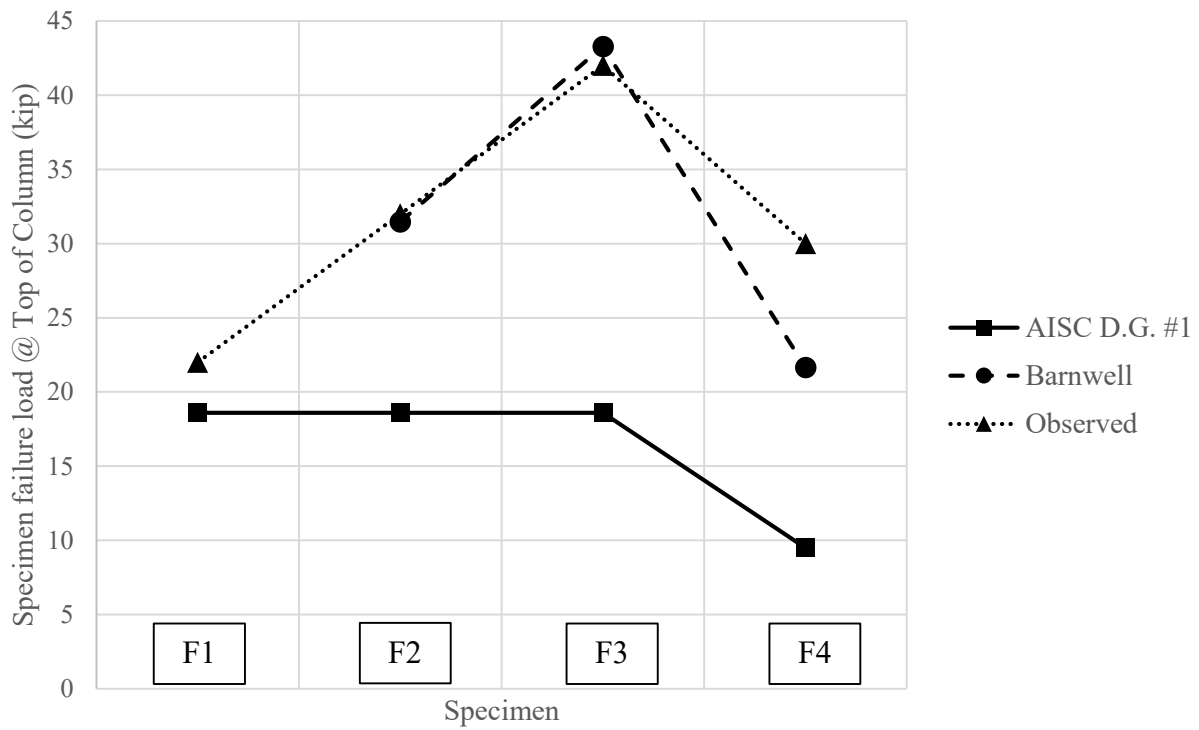


Figure 5-14: Observed Specimen Strength vs. Predicted Strengths, F-Specimens

This data suggests that the current method of designing the connection as an exposed base plate, ignoring any contribution of the embedment concrete, is a conservative approach. Even a small embedment (8 inches: specimens D2, and F2) exhibit strength that was 69%-72% greater than that predicted by this method. The deeper embedment (16 inches: specimens D3, D4, F3, & F4) exhibited strengths that were 126% - 216% greater than the conventional method; more than a two-fold increase for all specimens. The contribution of the block out concrete may be ignored when determining the strength of a connection, but this results in a very conservative estimate.

The method proposed by Barnwell is an adequate method of predicting the strength of a shallowly embedded connection with block out concrete. This model predicted strengths that were between -5% and 39% of the observed tests values. The model was extremely accurate (within 5% of observed strength) for specimens D2, D3, F2, & F3. The larger deviations occurred in specimens D4 and F4, when the number of anchor bolts was reduced. These two specimens represent a design that would be impractical for use, because the number of anchor bolts is grossly undersized compared to the required strength of the connection for actual design (see Section 3.3.2 for an explanation of the design of each specimen, and specifically Section 3.3.2.3 for an explanation of the design of the anchor bolts). This suggests that the model becomes increasingly conservative for specimens whose anchor bolts are undersized compared to the flexural strength of the column and base plate. A possible explanation to this could be related to the non-linear relationship between the anchor bolt and connection strength noted above. Barnwell's model suggests a linear relationship: i.e., reducing the amount of steel resisting tension (A_s) by $\frac{1}{2}$ would result in an equal reduction in the strength of the connection. The data from this test indicates that the specimens behave differently.

Another possible cause for the discrepancy noted above is that in applying Barnwell's model, the downward force caused by the weight of the column, base plate, and block out concrete was ignored. In reality, these elements cause a net downward force that reduces the amount of tensile force resisted by the anchor bolts. Thus, for specimens with a reduced amount of anchor bolt steel resisting the tensile resultant (D4, and F4), it would be expected that Barnwell's model would be relatively more conservative.

Though these data show that an increase in the depth of the embedment concrete correlates to an increase in the connection strength, there exists a theoretical limit to the embedment depth where a further increase would give no additional benefit. At this point, the connection itself is strong enough that the bending capacity of the column would theoretically govern the strength of the connection. These data do not reveal what this theoretical limit would be, and further study is needed to identify this limiting embedment depth.

5.4 Connection Stiffness

The rotational stiffness of a column base is an important characteristic of the connection, and has implications for the performance of the structure under lateral, vibration, and vertical gravity loads. See Figure 5-15 for a simplified representation of the rotational stiffness of the connection. Being able to accurately model the rotational stiffness of the base connection allows design engineers to more accurately predict the behavior of a structure under these loads.

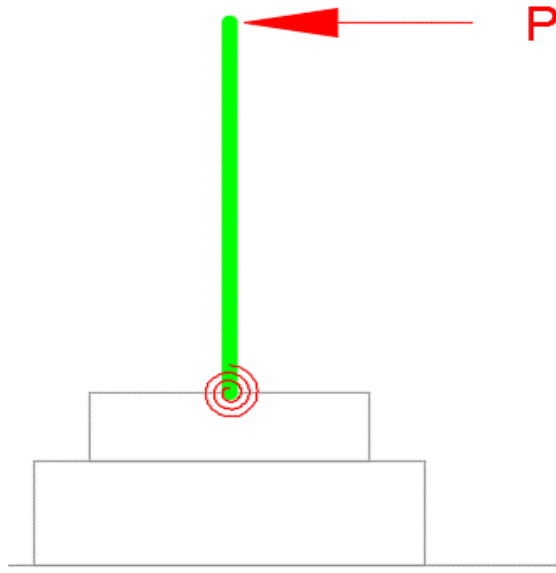


Figure 5-15: Rotational Stiffness of Column Base Connection at Top of Embedment Concrete, Modelled as a Rotational Spring

At low deflection cycles (less than 1% story drift), the rotational stiffness of the specimens increases with the addition of the block out embedment concrete. The specimens with a block out increased in stiffness by an average of 119% (D-Specimens), and 40% (F-Specimens). See Table 4-5. Interestingly, again for the low deflection cycles, the *amount* of block out concrete did not significantly affect the rotational stiffness. All three specimens for each specimen series had nearly identical stiffness, regardless of the actual amount of concrete.

The specimens did show a drop in the rotational stiffness after the concrete cold joint between the base mat and top mat broke. At this point, the stiffness for specimens with fewer anchor bolts (D4, and F4) was significantly lower than their counterparts with more anchor bolts. This indicates that after the cold joint has broken at higher deflection cycles, the anchor bolts are

engaged and resist the rotational movement of the connection. Thus, the fewer anchor bolts present to resist this motion, the lower the rotational stiffness.

Three methods of predicting the rotational stiffness of the connection have been proposed, and the results of the tests are compared to these three methods. The first method, proposed by (Kanvinde, Grilli et al. 2011), is an attempt to predict the stiffness for a simple exposed base plate connection, ignoring any contributions that the block out concrete may make. This represents the current industry practice of designing the base plate as if the embedment concrete does not exist. This method would thus predict equal values for the first three specimens of each series, which differ only in the amount of embedment concrete they have. See Section 0 for additional information on this method, and its application to these test specimens.

Until recently, if a designer wished to model the base connection as a rotational spring rather than the idealized “pinned” or “fixed” connection, Kanvinde’s method was the only option. Again, this method neglects any contribution of the block out embedment concrete to the stiffness of the connection. Two researchers have attempted numerical models that predict the behavior of shallowly embedded column connections, considering the additional influence of the embedment concrete. Their work is summarized in Sections 2.5.3 and 2.5.4.

(Jones 2016) obtained the test design and matrix for this thesis research, and used that information to produce predictions for the rotational stiffness based on his numerical modeling.

Similarly, (Tryon 2016) used numerical and finite element modeling to produce predictions about the rotational stiffness of an embedded column base connection. He produced a set of normalized graphs and accompanying equations to produce these predictions. The equation pertinent to these tests (common steel shape bent about its strong axis; see Section 2.5.4) was used to produce the predictions.

The results of these three methods are shown below in Table 5-3, along with the observed stiffness first presented in Section 4.5. The data is also presented graphically in Figure 5-16 and Figure 5-17.

Table 5-3: Predicted vs. Observed Rotational Stiffness, β

Specimen	Predicted			Observed
	Kanvinde Model	Jones Model (kips·in./rad)	Tryon Model	<i>small deflections</i> (kips·in./rad)
D1	5.70E+05	*	*	4.26E+05
D2	5.70E+05	8.80E+05	6.66E+05	9.63E+05
D3	5.70E+05	9.40E+05	9.77E+05	9.14E+05
D4	2.80E+05	9.14E+05	9.77E+05	9.20E+05
F1	5.11E+05	*	*	6.21E+05
F2	5.11E+05	8.32E+05	7.02E+05	10.31E+05
F3	5.11E+05	7.66E+05	10.84E+05	10.12E+05
F4	2.57E+05	7.20E+05	10.84E+05	10.56E+05

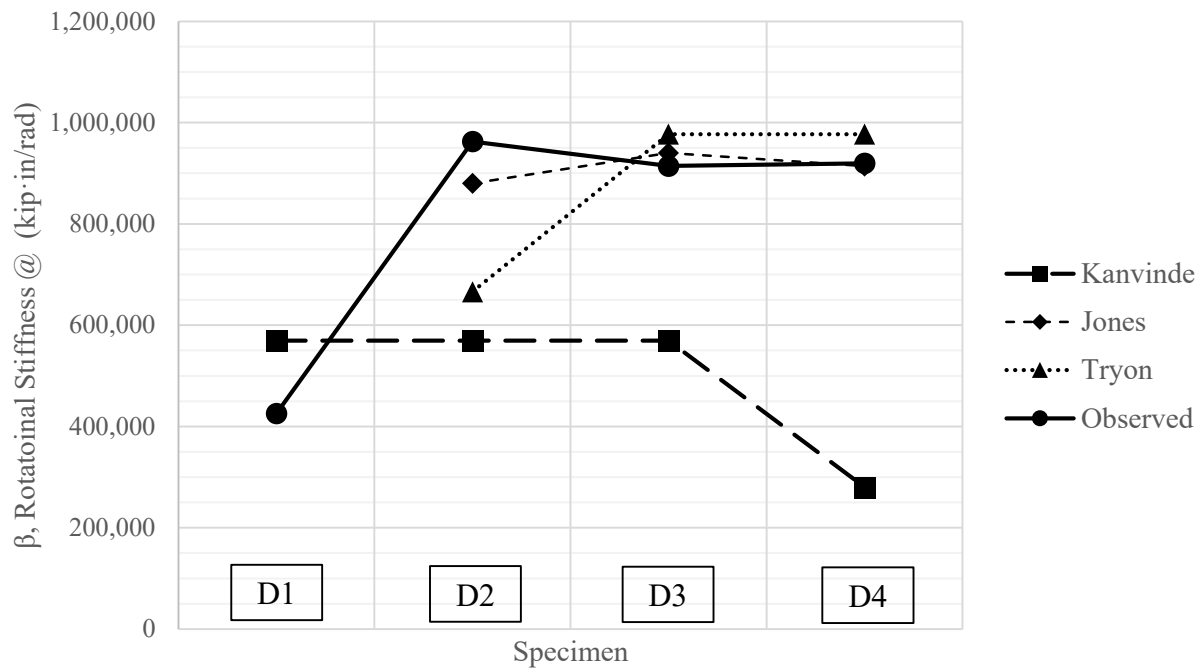


Figure 5-16: Predicted vs. Observed Rotational Stiffness, D-Series Specimens

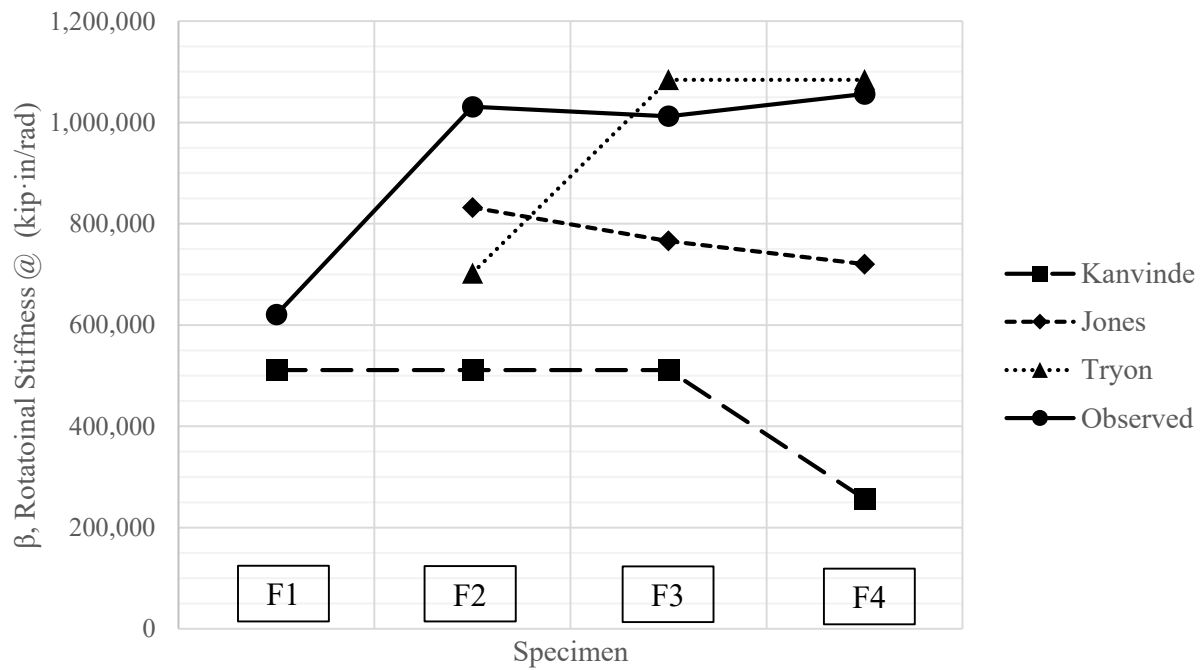


Figure 5-17: Predicted vs. Observed Rotational Stiffness, F-Series Specimens

The data suggests that all three predictive methods are reasonable and usable. Kanvinde et al's model produced predictions that were reasonable (within 25%) for specimens D1, and F1. These specimens represent the condition that Kanvinde et al's equations were meant for, so this was expected. His equations proved extremely conservative for the next two specimens in each series. Observed values were between 61% and 69% greater than the predictions for the D specimens, and 98% and 102% greater than predictions for the F specimens. In the final specimen of each series, Kanvinde et al's model predicted a large drop in stiffness when the base plate and anchor bolts were less-robust. This drop in stiffness was not reflected in the observed specimens. The observed values were 229% greater for specimen D4, and 312% greater for specimen F4. This suggests that Kanvinde et al's model would produce extremely conservative predictions when used with connections with block out concrete.

Jones' model was accurate to within 9% for the D specimens, and 47% for the F specimens. A possible explanation to the difference in the results is the flange width/column depth ratio that differs between the specimen groups (see Section 3.3.1). It is possible that Jones' finite element model does not correctly account for this difference. This is pure speculation, however, and a much more detailed and exhaustive analysis would need to be done on Jones' finite element modeling to discover the complete reason for the difference in accuracy. Even with the discrepancy noted, Jones' method of predicting behavior would be appropriate for use.

Tryon's model predicted a lower stiffness for both of the 8 inch block out specimens, and observed values were 45% (D2) and 47% (F2) higher than their predictions. For the deeper block out specimens, the method was much more accurate. The observed values were within 6% of the D specimen predictions, and within 7% of the F specimen predictions. Tryon's model predicted that as the embedment depth deepened, the rotational stiffness would likewise increase, until an

upper bound limit was met, at which point the connection would not exhibit an increase in stiffness with an increased embedment depth. This was reflected in the observed results.

This study revealed an alternative to these three methods of predicting the rotational stiffness of a shallowly embedded column base plate. The specimens with deeper block outs (D3, D4, F3, & F4) demonstrated behavior consistent with a theoretical “fixed” connection at the base of the column. Both Jones and Tryon’s models make predictions assuming the connection point to be at the top of the embedment concrete (see Figure 5-15). If, instead, that connection point is moved into the embedment concrete to the top of the base mat concrete, that point can be considered “fixed”. See Figure 5-18.

Evidence of this behavior can be found in the backbone curves of the specimens with deeper block outs, mentioned above. See Figure 4-43, Figure 4-45, Figure 4-51, Figure 4-53. This data clearly shows that for small deflections (under 1% story drift), the column exhibits the behavior of a column with a “fixed” base. Further evidence of this conclusion can be found in the data retrieved from the strain gages on the column flanges. See Figure 4-88, Figure 4-89, Figure 4-92, and Figure 4-93. These figures show that for the columns with 16 inches of embedment, the strain at the base of the column (measured by strain gages C11 and C21) remain extremely low, while on a normal cantilevered column with an exposed base plate, the strain in the column flange would be highest at the base of the column. This indicates that the addition of the surrounding block out concrete reduces the strain at the base of the column. The mechanism providing the rotational resistance then, relies less on the base plate/anchor bolt assembly and more on the embedment concrete. When this mechanism does not rely on the base plate/anchor bolt assembly at all for rotational resistance, the rotational stiffness at that location approaches infinity, and the data suggests these column assemblies do just that.

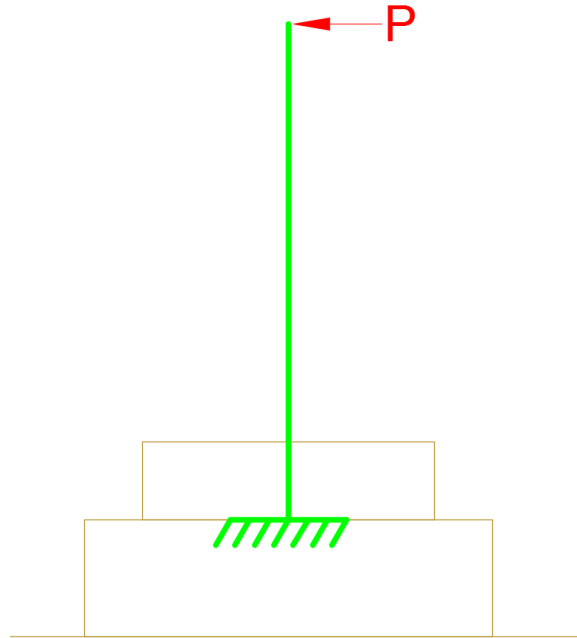


Figure 5-18: Rotational Stiffness of Column Base Connection, Modelled at the Base of the Column as a "Fixed" Connection

The two D-specimens in which this model are applicable have an embedment depth to column depth ratio (L/d) of $17 \text{ in} / 13.9 \text{ in} = 1.22$, whereas the ratio for the two F-specimens is $17 \text{ in} / 10.6 \text{ in} = 1.62$. Note that the embedment depth used in this ratio is the distance from the top of the block out concrete to the bottom of the column base plate. This suggests that for columns with similar ratios this proposed model would be appropriate. Obviously there would be a limit to how much embedment concrete would be needed, and demonstrated by the backbone curves for specimens D2 (Figure 4-41) and F2 (Figure 4-49). These specimens have a ratio of $7 \text{ in} / 13.9 \text{ in} = 0.50$ and $7 \text{ in} / 10.6 \text{ in} = 0.66$, respectively. The backbone curves show that these two

specimens exhibit backbone curves with less-stiff behavior than the theoretical fixed-base line, showing that this proposed model would be unacceptable for use with these two specimens.

This suggests that there exists an embedment depth to column depth ratio (d/L) that provides a limit to where this concept could be applicable. This limit lies somewhere in between the specimens tested here (0.66 – 1.22). Further research is needed to identify this ratio limit.

Regardless of what the lower limit is, the data from this research suggests that it would be appropriate to utilize this model in design for steel columns that have a d/L of 1.22 or more. The research done on composite moment connections by (Shahrooz, Remmetter et al. 1993) outlined in Section 0, also suggests that there is an upper limit to the validity of this ratio, at which point this method would be conservative. For extremely large d/L ratios (ie. very deep embedment depths), Shahrooz suggests that the point at which the column could be considered “fixed” may not be at the actual base of the column, but rather at some depth along the column, simply shortening the effective length of the column. This is similar to the observation made by (Shahrooz, Remmetter et al. 1993) about the effective embedment depth of a composite connection. Again, further research is needed to determine what this ratio would be.

5.5 Design Example

In order to understand the possible effects of this research, a series of design examples were performed. The purpose of these design examples was to perform the detailed design, fulfilling the same design requirements, but utilizing two different design approaches. The first approach would represent the current design methods employed by design professionals. The second approach represents the updated information and models discussed in this paper. This

example will answer the question as to whether or not the research presented here can translate into real-life differences in the design of structural members and column base connections.

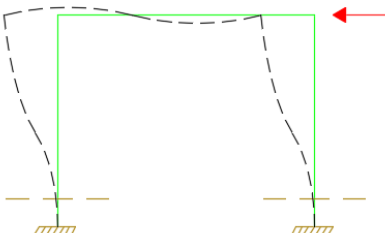
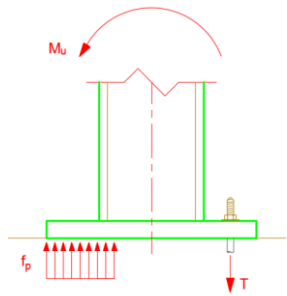
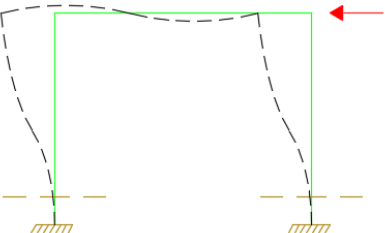
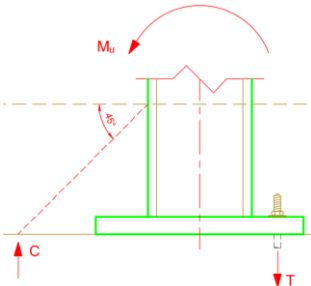
5.5.1 Design Example #1: Moment Frame with a “Fixed” Base

The first example is the detailed design of a moment frame subjected to a lateral load, and assumed to have a “fixed” column base. To account for the possibility of an uplift load on the column, there is no vertical load on the frame. The frame itself consists of wide flange shapes, oriented to bend about their strong axis. The column base is shallowly embedded in block out concrete, and attached via anchor bolts to a rigid concrete foundation. The beam is assumed to be connected rigidly to the column, and that detail will not be designed here.

The main objective of this design exercise is to determine appropriate member sizes for the columns and the beam, and to design the base plate connection to the foundation. There are two design constraints: the strength of the members must fulfill the requirements of AISC 360, and the serviceability of the frame must limit lateral deflection to 1.0% story drift, measured from the top of the floor to the top of the column.

The design is performed twice, using two separate approaches. First, the design follows conventional design methods, currently available to design engineers. The second method will follow the new methods discussed in this paper. Refer to (Appendix B.11 Design Example #1: Portal Frame Design with a “fixed” base), for the design calculations associated with both these methods. A summary of the design procedure and models used in the design is shown below in Table 5-4.

Table 5-4: Design Example #1: Summary of Design Methods

Conventional Design Methods	
Rotational Stiffness	<p>Assume a "fixed" column base, but only if the base connection is designed to develop the expected bending strength of the column.</p> 
Rotational Strength	<p>Design the Base according the Steps outlined in the AISC Steel Design Guide #1, chapter 3.4. The required strength (M_r) is the expected bending capacity of the column</p> 
New Design Methods	
Rotational Stiffness	<p>Since there is sufficient embedment depth (embed depth/column depth > 1.22), assume a "fixed" column base, regardless of the strength of the connection</p> 
Rotational Strength	<p>Design the Base using "Barnwell's Model". Choose a base plate thickness and anchor bolt size/quantity based on the tension resultant (T), determined from the model</p> 

The results of the detailed design are shown below in Figure 5-19, and Figure 5-20, and the design is summarized in Table 5-5. While there is no difference to the member sizes chosen, there is the potential for significant savings in the base elements by using the new methods.

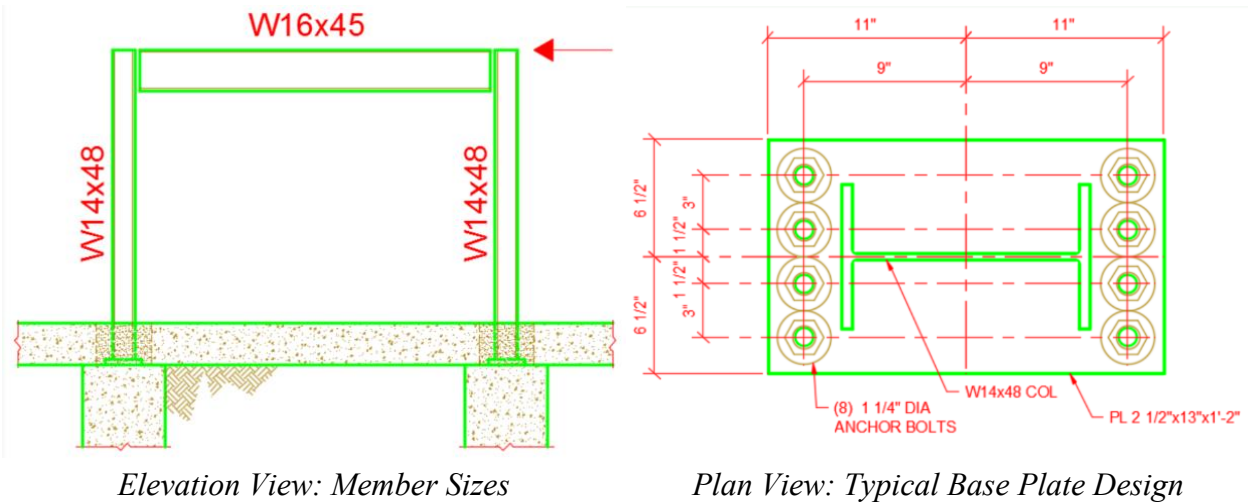


Figure 5-19: Design Example #1: Results of Design Using Conventional Design Methods

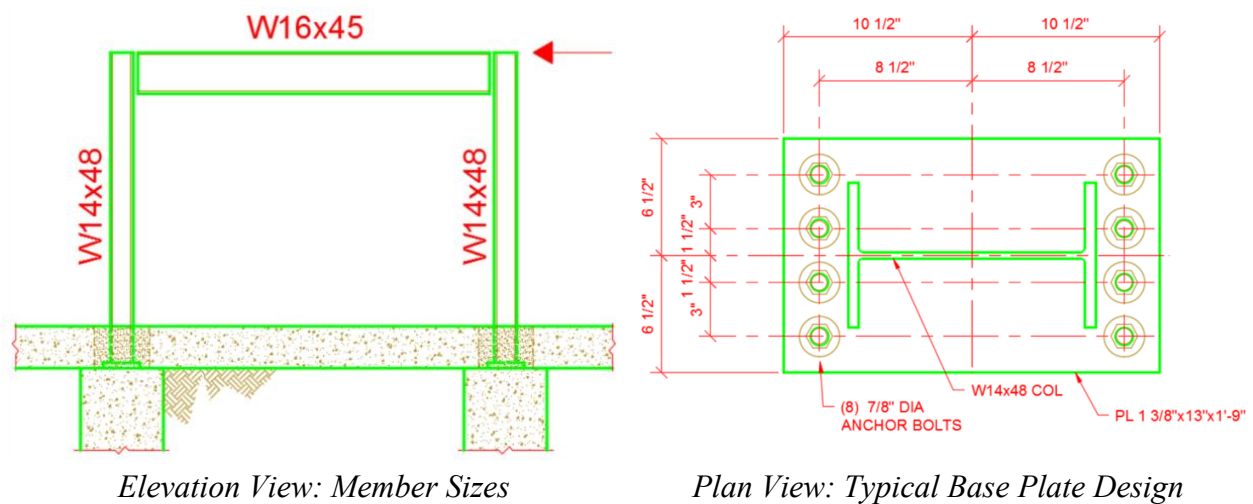


Figure 5-20: Design Example #1: Results of Design Using New Design Methods

Table 5-5: Design Example #1: Summary of Detailed Design Results

Design Method	Members			Base Plate				
	Columns	Beam	Weight	Width	Length	Thickness	AB	AB DIA
	size	size	lbs	inch	inch	inch	quantity	inch
Conventional	W14x48	W16x45	1734	13	22	2.5	8	1 ¼
New	W14x48	W16x45	1734	13	21	1.375	8	7/8

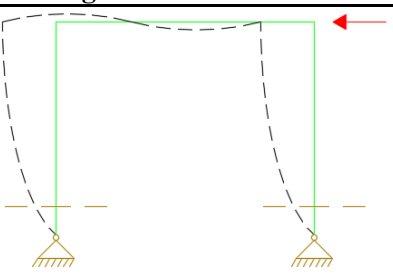
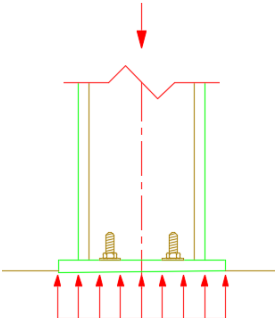
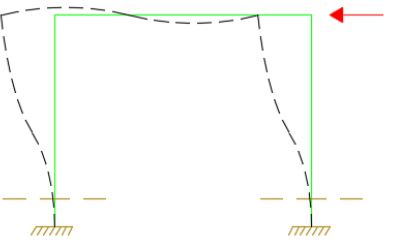
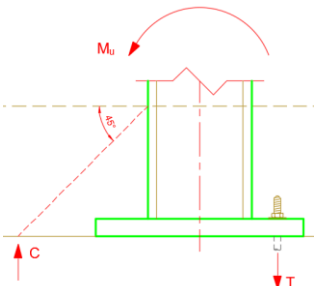
5.5.2 Design Example #2: Moment Frame with a “Pinned” Base

The second example is the detailed design of a moment frame subjected to a lateral load, and assumed to have a “pinned” column base. To account for the possibility of an uplift load on the column, there is no vertical load on the frame. The frame itself consists of wide flange shapes, oriented to bend about their strong axis. The column base is shallowly embedded in block out concrete, and attached via anchor bolts to a rigid concrete foundation. The beam is assumed to be connected rigidly to the column, and that detail will not be designed here.

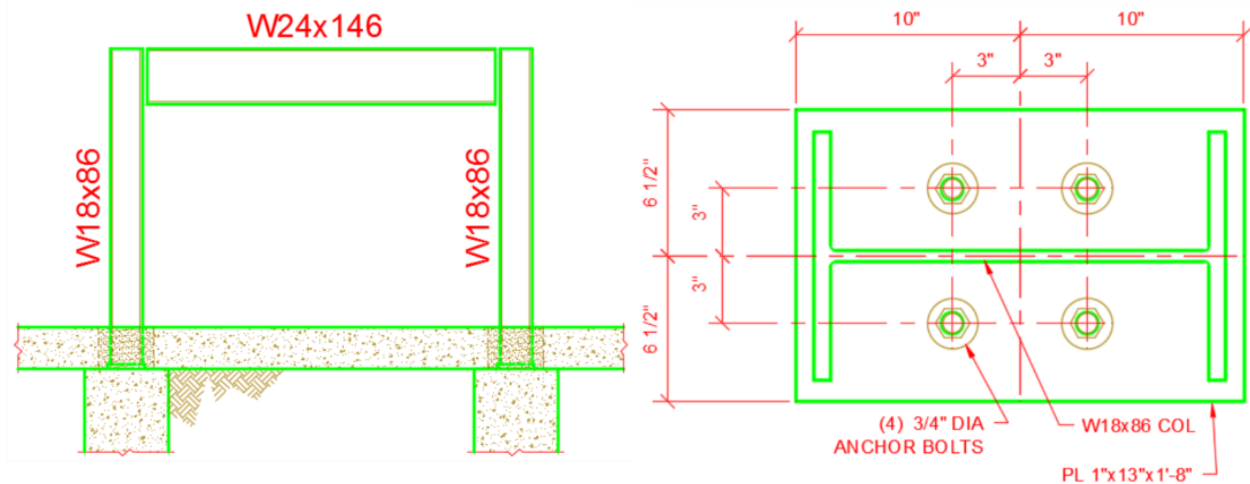
The main objective of this design exercise is to determine appropriate member sizes for the columns and the beam, and to design the base plate connection to the foundation. There are two design constraints: the strength of the members must fulfill the requirements of AISC 360, and the serviceability of the frame must limit lateral deflection to 1.0% story drift, measured from the top of the floor to the top of the column.

The design is performed twice, using two separate approaches. First, the design follows conventional design methods currently available to design engineers. The second method follows the new methods discussed in this paper. Refer to (Appendix B.12 Design Example #2: Portal Frame Design with a “Pinned” Base) for the design calculations associated with both these methods. A summary of the design procedure and models used in the design is shown below in Table 5-6.

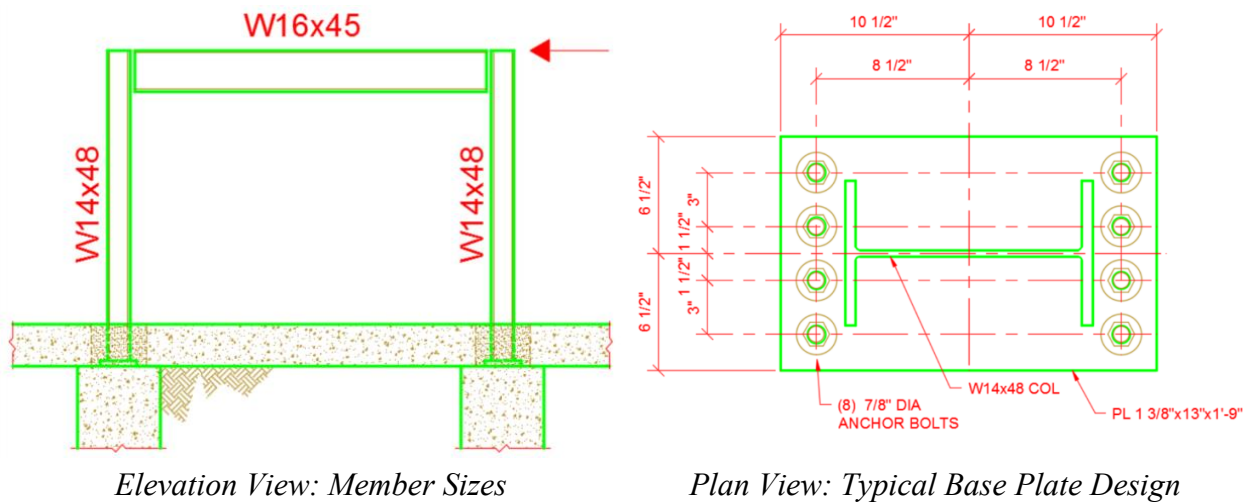
Table 5-6: Design Example #2: Summary of Design Methods

Conventional Design Methods	
Rotational Stiffness	<p>Assume a "pinned" column base, and the base connection need not be designed to resist any rotational forces</p> 
Rotational Strength	<p>Design the Base according the Steps outlined in the AISC Steel Design Guide #1, chapter 3.1. Design the base for gravity loads only</p> 
New Design Methods	
Rotational Stiffness	<p>Since there is sufficient embedment depth (embed depth/column depth > 1.22), assume a "fixed" column base, regardless of the strength of the connection</p> 
Rotational Strength	<p>Design the Base using "Barnwell's Model". Choose a base plate thickness and anchor bolt size/quantity based on the tension resultant (T), determined from the model</p> 

The results of the detailed design are shown below in Figure 5-21, and Figure 5-22, and the design is summarized in Table 5-7. The ability to model the base connection as “fixed” rather than “pinned” leads to a 43% decrease in the amount of steel utilized in the members.



Elevation View: Member Sizes *Plan View: Typical Base Plate Design*
Figure 5-21: Design Example #2: Results of Design Using Conventional Design Methods



Elevation View: Member Sizes *Plan View: Typical Base Plate Design*
Figure 5-22: Design Example #2: Results of Design Using New Design Methods

Table 5-7: Design Example #1: Summary of Detailed Design Results

Design Method	Members			Base Plate				
	Columns	Beam	Weight	Width	Length	Thickness	AB	AB DIA
	size	size	lbs	inch	inch	inch	quantity	inch
Conventional	W18x86	W24x146	3033	13	20	1.0	4	3/4
New	W14x48	W16x45	1734	13	21	1.375	8	7/8

6 CONCLUSIONS

This thesis continues a series of research performed at Brigham Young University that seeks to better understand the effects of block out concrete on shallow-embedded column base connections. To further this effort, eight physical test specimens were built and tested. The main results of the physical tests are given below:

1. The addition of the block out concrete increases the strength of the connection. Without any modifications to the connection design other than the addition of the embedment block out concrete, these tests show that the rotational strength of the connection increases between 74% (D-specimens) and 91% (F-specimens) over the corresponding exposed base plate connection without block out concrete. The shallower column (F-series) experiences a higher increase in strength than the deeper (D-series) specimens.
2. The model proposed by (Barnwell 2015) for predicting the rotational strength of shallowly embedded column base connections adequately predicts the behavior of the connection and is appropriate for use in estimating the capacity associated with the limit state of anchor bolt yielding. Other models may be required for designs where other limit states may govern. Barnwell's model predicted the strength of the physical specimens to between -5% and 39% of the observed values.
3. The proposed models for estimating the stiffness of a connection are also valid and appropriate for use. The model proposed by (Kanvinde, Grilli et al. 2011), while not

intended for use with a shallowly embedded connection, nevertheless produced predictions that were conservative, and useful. For those test specimens with block out concrete embedding the column base, his model made conservative predictions between 69% and 312% of observed values. The method proposed by (Jones 2016) is meant for shallowly embedded column base connections, and is thus much more accurate for use. Jones' model produced predictions that were between -3% and 47% of observed values. The method proposed by (Tryon 2016) is also designed for use with shallowly embedded column base connections. Tryon's method produced predictions that were between -7% and 47% of observed values.

4. The testing also indicates an alternate method for modeling the rotational stiffness of a connection. The methods outlined in the previous paragraph rely on modeling the connection as a rotational spring at the top of the block out concrete. If, however, there is a sufficient depth to the block out concrete, the connection may be modelled as a fixed connection (infinite rotational stiffness) at the base of the column. The exact embedment depth at which this model is accurate is not known, but these tests indicated that at a minimum, this method is appropriate when the embedment depth/column depth ratio is greater than 1.22.
5. Several design examples of a simple portal frame were performed using both the conventional design models and those newer models discussed here. These design examples show that by utilizing the newer models that account for the additional strength and stiffness afforded the connection by the block out concrete there is a potential for cost-saving designs in the sizes chosen for the members and in the detailing of the column base connection.

While appropriate for use in design, care should be taken when using any predictive models discussed herein. There were a limited number of variables in these tests, the main two being the column shape and the block out concrete depth. Other factors may influence the behavior of the connection that were not tested, including, but not limited to: the strength of the concrete, alternate reinforcing details in the floor mat, alternate base plate and anchor bolt configurations, and axial load/uplift on the column. Therefore, the models presented here should not be used for connections that have connection configurations or material properties significantly different than those tested here.

REFERENCES

AISC (2010). Seismic provisions for structural steel buildings. Chicago, Ill., American Institute of Steel Construction, Inc.

Barnwell, N. V. (2015). "Experimental Testing of Shallow Embedded Connections Between Steel Columns and Concrete Footings."

Bažant, Z. P. (1984). "Size effect in blunt fracture: concrete, rock, metal." Journal of Engineering Mechanics.

C39, A. (2001). "C39/C39M, Standard test method for compressive strength of cylindrical concrete specimens." ASTM International.

C143, A. (2015). "C143/C143M, Standard Test Method for Slump of Hydraulic-Cement Concrete." ASTM International.

C192, A. (2015). "C192/C192M Standard Practice for Making and Curing Concrete Test Specimens in the Laboratory." ASTM International.

Castilla, F., et al. (1984). Fixity of members embedded in concrete, DTIC Document.

Committee, A., et al. (2008). Building code requirements for structural concrete (ACI 318-08) and commentary, American Concrete Institute.

Cui, Y. and M. Nakashima (2011). "Hysteretic behavior and strength capacity of shallowly embedded steel column bases with SFRCC slab." Earthquake Engineering & Structural Dynamics 40(13): 1495-1513.

Deierlein, G. G., et al. (1989). "Beam-column moment connections for composite frames: Part 2." Journal of Structural Engineering 115(11): 2877-2896.

DeWolf, J. T. and E. F. Sarisley (1980). "Column base plates with axial loads and moments." Journal of the Structural Division 106(11): 2167-2184.

Eastman, R. S. (2011). Experimental Investigation of Steel Pipe Pile to Concrete Cap Connections. Civil & Environmental Engineering, Brigham Young University. MS.

Fisher, J. M. and L. A. Kloiber (2006). Base Plate and Anchor Rod Design, 2nd Ed. A. I. o. S. Construction.

Gomez, I., et al. (2010). "Exposed column base connections subjected to axial compression and flexure." Report Submitted to the American Institute of Steel Construction (AISC), Chicago, IL.

Grilli, D. A. and A. M. Kanvinde (2013). "Special Moment Frame Base Connection: Design Example 8." 2012 IBC SEAOC Structural/Seismic Design Manual 4: 255-280.

Grilli, D. A. and A. M. Kanvinde (2015). "Embedded Column Base Connections Subjected to Flexure and Axial Load: Tests and Strength Models."

Hetényi, M. (1971). Beams on elastic foundation: theory with applications in the fields of civil and mechanical engineering, University of Michigan.

Hutchinson, T. C., et al. (2005). "Simulation of full-scale cyclic lateral load tests on piles." Journal of geotechnical and geoenvironmental engineering 131(9): 1172-1175.

Jones, T. A. (2016). Finite Element Modeling of Shallowly Embeddeds Connections to Characterize Rotational Stiffness. Department of Civil and Environmental Engineering, Brigham Young University. Master of Science.

Kanvinde, A. and G. Deierlein (2011). Recent Research on Column Base Connections. Modern Steel Construction. 51: 42-44.

Kanvinde, A., et al. (2011). "Rotational stiffness of exposed column base connections: experiments and analytical models." Journal of Structural Engineering.

Kanvinde, A., et al. (2013). "Exposed column base plate connections in moment frames—Simulations and behavioral insights." Journal of Constructional Steel Research 84: 82-93.

Marcakis, K. and D. Mitchell (1980). Precast concrete connections with embedded steel members, McGill University.

Motter, C. J. (2014). Large-Scale Testing of Steel-Reinforced Concrete (SRC) Coupling Beams Embedded into Reinforced Concrete Structural Walls, University of California Los Angeles. Doctorate.

Myers, A., et al. (2009). "Effect of weld details on the ductility of steel column baseplate connections." Journal of Constructional Steel Research 65(6): 1366-1373.

Pertold, J., et al. (2000a). "Embedded steel column bases: I. Experiments and numerical simulation." Journal of Constructional Steel Research 56(3): 253-270.

Pertold, J., et al. (2000b). "Embedded steel column bases: II. Design model proposal." Journal of Constructional Steel Research 56(3): 271-286.

Richards, P. W., et al. (2011). "Experimental Testing of Pile-to-Cap Connections for Embedded Pipe Piles." Journal of Bridge Engineering 16(2): 286-294.

Shahrooz, B. M., et al. (1993). "Seismic design and performance of composite coupled walls." Journal of Structural Engineering 119(11): 3291-3309.

Sheikh, T. M., et al. (1989). "Beam-column moment connections for composite frames: Part 1." Journal of Structural Engineering 115(11): 2858-2876.

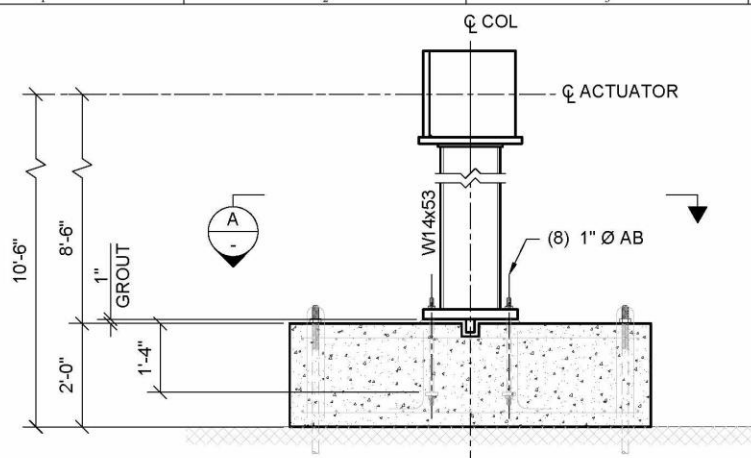
Thambiratnam, D. P. and P. Paramasivam (1986). "Base plates under axial loads and moments." Journal of Structural Engineering.

Tryon, J. E. (2016). "Simple Models for Estimating the Rotational Stiffness of Steel Column-to-Footing Connections."

Xiao, Y., et al. (2006). "Experimental studies on seismic behavior of steel pile-to-pile-cap connections." Journal of Bridge Engineering 11(2): 151-159.

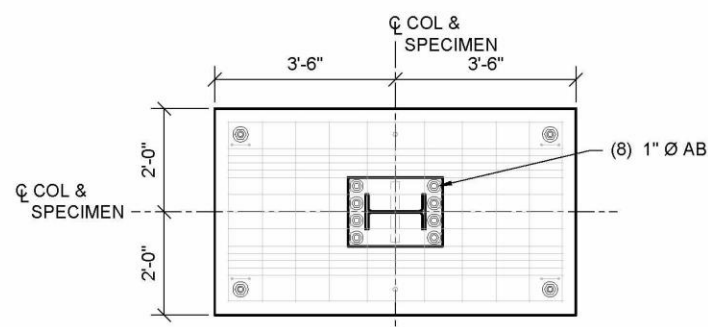
APPENDIX A: TEST SPECIMEN DESIGN DRAWINGS

A.1 Design Drawings for Specimen D1



ELEVATION
TEST SPECIMEN D1


0 6" 12" 24"
SCALE IN INCHES
1/2" = 1'-0"



SECTION

0 6" 12" 24"
SCALE IN INCHES
1/2" = 1'-0"

STEEL		
WEIGHT	641	lbs
CONCRETE		
VOLUME	56	ft³
WEIGHT	8400	lbs
ASSEMBLY		
TOTAL WEIGHT	9041	lbs



PROJECT
MS THESIS - KNH

DESIGNED
K. HANKS

APPROVED
P. RICHARDS

DATE
January 4, 2016

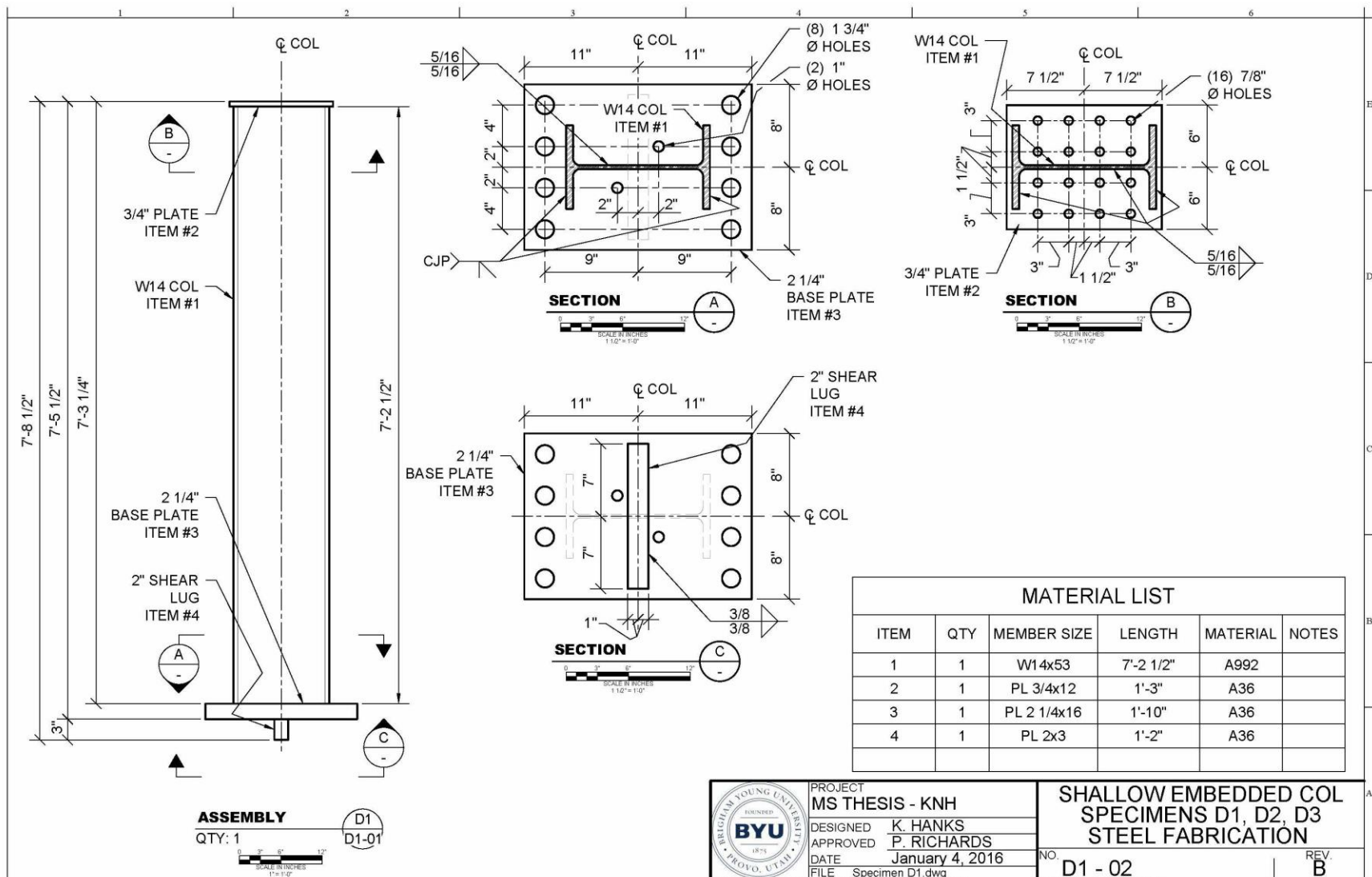
FILE
Specimen D1.dwg

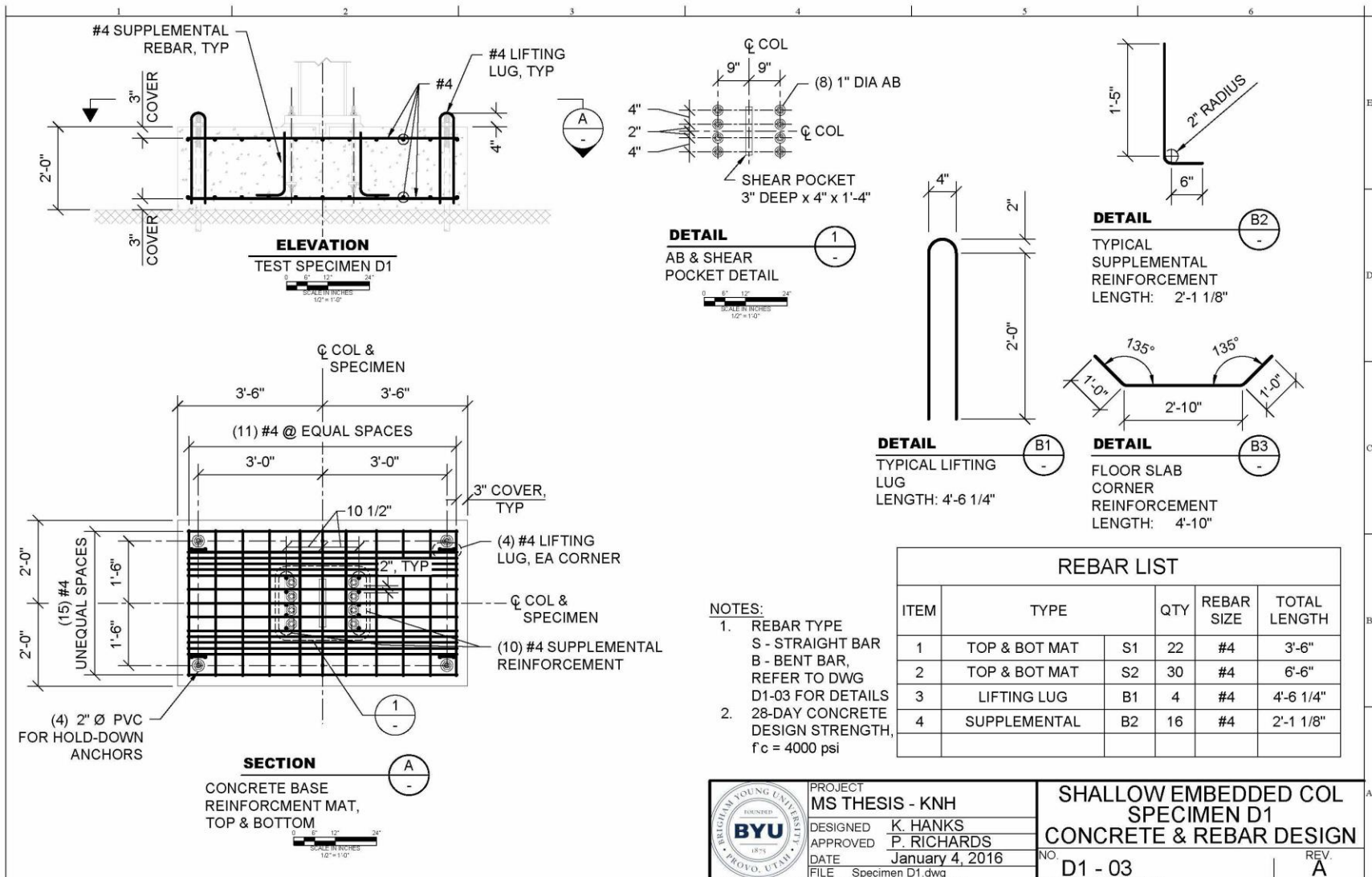
**SHALLOW EMBEDDED COL
SPECIMEN D1
OVERALL SPECIMEN DESIGN**

NO. **D1 - 01**

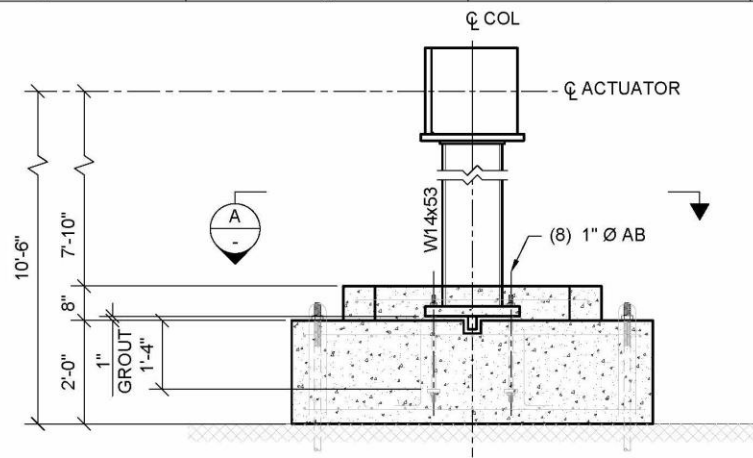
REV. **A**

C:\Users\hank\Documents\Masters Thesis\CAD\DRAWING\Specimen Drawing\Specimen D1.dwg PRINTED: Monday, March 7, 2016 6:42:06 AM

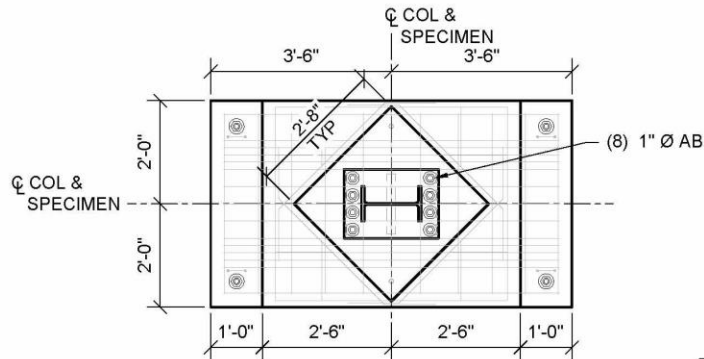
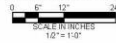




A.2 Design Drawings for Specimen D2



ELEVATION
TEST SPECIMENS D2



SECTION



STEEL		
WEIGHT	641	lbs
CONCRETE		
VOLUME	69	ft³
WEIGHT	10400	lbs
ASSEMBLY		
TOTAL WEIGHT	11041	lbs



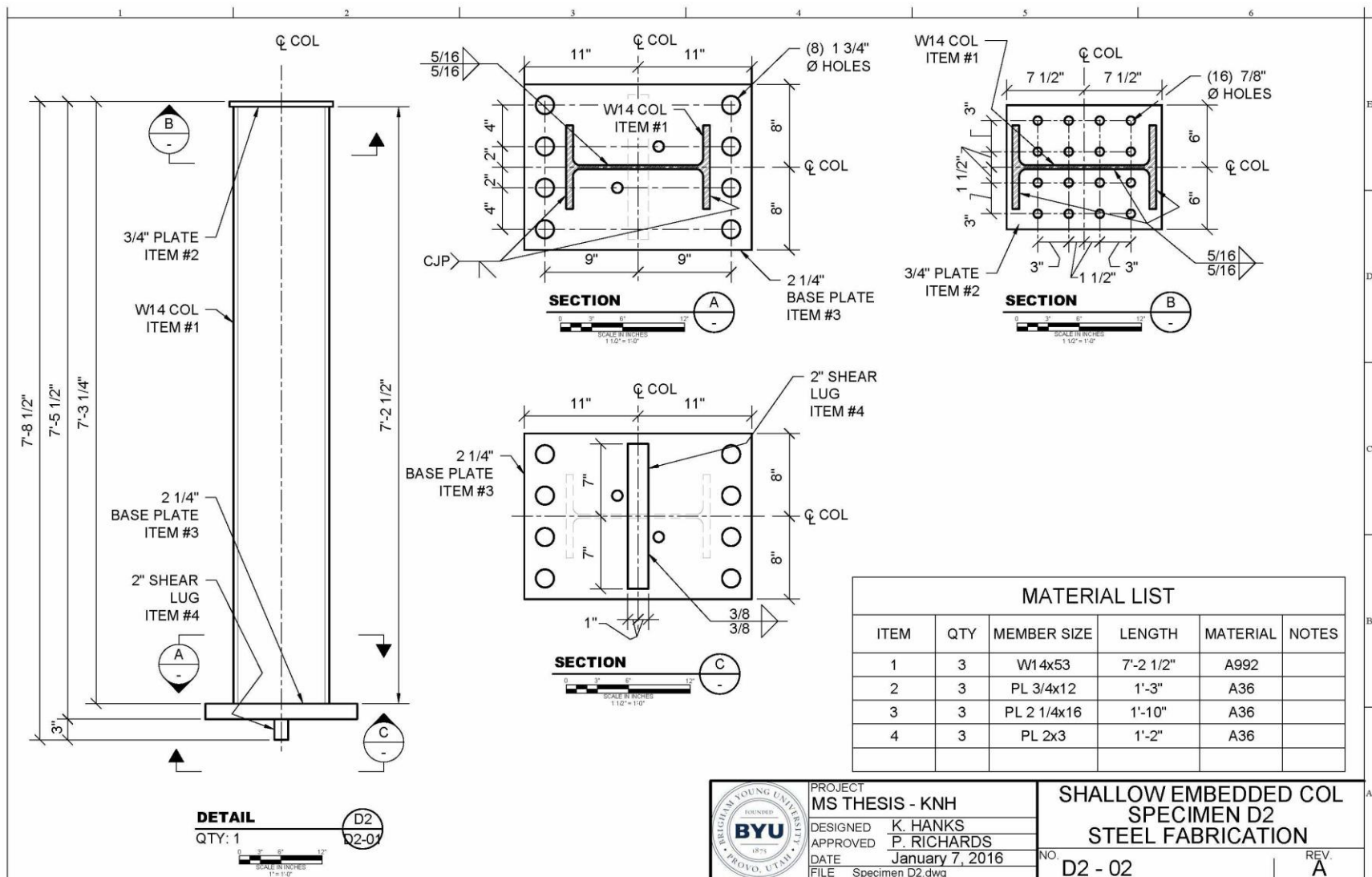
PROJECT
MS THESIS - KNH
DESIGNED K. HANKS
APPROVED P. RICHARDS
DATE January 7, 2016
FILE Specimen D2.dwg

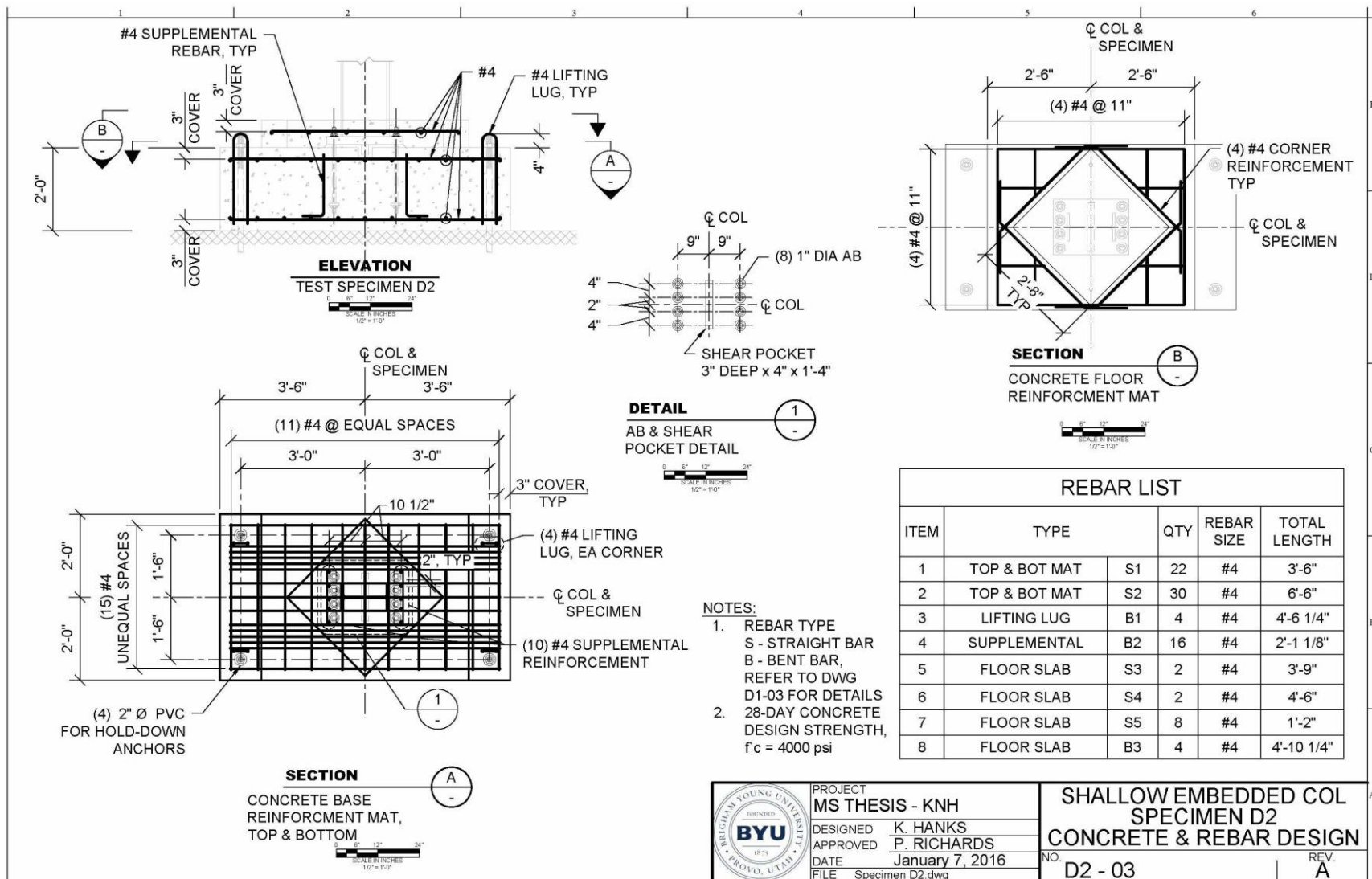
**SHALLOW EMBEDDED COL
SPECIMEN D2
OVERALL SPECIMEN DESIGN**

NO. D2 - 01
REV. A

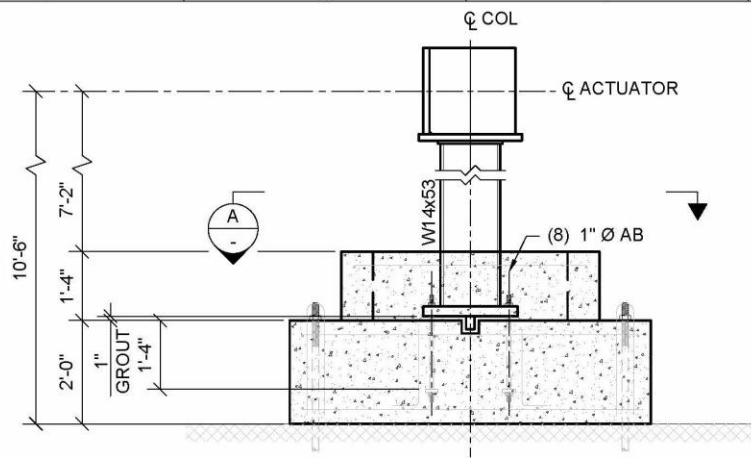
C:\Users\hank\Documents\Master Thesis\AD\DRAWING\Specimen Drawing\Specimen D2.dwg

PRINTED: Monday, March 7, 2016 6:42:40 AM

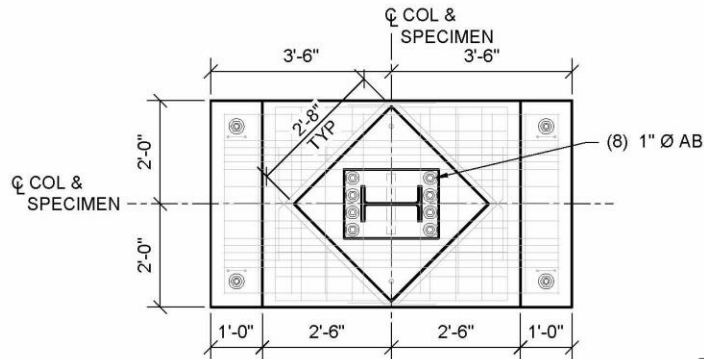
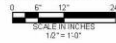




A.3 Design Drawings for Specimen D3



ELEVATION
TEST SPECIMENS D3



SECTION

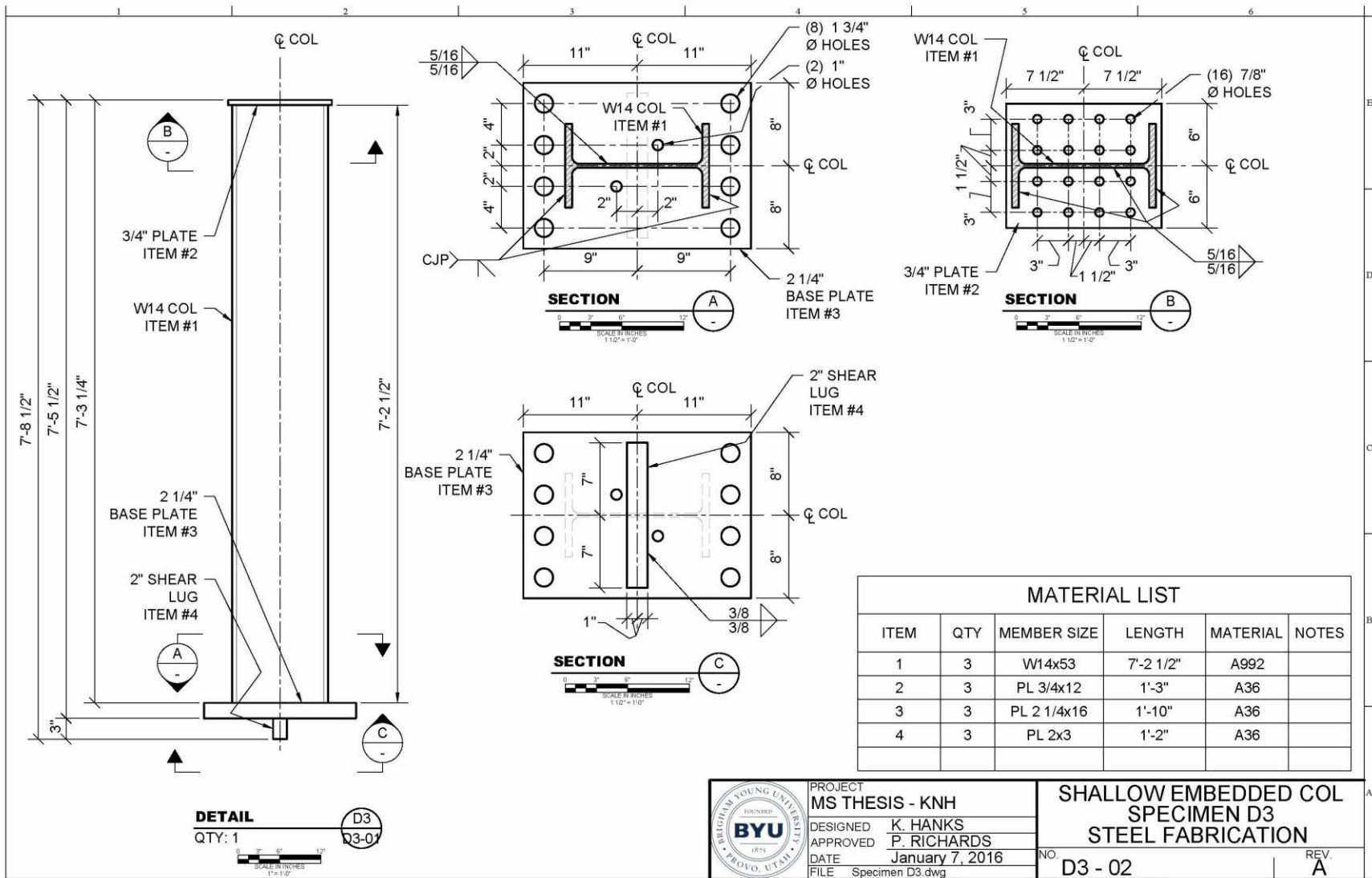


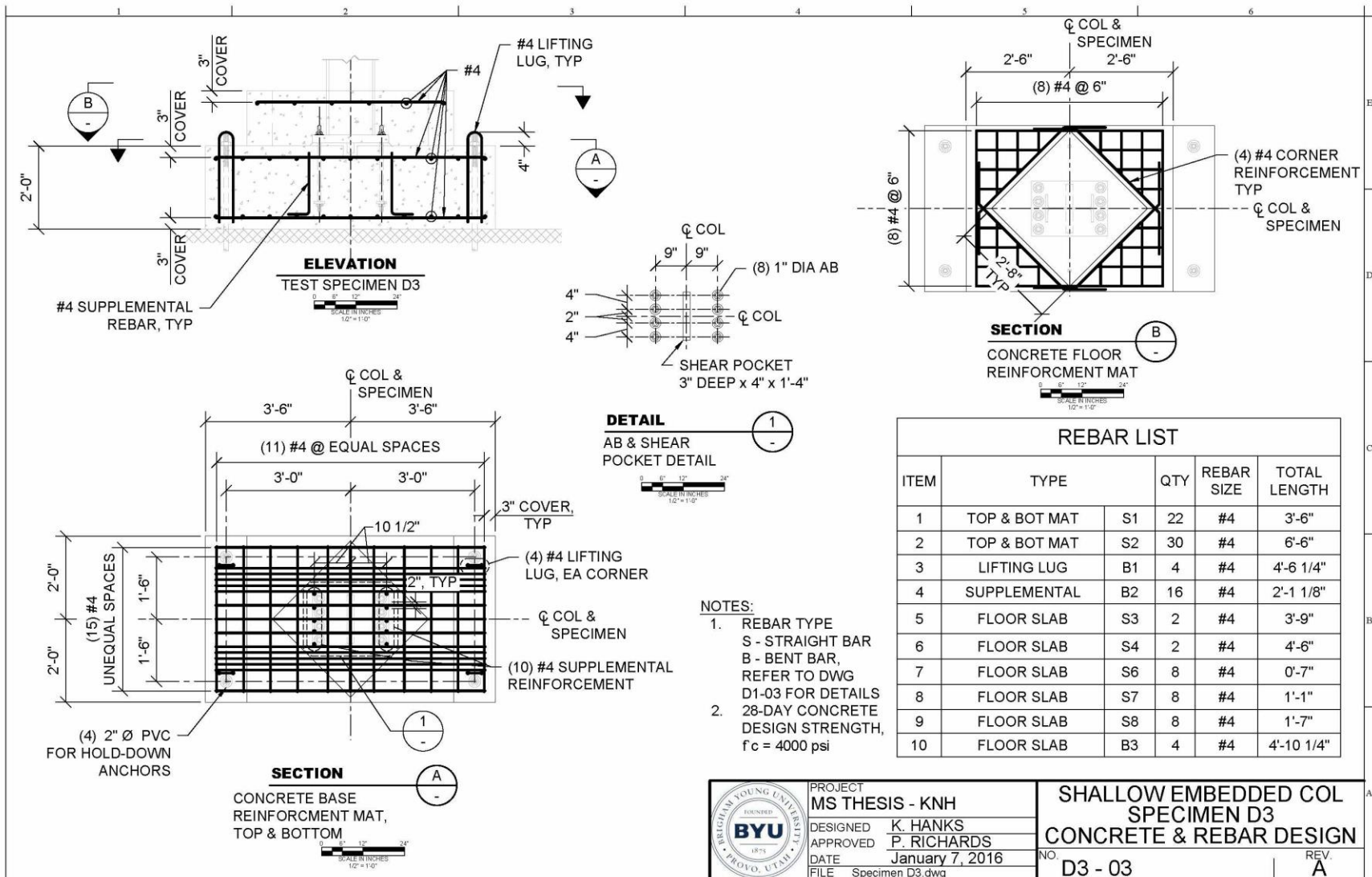
STEEL		
WEIGHT	641	lbs
CONCRETE		
VOLUME	83	ft³
WEIGHT	12400	lbs
ASSEMBLY		
TOTAL WEIGHT	13041	lbs



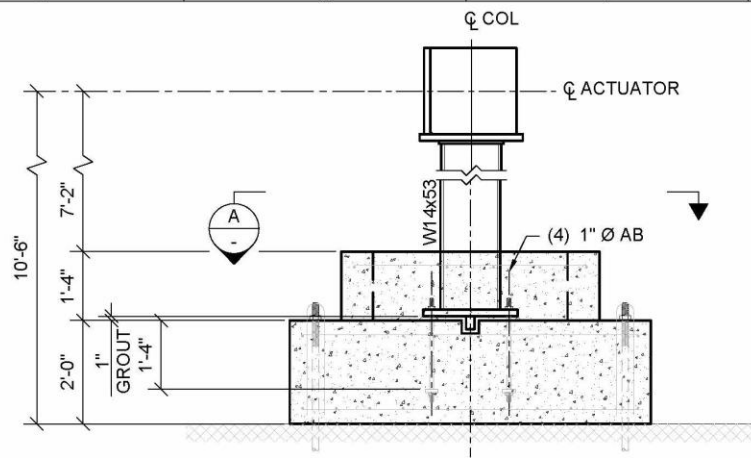
PROJECT
MS THESIS - KNH
DESIGNED
K. HANKS
APPROVED
P. RICHARDS
DATE
January 7, 2016
FILE
Specimen D3.dwg

SHALLOW EMBEDDED COL
SPECIMEN D3
OVERALL SPECIMEN DESIGN
NO.
D3 - 01
REV.
A

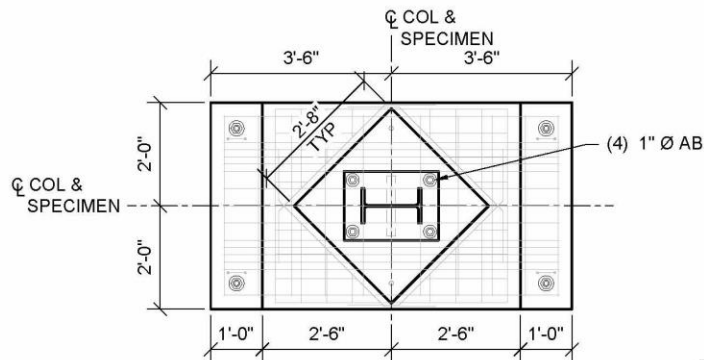
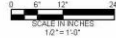




A.4 Design Drawings for Specimen D4



ELEVATION
TEST SPECIMENS D4



SECTION

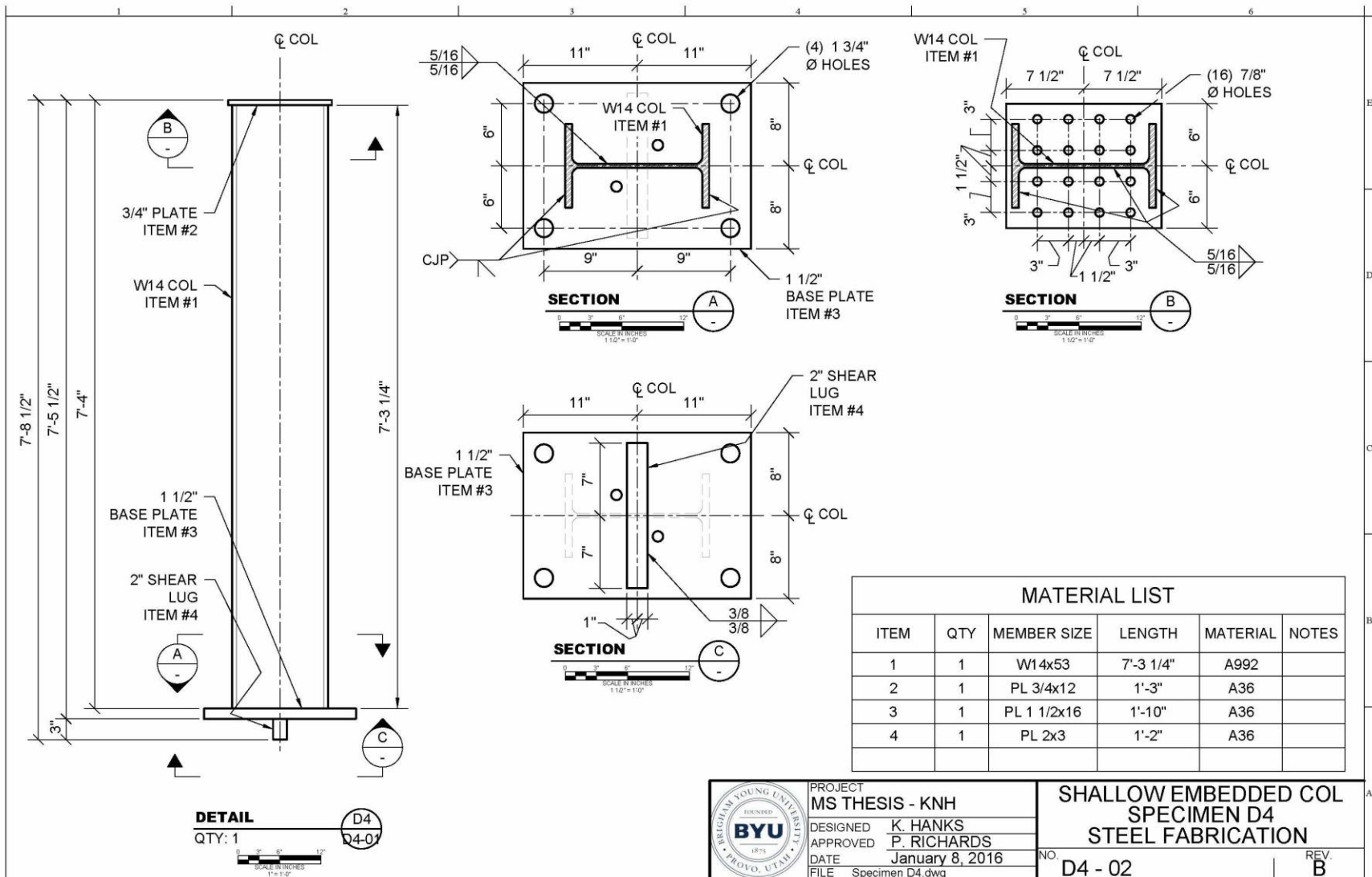


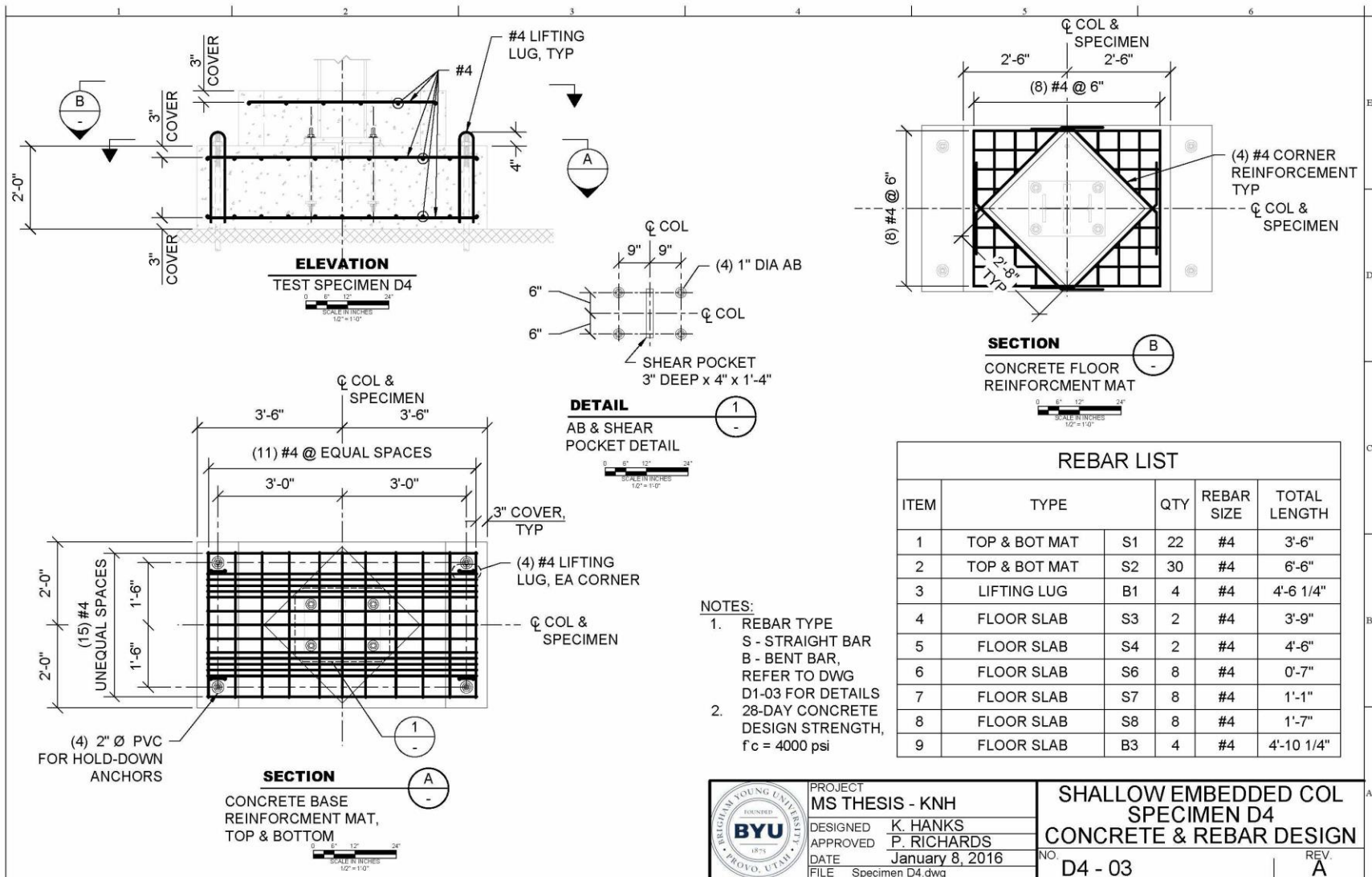
STEEL		
WEIGHT	583	lbs
CONCRETE		
VOLUME	83	ft³
WEIGHT	12400	lbs
ASSEMBLY		
TOTAL WEIGHT	13041	lbs



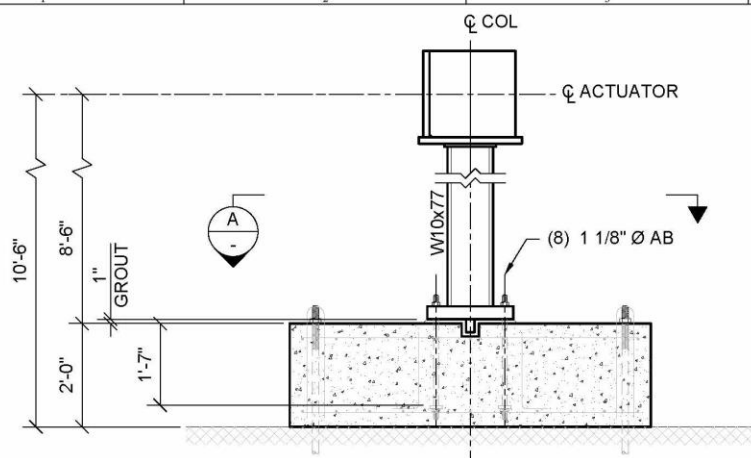
PROJECT
MS THESIS - KNH
DESIGNED
K. HANKS
APPROVED
P. RICHARDS
DATE
January 8, 2016
FILE
Specimen D4.dwg

**SHALLOW EMBEDDED COL
SPECIMEN D4
OVERALL SPECIMEN DESIGN**
NO.
D4 - 01
REV.
A

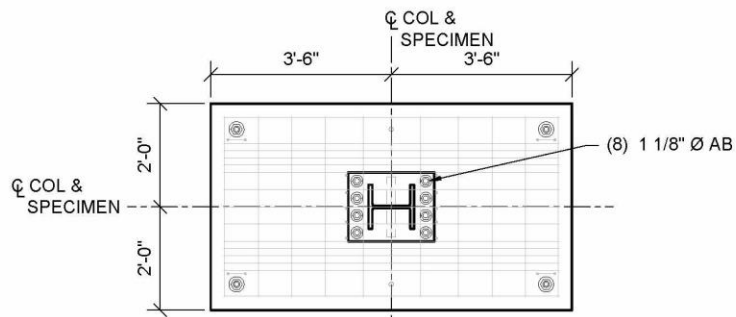
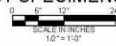




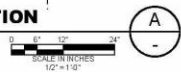
A.5 Design Drawings for Specimen F1



ELEVATION
TEST SPECIMENS F1



SECTION



STEEL		
WEIGHT	908	lbs
CONCRETE		
VOLUME	56	ft³
WEIGHT	8400	lbs
ASSEMBLY		
TOTAL WEIGHT	9308	lbs

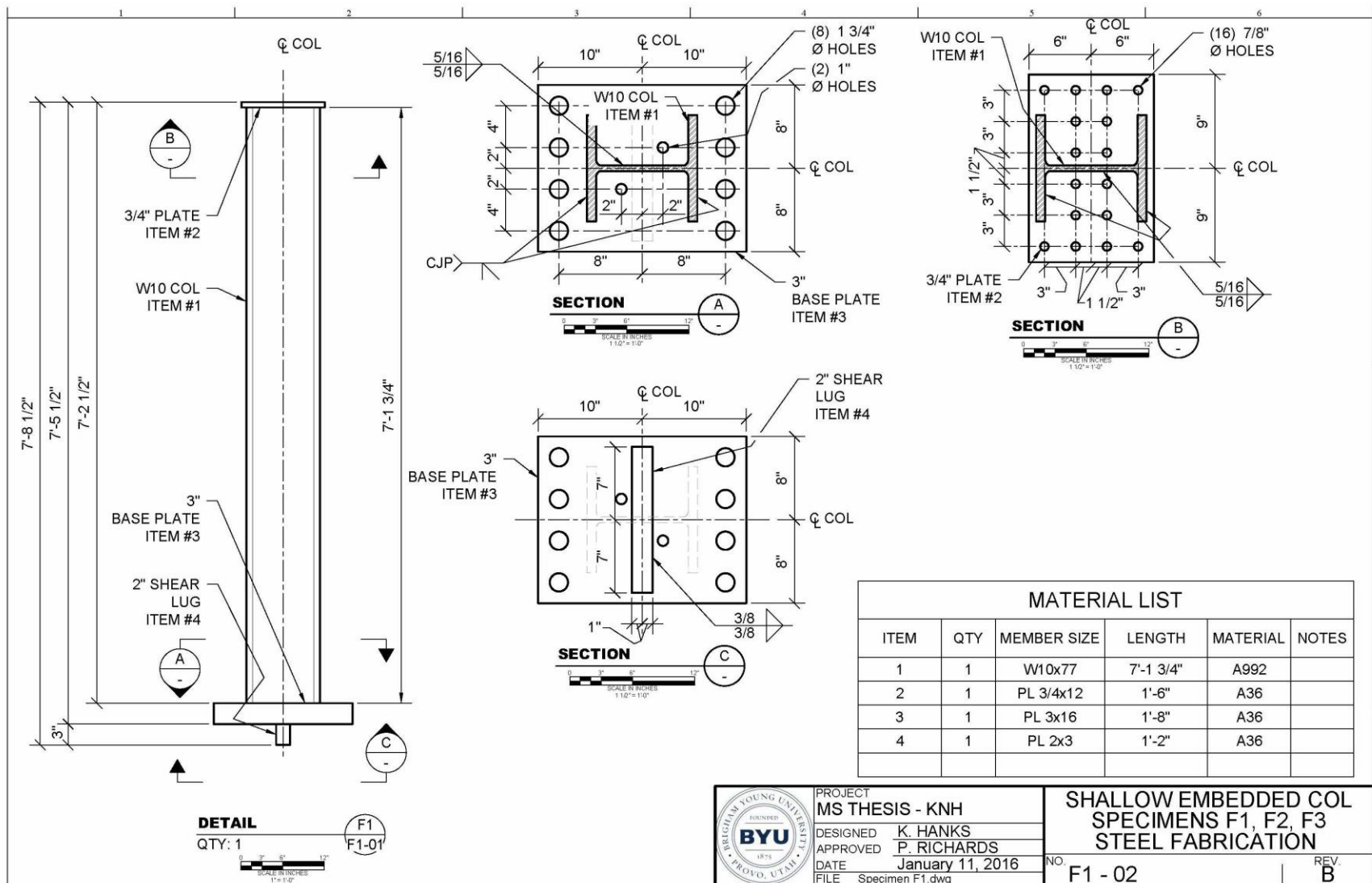


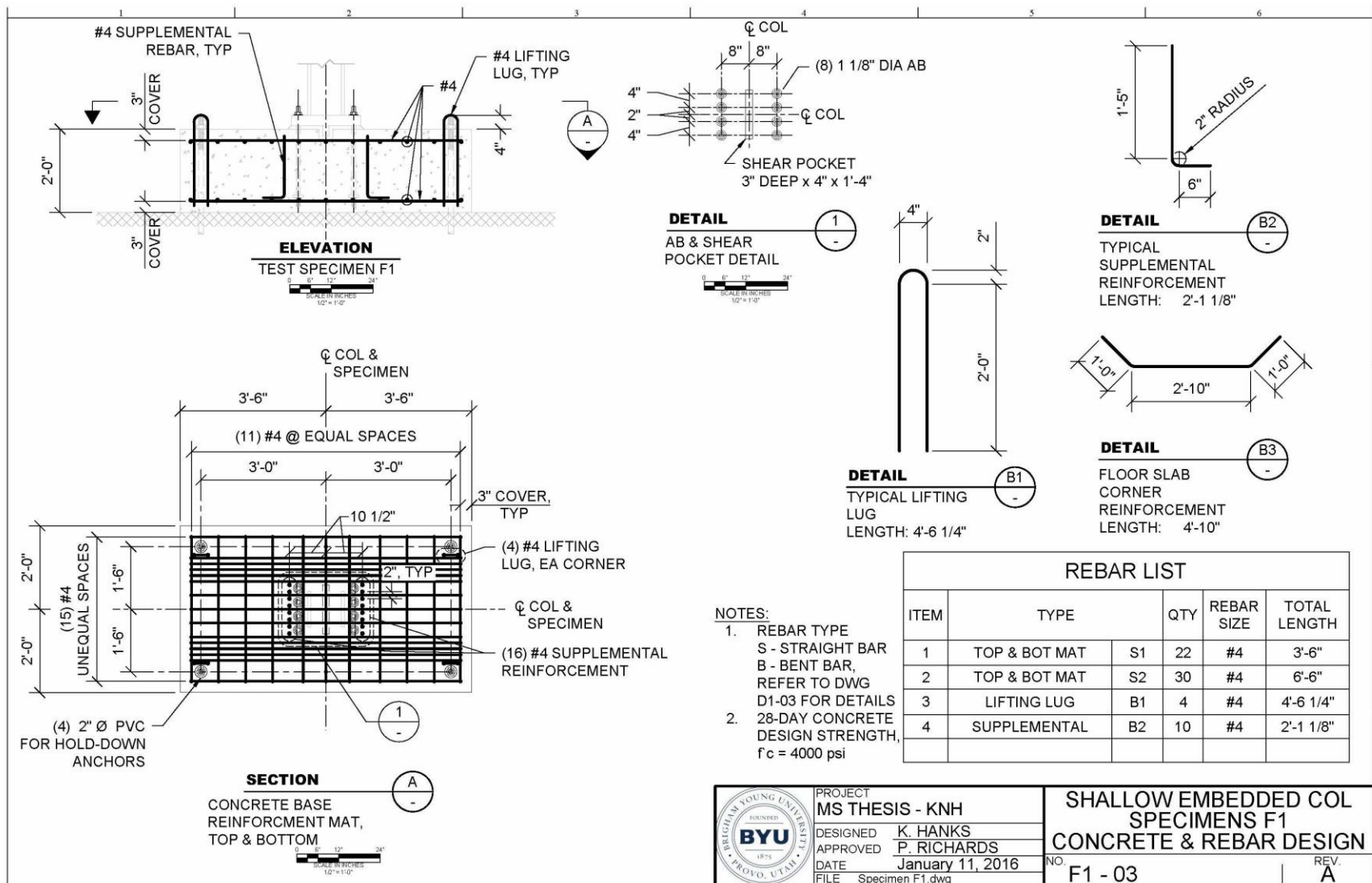
PROJECT	MS THESIS - KNH
DESIGNED	K. HANKS
APPROVED	P. RICHARDS
DATE	January 11, 2016
FILE	Specimen F1.dwg

SHALLOW EMBEDDED COL SPECIMEN F1 OVERALL SPECIMEN DESIGN	
NO.	F1 - 01
REV.	A

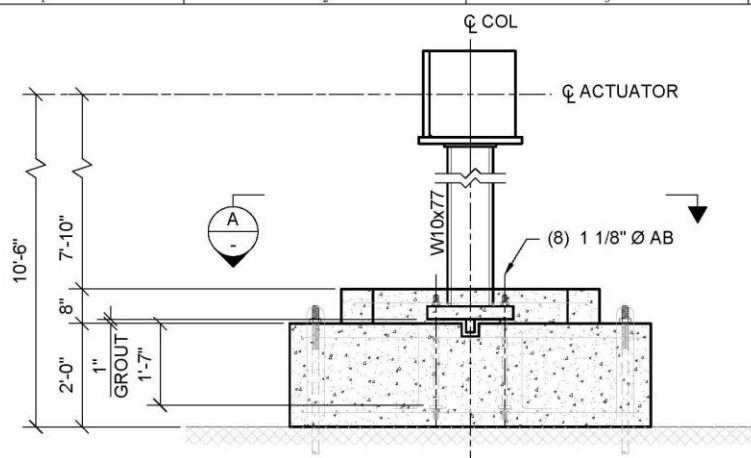
C:\Users\hank\Documents\Master Thesis\AD\DRAWING\Specimen Drawing\Specimen F1.dwg

PRINTED: Monday, March 7, 2016 2:01:30 PM

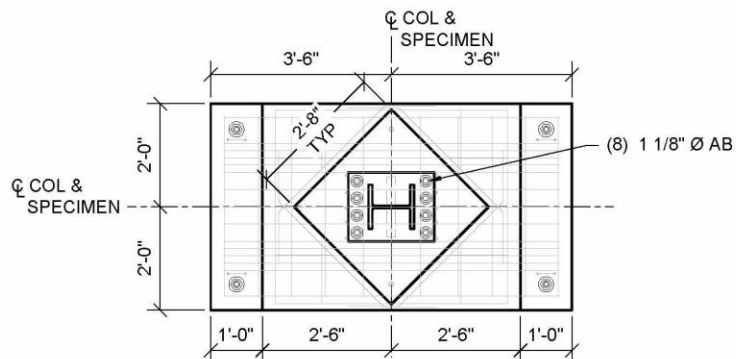
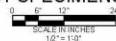




A.6 Design Drawings for Specimen F2



ELEVATION
TEST SPECIMENS F2



SECTION



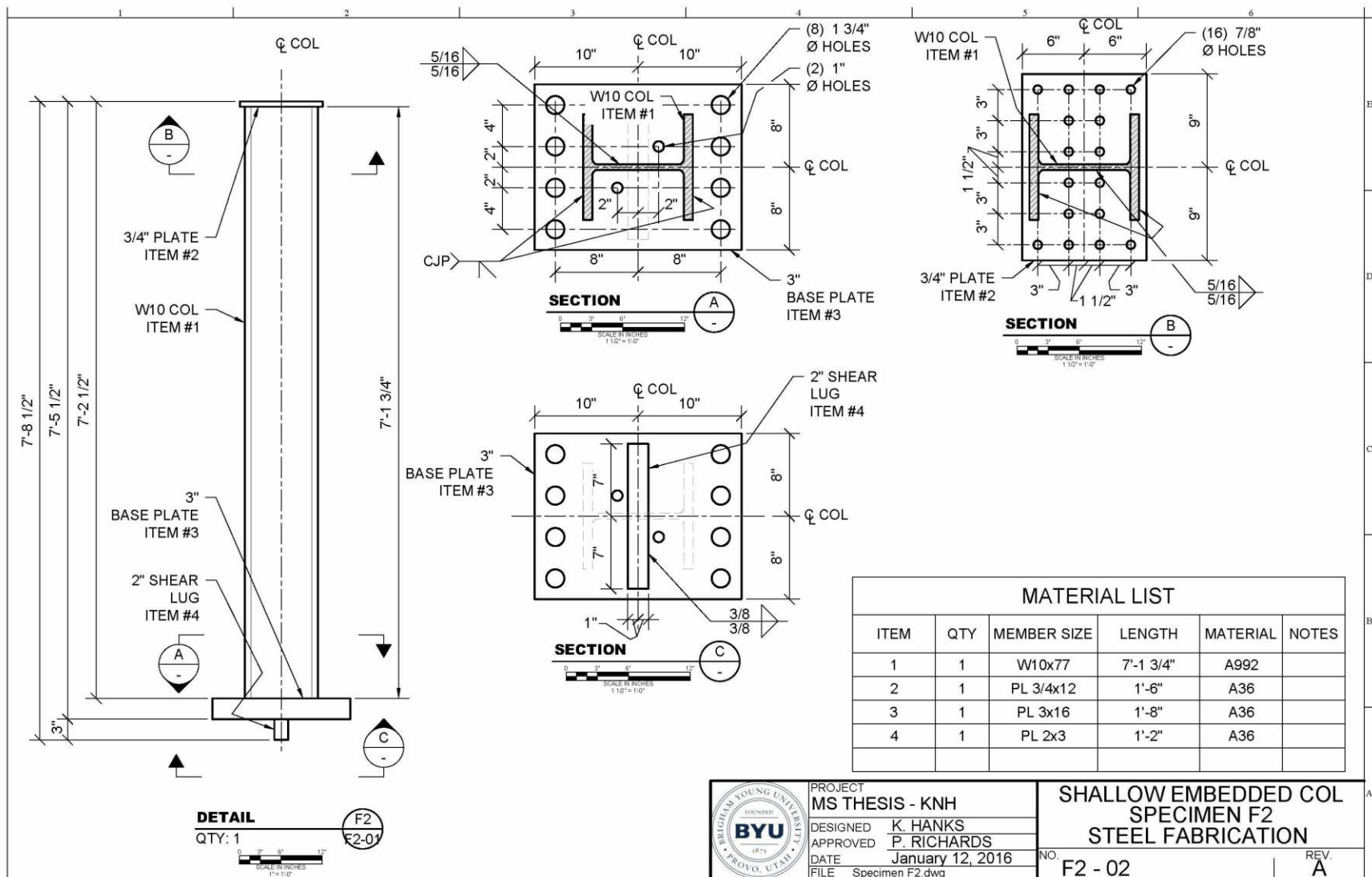
STEEL		
WEIGHT	908	lbs
CONCRETE		
VOLUME	69	ft³
WEIGHT	10400	lbs
ASSEMBLY		
TOTAL WEIGHT	11308	lbs

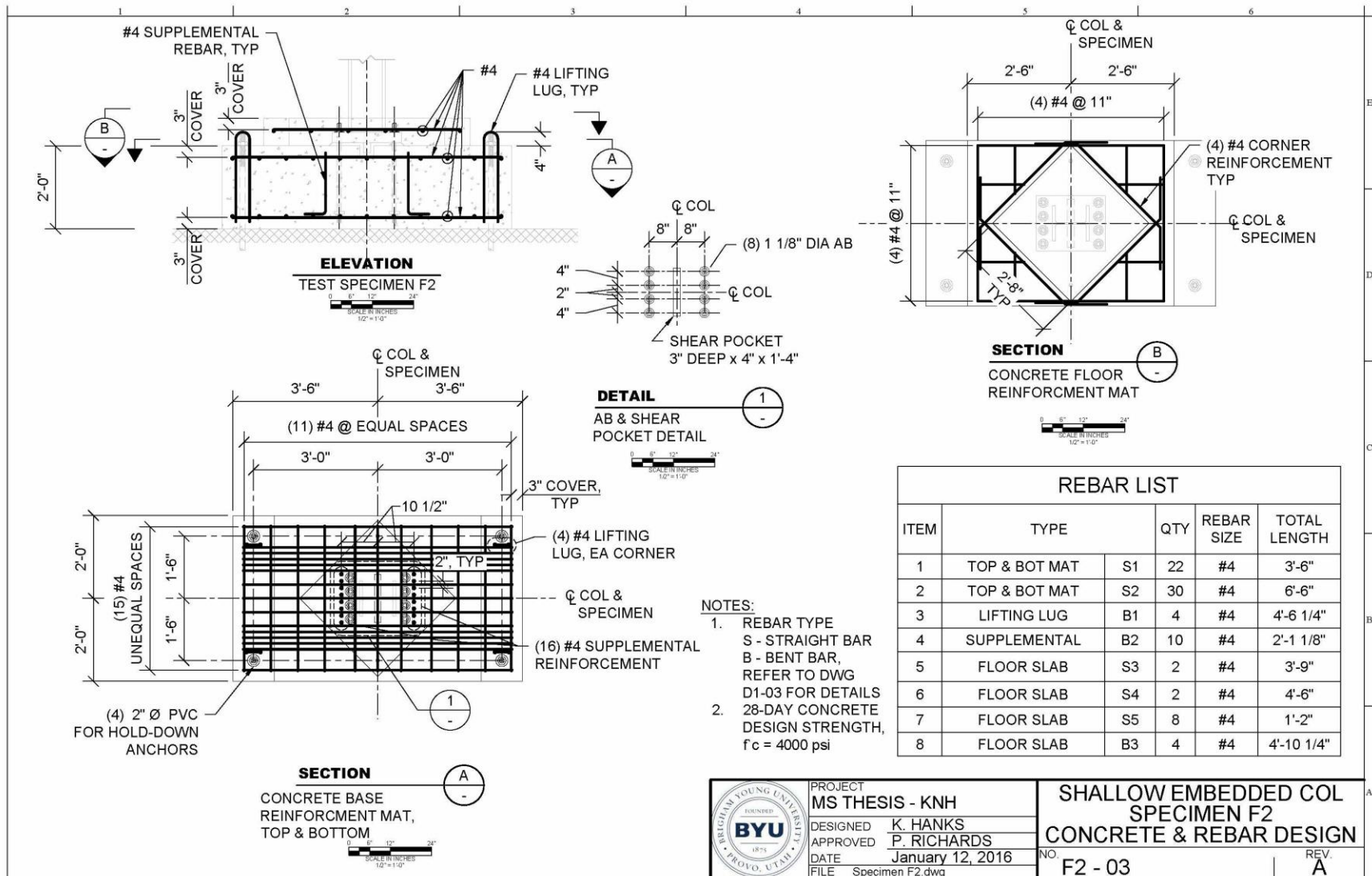


PROJECT	MS THESIS - KNH
DESIGNED	K. HANKS
APPROVED	P. RICHARDS
DATE	January 12, 2016
FILE	Specimen F2.dwg

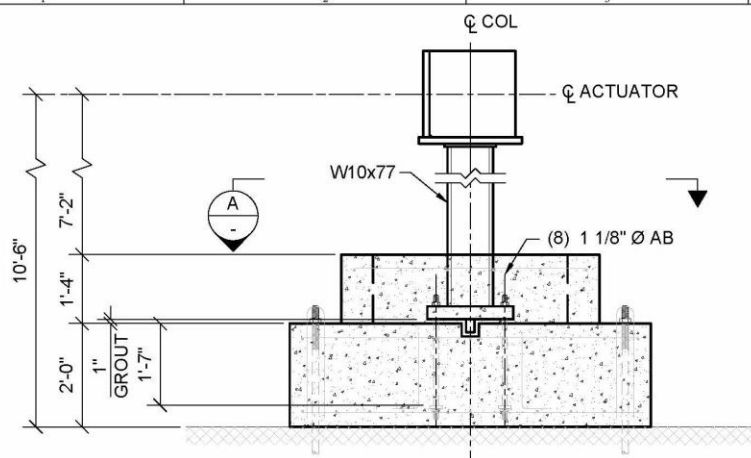
SHALLOW EMBEDDED COL SPECIMEN F2 OVERALL SPECIMEN DESIGN	
NO. F2 - 01	REV. A

PRINTED: Monday, March 7, 2016 2:13:10 PM

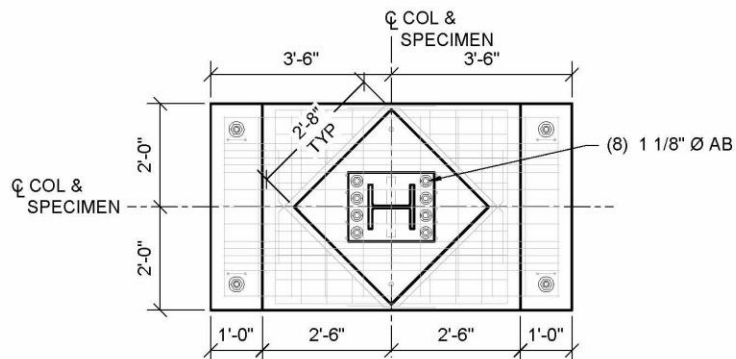
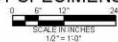




A.7 Design Drawings for Specimen F3



ELEVATION
TEST SPECIMENS F3



SECTION

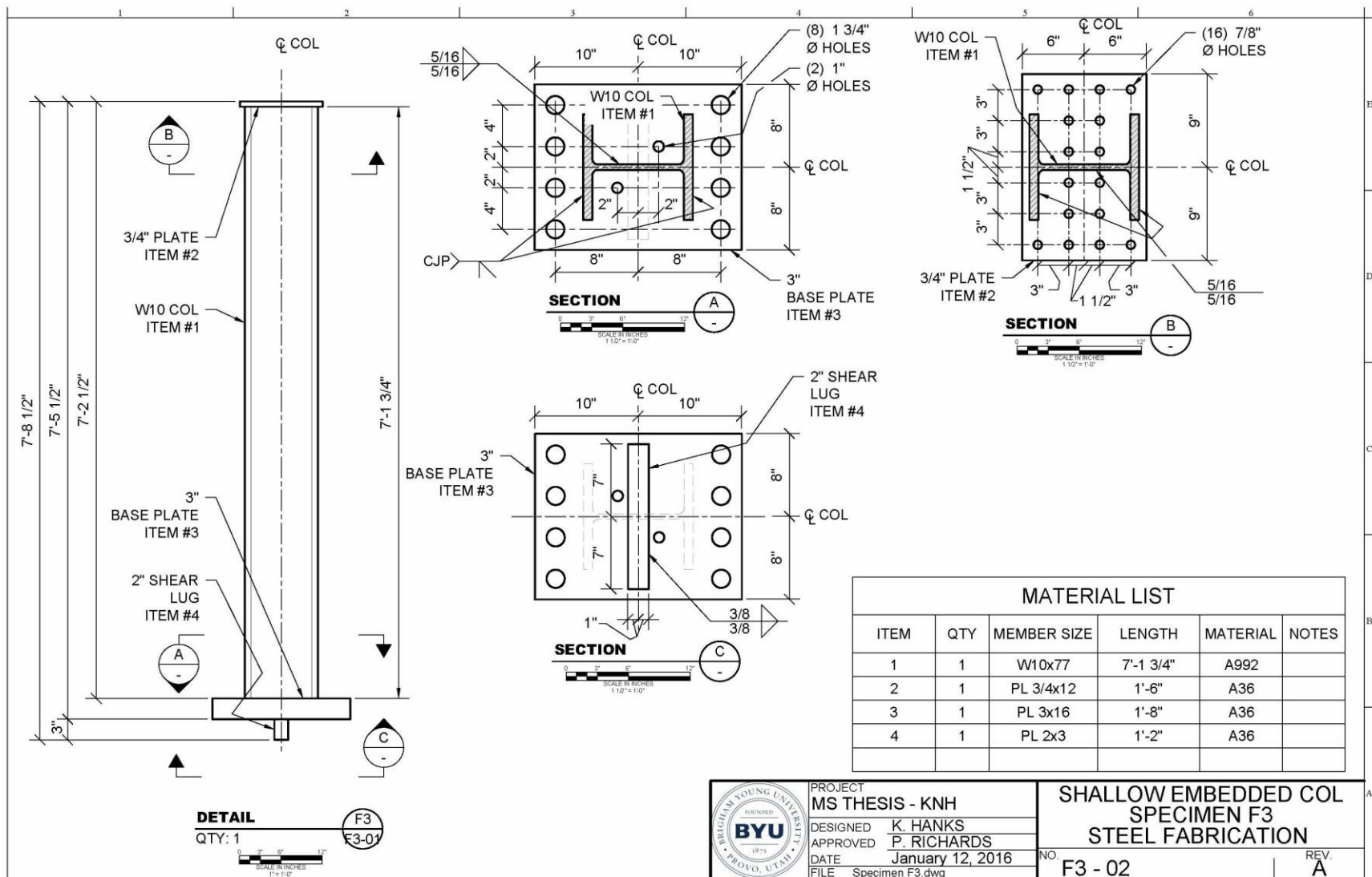


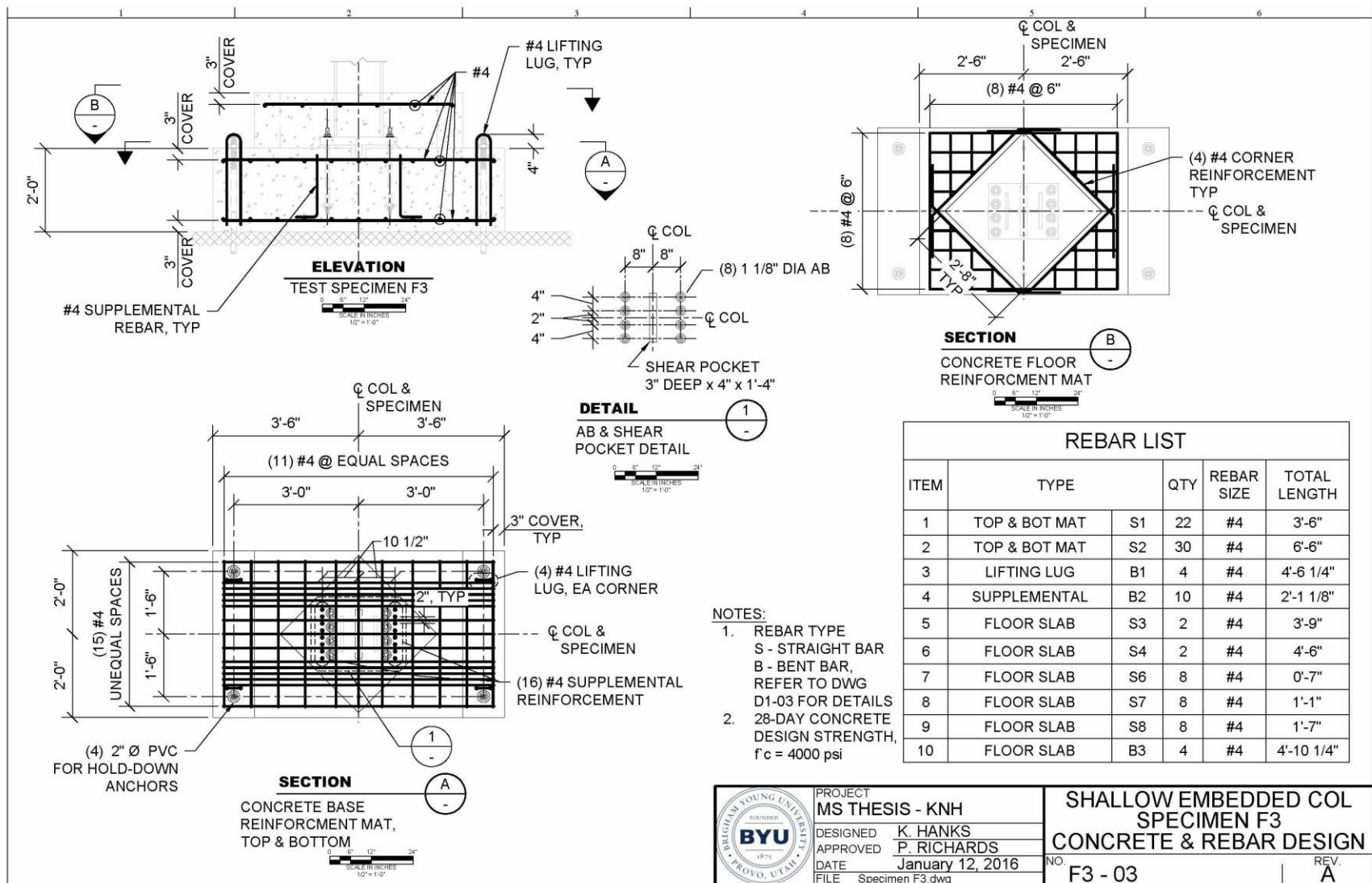
STEEL		
WEIGHT	908	lbs
CONCRETE		
VOLUME	83	ft³
WEIGHT	12400	lbs
ASSEMBLY		
TOTAL WEIGHT	13308	lbs



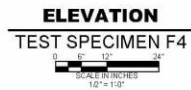
PROJECT
MS THESIS - KNH
DESIGNED K. HANKS
APPROVED P. RICHARDS
DATE January 12, 2016
FILE Specimen F3.dwg

SHALLOW EMBEDDED COL
SPECIMEN F3
OVERALL SPECIMEN DESIGN
NO. F3 - 01
REV. A

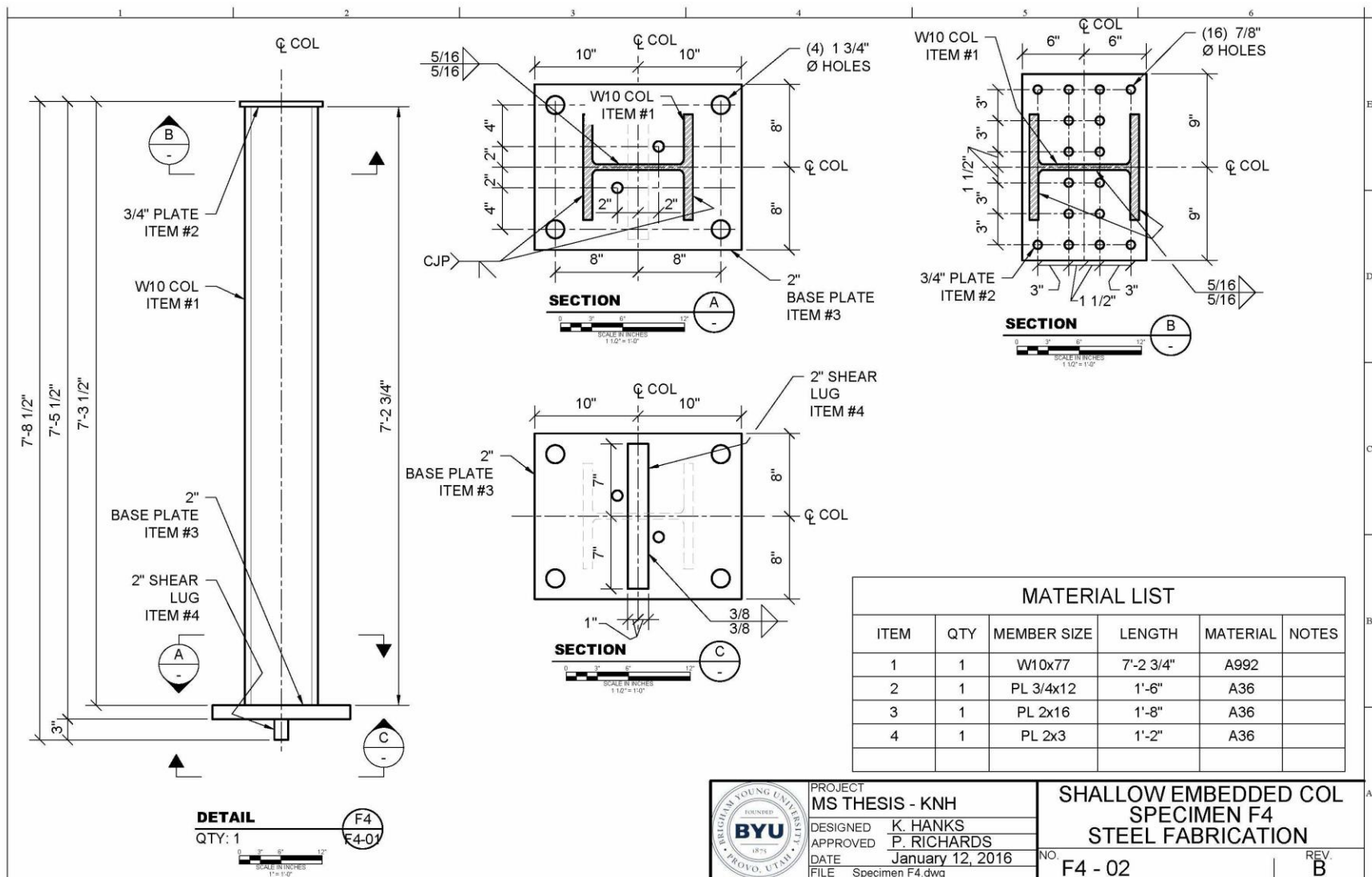




A.8 Design Drawings for Specimen F4



SHALLOW EMBEDDED COL SPECIMEN F4 OVERALL SPECIMEN DESIGN	
NO. F4 - 01	REV. A



APPENDIX B: DESIGN CALCULATIONS

B.1 Base Plate Design for Specimens D1, D2, D3, & D4

Given

Column

Column Size $Col := "W14 \times 53"$
 Column Height $h_{col} := 10 \text{ ft}$
 Steel Strength $f_{y,col} := 50 \text{ ksi}$ ASTM A992 Steel

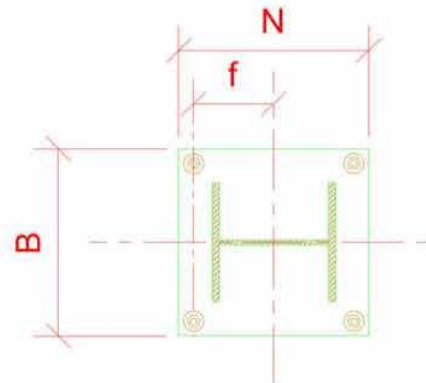
$M_p = 362.9 \text{ kip} \cdot \text{ft}$
 $R_y := 1.1$ [expected strength factor]

Base Plate

Width $N := 1 \text{ ft} + 10 \text{ in}$
 Length $B := 1 \text{ ft} + 4 \text{ in}$
 AB Locations $f := 9 \text{ in}$
 Yield Strength $f_{y,bspl} := 36 \text{ ksi}$

$$n := \frac{B - 0.8 \cdot b_f}{2} = 4.776 \text{ in}$$

$$m := \frac{N - 0.95 \cdot d}{2} = 4.398 \text{ in}$$



Concrete

Strength $f'_c := 4000 \text{ psi}$

Anchor Bolts

Material type: ASTM F1554 Gr 36

Yield Strength $f_{y,bolt} := 36 \text{ ksi}$

Ultimate Strength $f_{u,bolt} := 58 \text{ ksi}$

AB Quantity $num_b := 8$



Step 1: Determine the Axial and Moment Load on Column Base

$$P_r := h_{col} \cdot W_{col} = 530 \text{ lbf}$$

$$M_r := R_y \cdot M_p = 399.208 \text{ kip} \cdot \text{ft}$$

Step 2: Pick a trial base plate size ($N \times B$)

(defined previously)

$$N = 22 \text{ in}$$

$$B = 16 \text{ in}$$

Step 3: Determine the equivalent eccentricity (e), and the critical eccentricity (e_{crit})

$$e := \frac{M_r}{P_r} = 753.2 \text{ ft}$$

$$e_{crit} := \frac{N}{2} - \frac{P_r}{2 \cdot q_{max}} = 10.996 \text{ in}$$

$$\begin{array}{l|l} \text{if } e \geq e_{crit} & = \text{"GOOD!"} \\ \parallel & \\ \text{"GOOD!"} & \\ \text{else} & \\ \parallel & \\ \text{"NO GOOD!"} & \end{array}$$

Step 4: Determine the equivalent bearing length (Y) and the tensile force in the anchor rods (T).

$$Y := \left(f + \frac{N}{2} \right) + \left[\frac{1}{-1} \right] \cdot \sqrt{\left(f + \frac{N}{2} \right)^2 - \frac{2 \cdot P_r \cdot (e + f)}{q_{max}}} = \left[\begin{array}{c} 36.26 \\ 3.74 \end{array} \right] \text{ in}$$

$$Y := \text{if } 0 < Y_0 < N = 3.74 \text{ in}$$

$$\begin{array}{l|l} \parallel & \\ Y_0 & \\ \text{else} & \\ \parallel & \\ Y_1 & \end{array}$$

$$T := q_{max} \cdot Y - P_r = 263.964 \text{ kip}$$

Step 5: Determine the required minimum base plate thickness at the bearing and the tension interfaces.

Bearing Interface:

$$t_{p_req_b} := \begin{cases} \text{if } Y \geq \max(m, n) \\ 1.5 \cdot m \cdot \sqrt{\frac{f_{p_max}}{f_{y_bspl}}} \\ \text{else} \\ 2.11 \cdot \sqrt{\frac{f_{p_max} \cdot Y \cdot \left(m - \frac{Y}{2}\right)}{f_{y_bspl}}} \end{cases} = 2.273 \text{ in}$$

Tension Interface

$$t_{p_req_t} := 2.11 \cdot \sqrt{\frac{T \cdot \left(f - \frac{d}{2} + \frac{t_f}{2}\right)}{B \cdot f_{y_bspl}}} = 2.204 \text{ in}$$

Take maximum of the two:

$$t_{p_req} := \max(t_{p_req_b}, t_{p_req_t}) = 2.273 \text{ in}$$

Step 6: Determine the anchor rod size appropriate for the tensile loading
(assuming that the embedment is such that tensile fracture of the anchor bolt governs, and that shear load in the bolts is negligible)

Number of bolts in tension

$$N_{b_t} := \frac{num_b}{2} = 4$$

Tensile Force in each bolt (with factor - we want anchor bolt fracture to govern the strength of the connection)

$$T_u := 0.5 \cdot \frac{T}{N_{b_t}} = 32.995 \text{ kip}$$

required diameter $\phi := 0.75$

$$D_{req} := \sqrt{\frac{4 \cdot T_u}{\pi \cdot \phi \cdot f_{u_bolt}}} = 0.983 \text{ in}$$

B.2 Anchor Bolt Design for Specimens D1, D2, & D3

Calculations
Shear Lug
Per ACI 318 Appendix D

For Test Specimens:
D1, D2, & D3

Anchor Bolt Information

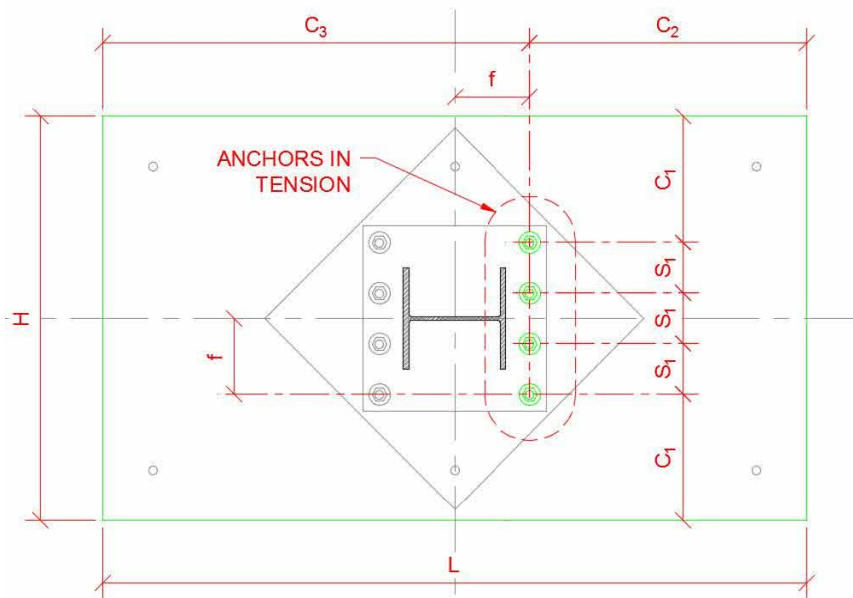
Anchor Bolt Diameter

$$D_b := 1.0 \text{ in}$$

Anchor Bolt Strength

$$f_{y_bolt} := 36 \text{ ksi}$$

$$f_{u_bolt} := 58 \text{ ksi}$$



IMPORTED

$$f := 9 \text{ in}$$

$$f'_c := 4 \text{ ksi}$$

INPUT

$$H := 4 \text{ ft}$$

$$L := 7 \text{ ft}$$

$$h_{ef} := 16 \text{ in}$$

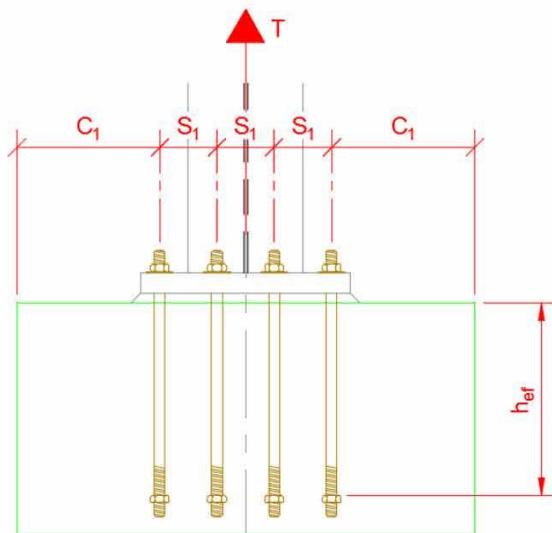
CALCULATED

$$s_1 := 4 \text{ in}$$

$$c_1 := \frac{H - 3 \cdot s_1}{2} = 18 \text{ in}$$

$$c_2 := \frac{L}{2} - f = 33 \text{ in}$$

$$c_3 := L - c_2 = 51 \text{ in}$$



Strength in Tension

D.5.1.2 - Nominal strength of a group of anchors in tension

$$N_{sa}$$

number of anchors in the group

$$n := 4$$

effective cross-sectional area
of a single anchor

$$A_{se.N} := 0.9 \cdot \pi \cdot \frac{D_b^2}{4} = 0.707 \text{ in}^2$$

strength of AB steel

$$f_{uta} := \min(1.9 \cdot f_{y_bolt}, f_{u_bolt})$$

$$f_{uta} = 58 \text{ ksi}$$

$$N_{sa} := n \cdot A_{se.N} \cdot f_{uta} = 164 \text{ kip}$$

D.5.2.1 - Nominal concrete breakout strength of a group of anchors in tension

$$N_{cbg}$$

projected concrete failure
area of a group of anchors

$$A_{Nc} := (3 \cdot s_1 + 2 \cdot \min(c_1, 1.5 \cdot h_{ef})) \cdot (\min(c_2, 1.5 \cdot h_{ef}) + \min(c_3, 1.5 \cdot h_{ef}))$$

$$A_{Nc} = 2304 \text{ in}^2$$

projected concrete failure
area of a single anchor

$$A_{Nco} := 9 \cdot h_{ef}^2 = 2304 \text{ in}^2$$

Eccentricity Factor

$$\psi_{ed.N} := 1$$

Modification factor for edge
effects

$$\psi_{ec.N} := \begin{cases} 1.0 & \text{if } \min(c_1, c_2, c_3) \geq 1.5 \cdot h_{ef} \\ 0.7 + 0.3 \cdot \frac{\min(c_1, c_2, c_3)}{1.5 \cdot h_{ef}} & \text{else} \end{cases}$$

$$\psi_{ec.N} = 0.925$$

Modification factor for
cracked/uncracked concrete

$$\psi_{c.N} := 1.25$$



Modification for post-installed anchors

$$\psi_{cp,N} := 1.0$$

Factor for post-installed/
cast-in-place anchor

$$k_c := 24$$

Modification factor for
lightweight concrete

$$\lambda := 1.0$$

Basic concrete breakout
strength of a single anchor in
tension in cracked concrete

$$N_b := k_c \cdot \lambda \cdot \sqrt{\frac{f'_c}{\text{psi}}} \cdot \left(\frac{h_{ef}}{\text{in}} \right)^{1.5} \cdot \text{lb}$$

$$N_b = 97.1 \text{ kip}$$

$$N_{cbg} := \frac{A_{Nc}}{A_{Nco}} \cdot \psi_{ec,N} \cdot \psi_{ed,N} \cdot \psi_{c,N} \cdot \psi_{cp,N} \cdot N_b$$

$$N_{cbg} = 112.3 \text{ kip}$$

Supplemental Reinforcement

steel strength of rebar

$$f_{y_rebar} := 60 \text{ ksi}$$

area of supplemental reinforcing steel
required to make up the difference
between the demand and the
capacity of the concrete

$$A_{s_req} := \frac{N_{sa} - N_{cbg}}{f_{y_rebar}} = 0.861 \text{ in}^2$$

Use #4 bars

$$A_{bar} := \pi \cdot \left(\frac{4 \text{ in}}{8} \right)^2 = 0.196 \text{ in}^2$$

Number of bars required

$$n_{bars} := \text{ceil} \left(\frac{A_{s_req}}{A_{bar}} \right) = 5$$



D.5.3.1 - Nominal pullout strength of a single anchor in tension

Bearing Area of the anchor
bolt head w/ 2"x2" plate
washer

$$A_{brg} := (2 \text{ in})^2 - \pi \cdot \frac{D_b^2}{4}$$
$$A_{brg} = 3.2 \text{ in}^2$$

Pullout strength of a single
headed bolt

$$N_p := 8 \cdot A_{brg} \cdot f'_c = 102.9 \text{ kip}$$

Factor to account for
cracked/uncracked concrete

$$\psi_{c,p} := 1.4$$

Nominal pullout strength of a
group of anchors in tension

$$N_{pn} := n \cdot \psi_{c,p} \cdot N_p = 576.1 \text{ kip}$$



B.3 Anchor Bolt Design for Specimen D4

Anchor Bolt Information

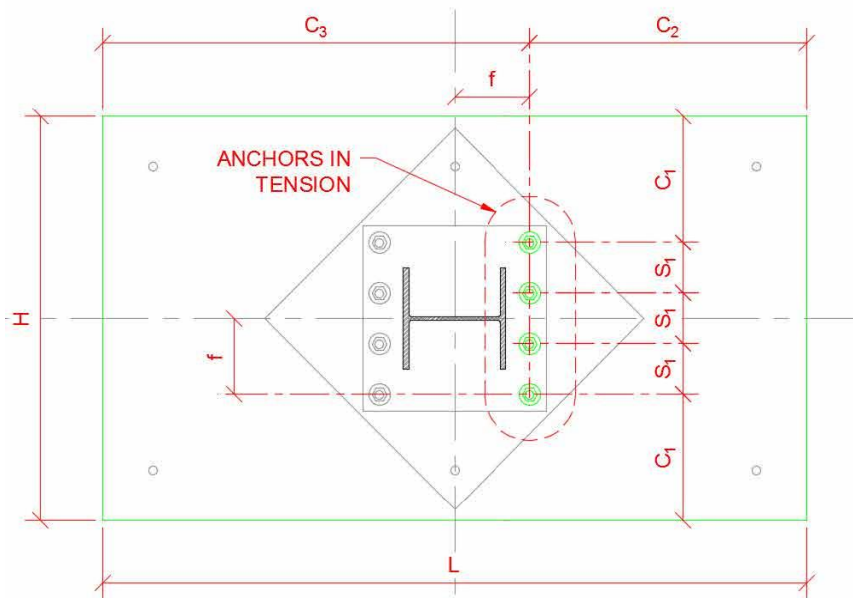
Anchor Bolt Diameter

$$D_b := 1.0 \text{ in}$$

Anchor Bolt Strength

$$f_{y_bolt} := 36 \text{ ksi}$$

$$f_{u_bolt} := 58 \text{ ksi}$$



IMPORTED

$$f := 9 \text{ in}$$

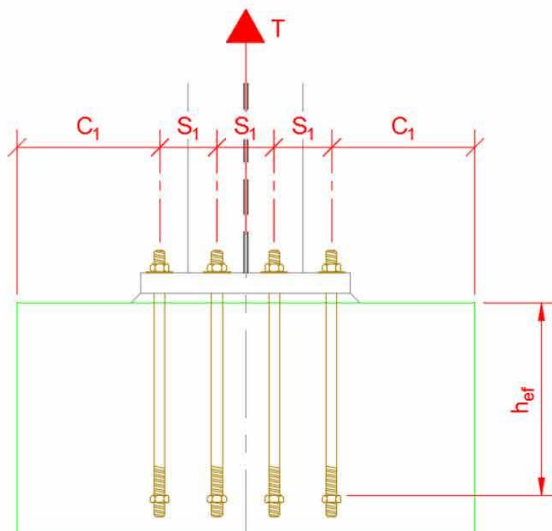
$$f'_c := 4 \text{ ksi}$$

INPUT

$$H := 4 \text{ ft}$$

$$L := 7 \text{ ft}$$

$$h_{ef} := 16 \text{ in}$$



CALCULATED

$$s_1 := 12 \text{ in}$$

$$c_1 := \frac{H - 1 \cdot s_1}{2} = 18 \text{ in}$$

$$c_2 := \frac{L}{2} - f = 33 \text{ in}$$

$$c_3 := L - c_2 = 51 \text{ in}$$

Strength in Tension

D.5.1.2 - Nominal strength of a group of anchors in tension

$$N_{sa}$$

number of anchors in the group

$$n := 2$$

effective cross-sectional area
of a single anchor

$$A_{se,N} := 0.9 \cdot \pi \cdot \frac{D_b^2}{4} = 0.707 \text{ in}^2$$

strength of AB steel

$$f_{uta} := \min(1.9 \cdot f_{y_bolt}, f_{u_bolt})$$

$$f_{uta} = 58 \text{ ksi}$$

$$N_{sa} := n \cdot A_{se,N} \cdot f_{uta} = 82 \text{ kip}$$

D.5.2.1 - Nominal concrete breakout strength of a group of anchors in tension

$$N_{cbg}$$

projected concrete failure
area of a group of anchors

$$A_{Nc} := (3 \cdot s_1 + 2 \cdot \min(c_1, 1.5 \cdot h_{ef})) \cdot (\min(c_2, 1.5 \cdot h_{ef}) + \min(c_3, 1.5 \cdot h_{ef}))$$

$$A_{Nc} = 3456 \text{ in}^2$$

projected concrete failure
area of a single anchor

$$A_{Nco} := 9 \cdot h_{ef}^2 = 2304 \text{ in}^2$$

Eccentricity Factor

$$\psi_{ed,N} := 1$$

Modification factor for edge
effects

$$\psi_{ec,N} := \begin{cases} 1.0 & \text{if } \min(c_1, c_2, c_3) \geq 1.5 \cdot h_{ef} \\ 0.7 + 0.3 \cdot \frac{\min(c_1, c_2, c_3)}{1.5 \cdot h_{ef}} & \text{else} \end{cases}$$

$$\psi_{ec,N} = 0.925$$

Modification factor for
cracked/uncracked concrete

$$\psi_{c,N} := 1.25$$



D.5.3.1 - Nominal pullout strength of a single anchor in tension

Bearing Area of the anchor
bolt head w/ 2"x2" plate
washer

$$A_{brg} := (2 \text{ in})^2 - \pi \cdot \frac{D_b^2}{4}$$

$$A_{brg} = 3.2 \text{ in}^2$$

Pullout strength of a single
headed bolt

$$N_p := 8 \cdot A_{brg} \cdot f'_c = 102.9 \text{ kip}$$

Factor to account for
cracked/uncracked concrete

$$\psi_{c,p} := 1.4$$

Nominal pullout strength of a
group of anchors in tension

$$N_{pn} := n \cdot \psi_{c,p} \cdot N_p = 288 \text{ kip}$$



Modification for post-installed anchors

$$\psi_{cp,N} := 1.0$$

Factor for post-installed/
cast-in-place anchor

$$k_c := 24$$

Modification factor for
lightweight concrete

$$\lambda := 1.0$$

Basic concrete breakout
strength of a single anchor in
tension in cracked concrete

$$N_b := k_c \cdot \lambda \cdot \sqrt{\frac{f'_c}{\text{psi}}} \cdot \left(\frac{h_{ef}}{\text{in}} \right)^{1.5} \cdot \text{lb}$$

$$N_b = 97.1 \text{ kip}$$

$$N_{cbg} := \frac{A_{Nc}}{A_{Nco}} \cdot \psi_{ec,N} \cdot \psi_{ed,N} \cdot \psi_{c,N} \cdot \psi_{cp,N} \cdot N_b$$

$$N_{cbg} = 168.5 \text{ kip}$$

Supplemental Reinforcement

steel strength of rebar

$$f_{y_rebar} := 60 \text{ ksi}$$

area of supplemental reinforcing steel
required to make up the difference
between the demand and the
capacity of the concrete

$$A_{s_req} := \frac{N_{sa} - N_{cbg}}{f_{y_rebar}} = -1.442 \text{ in}^2$$

Use #4 bars

$$A_{bar} := \pi \cdot \left(\frac{4 \text{ in}}{8} \right)^2 = 0.196 \text{ in}^2$$

Number of bars required

$$n_{bars} := \max \left(0, \text{ceil} \left(\frac{A_{s_req}}{A_{bar}} \right) \right) = 0$$



B.4 Maximum Expected Reaction Forces for Specimens D1, D2, D3, & D4

Calculations

Specimen Base Expected
Maximum Reaction Forces

For Test Specimens:

D1, D2, D3, & D4

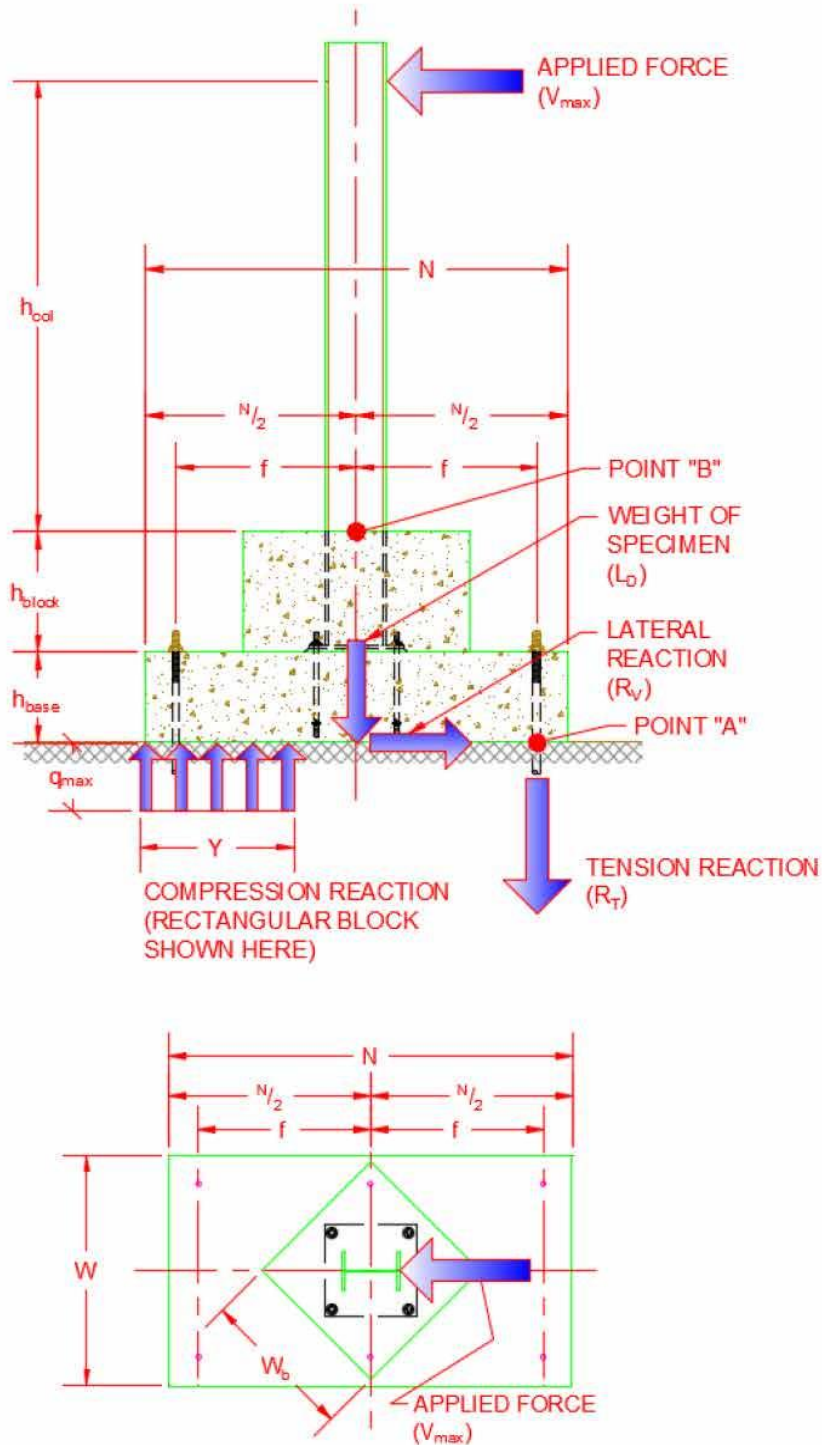
1. Overview - Purpose

Objective is to determine the maximum possible reaction loads imposed on the lab floor and anchorage during testing of specimens.

Specimens will be composed of a steel column anchored to a concrete base. The concrete base will be anchored to the lab floor (a "strong floor") via 4 steel threaded rods. Loads will be imposed on the specimen by means of an actuator at the top of the column creating both positive and negative lateral loads. This will create large moments in the base of the column. These moment forces will be resisted by a compression force in the leading edge of the concrete base, and a tensile force in the steel anchors on the trailing edge. The shear forces created will be resisted by both friction with the floor (ignored) and an external support system.



2. Specimen Info



Dimensions

$$N := 7 \text{ ft}$$

$$f := 3 \text{ ft}$$

$$W := 4 \text{ ft}$$

$$W_b := 2 \text{ ft} + 8 \text{ in}$$

$$h_{col} := 7.5 \text{ ft}$$

$$h_{block} := 16 \text{ in}$$

$$h_{base} := 24 \text{ in}$$

$$num_b := 2$$

number of anchors
in tension

Specimen Base Expected
Maximum Reaction Forces

Test Specimens: D1, D2, D3, D4

2 of 6

Material Properties
Steel Column

Steel Member Size	$Mem :=$ "W14x53"
Steel Grade	ASTM A992 Steel
yield strength	$F_y :=$ 50 <i>ksi</i>
ultimate strength	$F_u :=$ 65 <i>ksi</i>
Plastic Moment Capacity	$M_p := F_y \cdot Z_x =$ 363 <i>kip·ft</i>
Member Weight	$wt =$ 53 <i>plf</i>
Concrete Base	
Concrete Strength	$f'_c :=$ 4000 <i>psi</i>
Concrete Unit Weight	$\gamma_c :=$ 150 $\frac{lb_f}{ft^3}$



3. Determine Maximum Possible Applied Force on Column (V_{max})

The maximum possible lateral load, V_{max} , will occur when the column, bent about its strong axis, develops a plastic hinge at point "B".

$$R_y := 1.1$$

(note: the overstrength factor " R_y " is used to determine that maximum expected load in the column)

[from AISC "Seismic Design Manual", Table I-6-1, assuming A992 steel]

$$V_{max} := \frac{M_p \cdot R_y}{h_{col}} = 53.2 \text{ kip}$$

4. Determine total weight of specimen (L_D)

Base

$$L_{base} := \gamma_c \cdot (h_{base} \cdot W \cdot N) = 8.4 \text{ kip}$$

Blockout

$$L_{block} := \gamma_c \cdot (h_{block} \cdot W_b^2) = 1.42 \text{ kip}$$

Column (& base plate)

assume that base plate,
anchor bolts, etc. add 25%
of the weight of the column

$$pl := 0.25$$

$$L_{steel} := wt \cdot (h_{block} + h_{col}) \cdot (1 + pl) = 0.59 \text{ kip}$$

Total weight of specimen

$$L_D := L_{base} + L_{block} + L_{steel} = 10.41 \text{ kip}$$



5. **Determine width of compression block (Y)**

where:

$$q_{max} := f'_c = 4000 \text{ psi}$$

Sum moments about point "A"

$$[V_{max} * (h_{col} + h_{block} + h_{base})] + [L_D + f] - [(q_{max} * W * Y) * (f + N/2 - Y/2)] = 0$$

Simplify & convert to quadratic formula

$$Y^2 - (2 * f + N) * Y + \left(\frac{2}{q_{max} * W} \right) * [(q_{max} * (h_{col} + h_{block} + h_{base})) + (L_D + f)] = 0$$

$$A := 1$$

$$f = 3 \text{ ft}$$

$$B := -(2 * f + N)$$

$$C := \left(\frac{2}{q_{max} * W} \right) * (V_{max} * (h_{col} + h_{block} + h_{base}) + (L_D * f))$$

Using Quadratic Formula:

$$Y_q := \frac{-B + \left[\frac{1}{-1} \right] * \sqrt{B^2 - 4 * A * C}}{2 * A} = \left[\begin{array}{c} 155.511 \\ 0.489 \end{array} \right] \text{ in}$$

$$Y := |\min(Y_q)| = 0.489 \text{ in}$$

6. **Determine tension reaction in anchor rods (R_T)**

Sum all forces in the vertical direction

$$R_T := (q_{max} * Y * W) - L_D = 83.4 \text{ kip}$$

Load resisted by each anchor

$$R_{ab} := \frac{R_T}{num_b} = 41.7 \text{ kip}$$

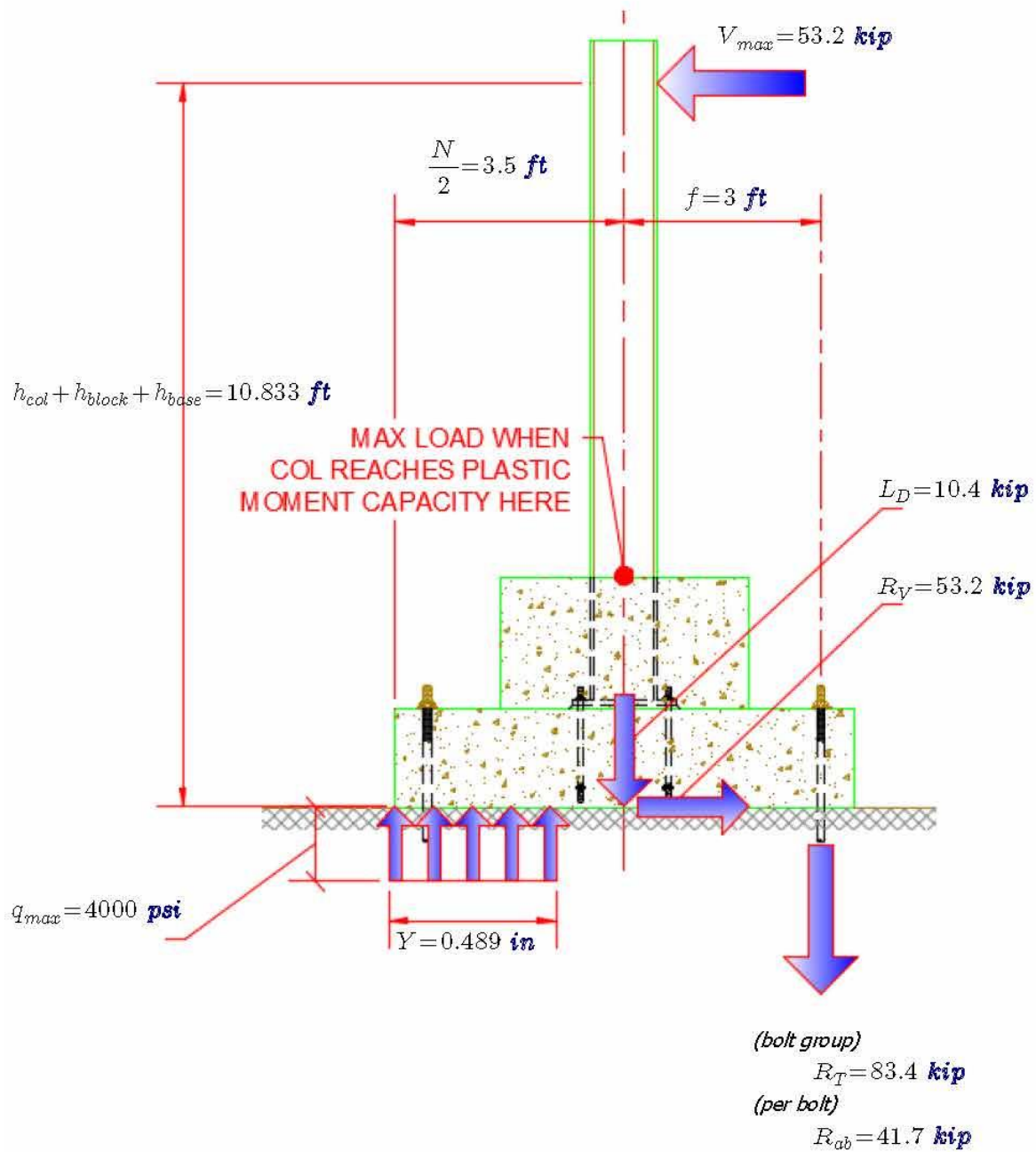
7. **Determine Lateral Reaction (R_V)**

Sum all forces in the horizontal direction

$$R_V := V_{max} = 53.2 \text{ kip}$$



8. Summary of Maximum Possible Loads and Reactions



Specimen Base Expected
Maximum Reaction Forces

Test Specimens: D1, D2, D3, D4

6 of 6

B.5 Base Plate Design for Specimens F1, F2, F3, & F4

Calculations

Base Plate Design

Per AISC Steel Design Guide 1, Section 3.4

For Test Specimens:

F1, F2, F3, & F4

Given

Column

Column Size $Col := "W10 \times 77"$

Column Height $h_{col} := 10 \text{ ft}$

Steel Strength $f_{y,col} := 50 \text{ ksi}$ ASTM A992 Steel

$$M_p = 406.7 \text{ kip} \cdot \text{ft}$$

$$R_y := 1.1 \quad [\text{expected strength factor}]$$

Base Plate

Width $N := 1 \text{ ft} + 8 \text{ in}$

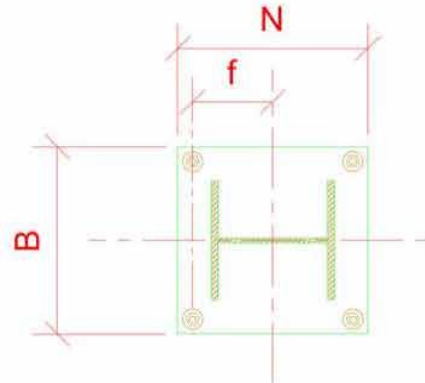
Length $B := 1 \text{ ft} + 4 \text{ in}$

AB Locations $f := 8 \text{ in}$

Yield Strength $f_{y,bspl} := 36 \text{ ksi}$

$$n := \frac{B - 0.8 \cdot b_f}{2} = 3.92 \text{ in}$$

$$m := \frac{N - 0.95 \cdot d}{2} = 4.965 \text{ in}$$



Concrete

Strength $f'_c := 4000 \text{ psi}$

Anchor Bolts

Material type: ASTM F1554 Gr 36

Yield Strength $f_{y,bolt} := 36 \text{ ksi}$

Ultimate Strength $f_{u,bolt} := 58 \text{ ksi}$

AB Quantity $num_b := 8$

Step 1: Determine the Axial and Moment Load on Column Base

$$P_r := h_{col} \cdot W_{col} = 770 \text{ lbf}$$

$$M_r := R_y \cdot M_p = 447.3 \text{ kip}\cdot\text{ft}$$

Step 2: Pick a trial base plate size ($N \times B$)

(defined previously)

$$N = 20 \text{ in}$$

$$B = 16 \text{ in}$$

Step 3: Determine the equivalent eccentricity (e), and the critical eccentricity (e_{crit})

$$e := \frac{M_r}{P_r} = 581 \text{ ft}$$

$$f = 0.667 \text{ ft}$$

$$e_{crit} := \frac{N}{2} - \frac{P_r}{2 \cdot q_{max}} = 9.995 \text{ in}$$

$$\begin{array}{l|l} \text{if } e \geq e_{crit} & = \text{"GOOD!"} \\ \parallel & \\ \text{"GOOD!"} & \\ \text{else} & \\ \parallel & \\ \text{"NO GOOD!"} & \end{array}$$

Step 4: Determine the equivalent bearing length (Y) and the tensile force in the anchor rods (T).

$$Y := \left(f + \frac{N}{2} \right) + \left[\begin{array}{c} 1 \\ -1 \end{array} \right] \cdot \sqrt{\left(f + \frac{N}{2} \right)^2 - \frac{2 \cdot P_r \cdot (e + f)}{q_{max}}} = \left[\begin{array}{c} 31.115 \\ 4.885 \end{array} \right] \text{ in}$$

$$Y := \text{if } 0 < Y_o < N \mid = 4.885 \text{ in}$$

$$\begin{array}{l|l} \parallel & \\ Y_o & \\ \text{else} & \\ \parallel & \\ Y_1 & \end{array}$$

$$T := q_{max} \cdot Y - P_r = 344.663 \text{ kip}$$



Step 5: Determine the required minimum base plate thickness at the bearing and the tension interfaces.

Bearing Interface:

$$t_{p_req_b} := \begin{cases} \text{if } Y \geq \max(m, n) \\ 1.5 \cdot m \cdot \sqrt{\frac{f_{p_max}}{f_{y_bspl}}} \\ \text{else} \\ 2.11 \cdot \sqrt{\frac{f_{p_max} \cdot Y \cdot \left(m - \frac{Y}{2}\right)}{f_{y_bspl}}} \end{cases} = 2.595 \text{ in}$$

Tension Interface

$$t_{p_req_t} := 2.11 \cdot \sqrt{\frac{T \cdot \left(f - \frac{d}{2} + \frac{t_f}{2}\right)}{B \cdot f_{y_bspl}}} = 2.89 \text{ in}$$

Take maximum of the two:

$$t_{p_req} := \max(t_{p_req_b}, t_{p_req_t}) = 2.89 \text{ in}$$

Step 6: Determine the anchor rod size appropriate for the tensile loading
(assuming that the embedment is such that tensile fracture of the anchor bolt governs, and that shear load in the bolts is negligible)

Number of bolts in tension

$$N_{b_t} := \frac{num_b}{2} = 4$$

Tensile Force in each bolt (with factor - we want anchor bolt fracture to govern the strength of the connection)

$$T_u := \frac{0.5 \cdot T}{N_{b_t}} = 43.083 \text{ kip}$$

required diameter $\phi := 0.75$

$$D_{req} := \sqrt{\frac{4 \cdot T_u}{\pi \cdot \phi \cdot f_{u_bolt}}} = 1.123 \text{ in}$$

B.6 Anchor Bolt Design for Specimens F1, F2, & F3

Calculations
Anchor Bolt Design
Per ACI 318 Appendix D

For Test Specimens:
F1, F2, & F3

Anchor Bolt Information

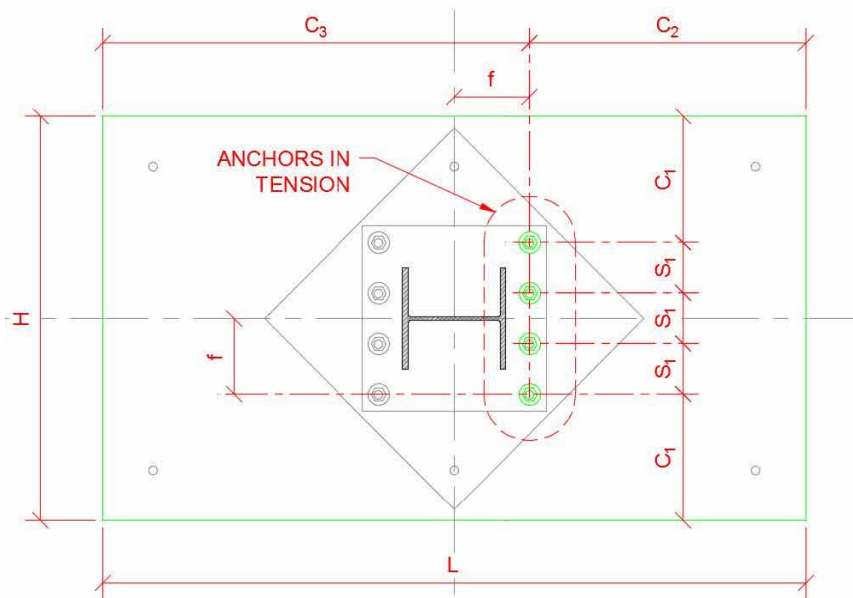
Anchor Bolt Diameter

$$D_b := 1.125 \text{ in}$$

Anchor Bolt Strength

$$f_{y_bolt} := 36 \text{ ksi}$$

$$f_{u_bolt} := 58 \text{ ksi}$$



IMPORTED

$$f := 8 \text{ in}$$

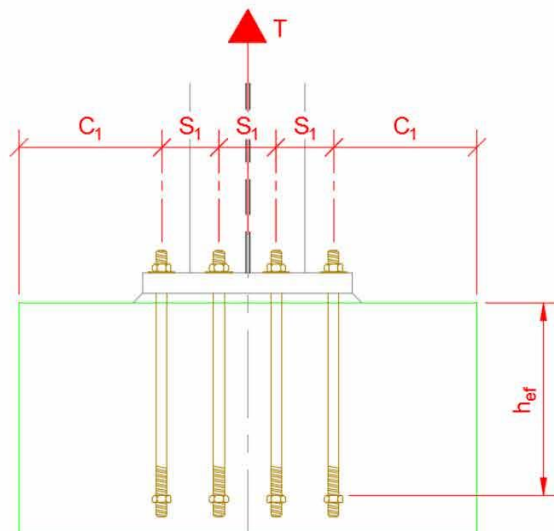
$$f'_c := 4 \text{ ksi}$$

INPUT

$$H := 4 \text{ ft}$$

$$L := 7 \text{ ft}$$

$$h_{ef} := 19 \text{ in}$$



CALCULATED

$$s_1 := 4 \text{ in}$$

$$c_1 := \frac{H - 3 \cdot s_1}{2} = 18 \text{ in}$$

$$c_2 := \frac{L}{2} - f = 34 \text{ in}$$

$$c_3 := L - c_2 = 50 \text{ in}$$

Strength in Tension

D.5.1.2 - Nominal strength of a group of anchors in tension

$$N_{sa}$$

number of anchors in the group

$$n := 4$$

effective cross-sectional area
of a single anchor

$$A_{se.N} := 0.9 \cdot \pi \cdot \frac{D_b^2}{4} = 0.895 \text{ in}^2$$

strength of AB steel

$$f_{uta} := \min(1.9 \cdot f_{y_bolt}, f_{u_bolt})$$

$$f_{uta} = 58 \text{ ksi}$$

$$N_{sa} := n \cdot A_{se.N} \cdot f_{uta} = 207.6 \text{ kip}$$

D.5.2.1 - Nominal concrete breakout strength of a group of anchors in tension

$$N_{cbg}$$

projected concrete failure
area of a group of anchors

$$A_{Nc} := (3 \cdot s_1 + 2 \cdot \min(c_1, 1.5 \cdot h_{ef})) \cdot (\min(c_2, 1.5 \cdot h_{ef}) + \min(c_3, 1.5 \cdot h_{ef}))$$

$$A_{Nc} = 2736 \text{ in}^2$$

projected concrete failure
area of a single anchor

$$A_{Nco} := 9 \cdot h_{ef}^2 = 3249 \text{ in}^2$$

Eccentricity Factor

$$\psi_{ed.N} := 1$$

Modification factor for edge
effects

$$\psi_{ec.N} := \begin{cases} \text{if } \min(c_1, c_2, c_3) \geq 1.5 \cdot h_{ef} \\ 1.0 \\ \text{else} \\ 0.7 + 0.3 \cdot \frac{\min(c_1, c_2, c_3)}{1.5 \cdot h_{ef}} \end{cases}$$

$$\psi_{ec.N} = 0.889$$

Modification factor for
cracked/uncracked concrete

$$\psi_{c.N} := 1.25$$

Modification for post-installed anchors

$$\psi_{cp,N} := 1.0$$

Factor for post-installed/
cast-in-place anchor

$$k_c := 24$$

Modification factor for
lightweight concrete

$$\lambda := 1.0$$

Basic concrete breakout
strength of a single anchor in
tension in cracked concrete

$$N_b := k_c \cdot \lambda \cdot \sqrt{\frac{f'_c}{\text{psi}}} \cdot \left(\frac{h_{ef}}{\text{in}} \right)^{1.5} \cdot \text{lb}$$

$$N_b = 125.7 \text{ kip}$$

$$N_{cbg} := \frac{A_{Nc}}{A_{Nco}} \cdot \psi_{ec,N} \cdot \psi_{ed,N} \cdot \psi_{c,N} \cdot \psi_{cp,N} \cdot N_b$$

$$N_{cbg} = 117.7 \text{ kip}$$

Supplemental Reinforcement

steel strength of rebar

$$f_{y_rebar} := 60 \text{ ksi}$$

area of supplemental reinforcing steel
required to make up the difference
between the demand and the
capacity of the concrete

$$A_{s_req} := \frac{N_{sa} - N_{cbg}}{f_{y_rebar}} = 1.498 \text{ in}^2$$

Use #4 bars

$$A_{bar} := \pi \cdot \left(\frac{4 \text{ in}}{8} \right)^2 = 0.196 \text{ in}^2$$

Number of Supplemental
bars required

$$n_{bars} := \text{ceil} \left(\frac{A_{s_req}}{A_{bar}} \right) = 8$$

D.5.3.1 - Nominal pullout strength of a single anchor in tension

Bearing Area of the anchor
bolt head w/ 2"x2" plate
washer

$$A_{brg} := (2 \text{ in})^2 - \pi \cdot \frac{D_b^2}{4}$$

$$A_{brg} = 3.0 \text{ in}^2$$

Pullout strength of a single
headed bolt

$$N_p := 8 \cdot A_{brg} \cdot f'_c = 96.2 \text{ kip}$$

Factor to account for
cracked/uncracked concrete

$$\psi_{c,p} := 1.4$$

Nominal pullout strength of a
group of anchors in tension

$$N_{pn} := n \cdot \psi_{c,p} \cdot N_p = 538.7 \text{ kip}$$



B.7 Anchor Bolt Design for Specimen F4

Calculations
Anchor Bolt Design
Per ACI 318 Appendix D

For Test Specimens:
F4

Anchor Bolt Information

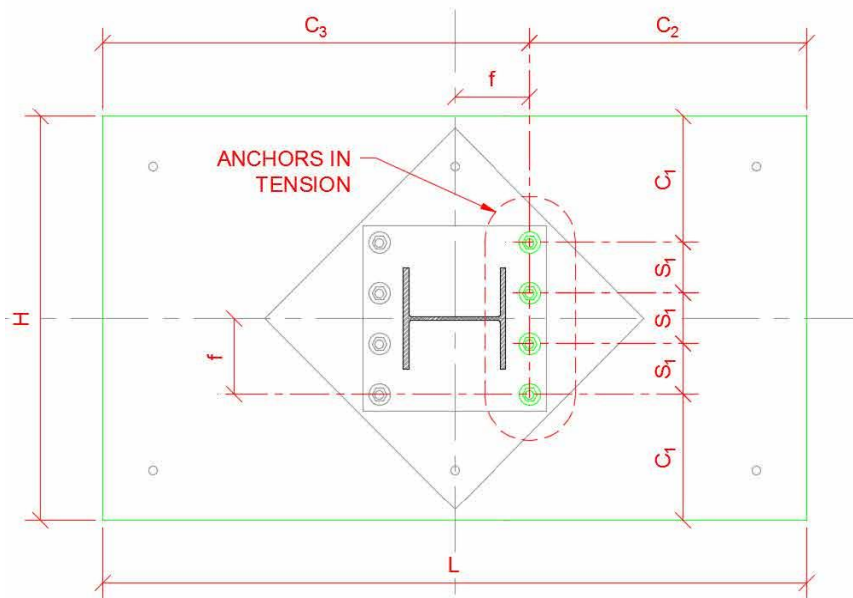
Anchor Bolt Diameter

$$D_b := 1.125 \text{ in}$$

Anchor Bolt Strength

$$f_{y_bolt} := 36 \text{ ksi}$$

$$f_{u_bolt} := 58 \text{ ksi}$$



IMPORTED

$$f := 8 \text{ in}$$

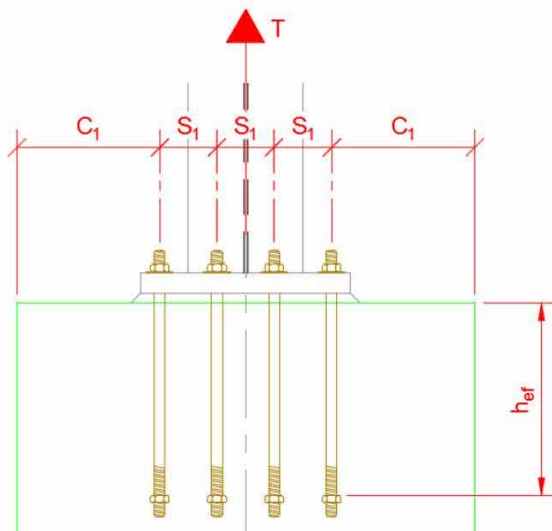
$$f'_c := 4 \text{ ksi}$$

INPUT

$$H := 4 \text{ ft}$$

$$L := 7 \text{ ft}$$

$$h_{ef} := 19 \text{ in}$$



CALCULATED

$$s_1 := 4 \text{ in}$$

$$c_1 := \frac{H - 1 \cdot s_1}{2} = 22 \text{ in}$$

$$c_2 := \frac{L}{2} - f = 34 \text{ in}$$

$$c_3 := L - c_2 = 50 \text{ in}$$

Strength in Tension

D.5.1.2 - Nominal strength of a group of anchors in tension

$$N_{sa}$$

number of anchors in the group

$$n := 2$$

effective cross-sectional area
of a single anchor

$$A_{se,N} := 0.9 \cdot \pi \cdot \frac{D_b^2}{4} = 0.895 \text{ in}^2$$

strength of AB steel

$$f_{uta} := \min(1.9 \cdot f_{y_bolt}, f_{u_bolt})$$

$$f_{uta} = 58 \text{ ksi}$$

$$N_{sa} := n \cdot A_{se,N} \cdot f_{uta} = 103.8 \text{ kip}$$

D.5.2.1 - Nominal concrete breakout strength of a group of anchors in tension

$$N_{cbg}$$

projected concrete failure
area of a group of anchors

$$A_{Nc} := (3 \cdot s_1 + 2 \cdot \min(c_1, 1.5 \cdot h_{ef})) \cdot (\min(c_2, 1.5 \cdot h_{ef}) + \min(c_3, 1.5 \cdot h_{ef}))$$

$$A_{Nc} = 3192 \text{ in}^2$$

projected concrete failure
area of a single anchor

$$A_{Nco} := 9 \cdot h_{ef}^2 = 3249 \text{ in}^2$$

Eccentricity Factor

$$\psi_{ed,N} := 1$$

Modification factor for edge
effects

$$\psi_{ec,N} := \begin{cases} 1.0 & \text{if } \min(c_1, c_2, c_3) \geq 1.5 \cdot h_{ef} \\ 0.7 + 0.3 \cdot \frac{\min(c_1, c_2, c_3)}{1.5 \cdot h_{ef}} & \text{else} \end{cases}$$

$$\psi_{ec,N} = 0.932$$

Modification factor for
cracked/uncracked concrete

$$\psi_{c,N} := 1.25$$



Modification for post-installed anchors

$$\psi_{cp,N} := 1.0$$

Factor for post-installed/
cast-in-place anchor

$$k_c := 24$$

Modification factor for
lightweight concrete

$$\lambda := 1.0$$

Basic concrete breakout
strength of a single anchor in
tension in cracked concrete

$$N_b := k_c \cdot \lambda \cdot \sqrt{\frac{f'_c}{\text{psi}}} \cdot \left(\frac{h_{ef}}{\text{in}} \right)^{1.5} \cdot \text{lb}$$

$$N_b = 125.7 \text{ kip}$$

$$N_{cbg} := \frac{A_{Nc}}{A_{Nco}} \cdot \psi_{ec,N} \cdot \psi_{ed,N} \cdot \psi_{c,N} \cdot \psi_{cp,N} \cdot N_b$$

$$N_{cbg} = 143.8 \text{ kip}$$

Supplemental Reinforcement

steel strength of rebar

$$f_{y_rebar} := 60 \text{ ksi}$$

area of supplemental reinforcing steel
required to make up the difference
between the demand and the
capacity of the concrete

$$A_{s_req} := \frac{N_{sa} - N_{cbg}}{f_{y_rebar}} = -0.667 \text{ in}^2$$

Use #4 bars

$$A_{bar} := \pi \cdot \left(\frac{\frac{4}{8} \text{ in}}{4} \right)^2 = 0.196 \text{ in}^2$$

Number of bars required

$$n_{bars} := \max \left(0, \text{ceil} \left(\frac{A_{s_req}}{A_{bar}} \right) \right) = 0$$



D.5.3.1 - Nominal pullout strength of a single anchor in tension

Bearing Area of the anchor
bolt head w/ 2"x2" plate
washer

$$A_{brg} := (2 \text{ in})^2 - \pi \cdot \frac{D_b^2}{4}$$

$$A_{brg} = 3.0 \text{ in}^2$$

Pullout strength of a single
headed bolt

$$N_p := 8 \cdot A_{brg} \cdot f'_c = 96.2 \text{ kip}$$

Factor to account for
cracked/uncracked concrete

$$\psi_{c,p} := 1.4$$

Nominal pullout strength of a
group of anchors in tension

$$N_{pg} := n \cdot \psi_{c,p} \cdot N_p = 269.3 \text{ kip}$$



B.8 Maximum Expected Reaction Forces for Specimens F1, F2, F3, & F4

Calculations

Specimen Base Expected
Maximum Reaction Forces

For Test Specimens:

F1, F2, F3, & F4

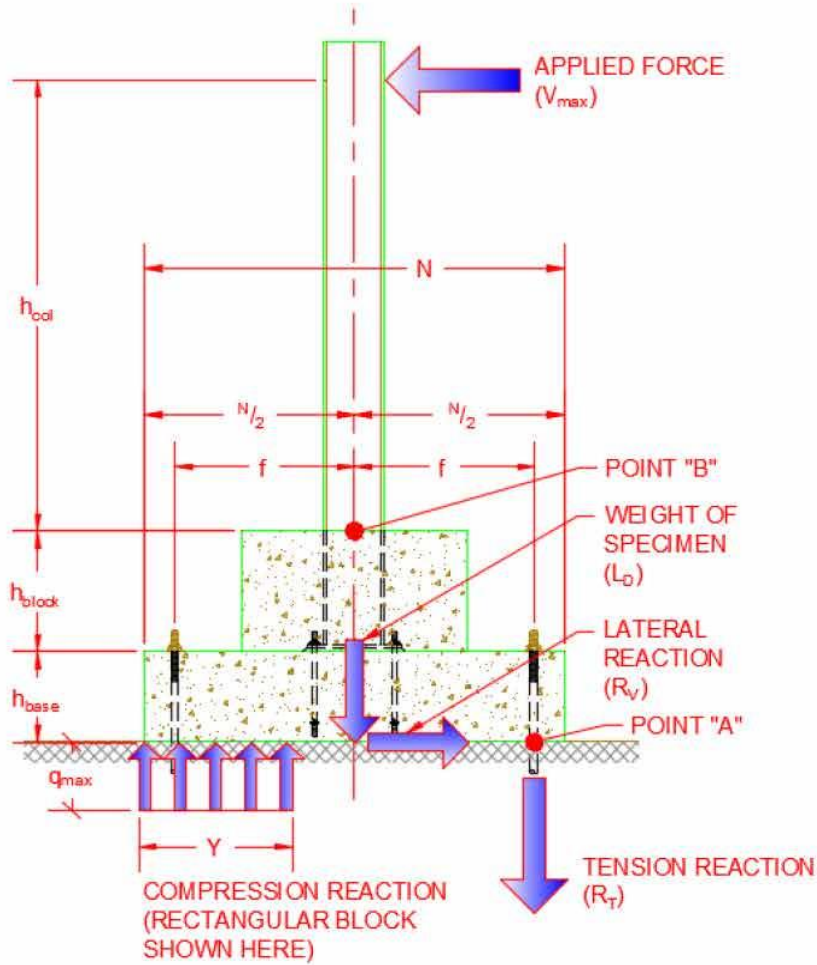
1. Overview - Purpose

Objective is to determine the maximum possible reaction loads imposed on the lab floor and anchorage during testing of specimens.

Specimens will be composed of a steel column anchored to a concrete base. The concrete base will be anchored to the lab floor (a "strong floor") via 4 steel threaded rods. Loads will be imposed on the specimen by means of an actuator at the top of the column creating both positive and negative lateral loads. This will create large moments in the base of the column. These moment forces will be resisted by a compression force in the leading edge of the concrete base, and a tensile force in the steel anchors on the trailing edge. The shear forces created will be resisted by both friction with the floor (ignored) and an external support system.



2. Specimen Info



Dimensions

$$N := 7 \text{ ft}$$

$$f := 3 \text{ ft}$$

$$W := 4 \text{ ft}$$

$$W_b := 2 \text{ ft} + 8 \text{ in}$$

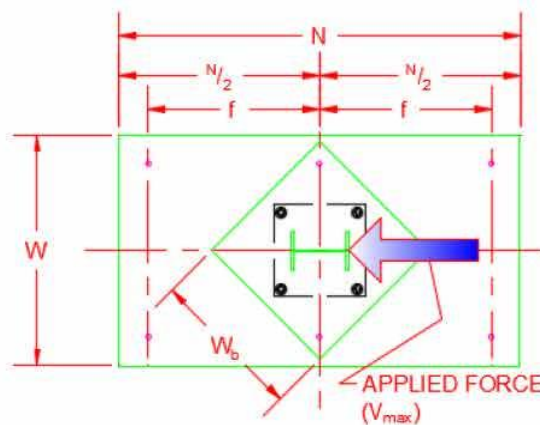
$$h_{col} := 7 \text{ ft} + 2 \text{ in}$$

$$h_{block} := 16 \text{ in}$$

$$h_{base} := 24 \text{ in}$$

$$num_b := 2$$

*number of anchors
in tension*



Specimen Base Expected
Maximum Reaction Forces

Test Specimens: F1, F2, F3, F4

2 of 6

Material Properties
Steel Column

Steel Member Size	$Mem := \text{"W10x77"}$
Steel Grade	ASTM A992 Steel
yield strength	$F_y := 50 \text{ ksi}$
ultimate strength	$F_u := 65 \text{ ksi}$
Plastic Moment Capacity	$M_p := F_y \cdot Z_x = 407 \text{ kip}\cdot\text{ft}$
Member Weight	$wt = 77 \text{ plf}$
Concrete Base	
Concrete Strength	$f'_c := 4000 \text{ psi}$
Concrete Unit Weight	$\gamma_c := 150 \frac{\text{lb}}{\text{ft}^3}$



3. Determine Maximum Possible Applied Force on Column (V_{max})

The maximum possible lateral load, V_{max} , will occur when the column, bent about its strong axis, develops a plastic hinge at point "B".

$$R_y := 1.1$$

(note: the overstrength factor " R_y " is used to determine that maximum expected load in the column)

[from AISC "Seismic Design Manual", Table I-6-1, assuming A992 steel]

$$V_{max} := \frac{M_p \cdot R_y}{h_{col}} = 62.4 \text{ kip}$$

4. Determine total weight of specimen (L_D)

Base

$$L_{base} := \gamma_c \cdot (h_{base} \cdot W \cdot N) = 8.4 \text{ kip}$$

Blockout

$$L_{block} := \gamma_c \cdot (h_{block} \cdot W_b^2) = 1.42 \text{ kip}$$

Column (& base plate)

assume that base plate,
anchor bolts, etc. add 25%
of the weight of the column

$$pl := 0.25$$

$$L_{steel} := wt \cdot (h_{block} + h_{col}) \cdot (1 + pl) = 0.82 \text{ kip}$$

Total weight of specimen

$$L_D := L_{base} + L_{block} + L_{steel} = 10.64 \text{ kip}$$



5. **Determine width of compression block (Y)**

where:

$$q_{max} := f'_c = 4000 \text{ psi}$$

Sum moments about point "A"

$$[V_{max} * (h_{col} + h_{block} + h_{base})] + [L_D + f] - [(q_{max} * W * Y) * (f + N/2 - Y/2)] = 0$$

Simplify & convert to quadratic formula

$$Y^2 - (2 * f + N) * Y + \left(\frac{2}{q_{max} * W} \right) * [(q_{max} * (h_{col} + h_{block} + h_{base})) + (L_D + f)] = 0$$

$$A := 1$$

$$f = 3 \text{ ft}$$

$$B := -(2 * f + N)$$

$$C := \left(\frac{2}{q_{max} * W} \right) * (V_{max} * (h_{col} + h_{block} + h_{base}) + (L_D * f))$$

Using Quadratic Formula:

$$Y_q := \frac{-B + \left[\frac{1}{-1} \right] * \sqrt{B^2 - 4 * A * C}}{2 * A} = \begin{bmatrix} 155.447 \\ 0.553 \end{bmatrix} \text{ in}$$

$$Y := |\min(Y_q)| = 0.553 \text{ in}$$

6. **Determine tension reaction in anchor rods (R_T)**

Sum all forces in the vertical direction

$$R_T := (q_{max} * Y * W) - L_D = 95.5 \text{ kip}$$

Load resisted by each anchor

$$R_{ab} := \frac{R_T}{num_b} = 47.7 \text{ kip}$$

7. **Determine Lateral Reaction (R_V)**

Sum all forces in the horizontal direction

$$R_V := V_{max} = 62.4 \text{ kip}$$

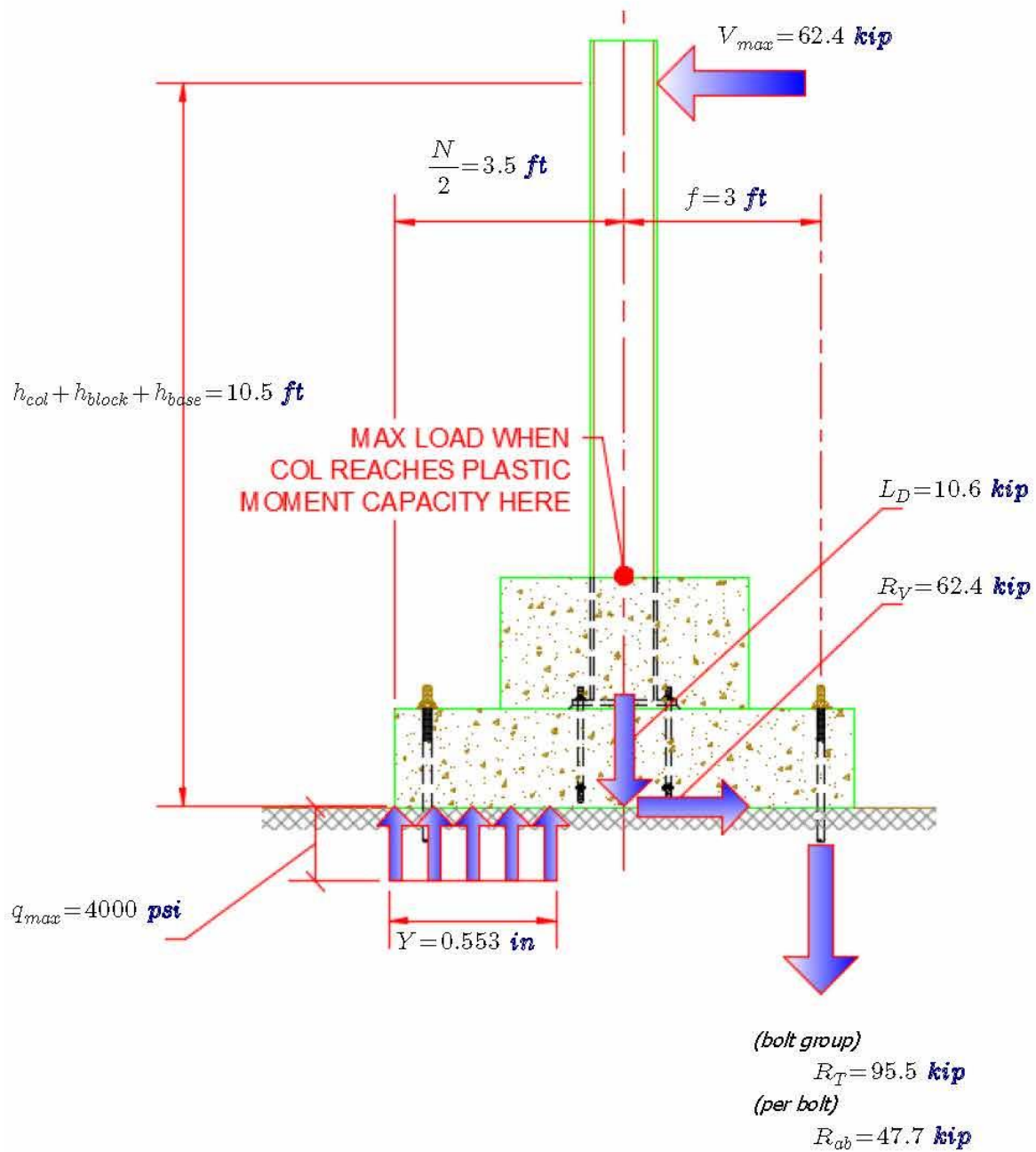
Specimen Base Expected
Maximum Reaction Forces

Test Specimens: F1, F2, F3, F4

5 of 6



8. Summary of Maximum Possible Loads and Reactions



Specimen Base Expected
Maximum Reaction Forces

Test Specimens: F1, F2, F3, F4

6 of 6

B.9 Shear lug weld design for all Specimens

Given

Weld

Weld metal
classification strength $F_{EXX} := 70 \text{ ksi}$

Base Plate

Yield Stress $f_{y_bspl} := 36 \text{ ksi}$

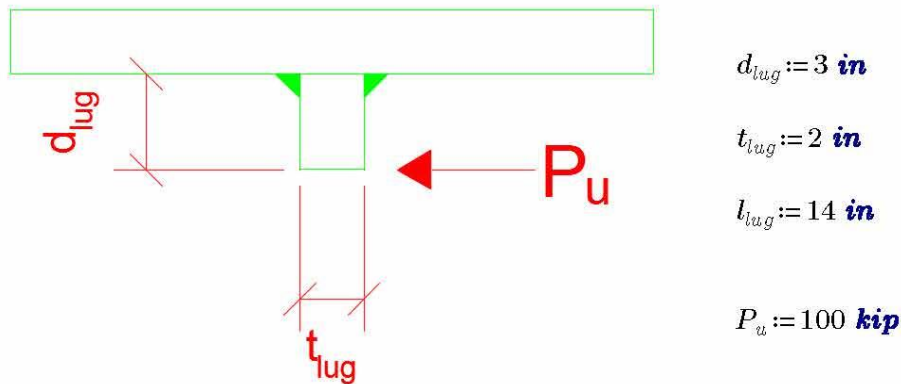
Ultimate Stress $f_{u_bspl} := 50 \text{ ksi}$

Shear Lug

Yield Stress $f_{y_lug} := 36 \text{ ksi}$

Ultimate Stress $f_{u_lug} := 50 \text{ ksi}$

Geometry



Note:

- 1) While the load against the shear lug is more accurately a pressure load on the lug caused by the resistance from the concrete base, it is conservative to assume that the entire lateral force will present itself as a point load at the base of the shear lug.
- 2) The lateral load (P_u) is taken as approximately 1.5 times the expected maximum possible lateral load experience by any of the Specimens (See appendix B4, and B8).

Step 1: Determine the demand on the weld per inch

Lateral Demand on the Weld

$$R_{lat} := \frac{P_u}{2 \cdot l_{lug}} = 3.57 \frac{\text{kip}}{\text{in}}$$

Vertical Demand on the Weld

$$R_{vert} := \frac{P_u \cdot \frac{d_{lug}}{t_{lug}}}{l_{lug}} = 10.71 \frac{\text{kip}}{\text{in}}$$

Resultant Demand on the Weld

$$R_u := \sqrt{R_{lat}^2 + R_{vert}^2} = 11.29 \frac{\text{kip}}{\text{in}}$$

Step 2: Determine minimum size of weld required

angle of loading measured
from the weld longitudinal
axis $\theta := 90^\circ$

a. Required size of weld based on failure of weld material

$$R_n = \phi \cdot F_{nw} \cdot A_{we}$$

strength reduction factor $\phi := 0.75$

$$R_n = R_u$$

$$F_{nw} = 0.6 \cdot F_{EXX} \cdot \left(1.0 + 0.5 \sin^{1.5}(\theta)\right)$$

$$A_{we} = \sin 45^\circ \cdot t_{weld} \cdot l_{weld}$$

$$R_u = \phi \cdot \left(0.6 \cdot F_{EXX} \cdot \left(1.0 + 0.5 \sin^{1.5}(\theta)\right)\right) \cdot \left(\sin 45^\circ \cdot t_{weld} \cdot l_{weld}\right)$$

solve for the minium required size of the weld

$$t_{weld_req1} := \frac{R_u}{\phi \cdot \left(0.6 \cdot F_{EXX} \cdot \left(1.0 + 0.5 \sin^{1.5}(\theta)\right)\right) \cdot \left(\sin(45^\circ)\right)} = 0.338 \text{ in}$$

b. Required size of weld based on failure of base material

$$R_n = \phi \cdot F_u \cdot A_e$$

strength reduction factor $\phi := 0.75$

$$R_n = R_u$$

$$F_u := f_{u_bspl} = 50 \text{ ksi}$$

$$A_e = l_{weld} \cdot t_{weld}$$

$$P_u = \phi \cdot F_u \cdot (l_{weld} \cdot t_{weld})$$

solve for the minium required size of the weld

$$t_{weld_req2} := \frac{R_u}{\phi \cdot F_u} = 0.3012 \text{ in}$$

c. Required size of weld

$$t_{weld_req} := \max(t_{weld_req1}, t_{weld_req2}) = 0.338 \text{ in}$$

$$t_{weld_min} := \text{Ceil}\left(t_{weld_req}, \frac{1}{16} \text{ in}\right) = 0.375 \text{ in}$$



B.10 Base Slab Bending Capacity and Reinforcement Design

Calculations

Base Slab bending moment capacity &
reinforcement design
Base Plate Capacity - per AISC Steel Design Guide 1
Base Slab Bending Capacity - Per ACI 318

For Test Specimens:

All

Given

Rebar

Steel Strength	$f_y := 60 \text{ ksi}$
Bar Size	#4
Bar Diameter	$d_b := \frac{4}{8} \text{ in}$
Area of a single bar	$a_s := \pi \cdot \frac{d_b^2}{4} = 0.2 \text{ in}^2$
Total Number of bars	$num_b := 15$
Total Area of steel	$A_s := a_s \cdot num_b = 2.95 \text{ in}^2$

Concrete

Concrete Strength	$f'_c := 4000 \text{ psi}$
-------------------	----------------------------

Geometry

Base Height	$h := 24 \text{ in}$
Base Width	$b := 4 \text{ ft}$
Rebar Cover	$cover := 3 \text{ in}$
Depth of Rebar	$d := h - cover - \frac{1}{2} \cdot d_b = 20.75 \text{ in}$



Bending Capacity

Depth of Compression block

$$a := \frac{A_s \cdot f_y}{0.85 \cdot f'_c \cdot b} = 1.08 \text{ in}$$

$$c := \frac{a}{0.85} = 1.27 \text{ in}$$

allowable compressive strain
in concrete

$$\varepsilon_{cu} := 0.003$$

Check strain in steel

$$\varepsilon_s := \varepsilon_{cu} \cdot \frac{(d - c)}{c} = 0.0459$$

strength reduction factor

$$\phi := \begin{cases} \text{if } \varepsilon_s \geq 0.005 & 0.9 \\ \text{else if } \varepsilon_s \leq 0.002 & 0.75 \\ \text{else} & 0.65 + \frac{250}{3} \cdot (\varepsilon_s - 0.002) \end{cases} = 0.9$$

bending capacity of bottom slab

$$\phi M_n := \phi \cdot A_s \cdot f_y \cdot \left(d - \frac{a}{2} \right) = 267.8 \text{ kip} \cdot \text{ft}$$

$$\phi M_n := \phi \cdot 0.85 \cdot f'_c \cdot a \cdot b \cdot \left(d - \frac{a}{2} \right) = 267.84 \text{ kip} \cdot \text{ft}$$



Demand on the Slab

The moment demand will be taken as the larger of two forces:

- 1) the moment imposed on the slab during lifting and maneuvering in the lab
- 2) the moment imposed on the slab from the column during testing

This load will be taken as the largest load transmitted to the system. Since the base plate was designed with the tensile failure of the anchor bolts as the governing failure, then the capacity of the base plate connection (again, governed by failure of the anchor bolts) will be used as the maximum load transmitted to the system.

1) Moment imposed on the slab during lifting and maneuvering in the lab

Weight of concrete $\gamma_c := 150 \text{ pcf}$

Dimensions of bottom slab
 $L := 7 \text{ ft}$
 $W := 4 \text{ ft}$
 $H := 2 \text{ ft}$

Dimensions of "floor" slab
 $L_f := 5 \text{ ft}$
 $W_f := 4 \text{ ft}$
 $H_f := 16 \text{ in}$

Total Concrete Weight
 $W_{conc} := \gamma_c \cdot (L \cdot W \cdot H + L_f \cdot W_f \cdot H_f)$
 $W_{conc} = 12.4 \text{ kip}$

Weight of Steel Column $wt_s := 77 \text{ plf}$

Height of Steel Column $L_{col} := 7.5 \text{ ft}$

Total Steel Weight (25% added to steel weight for plates, anchor bolts, etc.)
 $W_{steel} := wt_s \cdot L_{col} \cdot 1.25 = 0.72 \text{ kip}$

Total Weight of heaviest specimen: $W_{specimen} := W_{conc} + W_{steel} = 13.1 \text{ kip}$

To calculate the moment demand on the slab during lifting procedures, I'll make three conservative assumptions:

- 1) The load is concentrated at the center of the slab, acting as a "point load"
- 2) The crane straps act as the beam "support", and will act at the ends of the slab, rather than at the actual lifting lug locations.
- 2) The load imposed is created by lifting the specimen with a crane, so the load will be treated as a crane live load, with the applicable factors and load combinations from ASCE 7.

The load is created when straps lift the specimen from its 4 corners, causing one-way bending in the slab along its long edge.

Crane Vertical Impact force: $I_v := 1.25$
(assume a "monorail powered crane")

Factored Vertical Demand on the slab using LRFD Load combination #2: $P_u := 1.6 \cdot I_v \cdot W_{specimen} = 26.24 \text{ kip}$

Factored Bending Moment demand on slab $M_{u1} := \frac{P_u \cdot L}{4} = 45.93 \text{ kip} \cdot \text{ft}$

2) Moment imposed on the slab from the column during testing

Determine the largest expected moment transferred from the larger base plate
Use the base plate configuration of test specimen #F1
Follow the "ultimate stress design" procedure

Column

Column Size	$Col := \text{"W10x77"}$	
Column Height	$h_{col} := 10 \text{ ft}$	
Steel Strength	$f_{y_col} := 50 \text{ ksi}$	ASTM A992 Steel

Base Plate

Width	$N := 1 \text{ ft} + 8 \text{ in}$
Depth	$B := 1 \text{ ft} + 4 \text{ in}$
AB Location	$f := 8 \text{ in}$
Steel Strength	$f_{y_bspl} := 36 \text{ ksi}$

Concrete

$$f'_c := 4000 \text{ psi}$$

Anchor Bolts

Material: ASTM F1554 Gr 36

$$f_{y_bolt} := 36 \text{ ksi}$$

$$f_{u_bolt} := 58 \text{ ksi}$$

$$num_b := 8$$

$$D_b := 1.125 \text{ in}$$

$$A_b := \frac{\pi \cdot D_b^2}{4} = 0.99 \text{ in}^2$$

Determine magnitude of the concrete compression block

$$f_p := 0.85 \cdot f'_c = 3400 \text{ psi}$$

Determine the magnitude of the tensile force from the anchor bolts

$$T := \left(f_{y_bolt} \cdot \frac{num_b \cdot A_b}{2} \right) = 143.14 \text{ kip}$$

Assume that the vertical load on the column is simply its own self-weight

$$P_r := W_{steel} = 0.72 \text{ kip}$$

solve for the width of the compression block

$$a := \frac{P_r + T}{B \cdot f_p} = 2.64 \text{ in}$$

Sum moments about centerline of column to solve for the Moment Capacity of the connection

$$M_{u2} := T \cdot f + a \cdot B \cdot f_p \cdot \left(\frac{N}{2} - \frac{a}{2} \right) = 199.46 \text{ kip} \cdot \text{ft}$$

Summary of Moment Demand on the Column**1) Moment imposed on the slab during lifting and maneuvering in the lab**

$$M_{u1} = 45.93 \text{ kip} \cdot \text{ft}$$

2) Moment imposed on the slab from the column during testing

$$M_{u2} = 199.46 \text{ kip} \cdot \text{ft}$$

Moment to be used in Design

$$M_u := \max(M_{u1}, M_{u2}) = 199.46 \text{ kip} \cdot \text{ft}$$

Comparison of Demand & Capacity

Demand

$$M_u = 199.46 \text{ kip}\cdot\text{ft}$$

Capacity

$$\phi M_n = 267.84 \text{ kip}\cdot\text{ft}$$

Demand/Capacity Ratio

$$\frac{M_u}{\phi M_n} = 0.745$$

if $\frac{M_u}{\phi M_n} \leq 1.0$	= "GOOD!"
"GOOD!"	
else	
"NO GOOD..."	

Note: The increased amount of rebar is intended to account for the possibility that the block-out will increase the bending capacity of the column base connection, and that the actual moment experienced by the connection (and thus transferred to the slab) will increase beyond that amount an anticipated 30-40%.

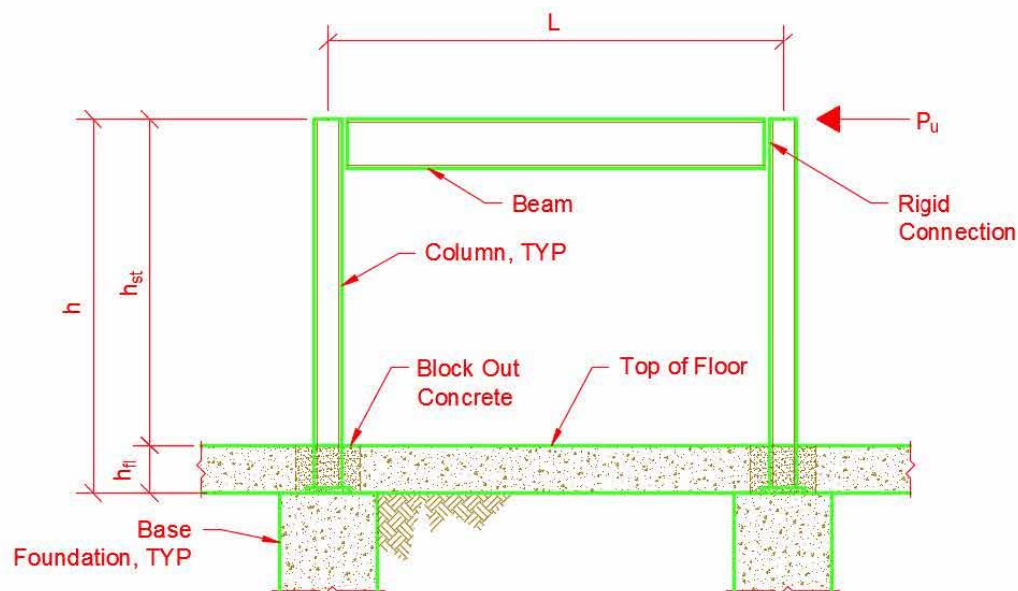


B.11 Design Example #1: Portal Frame Design with a “fixed” base

Design Example #1
Portal Frame Detailed Design
With "Fixed" Base

Given

1. A portal frame is subjected to a factored lateral load (wind load). Vertical Loads are ignored.
2. The portal frame consists of wide flange members, oriented to bend about their strong axis.
3. The Column bases are shallowly embedded in unreinforced block out concrete



story height $h_{st} := 10 \text{ ft}$

block out
(embedment depth) $h_{fl} := 18 \text{ in}$

Total Column Length $h := h_{st} + h_{fl} = 11.5 \text{ ft}$

Center-to-Center
Column Spacing $L := 14 \text{ ft}$

Factored LRFD lateral load
on Frame (Wind Loads) $P_u := 100 \text{ kip}$

Material Properties

Column & Beam

Steel Grade	ASTM A992 Steel
yield strength	$F_y := 50 \text{ ksi}$
ultimate strength	$F_u := 65 \text{ ksi}$
Modulus of Elasticity	$E := 29000 \text{ ksi}$
Shear Modulus of Elasticity	$G := 11200 \text{ ksi}$

Anchor Bolts

Steel Grade	ASTM F1554 Gr. 55
yield strength	$F_{y_b} := 55 \text{ ksi}$
ultimate strength	$F_{u_b} := 75 \text{ ksi}$

Base Plate

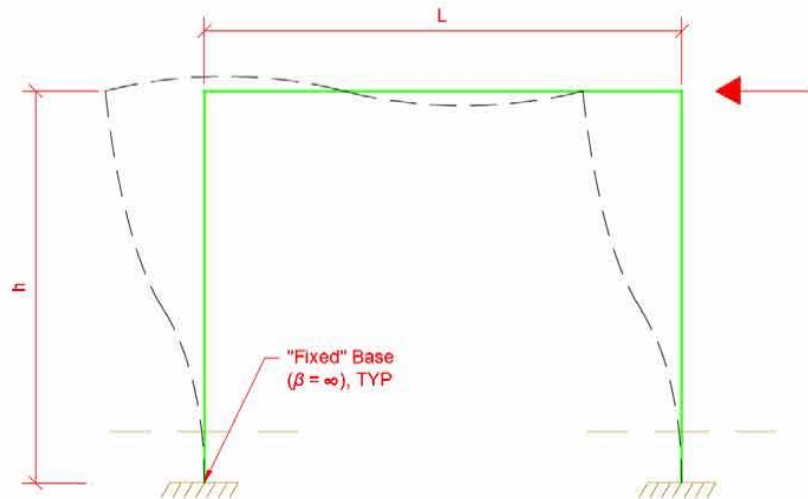
Steel Grade	ASTM A36
yield strength	$F_{y_{spl}} := 36 \text{ ksi}$
ultimate strength	$F_{u_{spl}} := 58 \text{ ksi}$

Concrete

28-day compressive strength	$f'_c := 4000 \text{ psi}$
-----------------------------	----------------------------

CONVENTIONAL DESIGN METHODS

Model



Column Base Design Methodology:

Rotational Stiffness

Assume a "fixed base" at the base of the column, but ONLY IF the strength of the base elements are designed to develop the expected bending capacity of the column.

Rotational Strength

Design the Base Connection in accordance with AISC Steel Design Guide #1, chapter 3.4 "Design of column base plates with large moments", with the required strength being the expected bending capacity of the column steel.

Design Member Sizes

Assume that the portal frame lateral deflection will govern the size of the members, then check those member sizes to ensure they fulfill the strength requirements.

Maximum Moment Demand in the Column

$$M_{u_c} := \left(\frac{P_u}{2} \right) \cdot \left(\frac{h}{2} \right) = 287.5 \text{ kip}\cdot\text{ft}$$

Maximum Moment Demand in the Beam

$$M_{u_b} := M_{u_c} = 287.5 \text{ kip}\cdot\text{ft}$$

Strength Reduction Factor for Bending

$$\phi_b := 0.9$$

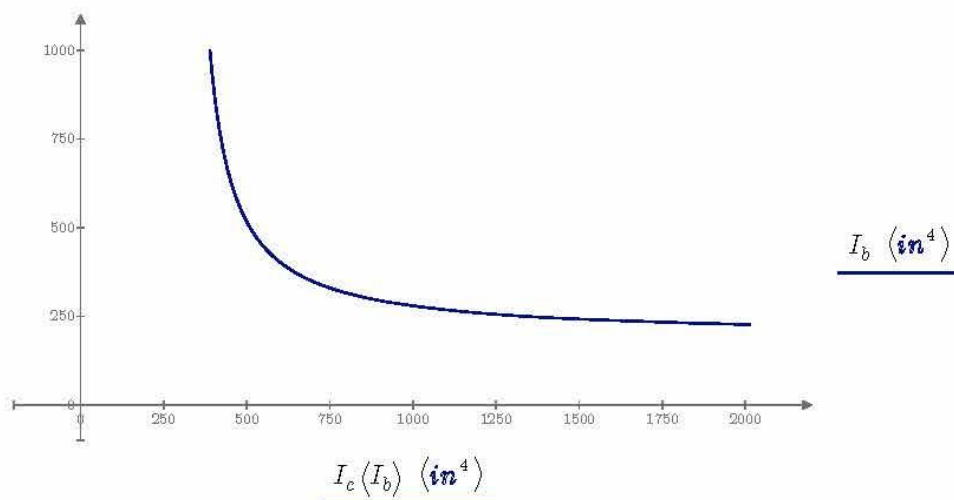
Maximum Deflection of portal frame

$$\Delta_{max} := (1\%) \cdot h_{st} = 1.2 \text{ in}$$

Deflection of portal frame, with a fixed base
(as a function of the stiffness of the column and the beam)

$$\Delta_p(I_c, I_b) := \frac{P_u \cdot h^2}{24 \cdot E} \cdot \left(\frac{h}{I_c} + \frac{L}{2 \cdot I_b} \right)$$

Given the maximum permissible lateral deflection, the Stiffness of the Column and the Beam must be related by the following graph:



Choose Member Sizes (Optimized Process Not Shown Here)

Column	$Mem := "W14 \times 48"$
nominal bending strength	$M_{p_col} := F_y \cdot Z_x = 326.67 \text{ kip} \cdot \text{ft}$
stiffness	$I_c := I_x = 484 \text{ in}^4$
Strength Check	$\left \begin{array}{l} \text{if } \phi_b \cdot M_{p_col} \geq M_{u_c} \\ \parallel \\ \text{"G"} \\ \text{else} \\ \parallel \\ \text{"NG"} \end{array} \right = \text{"G"}$
Beam	$Mem := "W16 \times 45"$
nominal bending strength	$M_{p_beam} := F_y \cdot Z_x = 342.92 \text{ kip} \cdot \text{ft}$
stiffness	$I_b := I_x = 586 \text{ in}^4$
Strength Check	$\left \begin{array}{l} \text{if } \phi_b \cdot M_{p_beam} \geq M_{u_c} \\ \parallel \\ \text{"G"} \\ \text{else} \\ \parallel \\ \text{"NG"} \end{array} \right = \text{"G"}$

Deflection Check with the members chosen

$$\Delta_{actual} := \Delta_p(I_c, I_b) = 1.17 \text{ in}$$

$$\frac{\Delta_{actual}}{\Delta_{max}} = 0.98$$

$$\left| \begin{array}{l} \text{if } \frac{\Delta_{actual}}{\Delta_{max}} \leq 1.0 \\ \parallel \\ \text{"G"} \\ \text{else} \\ \parallel \\ \text{"NG"} \end{array} \right| = \text{"G"}$$

Design of Base Connection

In accordance with common practice, the block out concrete will be ignored, and the base will be designed as if it were an "exposed base connection". The base plate will be designed to develop the expected bending capacity of the column.

$$R_y := 1.1 \quad [\text{expected strength factor}]$$

Base Plate

$$\text{Width} \quad N := 1 \text{ ft} + 10 \text{ in}$$

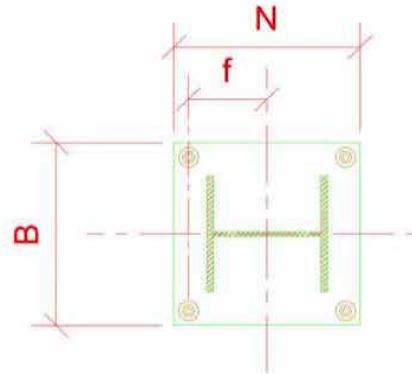
$$\text{Length} \quad B := 1 \text{ ft} + 1 \text{ in}$$

$$\text{AB Locations} \quad f := 9 \text{ in}$$

$$n := \frac{B - 0.8 \cdot b_{f_col}}{2} = 3.29 \text{ in}$$

$$m := \frac{N - 0.95 \cdot d_{col}}{2} = 4.45 \text{ in}$$

$$\text{AB Quantity} \quad num_b := 8$$



Step 1: Determine the Moment Load on Column Base

$$P_r := (h) \cdot wt_{col} = 552 \text{ lbf}$$

$$M_r := 1.1 R_y \cdot M_{p_col} = 395.27 \text{ kip} \cdot \text{ft}$$

Step 2: Pick a trial base plate size ($N \times B$)

(defined previously)

$$N = 22 \text{ in}$$

$$B = 13 \text{ in}$$

Step 3: Determine the equivalent eccentricity (e), and the critical eccentricity (ecrit)

$$e := \frac{M_r}{P_r} = 716.1 \text{ ft}$$

$$e_{crit} := \frac{N}{2} - \frac{P_r}{2 \cdot q_{max}} = 11 \text{ in}$$

$$\begin{array}{l} \text{if } e \geq e_{crit} \\ \quad \parallel \text{ "GOOD!"} \\ \text{else} \\ \quad \parallel \text{ "NO GOOD!"} \end{array} \quad \Bigg| = \text{"GOOD!"}$$

Step 4: Determine the equivalent bearing length (Y) and the tensile force in the anchor rods (T).

$$Y := \left(f + \frac{N}{2} \right) + \left[\begin{array}{c} 1 \\ -1 \end{array} \right] \cdot \sqrt{\left(f + \frac{N}{2} \right)^2 - \frac{2 \cdot P_r \cdot (e + f)}{q_{max}}} = \left[\begin{array}{c} 35.32 \\ 4.68 \end{array} \right] \text{ in}$$

$$\begin{array}{l} Y := \text{if } 0 < Y_0 < N \\ \quad \parallel Y_0 \\ \text{else} \\ \quad \parallel Y_1 \end{array} \quad \Bigg| = 4.68 \text{ in}$$

$$T := q_{max} \cdot Y - P_r = 268.31 \text{ kip}$$

Step 5: Determine the required minimum base plate thickness at the bearing and the tension interfaces.

Bearing Interface:

$$t_{p_req_b} := \begin{cases} \text{if } Y \geq \max(m, n) \\ 1.5 \cdot m \cdot \sqrt{\frac{f_{p_max}}{F_{y_bspl}}} \\ \text{else} \\ 2.11 \cdot \sqrt{\frac{f_{p_max} \cdot Y \cdot \left(m - \frac{Y}{2}\right)}{F_{y_bspl}}} \end{cases} = 2.34 \text{ in}$$

Tension Interface

$$t_{p_req_t} := 2.11 \cdot \sqrt{\frac{T \cdot \left(f - \frac{d_{col}}{2} + \frac{t_{f_col}}{2}\right)}{B \cdot F_{y_bspl}}} = 2.47 \text{ in}$$

Take maximum of the two:

$$t_{p_req} := \max(t_{p_req_b}, t_{p_req_t}) = 2.47 \text{ in}$$

$$t_p := \text{Ceil}(t_{p_req}, 0.125 \text{ in}) = 2.500 \text{ in}$$

Step 6: Determine the anchor rod size appropriate for the tensile loading

(assuming that the embedment is such that tensile fracture of the anchor bolt governs, and that shear load in the bolts is negligible)

Number of bolts in tension

$$N_{b_t} := \frac{num_b}{2} = 4$$

Tensile Force in each bolt

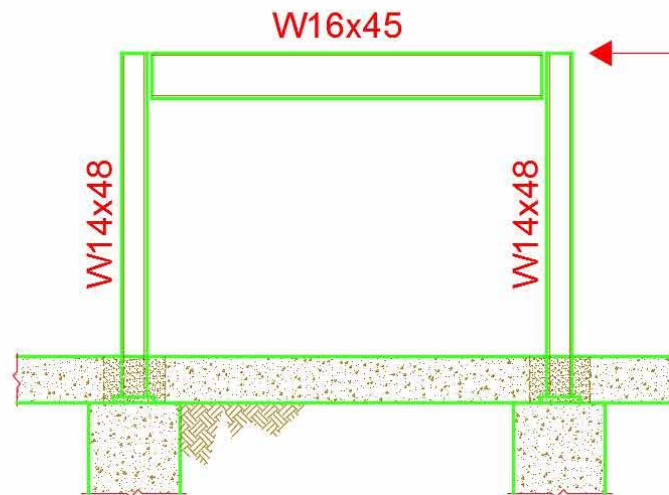
$$T_u := \frac{T}{N_{b_t}} = 67.08 \text{ kip}$$

required diameter $\phi := 0.75$

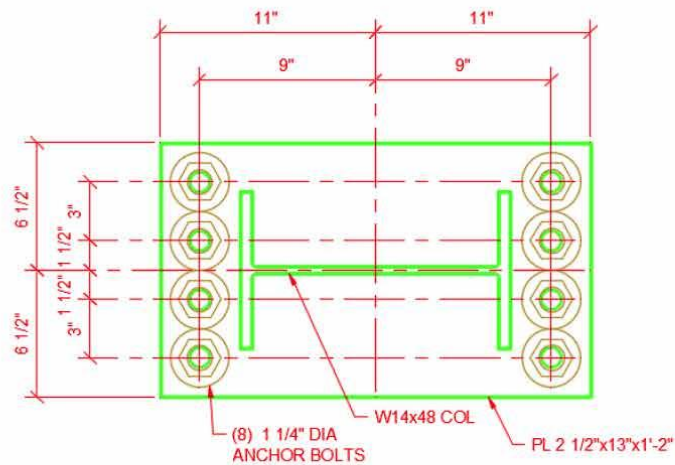
$$D_{req} := \sqrt{\frac{4 \cdot T_u}{\pi \cdot \phi \cdot F_{u_b}}} = 1.23 \text{ in}$$

$$D := \text{Ceil}(D_{req}, 0.125 \text{ in}) = 1.250 \text{ in}$$

Conventional Method, Design Summary



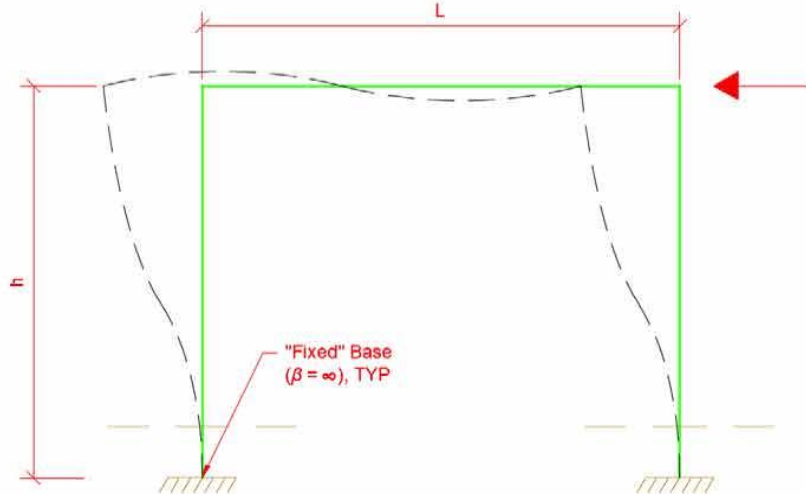
Elevation: Portal Frame Design - Member Sizes



Plan View: Typical Base Plate Design

NEW DESIGN METHODS

Model (Note that since the model is exactly the same as the conventional method, the member sizes chosen will be exactly the same)



Column Base Design Methodology:

Rotational Stiffness

depth of block out/depth of column $\frac{h_{fl}}{d_{col}} = 1.3$

Assume a "fixed base" at the base of the column, since the ratio of the block out depth to column depth is greater than 1.22. This is the case regardless of the strength of the connection

Rotational Strength

Design the base connection using Barnwell's Strength model to determine the tensile resultant of the moment force. That tensile resultant will determine both the size and quantity of the anchor bolts, and the thickness of the base plate.

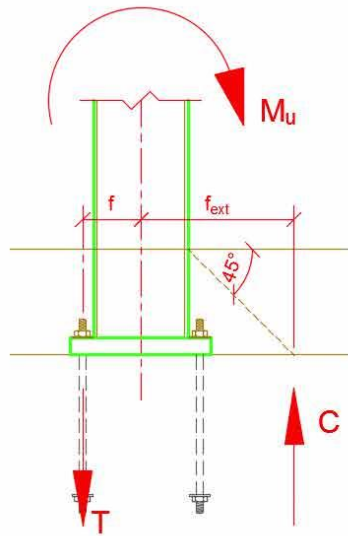
Design of Base Connection

Using Barnwell's Model for the strength design of the base connection.

Max Moment at the
column base

$$M_{u_c} := \frac{P_u \cdot h}{4} = 287.5 \text{ kip} \cdot \text{ft}$$

Barnwell's Model



$$f := 8.5 \text{ in}$$

$$f_{ext} := \frac{d_{col}}{2} + h_{fl} = 24.9 \text{ in}$$

$$T := \frac{M_{u_c}}{(f + f_{ext})} = 103.29 \text{ kip}$$

Design the Base plate thickness based on Tensile Resultant

$$t_{p_req_t} := 2.11 \cdot \sqrt{\frac{T \cdot \left(f - \frac{d_{col}}{2} + \frac{t_{f_col}}{2} \right)}{B \cdot F_{y_bspl}}} = 1.365 \text{ in}$$

$$t_p := \text{Ceil}(t_{p_req_t}, 0.125 \text{ in}) = 1.375 \text{ in}$$

Design the size of the anchor bolts

Total Number of Anchor Bolts

$$num_b := 8$$

Number of bolts in tension

$$N_{b_t} := \frac{num_b}{2} = 4$$

Tensile Force in each bolt

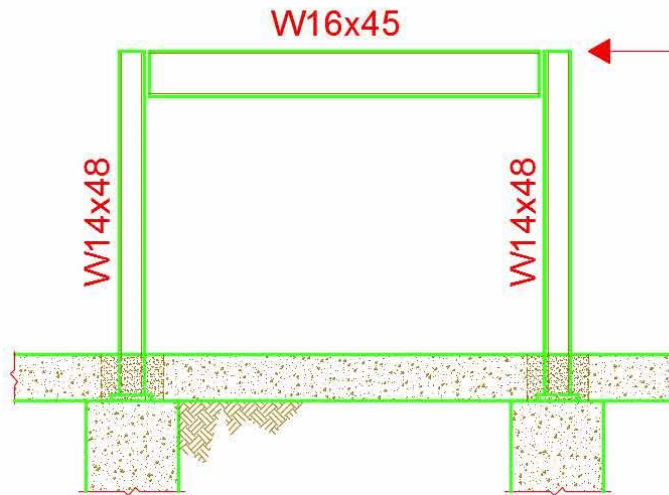
$$T_u := \frac{T}{N_{b_t}} = 25.82 \text{ kip}$$

required diameter $\phi := 0.75$

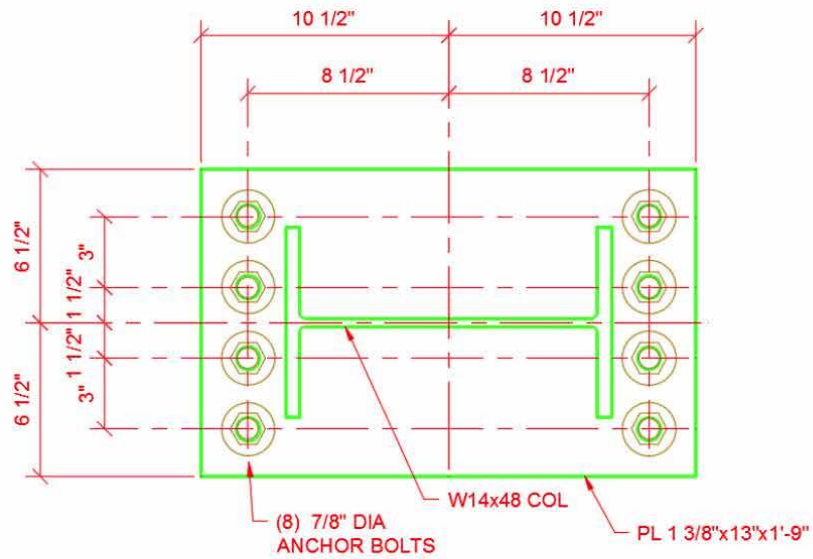
$$D_{req} := \sqrt{\frac{4 \cdot T_u}{\pi \cdot \phi \cdot F_{u_b}}} = 0.7645 \text{ in}$$

$$D := \text{Ceil}(D_{req}, 0.125 \text{ in}) = 0.875 \text{ in}$$

New Methods, Design Summary



Elevation: Portal Frame Design - Member Sizes



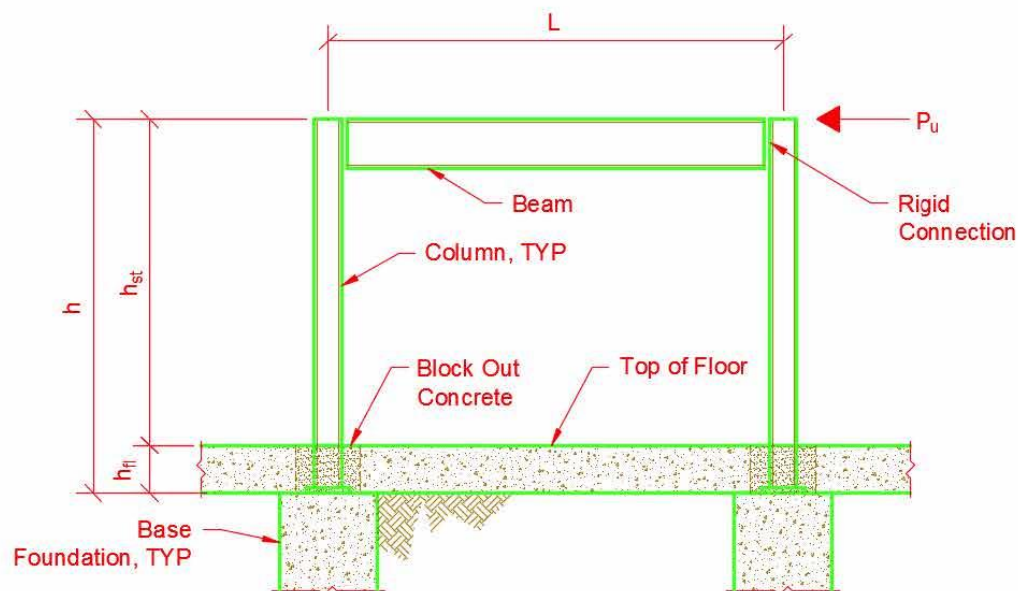
Plan View: Typical Base Plate Design

B.12 Design Example #2: Portal Frame Design with a “Pinned” Base

Design Example #2
 Portal Frame Detailed Design
 With "pinned" Base

Given

1. A portal frame is subjected to a factored lateral load (wind load). Vertical Loads are ignored.
2. The portal frame consists of wide flange members, oriented to bend about their strong axis.
3. The Column bases are shallowly embedded in unreinforced block out concrete



story height $h_{st} := 10 \text{ ft}$

block out
(embedment depth) $h_{fl} := 18 \text{ in}$

Total Column Length $h := h_{st} + h_{fl} = 11.5 \text{ ft}$

Center-to-Center
Column Spacing $L := 14 \text{ ft}$

Factored LRFD lateral load
on Frame (Wind Loads) $P_u := 100 \text{ kip}$

Material Properties

Column & Beam

Steel Grade	ASTM A992 Steel
yield strength	$F_y := 50 \text{ ksi}$
ultimate strength	$F_u := 65 \text{ ksi}$
Modulus of Elasticity	$E := 29000 \text{ ksi}$
Shear Modulus of Elasticity	$G := 11200 \text{ ksi}$

Anchor Bolts

Steel Grade	ASTM F1554 Gr. 55
yield strength	$F_{y_b} := 55 \text{ ksi}$
ultimate strength	$F_{u_b} := 75 \text{ ksi}$

Base Plate

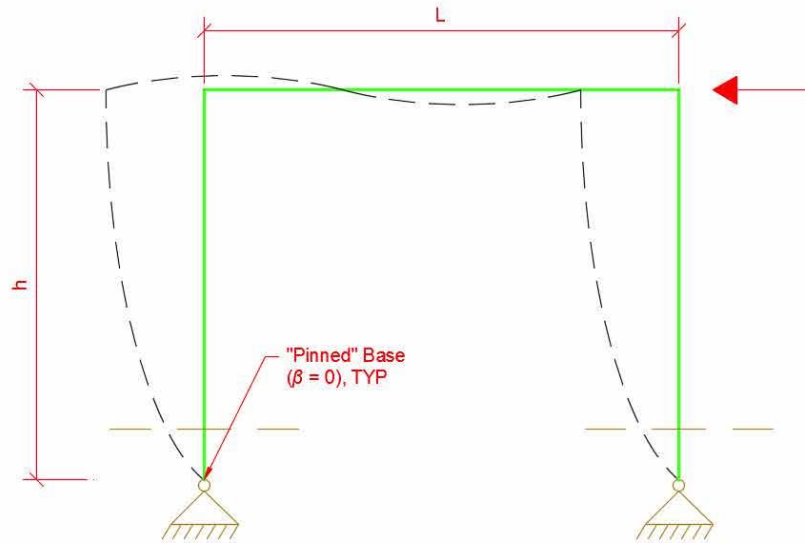
Steel Grade	ASTM A36
yield strength	$F_{y_{spl}} := 36 \text{ ksi}$
ultimate strength	$F_{u_{spl}} := 58 \text{ ksi}$

Concrete

28-day compressive strength	$f'_c := 4000 \text{ psi}$
-----------------------------	----------------------------

CONVENTIONAL DESIGN METHODS

Model



Column Base Design Methodology:

Rotational Stiffness

Assume a "pinned base" at the base of the column, thus the column base need only be designed for vertical loads.

Rotational Strength

Design the Base Connection in accordance with AISC Steel Design Guide #1, chapter 3.1 "Concentric Axial Loads", with the required strength being 50% of the axial capacity of the column.

Design Member Sizes

Assume that the portal frame lateral deflection will govern the size of the members, then check those member sizes to ensure they fulfill the strength requirements.

Maximum Moment Demand in the Column

$$M_{u_c} := \left(\frac{P_u}{2} \right) \cdot (h) = 575 \text{ kip}\cdot\text{ft}$$

Maximum Moment Demand in the Beam

$$M_{u_b} := M_{u_c} = 575 \text{ kip}\cdot\text{ft}$$

Strength Reduction Factor for Bending

$$\phi_b := 0.9$$

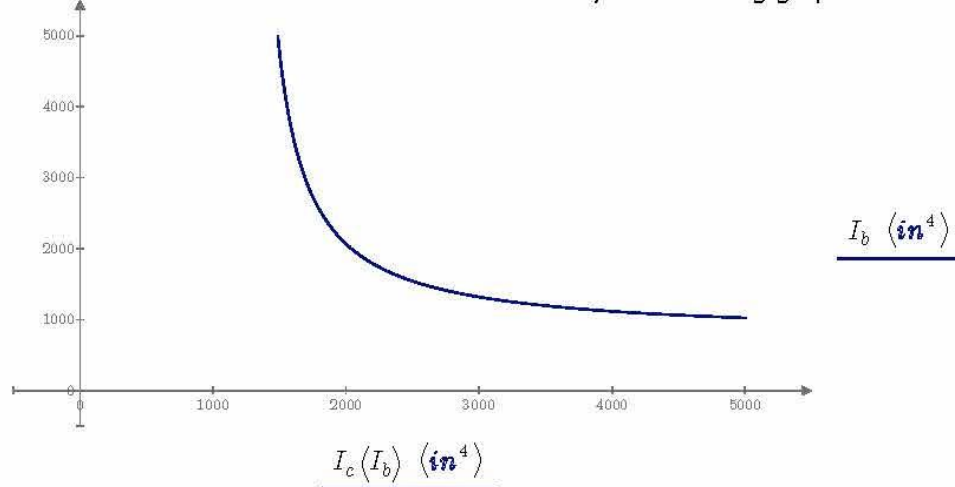
Maximum Deflection of portal frame

$$\Delta_{max} := (1\%) \cdot h_{st} = 1.2 \text{ in}$$

Deflection of portal frame, with a fixed base
(as a function of the stiffness of the column and the beam)

$$\Delta_p(I_c, I_b) := \frac{P_u \cdot h^2}{6 \cdot E} \cdot \left(\frac{h}{I_c} + \frac{L}{2 \cdot I_b} \right)$$

Given the maximum permissible lateral deflection, the Stiffness of the Column and the Beam must be related by the following graph:



Choose Member Sizes (Optimized Process Not Shown Here)

Column	$Mem := \text{"W18x86"}$
nominal bending strength	$M_{p_col} := F_y \cdot Z_x = 775 \text{ kip}\cdot\text{ft}$
stiffness	$I_c := I_x = 1530 \text{ in}^4$
Strength Check	$\begin{array}{l} \text{if } \phi_b \cdot M_{p_col} \geq M_{u_c} \\ \parallel \\ \text{"G"} \\ \text{else} \\ \parallel \\ \text{"NG"} \end{array} = \text{"G"}$
Beam	$Mem := \text{"W24x146"}$
nominal bending strength	$M_{p_beam} := F_y \cdot Z_x = 1741.67 \text{ kip}\cdot\text{ft}$
stiffness	$I_b := I_x = 4580 \text{ in}^4$
Strength Check	$\begin{array}{l} \text{if } \phi_b \cdot M_{p_beam} \geq M_{u_c} \\ \parallel \\ \text{"G"} \\ \text{else} \\ \parallel \\ \text{"NG"} \end{array} = \text{"G"}$

Deflection Check with the members chosen

$$\Delta_{actual} := \Delta_p(I_c, I_b) = 1.19 \text{ in}$$

$$\frac{\Delta_{actual}}{\Delta_{max}} = 0.99$$

$$\begin{array}{l} \text{if } \frac{\Delta_{actual}}{\Delta_{max}} \leq 1.0 \\ \parallel \\ \text{"G"} \\ \text{else} \\ \parallel \\ \text{"NG"} \end{array} = \text{"G"}$$

Design of Base Connection

In accordance with common practice, the block out concrete will be ignored, and the base will be designed as if it were an "exposed base connection". The base plate will be designed to for 50% of the axial capacity of the column

required axial
compressive load $P_u := 0.5 \cdot 836 \text{ kip}$

Base Plate

Width $N := 1 \text{ ft} + 8 \text{ in}$

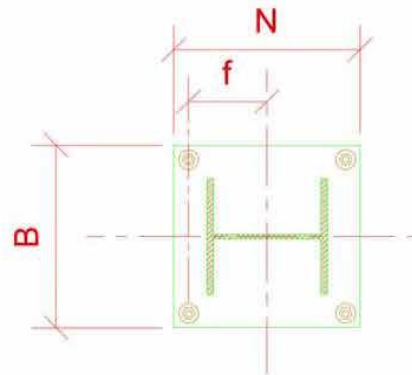
Length $B := 1 \text{ ft} + 1 \text{ in}$

AB Locations $f := 3 \text{ in}$

$$n := \frac{B - 0.8 \cdot b_{f_col}}{2} = 2.06 \text{ in}$$

$$m := \frac{N - 0.95 \cdot d_{col}}{2} = 1.26 \text{ in}$$

AB Quantity $num_b := 4$



Design Base Plate Thickness

$$\phi := 0.9$$

$$X := \left(\frac{4 \cdot d_{col} \cdot b_{f_col}}{(d_{col} + b_{f_col})^2} \right) \cdot \frac{836 \text{ kip}}{1672 \text{ kip}} = 0.47$$

$$\lambda := \frac{2 \cdot \sqrt{X}}{1 + \sqrt{1 - X}} = 0.79$$

$$\lambda n' := \lambda \cdot \frac{\sqrt{d_{col} \cdot b_{f_col}}}{4} = 2.83 \text{ in}$$

$$l := \max(m, n, \lambda n') = 2.83 \text{ in}$$

$$t_{min} := l \cdot \sqrt{\frac{2 \cdot P_u}{\phi \cdot F_{y_bspl} \cdot B \cdot N}} = 0.89 \text{ in}$$

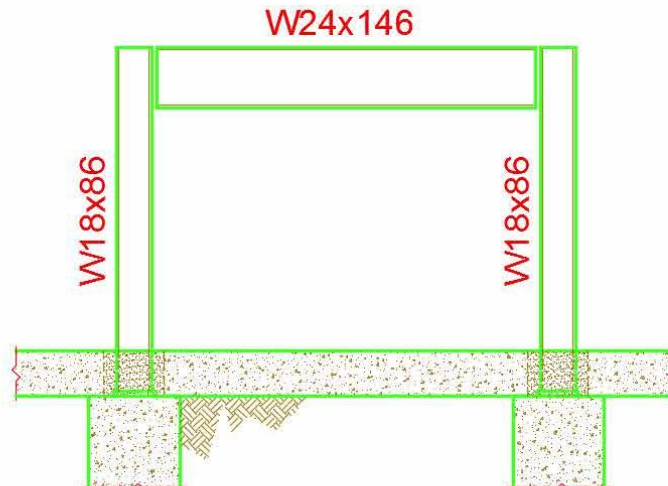
$$t_p := \text{Ceil}(t_{min}, 0.125 \text{ in}) = 1.0 \text{ in}$$

Determine the anchor rod size

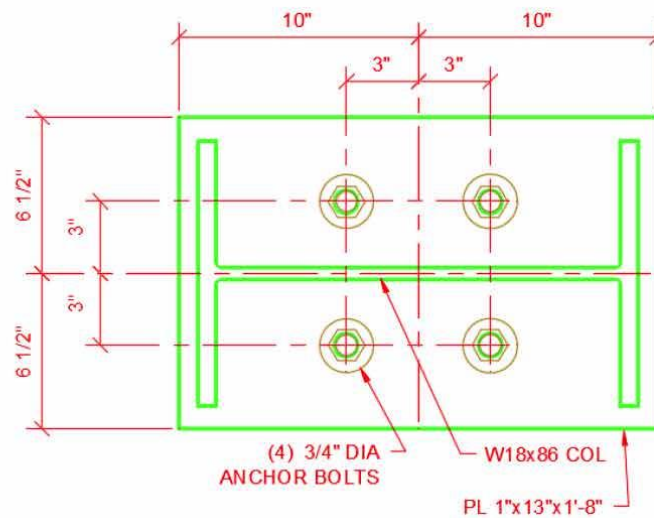
(provide the minimum required anchor bolts per OSHA)

$$D := \frac{3}{4} \text{ in} = 0.750 \text{ in}$$

Conventional Method, Design Summary



Elevation: Portal Frame Design - Member Sizes



Plan View: Typical Base Plate Design

NEW DESIGN METHOD

Design Example #2

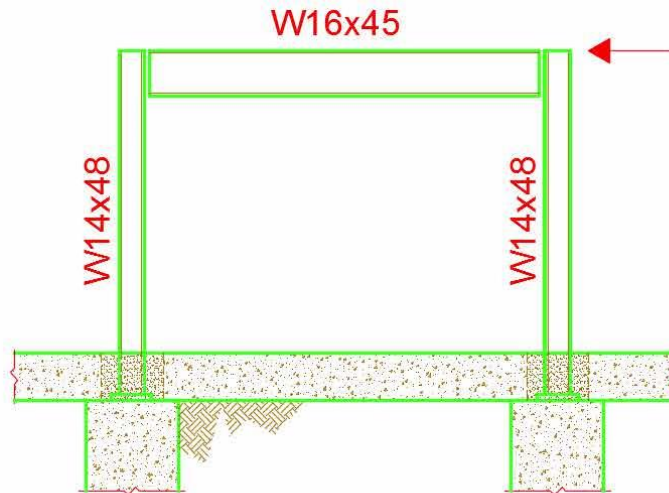
Portal Frame w/ "pinned" base

7 of 8

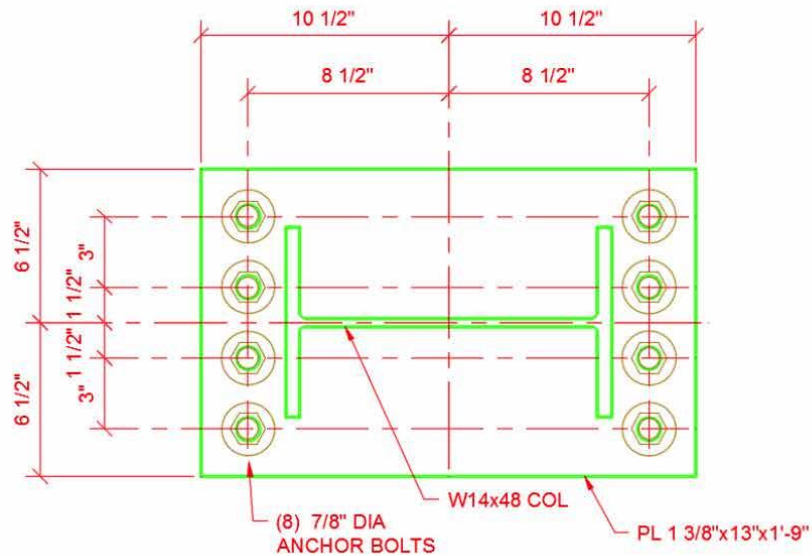
NEW DESIGN METHODS

Accounting for the block out concrete, the base can be considered fixed. Thus this design is identical to the design found on the partner document, "Design Example 1 - Moment Frame with Fixed Base". See that document for the detailed design.

New Methods, Design Summary



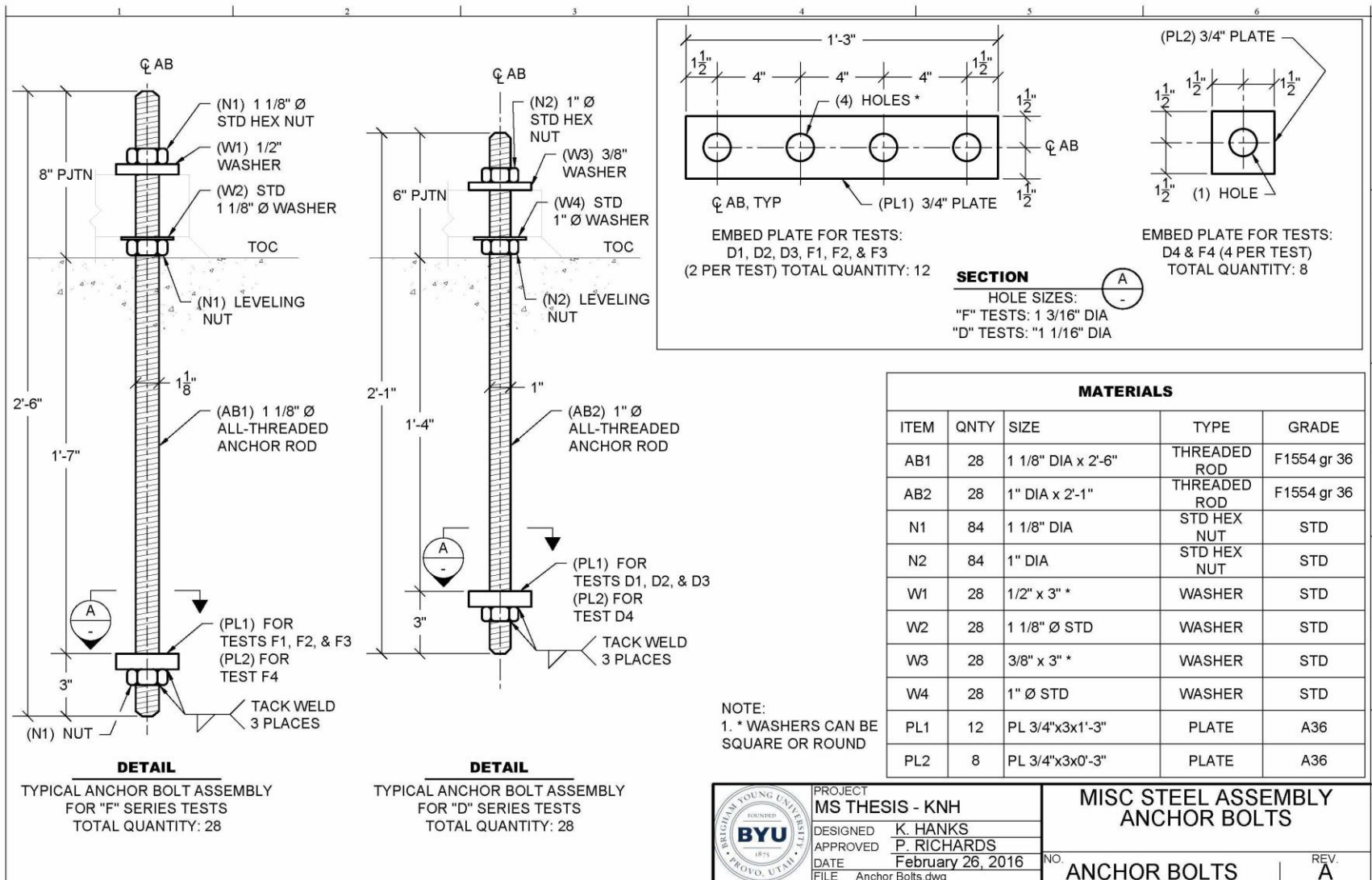
Elevation: Portal Frame Design - Member Sizes



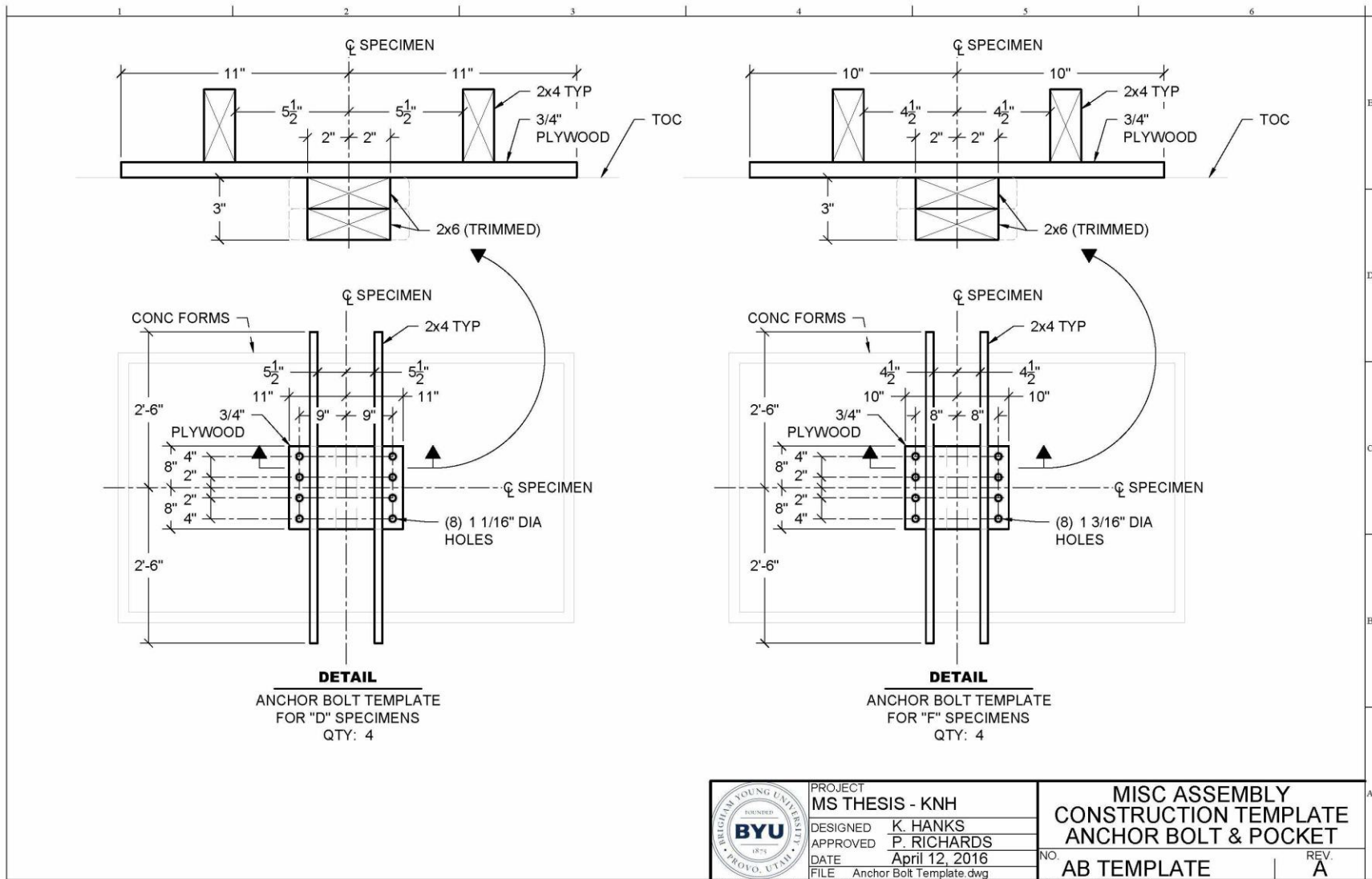
Plan View: Typical Base Plate Design

APPENDIX C: MISCELLANEOUS DRAWINGS

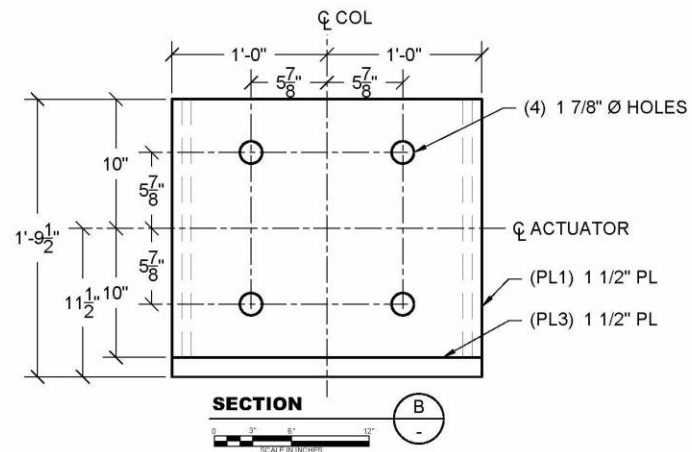
C.1 Design Drawing for the Anchor Bolts and Embedded Plates



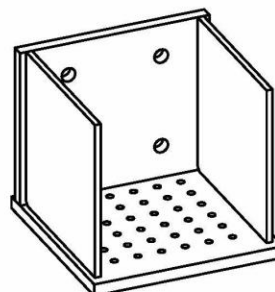
C.2 Design Drawing for the Anchor Bolt and Shear Key Pocket Template



C.3 Design Drawing for the Corbel



1. THIS CORBEL IS MEANT TO FIT A HYDRAULIC ACTUATOR, MANUFACTURED BY MTS SYSTEMS CORPORATION, EDEN PRARIE, MINNESOTA. MODEL NUMBER: 201.70. REFER TO DRAWING 100-318-636 REV C.



NOT TO SCALE
SHOWN FOR
REFERENCE ONLY

MATERIALS			
ITEM	QNTY	SIZE	GRADE
PL1	1	PL 1 1/2x20x2'-0"	A36
PL2	2	PL 3/4x19x1'-8"	A36
PL3	1	PL 1 1/2x24x2'-0"	A36



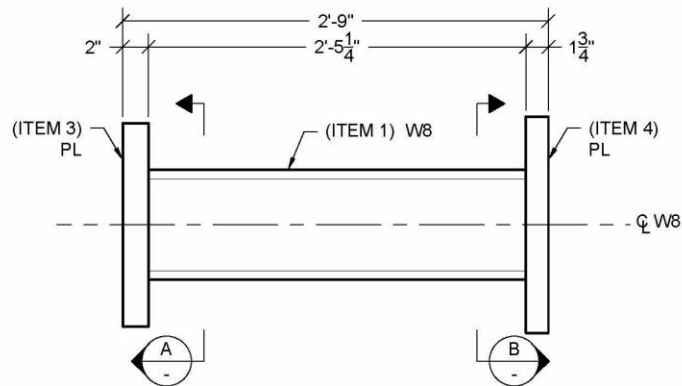
PROJECT	
MS THESIS - KNH	
DESIGNED	K. HANKS
APPROVED	P. RICHARDS
DATE	February 4, 2016
FILE	Corbel.dwg

MISC STEEL ASSEMBLY
CORBEL

NO. CORBEL

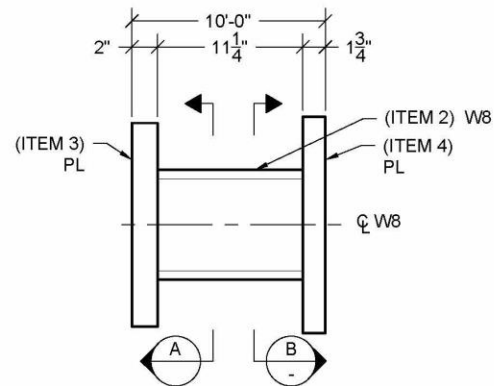
REV.
A

C.4 Design Drawing for the Actuator Extension Piece



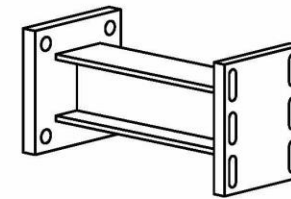
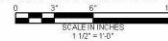
DETAIL

EXTENSION PIECE: TO BE USED WHEN ϕ OF ACTUATOR END SITS OVER BOLT HOLES



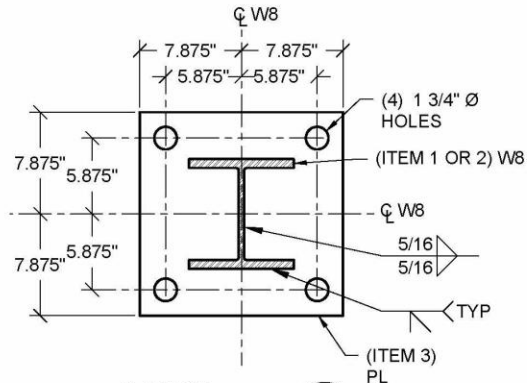
DETAIL

EXTENSION PIECE: TO BE USED WHEN ϕ OF ACTUATOR END STRADDLES BOLT HOLES



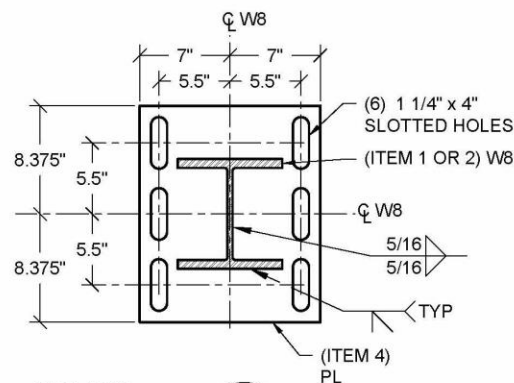
ISOMETRIC

NOT TO SCALE
SHOWN FOR
REFERENCE ONLY



SECTION

ACTUATOR
SIDE



SECTION

REACTION FRAME
SIDE



NOTES:

1. THIS EXTENSION PIECE IS MEANT TO FIT A HYDRAULIC ACTUATOR, MANUFACTURED BY MTS SYSTEMS CORPORATION, EDEN PRARIE, MINNESOTA. MODEL NUMBER: 201.70. REFER TO DRAWING 100-318-636 REV C.

MATERIALS

ITEM	QNTY	SIZE	GRADE
1	1	W8x48x2'-5 1/4"	A992
2	1	W8x48x0'-11 1/4"	A992
3	2	PL 2x15.75x1'-3 3/4"	A36
4	2	PL 1 3/4x14x1'-4 3/4"	A36



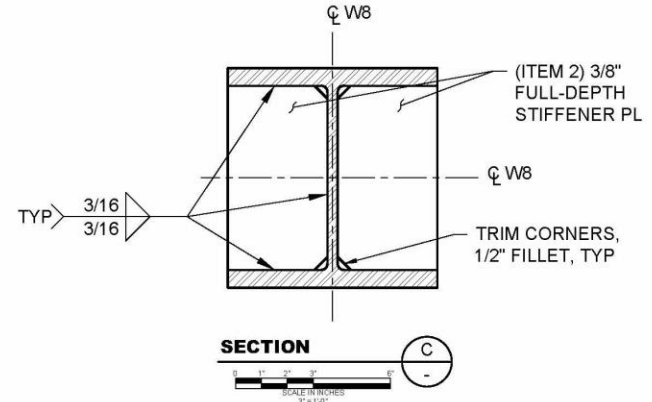
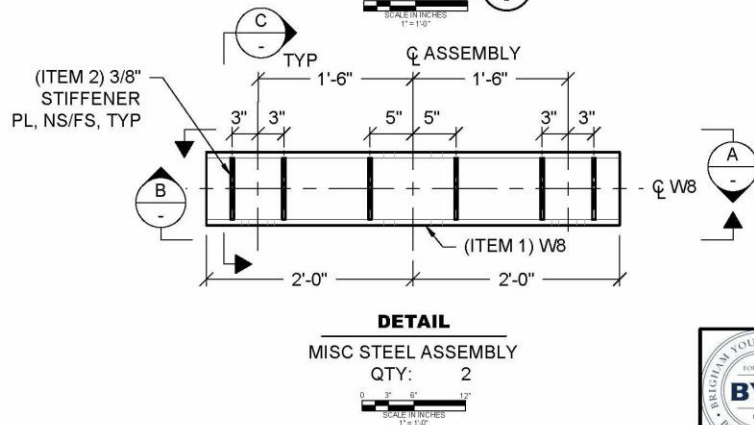
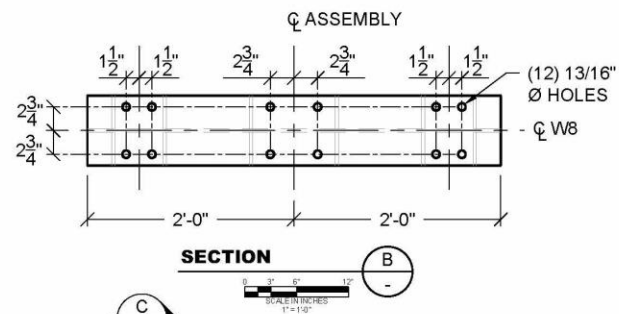
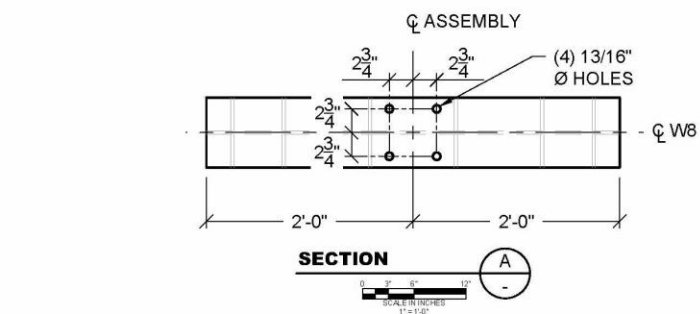
PROJECT
MS THESIS - KNH
DESIGNED **K. HANKS**
APPROVED **P. RICHARDS**
DATE **February 5, 2016**
FILE **Extension.dwg**

**MISC STEEL ASSEMBLY
EXTENSION PIECE**

NO. **EXTENSION**

REV. **A**

C.5 Design Drawing for the Base Lateral Support Steel



MATERIALS			
ITEM	QNTY	SIZE	GRADE
1	2	W8x48x4'-0"	A992
2	24	PL 3/8x3.8125x0'-7 1/8"	A36

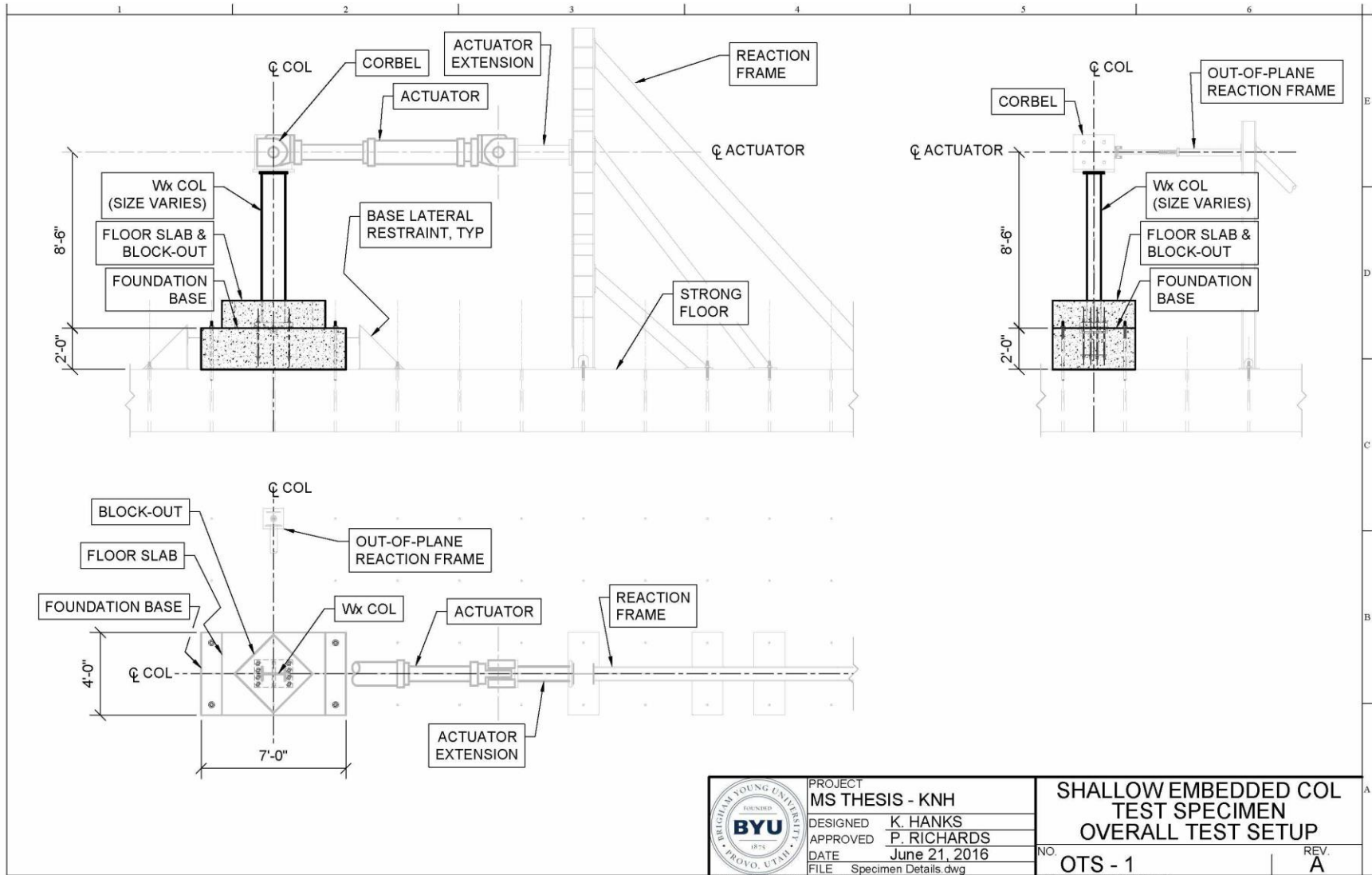


PROJECT
MS THESIS - KNH
DESIGNED
K. HANKS
APPROVED
P. RICHARDS
DATE
February 16, 2016
FILE
Extension.dwg

MISC STEEL ASSEMBLY
SUPPORT 2

NO. SUPPORT 2
REV. A

C.6 Design Drawing for the Overall Test Specimen Setup



C.7 Actuator Schematic

SPECIFICATIONS

MODEL NUMBER: 201.70

PRESSURE RATING: 3000 psi [207 bar]

FORCE RATING:

TENSION 216 kip [962 kN]

COMPRESSION 328 kip [1459 kN]

PISTON AREA:

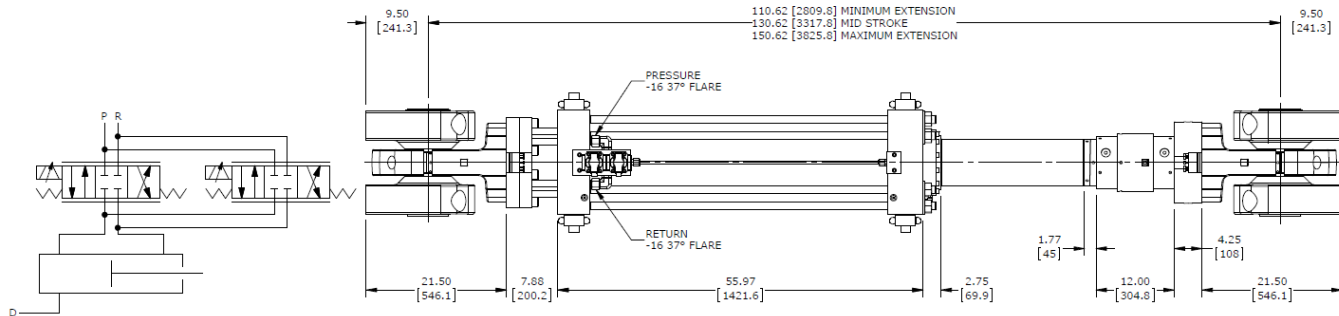
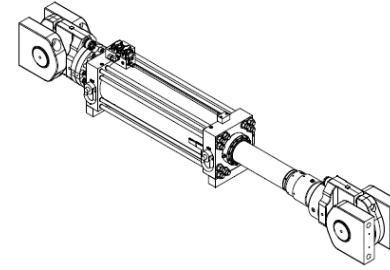
TENSION 74.61 in² [481.4 cm²]

COMPRESSION 113.10 in² [729.7 cm²]

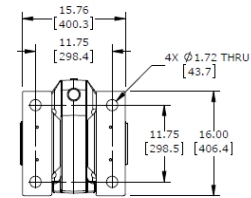
ROD DIAMETER: 7.000 [117.80]

DYNAMIC STROKE: 40.00 [1016.0]

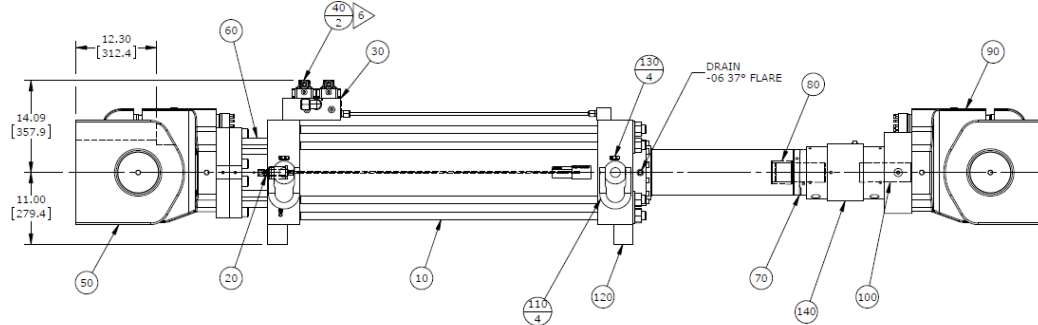
ESTIMATED WEIGHT: 4600 lbs [2090 kg]



HYDRAULIC SCHEMATIC



SWIVEL MOUNTING PATTERN TYPICAL BOTH ENDS



- (150) MOLYKOTE LUBE
- (160) ANTI GALL COMPOUND
- (170) SPANNER WRENCH
- (180) REBUILD KIT-SEALS
- (190) CABLE ASSY-493.XX TO 252 S/V
- (200) CABLE ASSY-SYSTEM GROUND
- (210) CABLE ASSY-493 TO TEMPO
- (220) CABLE ASSY-661.XX LOAD CELL
- (230) CABLE ASSY-P49 AUX PWR
- (240) MANUAL

NOTES:

- REVIEW ALL SUB-ASSEMBLY DOCUMENTS FOR ADDITIONAL INSTRUCTIONS, TORQUE VALUES, AND TEST PROCEDURES.
- ALL DIMENSIONS ARE FOR REFERENCE ONLY.
- UNITS ARE "INCHES [MILLIMETERS]" UNLESS OTHERWISE SPECIFIED.
- TORQUE ALL FASTENERS PER MTS DOCUMENT 700-005-727 TO VALUES PER MTS DOCUMENT 700-005-602.
- TORQUE ALL FITTINGS PER MTS DOCUMENT 700-005-727 TO VALUES PER MTS DOCUMENT 700-006-723.
- LUBE AND TORQUE TO 19 LB-FT [26 N-m].

REVISIONS

DESCRIPTION

DRAWN ENGR DATE

LETTER

REVNO

UNLESS OTHERWISE SPECIFIED:				DRAWN				CHECK				ENGR				MFG			
MATERIAL DESCRIPTION				XXX HOLE SIZE TOLERANCE				N/A				DATE				DATE			
SEE BOM				0.000				OVER 750				DATE				DATE			
MATERIAL SIZE				TO .750				TO 1.500				DATE				DATE			
FINISH				+ .010 / - .002				+ .010 / - .003				DATE				DATE			
TOLERANCE				NONE				NONE				DATE				DATE			
THREAD DEPTHS ARE TO MIN FULL THDS				SCALE				NONE				DATE				DATE			
+ DRILL DEPTHS ARE TO FULL DIA				XXX				1.00				DATE				DATE			
+ REMOVE BURRS AND CHAMF EDGES				XXX				1.00				DATE				DATE			
+ DO NOT SCALE PRINT				XXX				1.00				DATE				DATE			
MTS SYSTEMS CORPORATION				MTS				MTS				MTS				MTS			
ECON PARK, MINNESOTA U.S.A.				ECON				ECON				ECON				ECON			
PRODUCT CODE				201.70				201.70				201.70				201.70			
SHEET				1				1				1				1			
OF				1				1				1				1			